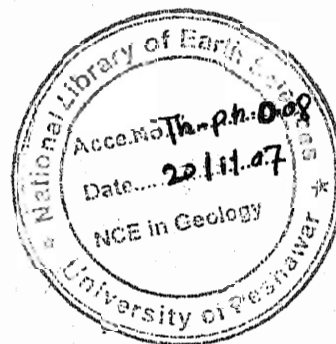
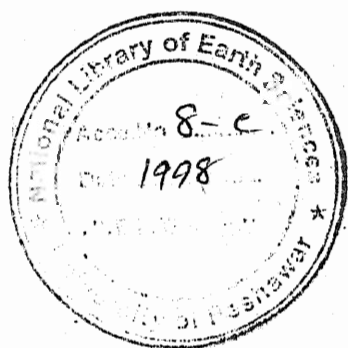


1
Ph.D.

GEOCHEMISTRY, MINERALOGY AND PETROLOGY OF THE
SULFIDE MINERALIZATION AND ASSOCIATED ROCKS
AROUND DROSH, CHITRAL (NORTHERN PAKISTAN)

549.
Mineralogy

Dissertation submitted to the
National Centre of Excellence in Geology, University of Peshawar,
in partial fulfillment of the requirement for the degree of
Doctor of Philosophy



Tazeem P. Tahirkheli

National Centre of Excellence in Geology
University of Peshawar

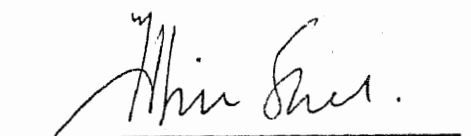
1998.

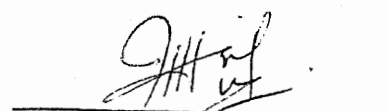
No. 8-c

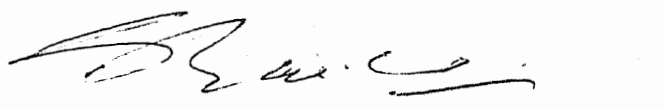
No. 8-c

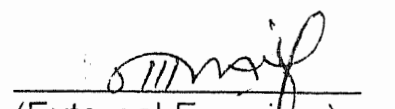
Seminar Library
Centre of Excellence
in Geology
University of Peshawar

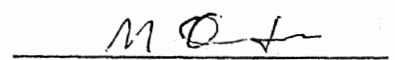
APPROVED BY


(Supervisor)
Dr. M. Tahir Shah
Associate Professor
NCE in Geology
University of Peshawar


(Co-Supervisor)
Dr. M. Asif Khan
Professor
NCE in Geology
University of Peshawar


(External Examiner)
Dr. Shamim Ahmed Siddiqui
Associate Professor
Centre of Excellence in Mineralogy
University of Baluchistan
Quetta


(External Examiner)
Dr. M. Arif
Assistant Professor
Department of Geology
University of Peshawar
Peshawar


Dr. M. Qasim Jan (T.I.)
Director
NCE in Geology
University of Peshawar

CONTENTS

	Page
ABSTRACT	
ACKNOWLEDGEMENTS	
LIST OF FIGURES	
LIST OF TABLES	
LIST OF PLATES	
.....	
<u>CHAPTER 1</u>	
INTRODUCTION	1
AIMS AND OBJECTIVES	2
PREVIOUS WORK	2
METHODOLOGY	4
Whole-Rock Analyses	4
Wet Chemical Method	5
Preparation Of Stock Solutions	5
Hf + HClO ₃ Digestion Method	6
Hf + HNO ₃ Digestion Method	6
Aqua Regia Digestion Method For Gold	6
X-Ray Fluorescence	7
Mineral Analyses	8
Electron Microprobe	8
X-Ray Diffraction	8
Fluid-Inclusion Studies	8
Lead-Isotope Analyses	9
Oxygen Isotope Analyses	9
<u>CHAPTER 2</u>	
REGIONAL TECTONICS	10
THE KOHISTAN TERRANE	13
TECTONIC EVOLUTION OF KOHISTAN AND NW HIMALAYA	20
REGIONAL GEOLOGY OF CHITRAL AND DROSH AREA	22

CHAPTER 3

LOCAL GEOLOGICAL SETTING & FIELD RELATIONS	27
LOCAL GEOLOGY	27
The Northern Suture Melange	27
The Upper-Crustal Arc Volcanic-Sedimentary Succession	27
FIELD RELATIONSHIPS	31
Kaldam Gol section	33
Gawuch Gol Section	34
Langar Gol Section	37
Gorin Gol Section	37

CHAPTER 4

PETROGRAPHY	40
METAVOLCANIC ROCKS	40
Gawuch Formation	40
Porphyritic volcanics	41
Fine grained volcanic rocks	42
Drosh Formation	44
Diorites/ Granodiorites	45
1) Diorites / Granodiorite	45
2) Altered Diorites/granodiorites	48
3) Diorite/Granodiorite Gneisses	52

CHAPTER 5

WHOLE-ROCK GEOCHEMISTRY	55
THE METAVOLCANIC ROCKS	55
Major-Element Chemistry	56
Trace Element Chemistry	62
Tectonic Setting	64
DROSH DIORITE COMPLEX	70
Major-Element Chemistry	70
Trace-Element Variations	74
Tectonic Setting of Magma Generation	74

DISCUSSION AND CONCLUSION	77
<u>CHAPTER 6</u>	
GEOLOGY OF THE MINERALIZED ROCKS	80
1- Sulfide-bearing quartz veins	80
2- Sulfide-bearing altered diorites	88
3- Sulfide- Bearing Shear Zones	90
TYPES OF COPPER MINERALIZATION	95
1- Copper mineralization along quartz Veins	95
2- Copper mineralization along the foliation planes	95
3- Disseminated copper mineralization	95
ORE MINERALOGY	96
Tetrahedrite	96
Galena	100
Chalcopyrite	100
Sphalerite	102
Pyrite	104
Magnetite	104
Bornite	105
CHEMICAL GAIN / LOSS ACCOMPANYING MINERALIZATION	109
Kaldom Gol	114
Gawuch Gol	114
Gorin Gol	114
<u>CHAPTER 7</u>	
<u>FLUID-INCLUSION STUDIES</u>	120
INTRODUCTION	120
PREPARATION AND PROCEDURES	122
TYPES OF FLUID INCLUSIONS	122
DISCUSSIONS	123
<u>CHAPTER 8</u>	
<u>OXYGEN ISOTOPE GEOCHEMISTRY</u>	129

INTRODUCTION	129
TYPES OF WATER IN HYDROTHERMAL SYSTEM	130
Sea Water	130
Meteoric Water	130
Juvenile Water	131
Magmatic Water	131
Connate or Metamorphic water	131
$\delta^{18}\text{O}$ IN MINERALIZED QUARTZ VEINS	132
$\delta^{18}\text{O}$ VALUES OF THE HYDROTHERMAL FLUID	133
THE ORE-FORMING FLUID	135
<u>CHAPTER 9</u>	
LEAD ISOTOPE GEOCHEMISTRY	140
INTRODUCTION	140
RESULTS AND DISCUSSIONS	142
<u>CHAPTER 10</u>	
SUMMARY AND CONCLUSIONS	154
.....	
REFERENCES	165

ABSTRACT

Copper mineralization in the Drosh-Shishi area is localized in the upper crust of the Kohistan arc terrane in Chitral, northern Pakistan. It is confined to the Gawuch Formation in the area, comprising variably metamorphosed volcanics and sediments intruded by the plutons of diorite and granodiorite composition. The metavolcanics of the Gawuch Formation and the diorite-granodiorite minor plutons have calc-alkaline compositional characteristics. In comparison, the metavolcanics of the Drosh Formation, occupying the top of the succession, are island-arc tholeiites. Copper mineralization in the area is related to hydrothermal activity and is mainly associated with altered diorites and quartz veins. It occurs in different forms; in the quartz veins, along the foliation planes, in dissemination and as supergene enrichment. Tetrahedrite, chalcopyrite, pyrite and galena are the dominant ore minerals along with subordinate amounts of sphalerite, magnetite, malachite and azurite.

Fluid-inclusion studies indicate that the salinity of the hydrothermal solution is <26 equivalent wt% NaCl and the homogenization temperature is in the range of 160 to 350°C. Oxygen isotope data suggest that the quartz in the mineralized quartz veins has $\delta^{18}\text{O}$ values ranging from 14.49 to 18.32 per mil. with mean value of 16.63‰. This, when combined with the homogenization temperature obtained from the fluid-inclusion studies, indicates involvement of magmatic fluids ($\delta^{18}\text{O}=5.79\text{--}9.62$ ‰) in the formation of quartz veins and associated copper mineralization.

The lead isotopic compositions of three galena samples suggest that $^{206}\text{Pb}/^{204}\text{Pb}$ ranges from 18.728 to 18.793, $^{207}\text{Pb}/^{204}\text{Pb}$ from 15.658 to 15.728 and $^{208}\text{Pb}/^{204}\text{Pb}$ from 39.040 to 39.285. These Pb-isotope ratios yield model ages of 42 - 140

Ma with the μ values of 9.86 to 10.01. The minimum age (i.e., 42 Ma) is in close agreement with ^{40}Ar - ^{39}Ar age of the Lowari pluton, which is considered to be the source of hydrothermal solutions. The lead isotopic composition of studied galena samples indicate involvement of lead derived from older sources. These sources could be the arc volcanics or pelagic sediments of oceanic crust of Neotethys or the continental crust of the subducting Indian plate.

It is concluded from these studies that the copper mineralization in Drosh-Shishi area was produced by the hydrothermal activity related with syntectonic dioritic magmatism.

ACKNOWLEDGEMENTS

The author is greatly indebted to Dr. M. Tahir Shah, the Principal Supervisor of this research. Without his constant encouragement, which most often crossed limits to persuasion, it was impossible to complete this research. His guidance in the fieldwork, supervision in the laboratory and painstaking correction of several versions of this manuscript is thankfully acknowledged. Dr. Asif Khan, the co-supervisor, greatly helped in field and interpretation of the data; he read several of the chapters and offered useful suggestions.

The author is greatly obliged to Shakirullah Khan, Project Manager SDA, Chitral for arranging the fieldwork and help and guidance in the field.

Several aspects of this research were completed outside the premises of the Peshawar University. Dr. Tehseenullah Khan and Said Rahim Khan of Geoscience laboratory, Islamabad, arranged facilities for XRF analyses, ore microscopy and fluid-inclusion studies. Dr. M.U.K. Khattak arranged Electrom Microprobe analyses of the ore minerals at the University of South Carolina, USA. Dr. John Dilles made available the facilities for Oxygen isotope analyses at the Oregon State University, USA, while Professor R.J. Stern performed Pb isotope analyses of the Galena samples. The author extends her gratitude to all these friends for sparing time and efforts to help with my work.

Several of the faculty, staff and students from the Department and Centre of Excellence in Geology assisted this work in one way or the other. Dr. M. Rafiq supervised the XRD work. Razaq, Mumtaz, Rasoul Mohammad and Barkatullah helped with analytical equipment. Seemi & Fridoon were a great help with typing parts of the manuscript, while Durrani assisted with preliminary drafting of the figures. Fellow Ph.D. students; Dr. Ahmad Khan, Sufyan Qazi and Shahina Tariq were always there to help with problems related to computer applications. Dr. Tahir Shah, Dr. Asif Khan, Dr. Iftikhar Ahmed read all or parts of the manuscript while Dr. C. J. Moon (Leicester University), Dr. Shamim Siddiqui (University of Baluchistan) and Dr. M. Arif (University of Peshawar) critically reviewed the final manuscript and suggested innumerable suggestions for improvement, which I have tried my best to incorporate.

Finally, my gratitude to my family, particularly to my father, who arranged university education for me and my sisters against the norms of the society in this country in those days. I shall not finish without mentioning Professors R.A.K. Tahirkheli and M. Qasim Jan, whose influence in my life is probably no less than that of my father.

LIST OF FIGURES

Figure 2.1. Map of the Himalayan region showing the main tectonic units and structural trends.

Figure 2.2. Geological map of the Kohistan island arc terrane.

Figure 2.3. A profile across the crust of the Kohistan island arc terrane, showing major lithological units in stratigraphic order.

Figure 2.4. Regional geological map of Chitral and Ghizer districts.

Figure 3.1 Geological Map of Drosh area, Chitral, N. Pakistan.

Figure 3.2. Generalized lithostratigraphic details of the Gawuch Formation.

Figure 5.1. Major-element variations in the volcanic rocks of Gawuch and Drosh Formations.

Figure 5.2 (a-e). Variation diagrams highlighting the calc-alkaline character of the volcanic rocks from the Gawuch Formation relative to the tholeiitic composition of the volcanic rocks from the Drosh Formation.

Figure 5.3. Mantle-normalized trace-element patterns of the volcanic rocks from the Gawuch Formation.

Figure 5.4. Mantle-normalized trace-element patterns of the volcanic rocks from the Drosh Formation.

Figure 5.5. Primordial Mantle-normalized transitional-element patterns of the volcanic rocks from the Gawuch and Drosh formations.

Figure 5.6. Discrimination diagrams showing the tectonic setting of magam generation for the volcanic rocks from the Gawuch and Drosh formations.

Figure 5.7. Primordial Mantle-normalized trace-element patterns of the volcanic rocks from the Gawuch and Drosh formations compared to mid-oceanic ridge basalt, oceanic island basalt, island-arc thoelelitre and island-arc calc-alkaline volcanics.

Figure 5.8. Classification diagram of plutonic rocks of Gawuch Formation using scheme of Cox et al. (1979).

Figure 5.9. Classification of diorites from the Gawuch Formation on the basis of Shands indices (after Maniar and Piccoli, 1989).

Figure 5.10. SiO_2 versus FeO / MgO plot for diorites from the Gawuch Formation. The diagonal lines separates tholeiitic from calc-alkaline rocks (after Miyashiro, 1975).

Figure 5.11. AFM plot of Gawuch diorites. The line demarcating the division between calc-alkaline and athlete after Irvine and Baragar (1971).

Figure 5.12. Variation in some major elements TiO_2 , Al_2O_3 , Fe_2O_3 , MgO , CaO and $\text{Na}_2\text{O} + \text{K}_2\text{O}$ in diorites from the Gawuch Formation with increasing degree of fractionation.

Figure 5.13. Mantle-normalized spider diagrams for the trace elements of dioritic rocks from the Gawuch Formation.

Figure 5.14. Different discrimination diagrams showing the tectonic setting of diorites from the Gawuch Formation. Note that a subduction-related origin is

indicated in all the diagrams used.

Figure 6.1. X-Ray diffraction pattern of tetrahedrite from the Gawuch Formation.

Figure 6.2. X-Ray diffraction pattern of galena from the Gawuch Formation.

Figure 6.3. X-Ray diffraction pattern of chalcopyrite from the Gawuch Formation.

Figure 6.4. X-Ray diffraction pattern of magnetite from the Gawuch Formation.

Figure 6.5. Variation in some major elements in Gawuch mineralized diorites with increasing degree of fractionation.

Figure 6.6. Variation in transitional elements in mineralized diorites from the Gawuch Formation.

Figure 6.7. Comparison of major and trace elements from samples collected from four principal sections i.e., Kaldom Gol, Gawuch Gol, Langer Gol and Gorin Gol.

Figure 6.8. Enrichment and depletion in major and trace element abundances during alteration and mineralization of diorites/granodiorites from Gawuch Formation, exposed in Kaldom Gol.

Figure 6.9. Enrichment and depletion in major and trace element abundances during alteration and mineralization of diorites/granodiorites from Gawuch Formation, exposed in Gawuch Gol.

Figure 6.10. Enrichment and depletion in major and trace element abundances

during alteration and mineralization of diorites/granodiorites from Gawuch Formation, exposed in Gorin Gol.

Figure 6.11. Enrichment and depletion in major and trace element abundances during alteration and mineralization of diorites/granodiorites from Gawuch Formation, exposed in Langrer Gol.

Figure 7.1. Portion of the NaCl-H₂O phase diagram to show the temperatures at which phase changes occur in an inclusion containing 15 wt% NaCl (after Shepherd et al., 1985), $t_1 = -10$ °C (ice forms and continues to crystallize), $t_2 =$ eutectic -21.2 °C; $t_3 = -20$ °C (supercooled temperature). On warming the inclusion follows the same path as taken upon freezing until at t_2 the first liquid forms from melting of solid phases. For 13.40 to 12.28 equivalent wt% NaCl: $t_1 = -9.5$ - -8.5 °C; $t_2 =$ eutectic, -19.2 °C; $t_3 = -45$ °C (super-cool temperature).

Figure 7.2 Oxygen isotope composition of parental waters calculated at a series of temperatures from the measured oxygen isotope composition of quartz of Gawuch Formation. The shaded area represent the range of the fluid inclusion homogenization temperature (160-350°C) and the range of corresponding oxygen isotopic composition (calculated) of parental waters.

Figure 8.1. Oxygen isotope composition of parental water calculated at a series of temperatures from the measured oxygen isotope composition of quartz from the Gawuch Formation. The lightly shaded area represents the range of the fluid inclusion homogenization temperature (160-350 °C) and the range of corresponding oxygen-isotope composition (calculated) of parental waters. The inset with darker shades represents the range of oxygen-isotope composition of the magmatic water.

Figure 9.1a, b. Lead isotope ratio diagrams showing growth curve of Stacey and Kramers (1975). The data from Gowuch Cu-mineralization plot very close

to the evolutionary curve in $^{207}\text{Pb}/^{204}\text{Pb}$ vs. $^{206}\text{Pb}/^{204}\text{Pb}$ and Pb diagram and above the evolution curve in $^{208}\text{Pb}/^{204}\text{Pb}$ vs. $^{206}\text{Pb}/^{204}\text{Pb}$.

Figure 9.2. $^{206}\text{Pb}/^{204}\text{Pb}$ vs. $^{207}\text{Pb}/^{204}\text{Pb}$ diagram for isotopic composition of galena from quartz veins in Cu-mineralization from the Gawuch Formation.

Figure 9.3 a, b. Plots of lead-isotopic ratios used to define the modern fields for mantle, upper crust, lower crust, and orogene (after plumbotectonic model of Zartman and Doe 1981. A = mantle. B = orogene. C = upper crust. D = lower crust. The lead isotopic data from Gawuch Cu-mineralization g plots within the intersection of fields for upper crust and orogeny curve.

Figure 9.4a,b. The lead isotope ratio diagram showing growth curve of upper crust and orogene of Doe and Zartman (1979). One sample from the Gawuch copper mineralization plots above the upper continental crust and two other between the orogeny and upper crust (a). All the samples plot to the left of the orogeny curve (b).

Figure 9.5 a,b. Comparison of plot of $^{207}\text{Pb}/^{204}\text{Pb}$ vs. $^{206}\text{Pb}/^{204}\text{Pb}$ and $^{208}\text{Pb}/^{204}\text{Pb}$ vs. $^{206}\text{Pb}/^{204}\text{Pb}$ for galena from quartz veins of the Gawuch Formation with lead isotope field of 1. Mississippi-valley type deposits (Central Missouri, USA): Doe and Delevaux (1972); 2. Laisvall-type (Sweeden) deposits: Richarad et al. (1981); 3. Rossie-type veins: Flecher and Farquhar (1982); 4. Central Metasedimentaries: Flecher and Farquhar (1982); 5. Balmat-Edwards galena: (Flecher and Farquhar (1982).

LIST OF PLATES

Plate 3.1 Photograph showing the sharp contact between the phyllites of Gawuch Formation and the altered metadiorites of Lowari Pluton.

Plate 3.2 Photograph showing faulted contact between the melange zone and the Purit Formation.

Plate 3.3 Photograph showing faulted contact between the Purit Formation and the Gawuch Formation.

Plate 4.1. Photomicrograph showing porphyritic texture in an andesite from the Gawuch Formation.

Plate 4.2. Photomicrograph showing an amygdule filled by chlorite. Amygdaloidal basaltic andesite, Gawuch Formation.

Plate 4.3. Photomicrographic view of plagioclase phenocrysts which shows partial alteration to carbonate, epidote and sericite, Drosh Volcanic Formation.

Plate 4.4. Photomicrograph showing euhedral grains of clinopyroxene (left half and lower right of the view). Note pseudomorphs of euhedral plagioclase in a fine grained groundmass. Metavolcanic from the Gawuch Formation.

Plate 4.5. Photomicrograph of a hornblende diorite. Note the tabular subhedral shape of plagioclase grain and anhedral shape of hornblende grains.

Plate 4.6. Photomicrograph showing a view of an intensively altered diorite, where the plagioclase is mainly altered to carbonates and epidote in the groundmass.

Plate 4.7a. Photomicrograph showing carbonates veining in the intensively altered diorites. The hydrothermal alteration has imparted brecciated appearance to the rock.

Plate 4.7b. Photomicrograph showing hydrothermal alteration of a diorite imparting a brecciated appearance to the rock. The carbonate masses enclose the rounded to sub-rounded aggregates of plagioclase and quartz.

Plate 4.8. Photomicrograph showing fracture-fill limonitic material in an altered diorite, enclosing the rounded to sub-rounded grains of plagioclase and quartz.

Plate 4.9. Photomicrograph showing a mylonitized dioritic rock. Rounded to sub-rounded, partially altered plagioclase grains are corroded along the margins and form asymmetrical porphyroclasts set in a fine-grained mylonitic matrix.

Plate 6.1. Photograph showing a one meter thick mineralized zone associated with a quartz vein. Malachite and azurite (green and bluish green in colour) occur as supergene enrichment along the mineralized zone.

Plate 6.2. Photograph of the same mineralized zone as above which is vanishing as the quartz vein pinches out.

Plate 6.3. Photomicrograph showing a large grain of galena in contact with an irregular grain of tetrahedrite. Note the presence of triangular pits in galena.

Plate 6.4a. Photomicrograph showing irregular grains of chalcopyrite (cp) within the tetrahedrite (tet) grains in a quartz vein (reflected light).

Plate 6.4b. Photomicrograph showing a grain of tetrahedrite (tet) as viewed in the reflected light. Note the presence of inclusions of chalcopyrite (cp). The tetrahedrite shows oxidation to limonite material along fractures.

Plate 6.5. Photomicrograph of a tetrahedrite (Tet) grain in the reflected light showing oxidation alteration to magnetite (Mt) and limonite (lm) at the margins and along the fractures. Note that the tetrahedrite host is now left as relics.

Plate 6.6. Photomicrograph of a tetrahedrite (Tet) grain in the quartz veins showing replacement to chalcocite (Ch) along the fractures.

Plate 6.7a. Photomicrograph showing an irregular and fractured grain of galena (Gl) with typical triangular pits. The abnormal morphology suggests strain post-dating the mineralization.

Plate 6.7b. Photomicrograph of a galena (Gl) grain in a quartz veins. Note the irregular grain boundaries suggesting precipitation in a pre-existing fracture.

Plate 6.8. Photomicrograph showing a grain of tetrahedrite (in full view) having inclusions of pale yellow chalcopyrite.

Plate 6.9. Photomicrograph showing irregular grains of pyrite (Py) (bright reflectance) in a quartz vein.

Plate 6.10. Photomicrograph showing cubic to subcubic grains of pyrite (Py) as observed in reflected light.

Plate 6.11. Photomicrographs showing intergrowth between tetrahedrite (Tet) and chalcopyrite (Cp) suggesting simultaneous crystallization of the two phases.

Plate 6.12. Photomicrograph showing fractured pyrite (Py). The fractures are filled by the chalcopyrite which suggest that the chalcopyrite (Cp) is the latter phase formed after pyrite.

Plate 6.13. A field view of the altered diorites showing surface staining due to the supergene enrichment of azurite and malachite.

Plate 6.14. Photomicrograph showing the precipitation of malachite (Mal) and limonite (Lm) along fractures within the altered diorites.

Plate 6.15. Photomicrograph showing irregular grains of chalcopyrite (Cp) which are precipitated as interstitial phase to the silicates.

Plate 6.16. Photograph showing a quartz vein (1/2 m thick) in the altered diorites which is enriched in the copper-bearing phases especially tetrahedrite.

CHAPTER 1

INTRODUCTION

This study is about the nature and genesis of copper mineralization exposed in the vicinity of Drosh, District Chitral, NWFP Pakistan. The studied mineralization occurs in the north-western part of the Kohistan terrane, immediately to the south of the Shyok Suture Zone, which separates the Eurasian plate to the north from the Kohistan Island-Arc Terrane to the south (Tahirkheli et al. 1979; Bard et al., 1980). The mineralized zone is 5 to 45 meters wide and laterally extends for a distance of 40 Km. It is confined to the upper part of a succession of intercalated metavolcanics and metasediments intruded by minor plutons of diorite and granodiorite composition, termed the Gawuch Formation (Pudsey et al., 1985). The mineralization is related to hydrothermal activity produced by diorite-granodiorite intrusions.

The studied area is located between latitude 60° - 70° N and longitude 87° - 97° E and covers about 40 km. The mineralized zone strikes NE-SW, more or less parallel to the Shyok Suture, which in turn, is parallel to the trend of the Shishi-Chitral rivers. The mineralized zone is accessible in the upper reaches of the Shishi valley. From here westward, accessibility is through the southern tributaries (called as Gol in the local language) of the Shishi and Chitral rivers. These include from east to west, Langer Gol, Gorin Gol, Gawuch Gol and Kaldom Gol. Except for the Kaldom Gol, where a jeepable fair-weather road leads all the way to the mineralized zone, the accessibility is by foot. However, everywhere the mineralized zone is more than 5 km away from the road.

AIMS AND OBJECTIVES

The main purpose of the present research was:

- Mapping of various lithological units and distribution of the mineralized zones with respect to these lithological units.
- Mineralogical and geochemical investigations of both mineralized and unmineralized rocks.
- Investigating the source of hydrothermal solutions and their metal enrichment processes using isotope and geochemical data.

PREVIOUS WORK

Prior to independence in 1947, a number of geoscientists (e.g., Hayden, 1916; Lydsker, 1882, 1883; McMahon, 1900; Wadia, 1932) carried out reconnaissance geological investigations, mostly during trekking/climbing expeditions, in the areas now constituting North Pakistan. The geological investigations in North Pakistan remained rare and fragmentary even after the independence mainly because of the lack of access to many of its parts. During the first thirty years after independence only a handful of geoscientists worked in North Pakistan (e.g., Misch, 1949; Desio, 1963, 1964; Ivanac et al., 1956; Martin et al., 1962; Matsushita and Huzita, 1965; Jan and Tahirkheli, 1969; Jan and Kempe, 1973; Shams, 1972). A major breakthrough came when the Karakoram Highway was opened for traffic in the late seventies. This coincided with first-time interpretation of the geology of north Pakistan in the light of the theory of plate tectonics (Tahirkheli et al., 1979). This discovery about the presence of two suture zones separating three plates (Eurasia, Kohistan and India) generated a profound

interest in the geology of North Pakistan attracting a great number of local and foreign geoscientists. Tahirkheli and Jan (1979) published first geological map of North Pakistan filling the gap in the maps published by the Geological Survey of Pakistan (e.g., Bakar and Jackson, 1964). A major contribution towards the geology of north Pakistan was made by the 1981-1988 British Universities-Peshawar University joint project (e.g., Coward et al., 1982, 1986; 1988; Petterson and Windley, 1985, 1991; Pudsey et al., 1985; Khan et al., 1989; Treloar et al., 1989). The more recent contributions towards the geology of north Pakistan are listed in Khan and Searle (1996).

In the north-west Pakistan (i.e., the Chitral region), the pioneering geological work is that of Hayden (1916), Tipper (1921) and Pascoe (1923, 1924). These workers described general geology and published accounts of fossil discoveries. The data on general geology was supplemented by Desio (1959, 1975). The first map of the Chitral region was published by Calkins et al. (1981) outlining the geology, stratigraphy and tectonic subdivision. Pudsey et al. (1985) carried out a more detailed work in the Chitral area adjacent to the Shyok suture zone and published a much improved version of the regional map of North-West Pakistan. The exploration of economic metal potential in Chitral and adjoining areas was first systematically under-taken by Sarhad Development Authority (SDA) in 1974-1978 in collaboration with Astrominerals. Subsequently several exploration studies were undertaken by SDA on a number of potential ore deposits. The area near Drosh was mapped by M. Nawaz Khan on a 1:50,000 scale, which is used as basis for the present investigation. Later in 1986 SDA submitted a report on Kaldam Gol copper of Drosh area based on a detailed

exploration program. Minerals and Metallurgy centre of PCSIR Lahore carried out geochemical studies in the Chitral region and published a report in 1991. Recently Kaneda et al. (1996) published a paper on ore mineralogy and geomagnetic anomaly of Kaldam Gol copper ore suggesting a origin as skarn-type deposits.

METHODOLOGY

This research project involved both field and laboratory work. The field work included detailed sampling from the mineralized zones using channel sampling method, accompanied by detailed field notes concerning mineral assemblages identifiable in the field, nature of the host rock in terms of composition, texture and origin (i.e., whether volcanic, plutonic or sedimentary), structure etc. Since the mineralized zone is oriented more or less along the south-eastern margin of the Chitral-Shishi rivers, it is intersected by several tributaries draining into the main rivers (e.g., Drosh Gol, Kaldam Gol, Gorin Gol and Langer Gol). Less detailed sampling was carried out from unmineralized rocks in the vicinity of the mineralized zones, including Gawuch and Drosh formations and diorites-granodiorites intruding them. A total of 45 rock samples were cut into thin sections to study petrographic aspects in terms of modal composition and textural characteristics.

WHOLE-ROCK ANALYSES

Based on petrographic studies, 40 samples from the unmineralized host rocks (diorites and volcanics) and 45 samples from mineralized rocks including

the quartz veins were chosen for major and trace element whole rock analyses. Majority of the whole-rock analyses reported in this thesis were obtained using a combination of Pye Unicam Sp 190\191 Atomic Absorption (AA) Spectrophotometer, Perkin Elmer 3300 (equipped with graphite furnace) and Sp8- 400 UV\VIS Spectrophotometer at the National Centre of Excellence in Geology, University of Peshawar. About 15 samples from the unmineralized rocks were analyzed using Rigaku XRF at the Geoscience Laboratory, Islamabad with objectives of assessment of the petrogenetic evolution.

Wet Chemical Method

The samples for the AA were prepared using 1) Hydrofluoric (HF) and perchloric (HClO_4) acid digestion for determination of major elements including Ca, Mg, Mn, Fe, Na, and K. Lanthanum solution was added to the digested sample for reducing the interference effect in case of Mg and Ca; 2) HF and HNO_3 digestion for the determination of trace element including Cu, Pb, Zn, Ni, Cr, Co and Ag. Gold was dissolved by Aqua Regia and extracted by Methyl Isobutyle Keton (MIBK). Cu, Pb, Zn, Ni, Cr and Co were determined by flame AA, while Au and Ag were determined by H 600 graphite furnace. The rest of the elements including Si, Al, P and Ti were analyzed by Pye Unicam 400 UV\VIS spectrophotometer.

Preparation of Stock Solutions

HF + HClO_4 Digestion Method: Accurately weighed 0.500g of finely powdered sample was taken in paleo crucible. 10ml of hydrofluoric acid and 4ml perchloric acid were added and was kept on a hot plate at a low temperature for 2 hours, then 2ml of perchloric acid was added and evaporated to complete dryness. Paste was

transferred to a glass beaker with deionized water and 4ml perchloric acid was added again. The solution was further heated, until completely dissolved. The volume was made to 250 ml with deionized water. This solution was used for major elements determination by using atomic absorption spectrophotometer and UV/VIS spectrophotometer.

HF + HNO₃ Digestion Method: Accurately weighed 0.50 g of finely powdered sample was taken in a 100ml teflon beaker. 5ml of hydrofluoric acid (HF) was added to it and was kept on hot plate at a temperature of approximately 75 °C. After 10 minutes about 15ml of concentrated HNO₃ was added and heating was continued until complete dryness. 3NHCl was added to the residue and was heated until the maximum dissolution of residue. The volume was made to 50 ml with 3NHCl and was stored in polythene bottle. This solution was then used for trace elements determination by using atomic absorption spectrophotometer.

Aqua Regia Digestion Method for Gold: 10-20 g of sample was weighed in 200ml Pyrex beaker. 50ml of aqua regia was added to it and was heated for about half an hour at low heat. After half an hour about 35ml of deionized water (D.I) was added. Heating and evaporation was continued until about 50ml solution was left in the beaker. The whole beaker content was then filtered in a test tube. The residue and beaker were washed several times with 6NHCL and the contents were collected in the test tubes. This filtrate was of about 50ml volume. The whole filtrate was then transferred to a 250ml separatory funnel. In order to keep normality of filtrate to 6N, about 50ml of D.I. water was added to it. Then 10ml of Methyl Isobutyle Ketone (MIBK) was added to separatory funnel. The

funnel was then shaken for 6-8 minutes on automatic flask shaker. The lower layer was removed and 20ml of 0.2NHCl was then added to M.I.B.K in the funnel and was shaken for about 5 more minutes. The most probable interference of Fe was removed by this process. The MIBK was collected and stored in glass test tube for further determination of gold on atomic absorption.

X-Ray Fluorescence

The analyses at the Geoscience Laboratory, Islamabad were conducted on a fully automated Rigaku 3370 EO X-Ray fluorescence (XRF) spectrometer. Sixteen elements were analyzed which included Si, Ti, Al, Fe, Mn, Mg, Ca, Na, and K as major elements and result were given in wt. % of oxides, whereas Ni, Cr, Ba, Rb, Cu, Zn, Co and Nb were analyzed as trace elements in part per million (ppm). The analyses were carried out on 5 : 1 lithium tetraborate : rock-powder fused disks commonly called glass beads. Rock powder under 200 mesh ($< 125 \mu\text{m}$) weighing 0.7 g was mixed with 3.5 g of lithium tetraborate to make a glass bead. Twelve Geological Survey of Japan (GSJ) standard reference samples were used for calibration of the instrument. The results of the analyses were compared with the values of 15 recommended U.S.G.S standards. A check of precision of the instrument was made using JA-3 standard reference sample. For both major and trace elements the standard deviation and variance fell within acceptable limits. Correction for line interference, matrix effect, and overlapping from all other analyzed elements were made from each elemental analysis. The empirical method for the calibration was used. The result were normalized on a volatile free basis with total iron expressed as Fe_2O_3 .

MINERAL ANALYSES

Electron Microprobe

Identification of ore minerals, in this study, was based on reflected-light microscopy, Electron Microprobe and X-Ray Diffractometry. About 25 sample were selected for petrographic study. Electron Probe Microanalyser (EPMA), model Cameca SX - 50 (University of S. Carolina, USA) was used to analyze metallic minerals. All the analyses were performed at 25 KV, using an energy dispersive system. Standards used were: pyrite, chalcopyrite, galena, sphalerite and tetrahedrite. The spots from both cores and margins were routinely analyzed. All the ore minerals were analyzed for Cu, Fe, Zn, Pb, As, Sb, Ag, Mn and S.

X-Ray Diffraction

The X-Ray diffraction analyses were performed only for metallic minerals. These analyses were carried out on a Rigaku . D. Max 111 X-Ray diffractometer at the National Center Of Excellence in Geology, University of Peshawar. The metallic minerals were separated from crushed sample. These metallic sample were scanned between 20° and 65° . This range is the important reflection of the common minerals . The d- spacing were listed with their intensities and the A. S. T. M. powder data file was used to identify the minerals.

FLUID-INCLUSION STUDIES

The analytical work for the fluid inclusion research was carried out in the Geological Survey of Japan, Tsukuba, Japan. A total of 8 samples of ore-bearing

quartz veins were selected for doubly polished sections preparation. The thickness of the sections obtained ranges from 100-150 μ m. The polished sections were studied under the petrographic microscope to observe the morphology of the inclusions and to select them for microthermometry measurements.

LEAD-ISOTOPE ANALYSES

Lead isotopic study of galena was carried out by separating galena grains from quartz veins, Small Chips of galena were dissolved in 6 N HCl to produce a concentration of approximately 1 microgram Pb per microliter solution was loaded with silica gel. These analyses were carried out at the University of Texas, Dallas, using a Mat 261 thermal ionization mass spectrometer in the static mode.

OXYGEN ISOTOPE ANALYSES

About 13 sample of mineralized quartz veins were selected and analyzed for oxygen isotopic studies. Quartz separates were made by standard techniques of heavy liquids, hand picking, and short cold HF bath. Quartz was 100% pure. Oxygen was extracted by a new technique, in which 1 mg of silicate was heated by laser and reacted with BrF₅ (Sharp, 1990), and then converted to CO₂ on a hot carbon rod (Taylor and Epstein, 1962). Isotopic composition of the prepared gas was measured on gas ratio (Nier type) mass spectrometers and are reported using the standard notation relative to SMOW (standard mean ocean water) in units of per mil (parts per thousand). Oxygen analyses were carried out at the Oregon State.

CHAPTER 2

REGIONAL TECTONICS

Northern Pakistan contains three mountain chains: Hindu Kush, Karakoram and Himalaya (Figure 2.1). The Hindu Kush stretches southwest from the Pamirs in Central Asia, passes across the northwestern extremities of Pakistan and enters into Afghanistan. The Karakoram has a NW-SE trend, at high angles to that of the Hindukush. It stretches along the northeastern borders of Pakistan, separating Kunlun Range in the NE (in China) from the Himalaya in the south. The Himalaya comprises a series of mountain ranges to the south of the Hindukush and Karakoram. They are subdivided, from north to south, into Higher, Lesser and Lower Himalaya (Gansser, 1964). The Kohistan region of north Pakistan occupies a transitional geographic position at the junction of the said three mountain chains. It will be later shown that Kohistan is defined by geological characteristics distinct from Hindukush, Karakoram and Himalaya, and thus may be considered a separate geographic entity.

The Himalaya and associated mountain ranges in south-central Asia formed in response to continent-continent collision between Eurasia and a series of continental blocks separated from Gondwana. The Karakoram plate (which includes the present Hindukush) collided with the southern margin of Eurasia about 145 Ma ago at the site of the Rushan-Pashart Suture Zone (Ruzhentsev and Shvolman, 1981). Lahasa block in the east and Afghan block in the west are marked by similar timing of accretion at the southern margin of Eurasia, suggesting that they were equivalent of or a part of the Karakoram plate.

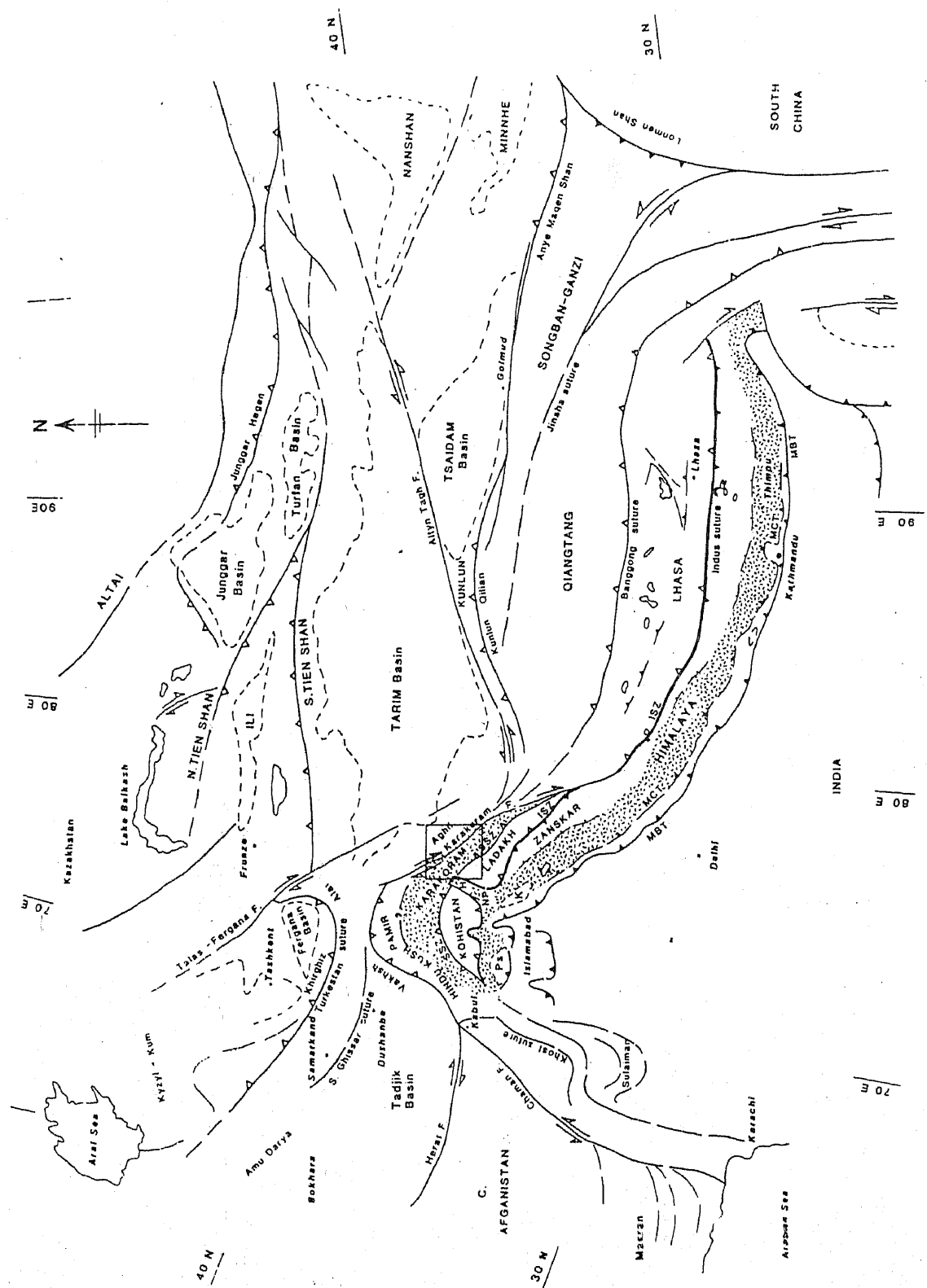


Figure 2.1. Map of the Pamir-Himalaya-Tibet region showing the main tectonic units and structural trends (After Searle, 1991).

In the eastern and Central Himalaya, the Lahasa plate was directly accreted at its southern margin by the Indian plate. In contrast, in the NW Himalaya, the Himalayan collision was preceded by accretion of an intraoceanic island arc (i.e., the Kohistan terrane) at the southern margin of the Karakoram plate (Tahirkheli, 1983). This accretion is believed to have occurred during the Early Cretaceous (i.e., 100-80 Ma) (Coward et al., 1985; Petterson and Windley, 1985).

The Himalayan orogeny is believed to have started about 65 Ma ago marking the initial contact of the Indian plate with the southern margin of Eurasia (Klootwijk et al., 1992). The north-western part of the Indian plate (i.e., Nanga Parbat and to its west) was probably the first to come in contact with the Eurasian plate, probably in the form of a promontory projecting northward from the mainland India. Fifty Ma age of high pressure metamorphism forming eclogites (Tonarini et al., 1993), 45 Ma age of the peak of the Himalayan metamorphism (Treloar et al., 1989) and the presence of leucogranites as old as 52 Ma (Zeitler and Chamberlain, 1991) all point out that the Nanga Parbat and the Kaghan region of the Indian plate collided with the Kohistan terrane sometime around 60-65 Ma. Like elsewhere, the collision of the Indian plate with Eurasia was highly diachronous. In most of the central and eastern Himalaya, sedimentation at the northern margin of the Indian plate continued until late Eocene. Fore-arc basins, both in Kohistan (e.g., Dir; Sullivan et al., 1993) and Ladakh (Indus Flysh; Albertson and Deggan, 1993), continued to be active until about Early Eocene. Thus all this evidence suggests that the Himalayan collision was not a short-lived event; rather took place in a span of over 20 Ma.

The mineralisation studied during the course of this study is from the NW marginal parts of the Kohistan terrane. Therefore, a more detailed account of the regional geology and tectonics of the Kohistan terrane is included in the following.

THE KOHISTAN TERRANE

The Kohistan terrane occupies the collision zone between the collided Indian and Karakoram plates (Figure 2. 2). Tahirkheli et al. (1979) interpreted the terrane to represent a fossil island arc formed in an intraoceanic setting during the Cretaceous and sandwiched between the collided Indian and Eurasian plate during the Himalayan collision. The Ladakh terrane to the east has a remarkable lithological and geochronological resemblance with the Kohistan terrane, suggesting their mutual continuity in the geological past. The Nanga Parbat crustal structure (Zeitler et al., 1982), currently separating the Kohistan and Ladakh terranes, formed only during the last 10 Ma.

The Kohistan terrane occupies the western branch of the Himalayan Syntaxis between 71° E (Kunhar river) and 75° E (Nanga Parbat antiform). On a regional scale, the terrane appears to be a thick, more or less monoclinial slab dipping 30° to 60° NW (Bard et al., 1980). The principal tectonic feature of the Kohistan geology is the occurrence of two major faults, the Main Karakoram thrust (MKT) and the Main Mantle Thrust (MMT), which bring the Kohistan terrane in direct contact with the rocks of the Karakoram plate in the north and the Indian plate in the south, respectively. The MKT (also known as the northern suture; Pudsey, 1986 or Shyok suture; Searle, 1991) is an up to 4 km thick melange zone comprising meter to hectometre scale blocks of limestone, marble, conglomer

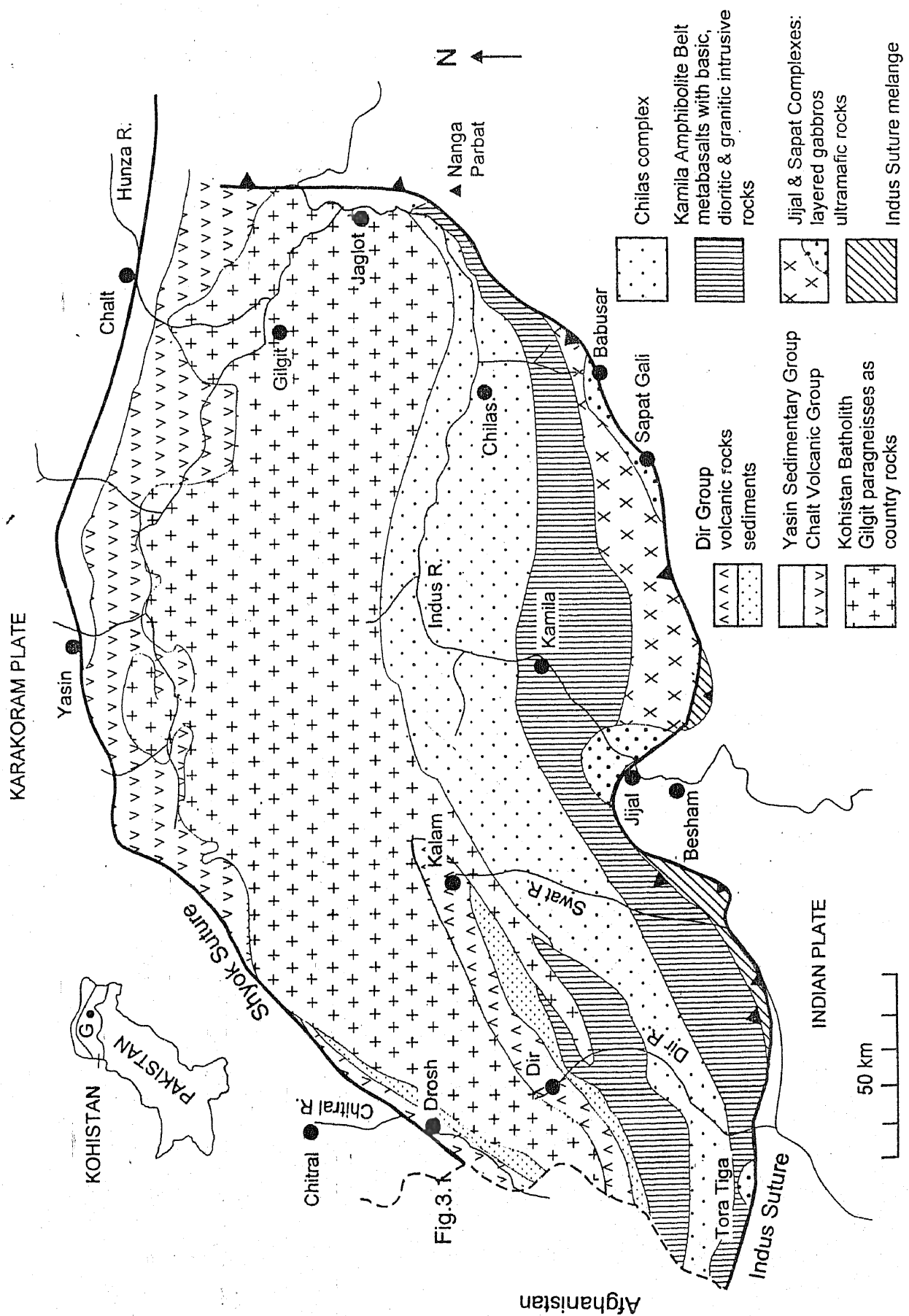


Figure 2.2. Regional geological map of Kohistan in North Pakistan (after Khan et al., 1993)

ate, serpentinitised metavolcanics and ultramafics set in a matrix of slates. Pudsey (1986) interpreted an olistostorm origin for the material in the MKT and suggested closure of a marginal basin at this site. Khan et al. (1997), on the basis of recently acquired isotope data, dispute this contention and suggest that Kohistan originated at latitudes 30°-50° degrees to the south of its present position, advocating a large oceanic basin between Kohistan and Karakoram prior to collision. Tahirkheli et al. (1979) and Bard et al. (1980) suggested a Himalayan (i.e., Eocene) age for the closure of the MKT, relatively later than the MMT. Later, however, Tahirkheli (1983) postulated a Cretaceous age for the formation of the MKT. Coward et al. (1986) supported a late Mid Cretaceous age for the formation of the MKT for two reasons; 1) absence of lithologies younger than Albian and Aptian from the MKT melange zone and 2) 80-90 Ma ($\text{Ar}^{39}\text{-Ar}^{40}$) ages from the deformed rocks associated with the MKT. Petterson and Windley (1985) noticed that 102 Ma old Matum Das pluton in the Hunza valley was deformed by structures associated with the MKT, which they interpreted to mark the upper limit on the age of the MKT. The younger age limit for the MKT is represented by 75 Ma ($\text{Ar}^{39}\text{-Ar}^{40}$) old suite of basic dykes cross-cutting the deformed Matum Das plutons (Coward et al., 1986).

The MMT is marked by existence of major ophiolites (Arif and Jan, 1993) and glaucophane schists (Shams, 1980) suggesting closure at the site of a subduction zone in a major oceanic basin. It is razor sharp at its type locality at Jijal, where the ultramafic rocks of the Kohistan terrane are in direct tectonic contact with the gneisses of the Indian plate. Elsewhere, like in Mingora (Kazmi et al., 1984) and Allai (Shah and Majid, 1985), the MMT is represented by

several hundreds of meters wide melange zone comprising ophiolite ultramafics and gabbroic rocks, greenschist, metavolcanics and glaucophane-bearing pelitic melanges. The available K/Ar and $\text{Ar}^{39}\text{-Ar}^{40}$ on glaucophane and phengite (Shams, 1980; Maluski and Matte, 1984; Treloar et al., 1989) range between 80 and 67 Ma. Obviously these ages cannot be taken as the age of closure of the MMT but they may indicate the age of glaucophane formation in a subduction zone. As discussed earlier, the minimum age of the closure of the MMT in Pakistan is constrained by Early Eocene fore-arc basin in Dir. The upper age limit on the closure of the MMT is between 55 and 65 Ma constrained by ~ 50 Ma age of high-pressure metamorphism in the Indian plate and those of the leucogranites (Tonarini et al., 1993; Zeitler and Chamberlain, 1991). The major lithotectonic units of the Kohistan terrane include the following (Figure 2.3)

The Jijal Complex: It is a 150 km² tectonic wedge comprising a) a 7 km thick slab of ultramafic rocks at base and b) overlain by ~4 km thick mass of garnet granulites derived from gabbroic rocks. The ultramafic body occurs directly on top of the southern suture or the MMT and includes serpentinites, diopsidites, harzburgites, dunites and websterites (Jan and Howie, 1981). The common presence of igneous stratification points to their origin as cumulates from a basaltic magma rather than a slab of mantle ultramafics. Jan and Windley (1990), on the basis of a detailed mineral chemistry, suggested that the Jijal ultramafic rocks were derived from a tholeiitic basaltic magma in a magma chamber at the base of an intraoceanic island arc. Jan and Howie (1981) esti-

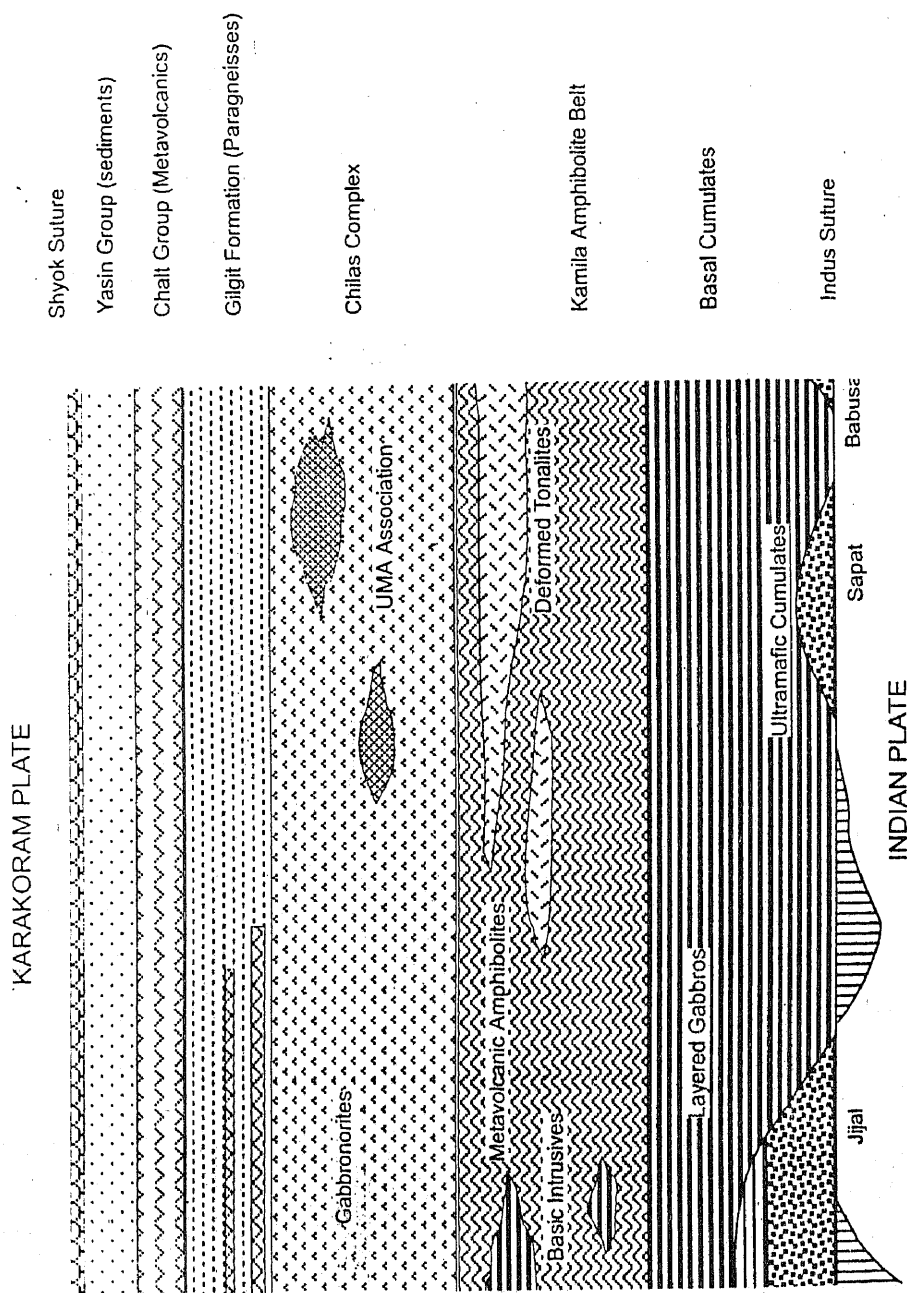


Figure 2.3. Crustal profile of the Kohistan island-arc terrane, showing principal lithological units (except the Kohistan batholith)
(After Khan et al. 1993)

mated 670-790 °C temperature and a pressure of 12 to 14 kbars for the metamorphic equilibration of the Jijal Complex.

Sapat Ultramafic-Mafic Complex: The Jijal Complex is tectonically overlain by a complex of gabbroic rocks. Miller et al. (1991) grouped these rocks into Patan Complex. Recently, Jan et al. (1993) described a complex of plutonic ultramafic and gabbroic rocks in the same strike direction from Kaghan Kohistan which they called Sapat Complex. Ultramafic and associated gabbroic rocks in the hanging wall of the MMT from Shergarh Sar (Shah and Majid, 1985), Babusar (Ahmed and Chaudhry, 1976) and Tora Tiga (Jan et al., 1983) are continuation of the Sapat Complex. These ultramafic and gabbroic rocks are stratiform in nature with a mineralogy similar to that of the Jijal Complex. However, unlike the Jijal Complex, they have undergone only a lower amphibolite facies metamorphism rather than a high-pressure granulite-facies metamorphism.

The Kamila Amphibolite Belt: This is a vast belt of amphibole-rich rocks overlying the ultramafic-mafic complexes at the base of the island arc sequence (i.e., Jijal and Sapat complexes). Kamila amphibolites include banded and homogenous amphibolites, hornblendites and hornblende schists, calc-silicates and quartzo feldspathic intrusions (Jan, 1979, Shah et al., 1995). Khan et al. (1993) divided the complex into two components. The fine-medium grained amphibolites, locally containing relict pillows, are interpreted to be metavolcanic in origin. Whole-rock chemistry of these amphibolites is typical of ocean-floor basalts. These amphibolites serve as the basement for the intrusion of the second principal component in the Kamila belt i.e., medium-coarse grained

gabbroic amphibolites which have a calc-alkaline subduction-related geochemistry.

The Chilas Complex: This is a vast body of mafic-ultramafic rocks, occasionally showing spectacular igneous layering (Jan et al., 1984). It contains rare calc-silicate inclusion but is mostly coherent making about 1/5 of the area occupied by Kohistan arc. It represents a relatively higher-level intrusion into the Kamila Amphibolite Belt and comprises ultramafics (dunites, peridotites, pyroxenites and minor chromitites), anorthosites and gabbro-norite/hypersthene diorites. The intrusion has a typical calc-alkaline geochemistry (Khan et al., 1989; 1993).

The Kohistan Batholith: More than two-third of the northern half of Kohistan arc is occupied by granitic rocks collectively called the Kohistan Batholith (Petterson and Windley, 1985). It consists of a calc-alkaline gabbro-diorite-granodiorite- granite plutonic suite, which intrudes a predominantly metasedimentary sequence in the south and chalt volcanics in the north. Three phases are recognised (Petterson and Windley, 1985); 102 Ma trondhjemites/ quartz diorites form the earliest phase generated in the intraoceanic phase of the island arc growth, 85-45 Ma old gabbros, diorites and granites form the principal component of the batholith formed during the continental-margin phase of the arc growth . The third phase of the batholith is represented by 33-28 Ma old leucogranites and pegmatites which represent the youngest phase of magmatism in Kohistan, probably derived by the partial melting of the thickened Kohistan crust subsequent to the Himalayan collision.

The Chalt Volcanics: This is a thick sequence of meta-volcanics, representing the main bulk of the volcanic cover of the Kohistan arc. They are frequently intruded by the plutons of the Kohistan batholith. In the upper, less metamorphosed parts of sequence, pillow structures are observed. Two phases are recognised (Petterson and Windley, 1991). Upper greenschist to amphibolite-facies metavolcanics are recognised in the Hunza areas. These include high-Mg basalts and andesites (bonninites). The other phase is restricted to the valleys west of Hunza (Ishkuman, Yasin and Shamran) and includes unmetamorphosed calc-alkaline basalts, andesites, dacites and rhyolites. In the upper part of the sequence, sedimentary intercalations have yielded Mid Cretaceous fossils (Albian-Aptian).

The Yasin Group Metasediments: These sediments crop out in 150 m thick linear belt on the northern edge of the Kohistan arc, and comprise conglomerates, limestone, sandstone and shales. They are frequently interbedded with volcanics. They overlie the Chalt Volcanics and represent either the cover sequence of the Kohistan arc (Pudsey, 1986) or sediments deposited in a back-arc basin (Khan et al., 1994).

TECTONIC EVOLUTION OF THE KOHISTAN AND NW HIMALAYA

Important evidence for the evolution of Himalaya has been presented in a number of papers published between 1979-1984 (Klootwijk et al., 1979; Molnar and Tapponier, 1975, 1977; Powell, 1979; Patriat and Achache, 1984). The salient features of the models explaining the tectonic evolution of the NW Himalaya include:

- 1) Prior to the separation of the Indian plate from the Gondwana, several microplates detached from Gondwana and, after drifting across the Palaeotethys, got accreted at the southern margin of Eurasia during the middle Jurassic (~145 Ma.). These microplates included, from west to east, the Afghan block, the Karakoram plate and the Lahasa plate. Hindukush region of N. Pakistan and eastern Afghanistan formed a part of the Karakoram plate.
- 2) The Indian plate got separated from the eastern Gondwana during the middle Cretaceous (i.e., 125-118 Ma). The controlling factors may be the initiation of a major subduction zone in the Neotethys responsible for the Ladakh-Kohistan island arc (Khan et al., 1997). The relative convergence between the Indian and Eurasian Plate was initially at the rate of 20 cm/yr, and then, since 50 Ma ago, at a reduced rate of 4-6 cm/yr probably as a consequence of the India-Eurasia collision.
- 3) The Kohistan Ladakh island arc had a span of some 30-40 Ma in an intraoceanic setting (Khan et al., 1993). The arc collided with the southern margin of the Eurasian plate around 100-80 Ma, probably in response to closure of a divergent set of subduction zones at the site of the MKT. Much of deformation in the Kohistan terrane is related with this tectonic event (Coward et al., 1986).
- 4) Several factors including presence of 50 Ma old eclogites (Tonarini et al., 1993), 52 Ma old leucogranites (Zeitler and Chamberlain, 1991). and >45 Ma age of the peak of the Himalayan metamorphism (Treloar et al., 1989) suggest that the Himalayan collision initiated around 65-60 Ma ago probably in the north western parts of the Indian plate. However, the final collision took

place some 20 Ma after the initial contact between two plates (i.e., at 40-45 Ma)(Patriat and Achache, 1984).

- 5) The tectonic activity continued subsequent to the India-Eurasia collision on the either side of the MMT. Shear zones, thrust, normal and strike-slip faults developed in the Karakoram plate some of which are still active (e.g., the Karakoram Fault of Searle, 1991). Likewise deformation front moved southward from the MMT inward in the Indian plate resulting in several regional thrust faults (e.g., Main Central Thrust, Main Boundary Thrust and Main Frontal Thrust). These south-verging thrust sheets are back-folded at several places giving rise to dome and basin structures (e.g., Nanga Parbat, Besham and Hazara-Kashmir and Indus syntaxis)(Bossart et al., 1988; Coward et al., 1988).

REGIONAL GEOLOGY OF CHITRAL AND DROSH AREA

The Chitral area of NW Pakistan is a part of the Karakoram plate. It is separated from the Kohistan terrane in the south by the MKT or the Northern Suture (Figure 2.4) which passes near Drosh (Chitral). The Karakoram plate in the Chitral area is itself divisible into two parts by a regional fault structure termed Reshun Fault. Pudsey et al. (1985) designated following nomenclature for the tectonic subdivision of the Chitral area (Figure 2. 4).

1. Lutkho-Turikho unit, between the Pakistan-Afghanistan border and Reshun fault.
2. Kunar-Yarkhun unit, between the Reshun fault and the MKT.
3. Kohistan unit, between the MKT and the Main Mantle Thrust.

The Lutkho-Turikho Unit: This unit comprises a small belt of Devonian carbonates and fine grained white quartzites, which extend from NNE of Chitral town through Buni to Baroghil. This sequence is overlain by a thick succession of fine grained shales, slates and limestone (called Lun shales) which is Devonian to Permian in age. The structure is complex with S-verging thrusts and isoclinal folds.

Kunar-Yarkhun unit: This unit forms a narrow (20-40 km) stripe between the Reshun fault and the Northern Suture. The unit is further subdivided into a Mastuj subunit, comprising sediments belonging to the Darkot group, and a Chitral subunit which is divided into Gahiret Limestone, Koghozi greenschists, Chitral slates, Krinj limestone and Reshun Formation.

Darkot group is a succession of slates and quartzose sandstones, with a few major carbonate units, first mapped as the Darkot Group in the Gilgit region

(Ivanac et al., 1956). Calkins et al. (1981) and Pudsey et al. (1985) found extensions of this group to the west of Mastuj, in the upper reaches of the Shishi valley. The group is in direct southern contact with the Northern Suture. To the north, the contact between the Darkot group and the Gahiret limestone is obliterated by the intrusion of the Kesu-Buni Zom pluton. Presence of intercalated cross-bedded quartzites and massive limestones indicate a shelf origin for the Darkot group, with local turbidite origin as shown by the graded-bedded Bouma sequences and sole structures (Pudsey et al., 1985). A Permo-carboniferous age is assigned to the Darkot group.

Within the Chitral subunit, the Chitral slates form the principal stratigraphic entity. These are monotonous dark grey slates with abundant graded bedding structures. Locally sandstones can form up to one-third of the sequence. Pudsey et al. (1985) suggested a deep-water origin for the Chitral slates on the basis of presence of graded bedding. The Chitral slates are bounded, on the both sides, by thick successions of marbles and limestones, called Gahiret and Krinj limestones. Of these the Krinj limestone has yielded fossils like *Orbitolinas* and rudistids (Pudsey et al., 1985), suggesting a lower Cretaceous age. Since there is a conformable contact between the Krinj limestone and the Chitral slates, the latter are assigned a Cretaceous age. The massive nature of the Krinj and Gahiret limestones is considered to represent platform-type carbonate depositional environments.

The Kunar-Yarkun unit is bounded on its north side by a regional fault called the Reshun fault. Associated with this fault is a succession of fluvial sediments of a distinct red colour called the Reshun Formation. A varied group of rocks including polymict pebble and cobble conglomerates, red shale and grey micritic limestone lie below the Reshun fault and above the Chitral slates and Darkot Group. The basal contact is marked by a sharp angular unconformity with conglomerates containing clasts of deformed Chitral slates. Micritic limestones near Bunni yield remains of rudists suggesting an Aptian-Albian age (Pudsey et al., 1985).

Kohistan unit: This unit includes northern-suture melange and everything to the south east of it. No fossils have been found in this unit except Cretaceous *Orbitolinas* in the limestone (Desio, 1959; Pudsey et al., 1985). Around Drosch

and in the Shishi valley, Pudsey et al. (1985) divided the Kohistan lithologies into three stratigraphic entities called Gawuch Formation, Purit Formation and Drosh Formation. The Gawuch Formation comprises mainly metavolcanics and carbonate sediments and is probably equivalent of the Chalt-Yasin succession in the eastern Kohistan (Hunza-Yasin areas). The Purit Formation, characteristically red in colour, comprises fluvial sediments and overlies the Gawuch Formation. The Drosh Formation comprises thickly bedded andesites. The melange comprises a 3 km wide zone of mainly strongly cleaved slates with interbedded clastic sediments, blocks of volcanic greenstone, limestone, red shale and serpentinites.

CHAPTER 3

LOCAL GEOLOGICAL SETTING & FIELD RELATIONS

LOCAL GEOLOGY

The studied area in Drosh-Shishi valley hosting the copper mineralization forms a part of the upper crust of the Kohistan island arc terrane and comprises variably metamorphosed volcanics and sediments intruded by plutons of diorite-granodiorite-granite composition. The local geology of this area is divisible into two broad units; 1) Northern or the Shyok Suture Melange and 2) the upper-crustal arc volcanic-sedimentary succession.

The Northern Suture Melange

Shyok or the Northern Suture Melange occupies a 3 km wide zone near Drosh near the Chitral-Shishi confluence. The principal component of the melange is a cleaved slate with interbedded clastic sediments, which contain blocks of volcanic greenstone, limestone, red shale and serpentinites. The grey slate matrix contains, locally up to about 10% of the outcrops, lithic sandstones and matrix-supported pebble conglomerates. Amongst the blocks, limestone and volcanic greenstone are the most abundant. Limestones, however, occur both as original beds as well as blocks. Similarly, red shales form blocks as well as original beds within the melange zone. In the conglomerates, the most abundant clasts are of volcanic rocks (rounded) and limestone (angular), each of them forming monomict conglomerates with lithic sandstone matrix. Polymict types may contain, in addition, quartzite, diorite and intraformational slate.

The Upper-Crustal Arc Volcanic-Sedimentary Succession

The upper crust of the Kohistan terrane is best exposed in the southern tributaries of the Shishi and Kunar (Chitral) rivers, in the vicinity of Drosh.

According to Pudsey et al. (1985), it is divisible into three stratigraphic units, which from bottom to the top, include Gawuch Formation, Purit Formation and Drosh Formation (Table 3.1).

Gawuch Formation: The Gawuch Formation consists of metavolcanics and metasediments and is about 2 km thick in the Drosh-Shishi area. The basal part of the formation is exposed in the upper reaches of Kaldam Gol and comprises phyllites of green colour, having chlorite albite and quartz together with minor amount of illite and amphibole. Presence of strong mylonitic fabric suggests that these phyllites are product of mylonitization at the expense of a sequence of metavolcanics in a greenschist facies shear zone. Observations in the Kaldam Gol suggest that the lower half of the formation consists of either the green phyllites or greenschist facies metavolcanics. The upper half of the formation contains metavolcanics together with common intercalations of metasediments like quartzites and marble. Most of the volcanics are probably andesites in composition and are strongly foliated and commonly altered. Tuffites are commonly associated with the metavolcanics. They are fine-grained porcellaneous tuffites. They consist of alternating graded beds of light and dark green lithologies which range in thickness from less than 1 cm to over 30 cm. Fracture, minor faults and thin calcite veins commonly cut the tuffites.

Amongst the sediments, limestone occurs both as very thick units and as thinly interbedded limestone-phyllite-minor quartzite units. Several distinctive light grey to green cryptocrystalline limestones occur interbedded with the phyllite. They form discontinuous beds up to 10m thick and show a light colour banding which may represent original bedding. At places the

limestones become more dominant with the development of layered marbles showing complex fold patterns. Talc schist occurs in association with light brown irregular pods of dolomites within the phyllites. The talc-bearing rocks generally are highly schistose and some contain the chrome mica (fuchsite).

Table 3.1 Stratigraphy of the upper-crustal sequence of the Kohistan island-arc terrane near Drosh (after Pudsey et al., 1985).

Formation	Type sections	Base	Top	Lithology	Thickness
Drosh	Drosh Gol	Porphyritic andesitic lavas overlying red shale	faulted against slates of Northern suture melange	Andesitic lavas and red shales	1.5 Km
Purit	Drosh Gol	Red-shale overlying limestone, locally faulted against Gawuch Formation or unconformable on diorite.	Base of Drosh Formation	Red shales, sandstones and conglomerates	1 Km
Gawuch	Gawuch Gol	Green phyllites intruded by diorite.	Base of Purite Formation; locally faulted.	Green phyllites and limestones	2Km

The Gawuch Formation is commonly intruded by plutons of diorite, granodiorite and granite composition belonging to the Kohistan batholith. Other intrusions include basic and andesitic dykes, and quartz veins. Cu-mineralization, the subject of this study is restricted to this formation.

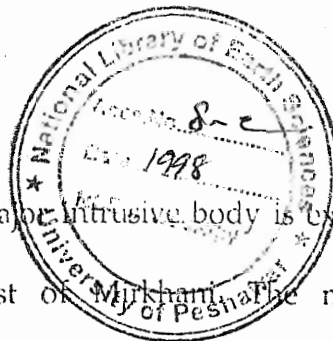
Purit Formation: Calkins et al. (1981) mapped this formation as a part of Reshun Formation due to occurrence of red beds. Since the Reshun Formation proper is part of the Karakoram plate exposed along the Reshun fault in upper-

middle Chitral, Pudsey et al. (1985) distinguished the red beds exposed to the south of the Shyok suture as the Purit Formation. Unlike the Gawuch Formation, the Purit Formation is fluvial in origin and comprises conglomerate, sandstone, siltstone and shale. Red shale is the most abundant rock type having abundant calcite veins at high angles to the bedding.

The conglomerate and sandstone are the dominant rocks in the lower half of the formation. At places the red sandstone matrix contains granodiorite and porphyritic andesite clasts. Red shale containing clast supported conglomerate and fine to medium grained sandstone, predominates in this formation to the SE of Drosh.

Drosh Formation: The Drosh Formation comprises a sequence of thickly bedded porphyritic andesites with phenocrysts of plagioclase, hornblende, and pyroxene. It is very well exposed along the road, south of Drosh and in the Shishi valley. Some lava flows are highly vesicular and few are brecciated, some thin red shales are interbedded with the andesite flow. This formation conformably overlies the Purit Formation.

Intrusive Rocks: The Drosh-Shishi area hosts several major plutons belonging to the Kohistan and Karakoram batholiths. The Northern Suture melange, at its northern margin is intruded by a WSW-ENE trending granitic plutonic body called Kesu-Buni Zom pluton (Pudsey et al., 1985). Very little petrological information is available from this pluton. It is intruded in the Karakoram plate and is in line with the Karakoram batholith (Searle, 1991) and thus may be considered to be part of the same. The Gawuch Formation is bounded on its south-eastern contact by a major pluton belonging to the Kohistan batholith



No. 8-c

called Lowari pluton. The third major intrusive body is exposed in the lower reaches of the Kunar river west of Mirkham. The metasediments and metavolcanics of the upper arc crust of the Kohistan terrane are restricted to a triangular wedge-like area near Drosh, squeezed between these three intrusive bodies (Figure 2.4).

The Kesu-Buni-Zom pluton, in its exposures north of Drosh consists of steeply foliated dioritic rocks with relatively undeformed intermediate and acidic minor intrusions. The part of the pluton exposed in the upper reaches of the Shishi valley consists of medium-grained diorites and granodiorites.

The Lowari pluton ranges in composition from quartz monzodiorite to tonalite through a gradational variation. The pluton is commonly intruded by pegmatite and aplite sheets. Zeitler (1985) reported an age of 45.2 ± 0.4 Ma (Ar^{40} - Ar^{39} on hornblende) and therefore, is classified as stage II intrusion of the Kohistan batholith (Sullivan et al., 1993).

FIELD RELATIONSHIPS

The local geology and field relations of the Drosh-Shishi area is best studied either along the Kunar river, or in the Shishi valley. The southern tributaries of the Shishi valley and the Chitral river, however, provide sections perpendicular to the strike direction and hence are better suited for detailed geological investigations. In the following, geology of the Drosh-Shishi area is described on the basis of observations made in valley sections formed by the southern tributaries of the Shishi river (e.g., Kaldam Gol (stream), Gawuch Gol, Langar and Gorin Gol), (Figure 3.1).

No. 8-c

Geological Map of Drosh Area, Chitral, N. Pakistan

(Modified after
M. Nawaz Khan
Unpublished SDA report)

Scale
6 km

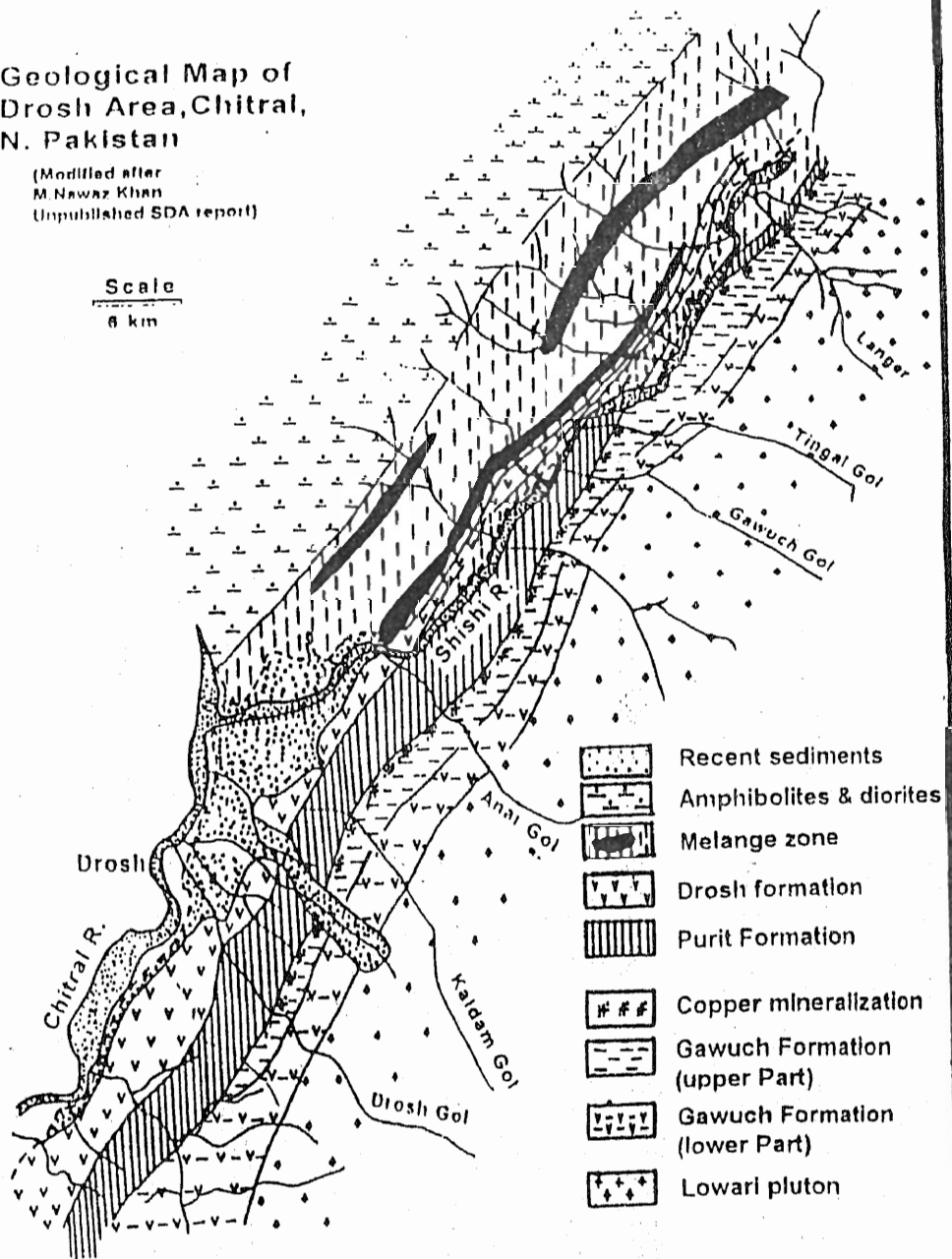


Figure 3.1 Geological map of Drosh Shishi area

Kaldam Gol section

Kaldam Gol is situated about 5 Km east of Drosh on the southern side of the Shishi valley. Much of the mouth of the valley is covered with flood-plain deposits, with minor outcrops of Drosh Formation, comprising green coloured rocks of basaltic composition. Little upstream in the valley, the first continuous outcrops are reddish conglomerates of Purit Formation. These conglomerates pass upstream into interbedded red sandstone and shale, which have a general strike of N40°E. The succession is highly sheared and is commonly cross cut by carbonate and quartz veins. These veins are selectively eroded leaving behind open channels. Middle and upper reaches of the Kaldam Gol comprise the Gawuch Formation. The Gawuch Formation in its upper most part is represented by a 10 metre thick band of marble which is in unconformable contact with the overlying Purit Formation. The marble has its southern contact with sheared volcanics which, in turn, are in contact with a sheet of altered mineralized diorites-granodiorites. The contact between marble and the sheared volcanics is marked by a strongly mineralized zone of about 1/2 m thickness. Rest of the formation exposed in the middle and upper reaches of Kaldam Gol can be divided into two units. The upper half of the formation consists of more or less equal proportions of intercalated greenschist metavolcanics and marbles, with minor quartzites and granodiorite sills. The lower half of the formation comprises greenschist metavolcanics with little or no metasedimentary component. In this respect, the lower half of the Gawuch Formation is equitable with the Chalt Formation while the upper half is equitable with the Yasin Group.

The basal contact of the Gawuch Formation is with the Lowari pluton (Figure 3.1). Fine grained granodiorites have a planar knife-edge contact with green phyllites of the Gawuch Formation (Plate 3.1). The green phyllites in the southern parts of the Gawuch Formation are derived from a ductile shear zone with steep foliations defining the steep mountain front of the Lowari ridge. Figure (3.2) shows a detailed lithological profile along Kaldom Gol.

Gawuch Gol Section

The general attitude of the rocks in this section is $N40^{\circ}-50^{\circ}E/18^{\circ}NW$. From south to north, the Lowari diorites are overlain by phyllites at the base of the Gawuch Formation. These phyllites are overlain by a thick zone of metavolcanics, which are massive greenstones. After the metavolcanics, there is an 8 m thick zone of meta-diorites/granodiorites, which are altered to silicified rocks. This zone is sheared at its both contacts and is mineralised containing disseminated tetrahedrite. It appears that it was the deformation which provided conduits for hydrothermal solutions which caused mineralization and silicification. There are abundant quartz veins in this zone which have a thickness of $<1/2$ meter and are parallel to the foliation direction ($N60^{\circ}E$), which is also the general attitude of the zone. These veins have Cu-bearing phases, especially tetrahedrite and chalcopyrite with supergene enrichment of malachite and azurite at the surface. To the north of the mineralised zone, metavolcanics contain locally up to 2 m thick zones of silicified rocks, mostly in the shear zones. These metavolcanics also contain <6 cm thick quartz veins with silicification associated with the outer contacts of the quartz veins. There is a 50 m thick crystalline limestone at the northern contact of the volcanics. The

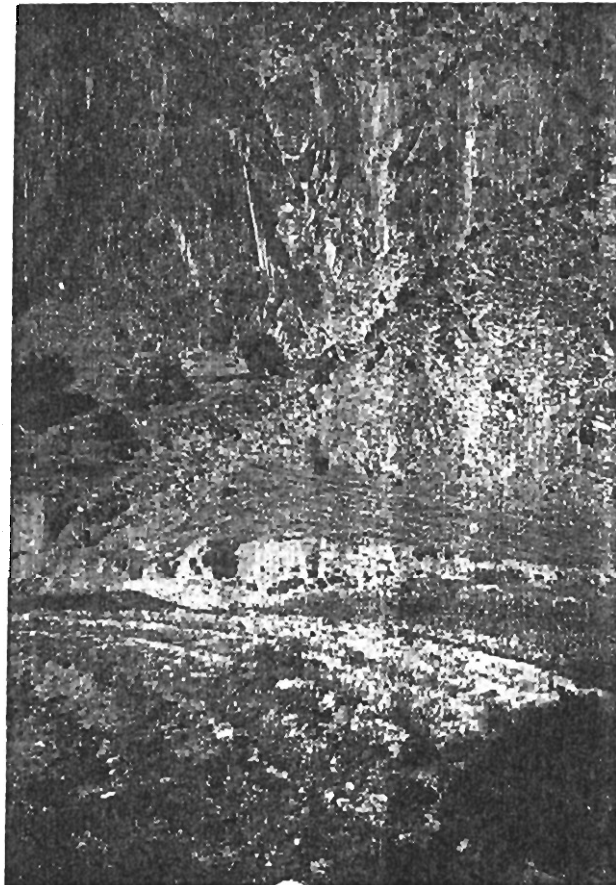


Plate 3.1 Photograph showing the sharp contact between the phyllites of Gawuch Formation (upper left) and the altered metadiorites of Lowari Pluton (middle right).

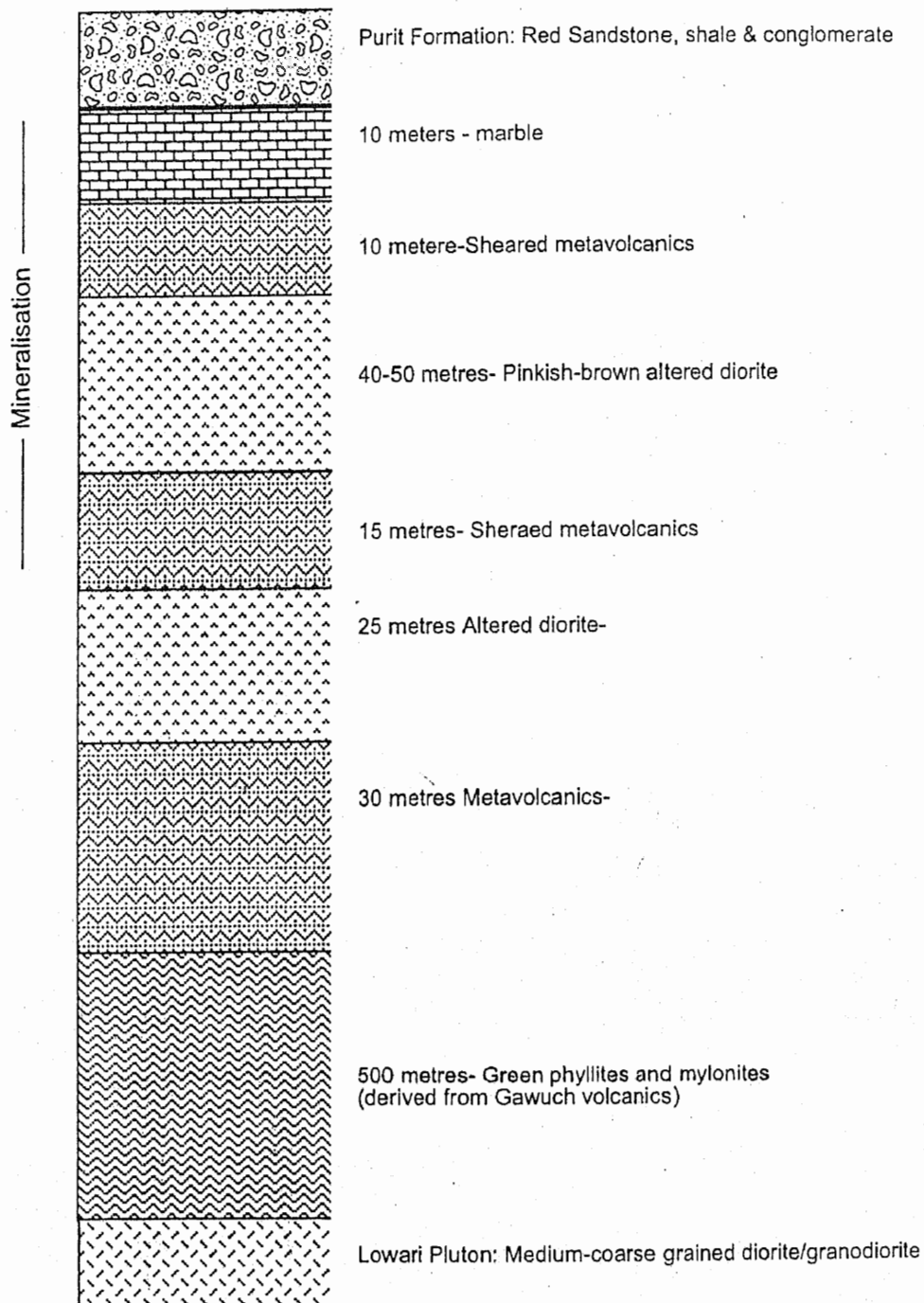


Figure 3.2. Generalised lithostratigraphic column for the Gawuch Formation.

contact is marked by a mineralised zone although much of it is covered by scree. Like in Kaldam Gol, a marble unit marks the uppermost part of the Gawuch Formation, overlain unconformably by the Purit Formation. The Purit Formation is highly sheared and typically comprises reddish claystone, sandstone, siltstone and conglomerate.

Langar Gol Section

Again the southern part of the section is marked by the presence of phyllites at the base of the Gawuch Formation defining the tectonic contact between the Lowari pluton and the Gawuch Formation. The phyllites are brown in colour and extensively weathered. They are highly foliated and contain carbonate veins along the foliation plane, but some veins cut across the foliation. The general attitude of the foliations remains same as in the Kaldam Gol (i.e., N60°E/75°NW). These phyllites are in contact with altered felsic material derived from diorites. This zone is about 30 m thick and is extensively sheared both at the contacts as well as in the interiors. The zone is overlain by a thick mass of metavolcanics. These metavolcanics are highly sheared, locally serpentinized and contain microveins of quartz and carbonate cutting across the entire rock body. The volcanics are overlain by marble. Again at the contact between the volcanics and marble, there is a 2 m thick, strongly sheared and oxidised zone. This zone is highly silicified and mineralised.

Gorin Gol Section

In the Gorin Gol, the melange zone has a direct lower contact with the Purit Formation (Plate 3.2). In the lower reaches of the valley both the Purit Formation and the melange zone dip to the north. However, upstream the

Purit Formation dips to the south, and the Gawuch Formation overlies the Purit Formation along a north-verging ductile-brittle thrust (Plate 3.3). The presence of an anticline in the Purit Formation raises the possibility that the Drosh Formation at the northern limb and the Gawuch Formation at the southern limb are equivalent rather than separate stratigraphic entities, opposite to what was suggested by Pudsey et al. (1985). However, the thrust nature of the southern contact suggests that Gawuch Formation is older than the Purit Formation, and the stratigraphic scheme suggested by Pudsey et al. (1985) is valid. The Gawuch Formation in this stream, comprises phyllites with sheets of diorites. Diorites, intruded by quartz veins are commonly sheared and mineralised. The copper mineralization is generally confined to or associated with quartz veins. One such mineralised zone is about 1 m thick and extends some 30 m along the strike. Copper mineralization includes tetrahedrite, chalcopyrite, azurite, malachite.

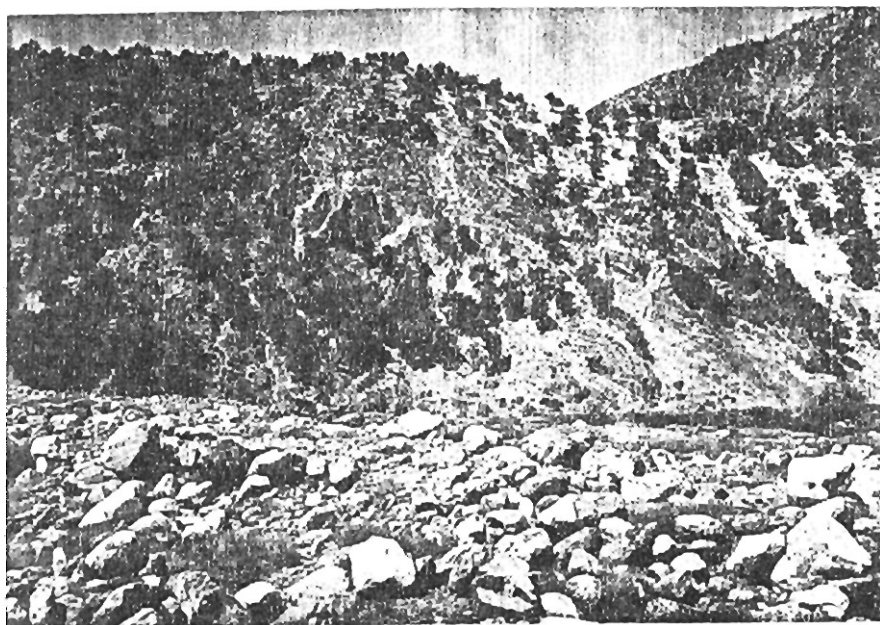


Plate 3.2 Photograph showing faulted contact between the melange zone (upper right) and the Purit Formation (left).

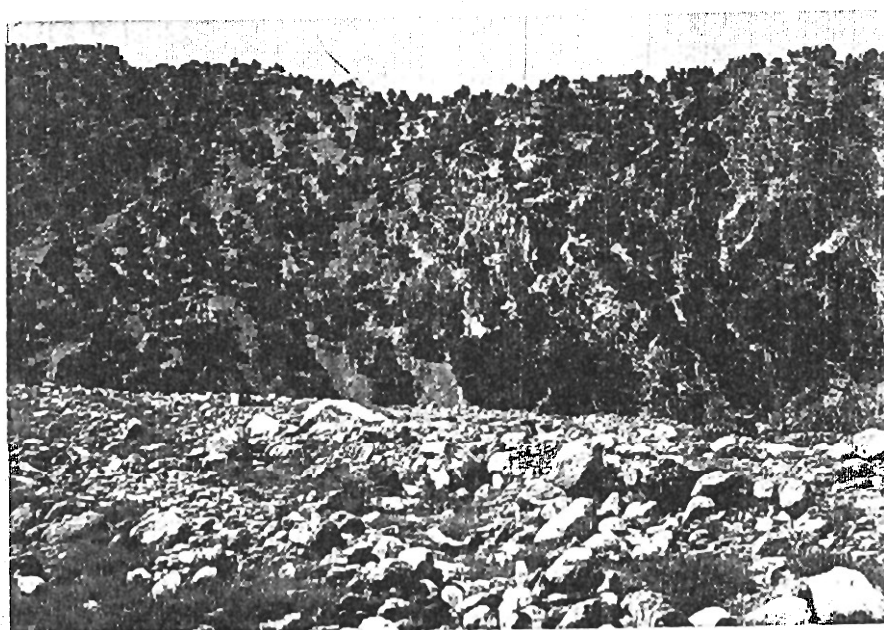


Plate 3.3 Photograph showing faulted contact between the Purit Formation (right) and the Gawuch Formation (left).

CHAPTER 4

PETROGRAPHY

A variety of lithologies, including metavolcanics, diorites, granodiorites, marbles, conglomerates, sandstones and shales occur in the studied area (see Chapter 3 for details). However, petrographic studies have been restricted only to the lithologies forming the Gawuch Formation which hosts the Cu-mineralization. The Gawuch Formation comprises mainly of volcanic and sedimentary rocks, metamorphosed under greenschist facies conditions. This formation is in contact with Lowari pluton of the Kohistan batholith in the south. Additionally several minor plutons in the form of irregular intrusions, dykes / sills and veins intrude the Gawuch Formation. All the lithologies of the Gawuch Formation are intruded by a network of veins comprise either quartz or carbonate. Petrographic accounts of metavolcanics, diorite/granodiorite rocks and quartz/carbonate veins from the Gawuch Formation are presented in this Chapter. A brief account of petrography of the metavolcanic rocks constituting the Drosh Formation is also included for comparison.

METAVOLCANIC ROCKS

Metavolcanic rocks constitute an important lithology in the studied area. As described in the local geology (Chapter 3), the metavolcanics occur as two stratigraphic entities i. e. Gawuch and Drosh formations.

Gawuch Formation

On the basis of grain size and texture, volcanics from the Gawuch Formation are divided in to two types:

(1) Porphyritic Volcanics

(2) Fine Grained, Glassy Volcanic

Porphyritic volcanics: These volcanics are characterized by fine grained groundmass, with phenocrysts ranging between medium- and coarse-grain size. These are characteristically porphyritic and less commonly aphyric with seriate texture. These range from being fresh to highly altered and are dissected by quartz and calcite veins. The principal constituent minerals include amphibole, pyroxene, feldspar and chlorite, whereas quartz, epidote, clay and ore occur as minor constituents. Nearly all the major constituents are subhedral to anhedral.

Most of the metavolcanic rocks are altered. Fresh rocks with original volcanic textures are relatively rare. The phenocrysts are mainly plagioclase, amphibole and ore minerals. while clinopyroxene, epidote, chlorite, sericite, carbonate and quartz occur in the groundmass.

Plagioclase (5-35%) occurs as a phenocryst phase as well as in the groundmass. In the fresh samples, plagioclase composition is in the range of $An_{39}-An_{42}$. In most cases, however, the plagioclase is turbid and shows development of carbonates and epidote in the cores (Plate 4.1). The rocks with a greater degree of alteration contain plagioclase which is sometime completely altered to epidote, carbonates, sericite and kaolinite.

Amphibole (25-60%) occurs in two varieties (1) light green to bluish green hornblende (2) light-green actinolite. Hornblende is prismatic to tabular in form, while actinolite is fibrous. Hornblende is a primary phase occurring both in the phenocryst phase and in the groundmass. Actinolite is probably secondary in origin developed at the expense of plagioclase and amphibole.

Pyroxene (2-10%) is colourless to pale and augitic in composition. It is usually associated with amphibole. Some grains show exsolution.

Quartz (0-5%) is mostly fine-grained and occurs in the groundmass, but in some rocks, it forms a minor fraction of the phenocrysts. The quartz phenocrysts are turbid and exhibit undulus extinction. In the groundmass it is very fine grained commonly intermixed with sericite, epidote and kaoline. Fine-grained recrystallized quartz occurs in the form of microveins and patches.

Chlorite (0-20%) is fine-grained, occurring as green patches and is secondary after amphibole. Locally, however, it is a cavity filling material contained in amegdules (Plate 4.2). Epidote (4-15%) is mostly fine grained, occurring as anhedral granular aggregates pseudomorphically replacing the plagioclase. It occurs as irregular patches in the groundmass and is locally very abundant in the fractures and veins. These epidote grains are highly birefringent. Biotite and muscovite occur in trace amounts in the form of flakes and mostly associated with epidote and ore minerals.

Parts of the metavolcanic rocks in the study area are completely altered. For instance, the mineralized rocks in the Gawuch Formation are completely recrystallized and altered with phenocrysts completely replaced by pseudomorphs comprising secondary minerals. These rocks consist of chlorite, epidote, and carbonate with lesser amount of actinolite and fine grained felsic phases.

2) Fine grained volcanic rocks: These are very fine-grained to glassy, composed of chlorite, epidote, carbonate, clay, quartz, ore, feldspar and glass. Chlorite is 20-65% by volume, mostly forming green patches. It is distributed throughout the

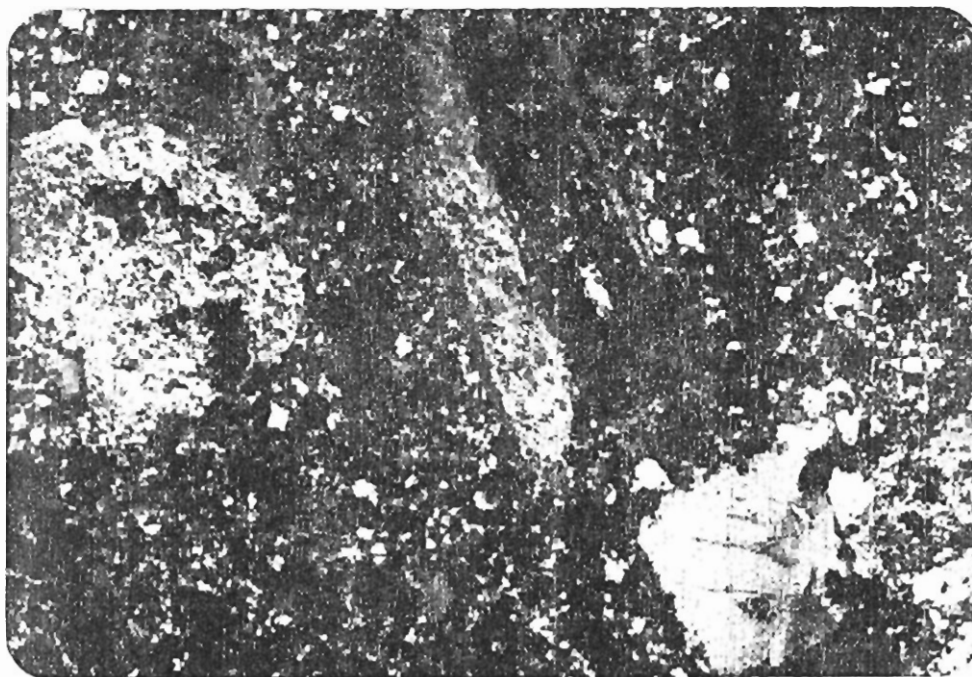


Plate 4.1. Photomicrograph showing porphyritic texture in an andesite from the Gawuch Formation. Partially altered plagioclase phenocrysts are embedded in a felsic ground mass (X 2.5 cross light).

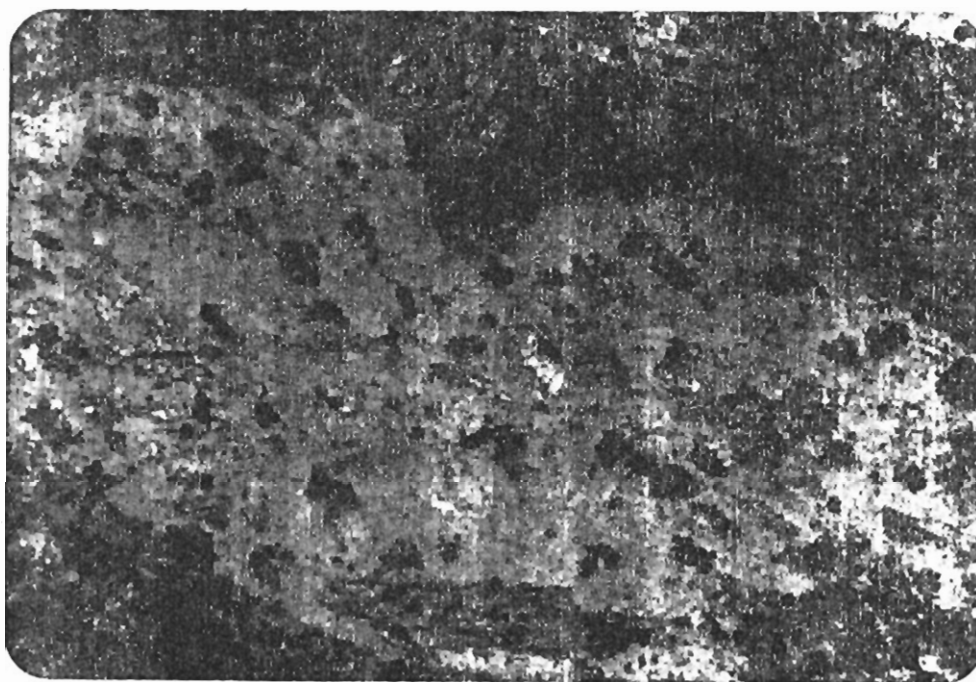


Plate 4.2. Photomicrograph showing an amygdule filled by chlorite. Amygdaloidal basaltic andesite, Gawuch Formation (X 2.5).

rock mostly intermixed with disseminated ore and epidote and is secondary in origin. It may have been formed at the expense of feldspar and amphibole. Sometimes it occurs as pseudomorphs after primary amphibole. Epidote is the next dominant phase (10-60%). It is an alteration product of feldspar. It generally occurs as granular aggregate. Quartz is mostly less than 10%, but some rocks might contain up to 30%. It is very fine-grained, inter-mixed with chlorite and epidote. Some rocks are criss crossed by a network of veins. These veins are filled with quartz and carbonate. These veins are enriched in ore minerals like tetrahedrite, galena, pyrite, magnetite etc. Feldspar is usually altered but some rocks show the pseudomorph of feldspar, replaced by epidote and carbonate. Carbonate, clay and ore are all very fine-grained disseminated throughout the rock.

Drosh Formation

The volcanic rocks are massive to weakly foliated, fine-grained and commonly altered. Compositionally they are mostly andesites. In terms of mineral composition, feldspars, amphibole, clinopyroxene, quartz and ore are the principal primary constituents, with chlorite, sericite, epidote, clay and sphene as secondary minerals. These volcanics are typically porphyritic in texture, with well developed euhedral to subhedral medium to coarse-grained phenocrysts set in a fine-grained groundmass (Plate 4.3).

Feldspars occur both as phenocrysts and in the groundmass. Commonly it shows alteration to carbonate, epidote, sericite and clay (Plate 4.3), but in a few sections it survives as relicts. Altered plagioclase ranges in composition between An_{32} and An_{38} .

Amphibole and clinopyroxene occur both as phenocrysts as well as in the groundmass. They commonly show partial alteration to chlorite and epidote. Brown amphibole is rarely left as relicts. Clinopyroxene is fresh. It is fine-medium grained in size and sub- to euhedral in shape. The phenocrysts are typically tabular or prismatic (Plate 4.4). Magnetite occurs as inclusions in some clinopyroxene grains.

Chlorite forms patches along with epidote. They are replacement minerals after ferromagnesian minerals like amphibole and clinopyroxene. At places chlorite and epidote also occur as a cavity filling material.

Ore minerals include magnetite and ilmenite. Sometime they are enclosed in leucoxene as relics. Sphene is also present in trace amounts and is usually associated with magnetite.

Diorites/ Granodiorites

Three varieties of diorites/granodiorite are distinguished in the studied area on the basis of texture and degree of alteration. These include 1) diorites/granodiorites, 2) altered diorites/granodiorites and 3) gneissose diorites/granodiorites.

1) Diorites / Granodiorite: Plutonic igneous rocks occur in Kaldom Gol, Gorin Gol and Gawuch Gol parts of the studied area. These rocks comprise plagioclase (25-70 vol%), hornblende (traces-35 vol%), quartz (5-30 vol%) and k-feldspar (10-25 vol%), and are classified as diorite/granodiorites. Some samples contain up to 35 vol% of hornblende are classified as hornblende diorites.

The diorites/granodiorites of the studied area are medium- to coarse-grained, equigranular to inequigranular, and subhedral in shape. Some rocks

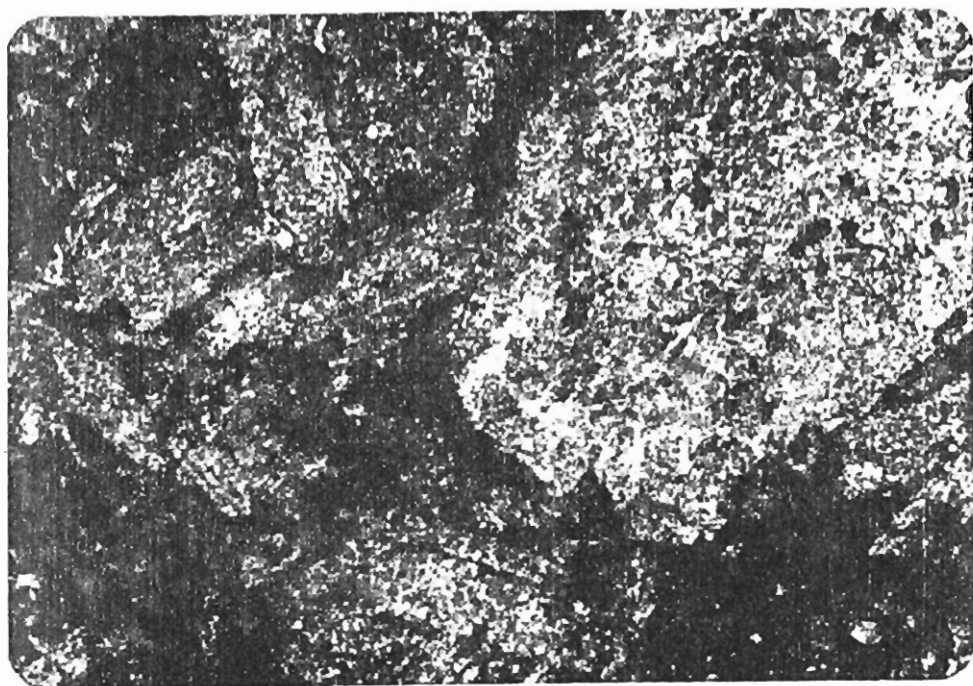


Plate 4.3. Photomicrographic view of plagioclase phenocrysts which shows partial alteration to carbonate, epidote and sericite, Drosh Volcanic Formation (X 2.5 cross light).

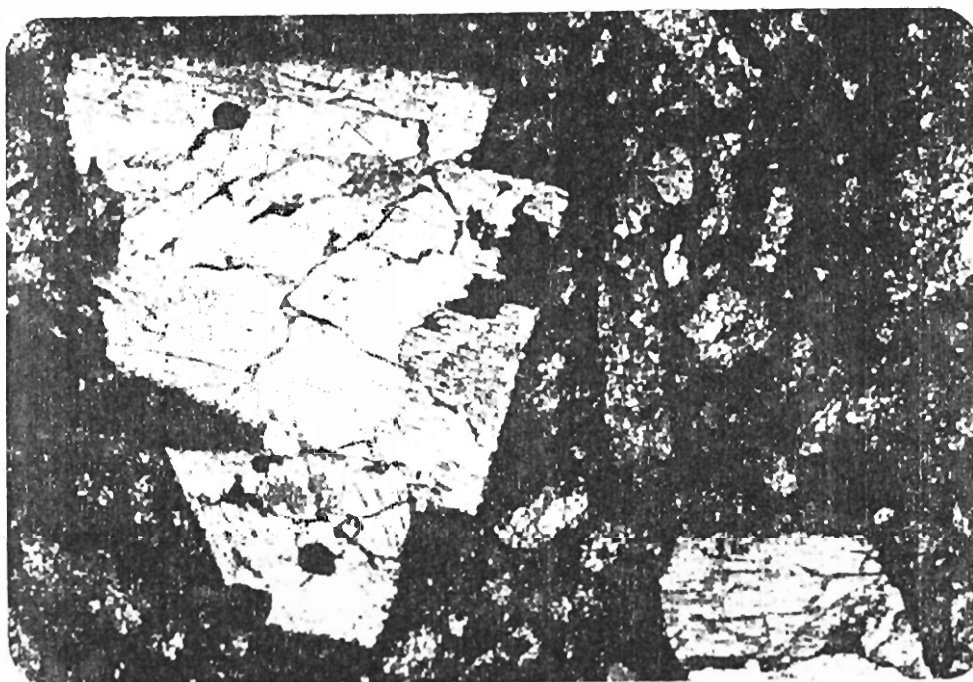


Plate 4.4. Photomicrograph showing euhedral grains of clinopyroxene (left half and lower right of the view). Note pseudomorphs of euhedral plagioclase in a fine grained groundmass. Metavolcanic from the Gawuch Formation (X 2.5 cross light).

show allotriomorphic and poikilitic textures. The major constituent minerals are plagioclase, orthoclase, amphibole and quartz. Calcite, chlorite and epidote occur as minor constituents while muscovite, biotite and ore are accessory phases.

Plagioclase is mostly subhedral to anhedral, commonly fresh and shows zoning and albite twinning (Plate 4.5). Some of the plagioclase grains show alteration to epidote, carbonates and clay (sericite) while other have turbid surface due to static alteration. Few plagioclase crystals are zoned with cores preferentially more altered than the margins. Optical determinations suggest an andesine composition ($An_{40} - An_{48}$).

Orthoclase is second most abundant feldspar. It is medium- to coarse-grained and mostly fresh, however some grains have cloudy appearance containing quartz inclusions.

Quartz is fine- to medium-grained. The larger grains commonly show undulose extinction suggesting strain in ductile conditions of deformation. In some rocks it is found in aggregates as well as individual grains. In hornblende diorites, quartz occurs in small amounts, while in the case of granodiorites it reaches up to 50 %. Locally veins and veinlets comprising exclusively of quartz, cut across the diorites.

Amphibole is light green to brown in colour, medium- to coarse-grained and generally anhedral and tabular in shape, particularly where it is associated with opaque phases (Plate 4.5). In a few sections granulation of amphibole to finer phases is also observed. Commonly, the amphibole grains are fresh, showing well developed rhombic cleavages, but in some rocks amphibole is altered to chlorite, epidote and clay, specially at the margins.

Carbonates are mainly calcites with lesser amount of dolomite. They occur as interstitial and vein material. Rarely, quartz and feldspars grains are enclosed in carbonate matrix.

Chlorite, epidote, sericite, clay occur as alteration products of amphibole and plagioclase. Muscovite is fine- to medium-grained. It occurs as irregular aggregates. Tiny grains of biotite spread all over the rock in some samples. At places it is chloritized having chlorite tint. Opaque phases (traces-1%) occur as subhedral to rounded disseminated grains. Few irregular grains of reddish-brown colour are also noticed as aggregates in the interstices and fractures in previously existing silicate phases.

2) Altered Diorites/granodiorites: Altered diorites are present in all sections (i.e., Kaldam Gol, Gawuch Gol, Langer and Gorin Gol) of the studied area. These are significant for being host to the copper mineralization. They are mineralogically similar to the fresh diorites and granodiorites, but are different in texture. The principal difference, however, is the degree of alteration. The alteration is commonly so intense that the primary texture is no more intact and the primary mineralogy is almost completely obliterated. It is not possible to identify these rocks as diorite/granodiorite purely on petrography basis. However, in the field these diorites are closely associated with or found within the fresh diorites and are, therefore, considered as the same unit. For the same reason, the modal composition of these rocks is not given in the text. The altered diorites are fine- to coarse-grained, inequigranular and are characteristically porphyritic, but some rocks show typically idiomorphic porphyritic and poikilitic textures. In some samples fine-grained quartz veins are also noticed. The important mineral

constituents are feldspar (both plagioclase and orthoclase) and quartz as the primary minerals, calcite, sphene and ore as the accessory minerals while chlorite, epidote, sericite and calcite as the secondary minerals. At places relicts of hornblende are also present in the aggregate of chlorite.

Plagioclase, orthoclase and quartz are the principal silicate phases occurring in these rocks. These are inequigranular, ranging from fine- to coarse-grained, occurring as large grains and also as matrix. Plagioclase is strongly altered to carbonates and epidote (Plate 4.6). In most samples the plagioclase is so intensively altered, that only pseudomorphs of plagioclase can be seen. In comparatively less altered rocks, the plagioclase grains are cloudy, and are enclosed by chlorite and sulfide minerals.

Quartz occurs as large grains but mostly it is present in fine grained matrix. The large grains showing undulatory extinction. Commonly anhedral quartz grains occupy interstices between plagioclase and orthoclase. At some places, quartz also occurs as veins.

Calcite is fine- to medium-grained in size, usually subhedral in shape, and occurs as irregular aggregates, interstitial material or in the form of microveins (Plate 4.7a). In some cases carbonate mass encloses rounded to sub-rounded plagioclase and quartz aggregates (Plate 4.7b). Some of the carbonate minerals appear to have formed by the alteration of plagioclase, but most are metasomatic in origin.

Chlorite occurs as fine-grained irregular aggregates or flakes. It is a common alteration product of amphibole. Amphibole, if present, is generally altered to chlorite and epidote in these rocks.

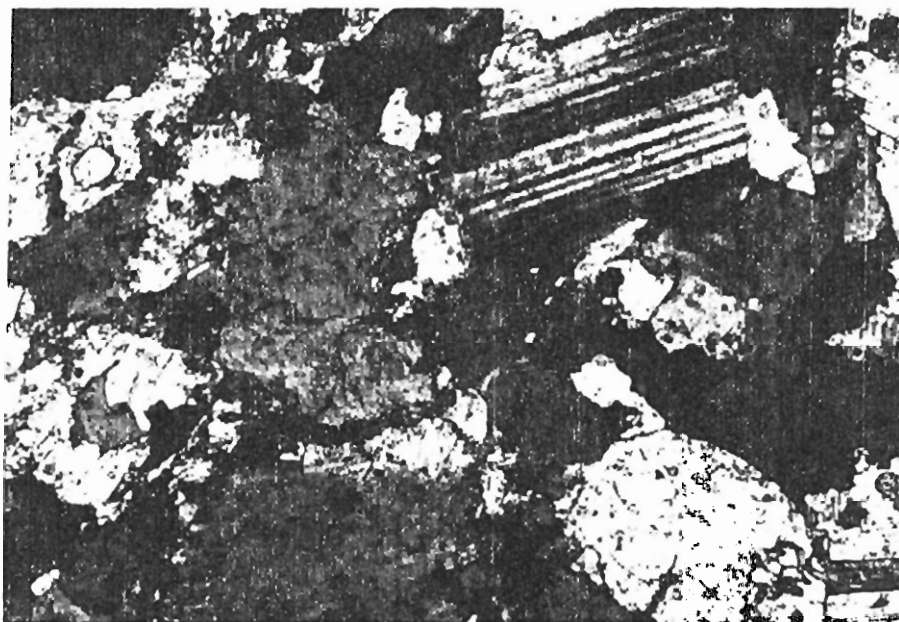


Plate 4.5. Photomicrograph of a hornblende diorite. Note the tabular subhedral shape of plagioclase grain and anhedral shape of hornblende grains (X 4 cross light).

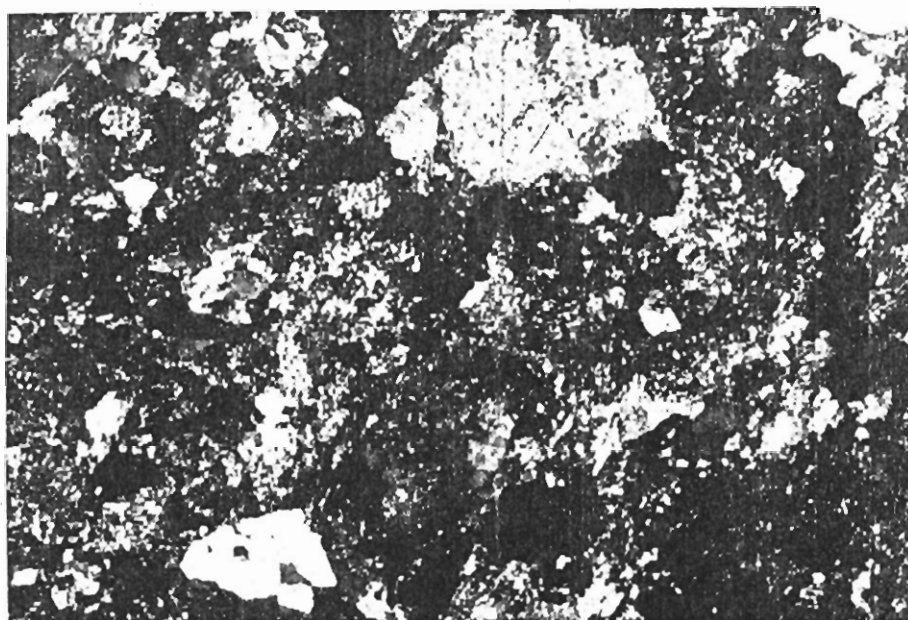


Plate 4.6. Photomicrograph showing a view of an intensively altered diorite, where the plagioclase is mainly altered to carbonates and epidote in the groundmass (X2.5 cross light).

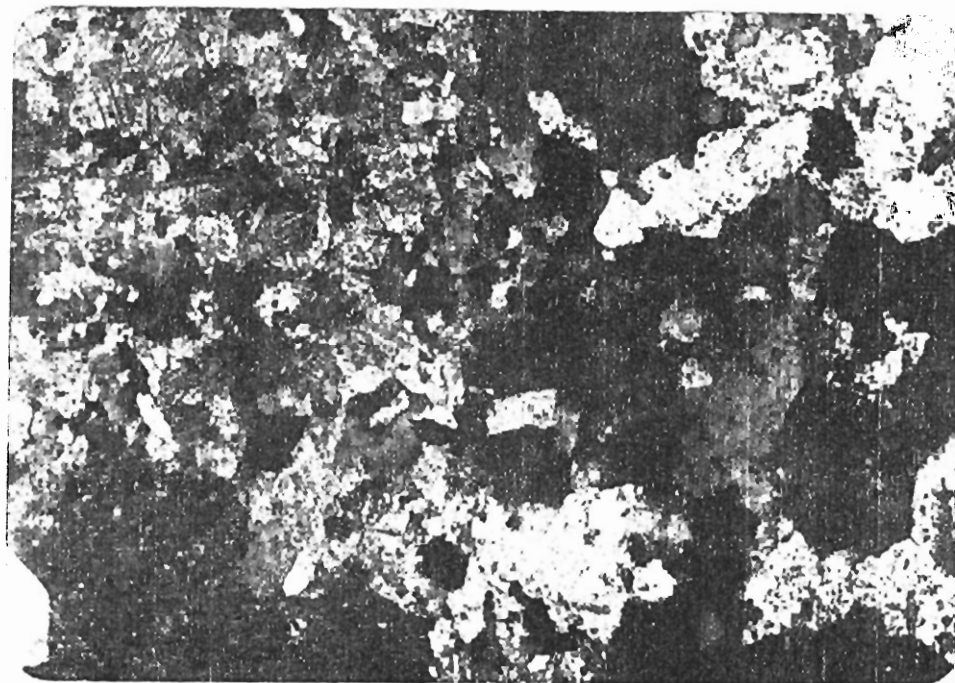


Plate 4.7a. Photomicrograph showing carbonates veining in the intensively altered diorites. The hydrothermal alteration has imparted brecciated appearance to the rock (X2.5, cross light).

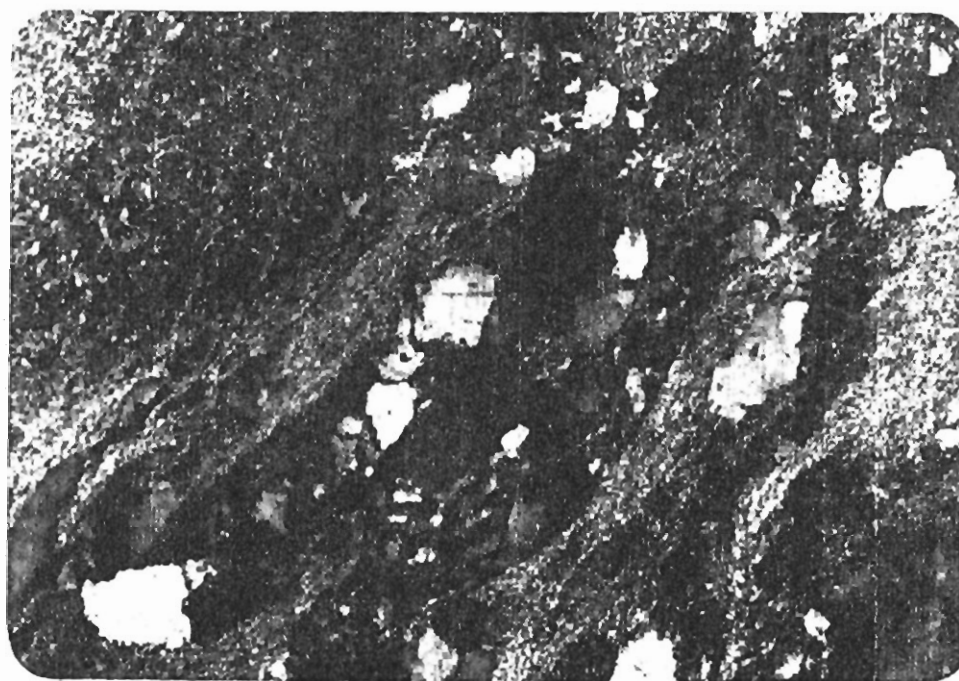


Plate 4.7b. Photomicrograph showing hydrothermal alteration of a diorite imparting a brecciated appearance to the rock. The carbonate masses enclose the rounded to sub-rounded aggregates of plagioclase and quartz (X 2.5, cross light).

Epidote occurs as subhedral elongated grains and also as granular aggregates. The elongated grains are zoned, having anomalous blue cores and brownish margins. Fine-grained epidote is disseminated throughout the matrix in association with carbonates and is usually the alteration product of the plagioclase.

Sericite is very fine-grained and occurs in association with muscovite, chlorite, epidote and ore. It is commonly an alteration product of feldspar. Muscovite is associated with chlorite and epidote, and is secondary in origin. Ore, in the form of sulphides, occurs as anhedral large grains and irregular masses within the interstices and along fractures. Iron oxide and limonite of yellowish- to brownish-red colour occur as a fracture-fill material in these rocks. In some rocks limonite occurs as a fracture-fill material enclosing quartz and plagioclase grains (Plate 4.8).

3) Diorite/Granodiorite Gneisses: Most of the diorites/granodiorites are strongly foliated and have a banded appearance in the handspecimen. Some of the samples are porphyroclastic with eye-shape appearance of the feldspar grains set in a matrix of fine-grained dynamically recrystallized matrix, imparting a gneissose texture. As far as the mineral composition is concerned, there are only subtle differences between these and non-foliated diorites/granodiorites described above. The major constituents of diorite gneisses are plagioclase, quartz and amphibole. Chlorite, epidote, sericite, clay and ore occur as minor constituents. Plagioclase and quartz are coarse grained and are enclosed by fine grained matrix of quartz, feldspar, hornblende, chlorite, muscovite, biotite and ore.

A few samples show growth of chlorite, epidote and muscovite along the foliation planes. These minerals occur in close association with each other and are found as very thin elongated tabular grains. Epidote typically occurs in aggregates of small rounded grains. Magnetite itself occurs as irregular grains associated with muscovite. Evidence of high strain has been noticed in feldspar and quartz in the form of pressure shadows. The porphyroclasts, set in a fine-grained matrix, are deformed and rotated, and in certain cases, show granulation at their margins (Plate 4.9). The matrix shows abrupt changes in grain size and in certain cases it becomes very fine grained and strongly foliated, indicating mylonitization.

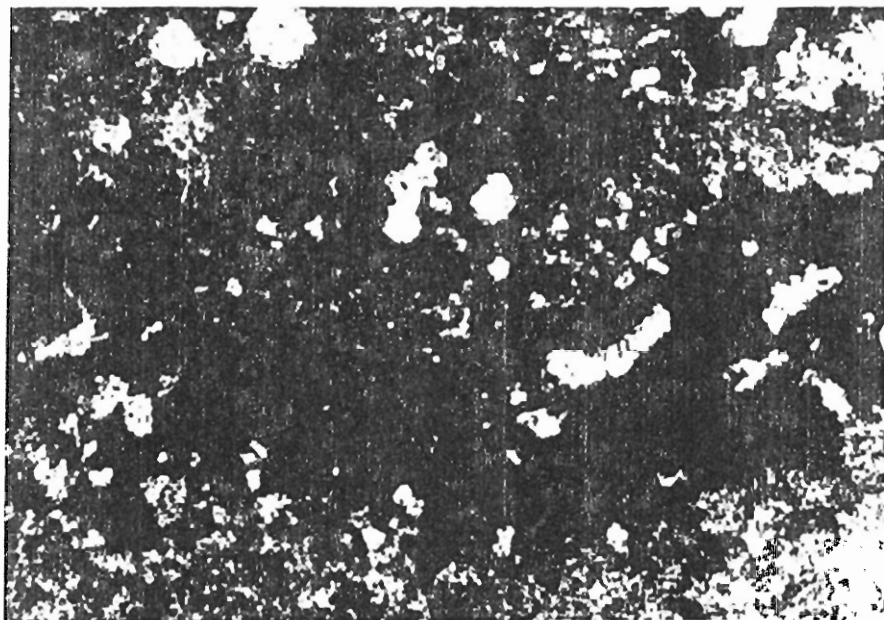


Plate 4.8. Photomicrograph showing fracture-fill limonitic material in an altered diorite, enclosing the rounded to sub-rounded grains of plagioclase and quartz (X 2.5, plane light).

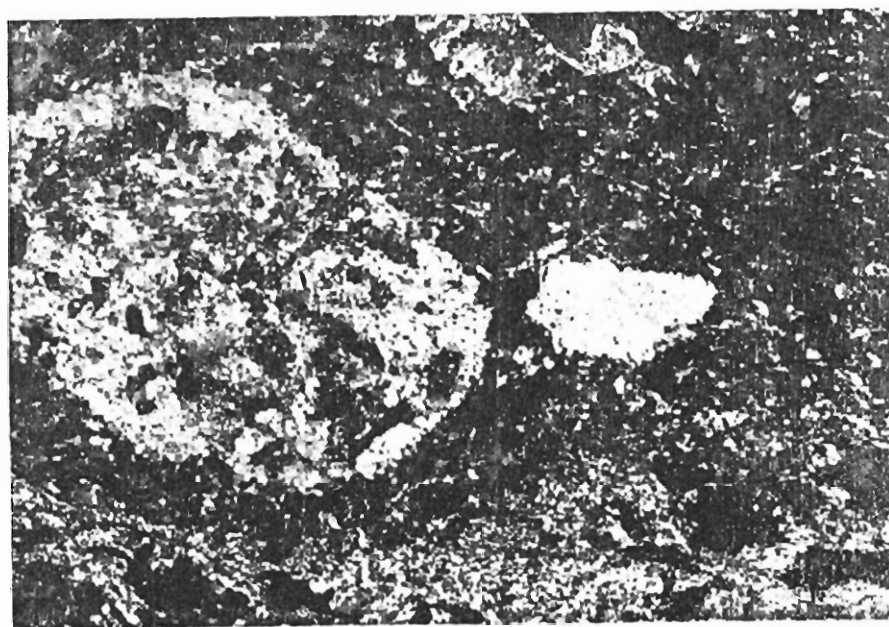


Plate 4.9. Photomicrograph showing a mylonitized dioritic rock. Rounded to sub-rounded, partially altered plagioclase grains are corroded along the margins and form asymmetrical porphyroclasts set in a fine-grained mylonitic matrix (X 2.5, cross light).

CHAPTER 5

WHOLE-ROCK GEOCHEMISTRY

The studied area comprises two groups of igneous rocks; metavolcanics and diorites. These are generally altered due to the hydrothermal activity and associated Cu-mineralization. This has rendered the mineralized rocks unsuitable for geochemical investigations. Keeping this in view, a number of representative samples were collected from the unmineralized parts of the metavolcanics and diorites. In this chapter, the igneous rocks from the studied area are treated in terms of their whole-rock geochemistry in order to characterize their petrology, genesis and tectonic setting of origin.

METAVOLCANIC ROCKS

The metavolcanic rocks of the Drosh-Shishi area, as defined in Chapter 2, belong to two different stratigraphic entities (i.e., Gawuch Formation and Drosh Formation). The age difference between these two formations is unknown, but in the stratigraphic column of Pudsey et al. (1985) (Table 2.1), they are separated from each other by the Purit Formation of fluvial origin. In the context of the Kohistan geology, two groups of volcanic rocks are also identified in the Shamran (Shandur Pass) area, to the east of the presently studied area (Pudsey et al., 1985). The age relationship between the two groups of volcanics in the Shamran area is controversial; Pudsey et al. (1985) consider them both to be stratigraphically below the Aptian-Albian Yasin Group and thus lower Cretaceous in age, while Sullivan et al. (1993) differentiate the fresh volcanics of andesite-dacite-rhyolite composition from those metamorphosed to amphibolite-greenschist facies and assign them an age of 58 Ma on the basis of ^{40}Ar - ^{39}Ar on hornblende, equating

them with the volcanic rocks in the Dir area (Sullivan et al., 1993; Shah et al., 1994). Field observations during the course of this study suggest that the Gawuch Formation of the Drosh-Shishi area has lithological similarities with the Chalt volcanics and the Yasin group combined, and a lower Cretaceous age may be assigned to the Gawuch Formation on the basis of this correlation. However, there is no control on the age of the Drosh Formation at the moment. In this chapter an attempt is made to evaluate differences between the volcanic components of the Gawuch and Drosh Formations on the basis of both major and trace element chemistry.

Eighteen representative samples were analyzed from the metavolcanics of the Gawuch (15 sample) and Drosh (3 sample) formations (Table 5.1). Of these eight were analyzed by using Rigaku X-ray fluorescence (XRF) at the Geoscience Laboratory, Islamabad, while the rest were analyzed by atomic absorption spectrometry, at the National Center of Excellence in Geology, University of Peshawar. Both sets of analyses include major elements. Amongst the trace elements, Cu, Pb, Zn, Ni, Co and Cr are present in both sets of analyses while Nb, Zr, Y, Sr, Rb, U, Ga, Sc, and Th are restricted only to the set of analyses obtained by using the XRF.

Major-Element Chemistry

The metavolcanics of the area are classified on the basis of SiO₂ content (Gill, 1980) as basalt (< 53 wt% SiO₂), basaltic-andesite (53-57 wt% SiO₂) and andesite (57-63 wt% SiO₂). Major element variations in the studied samples are presented in Figure (5.1). The TiO₂ vs SiO₂ plot clearly discriminates between the samples from the Gawuch and Drosh Formations. The Drosh Formation metavolcanics are high

Table 5.1 Major- and trace-element composition of volcanic rocks from Gawuch and Drosh Formations.

SAMPLE	KG2	KG7	KG8	KG9	KG12	KG15	KG172	KG210	GOG27
SiO ₂	46.60	55.98	54.87	57.32	53.67	48.89	55.12	52.76	48.67
TiO ₂	0.68	0.92	0.84	0.55	0.86	0.43	0.65	0.82	0.80
Al ₂ O ₃	17.89	19.87	18.76	17.76	17.34	16.98	14.47	18.98	20.56
Fe ₂ O ₃	5.65	5.18	6.11	4.12	6.11	8.18	8.94	5.34	5.12
MnO	0.15	0.07	0.07	0.09	0.08	0.11	0.13	0.09	0.07
MgO	3.41	3.59	4.46	3.68	4.43	10.28	6.17	3.32	5.04
CaO	11.93	3.39	4.27	4.60	5.07	8.88	5.67	5.19	7.20
Na ₂ O	1.69	1.85	0.79	0.54	0.80	1.57	3.29	0.72	3.88
K ₂ O	0.67	3.16	3.68	2.17	2.17	0.33	0.59	2.26	1.43
P ₂ O ₅	0.13	0.17	0.17	0.25	0.23	0.12	0.15	0.17	0.27
LOI	10.47	4.43	5.20	7.10	8.67	2.86	4.82	9.57	5.50
TOTAL	99.27	98.61	99.22	98.18	99.43	98.63	100.00	99.22	98.54
Nb		6				7	4		
Zr		130				136	73		
Y		42				18	17		
Sr		228				255	380		
Rb		40				18	26		
Cu	38	85	39	45	76	448	180	345	56
Pb	59	62	39	31	37	47	42	52	42
Zn	68	78	72	74	117	73	73	79	69
Ni	28	80	85	52	95	176	45	58	54
Cr	29	118	108	114	371	481	268	82	103
V		426				309	395		
Ba		150				61	164		
CO	35	59	50	35	47	1173	48	36	44
Th		4				999	2		
Sc		49				51	34		
Ga		8				7	12		
U		2					1		

The samples with KG, GOG, GR and GL prefixes are from the Gawuch Formation and DRO from the Drosh Formation.

Table 5.1 continued

SAMPLE	GOG34	GL48	GR78	GR79	GR80	GR98	DRO232	DRO 23E	DRO240
SiO ₂	55.30	46.67	46.34	52.62	48.67	53.78	48.72	46.57	48.82
TiO ₂	0.47	1.64	0.46	0.47	0.68	0.65	1.36	1.29	1.30
Al ₂ O ₃	15.12	16.23	16.32	13.90	20.23	18.65	17.19	15.83	17.48
Fe ₂ O ₃	4.92	6.96	5.48	6.72	6.04	3.46	11.26	11.93	10.02
MnO	0.06	0.08	0.11	0.13	0.12	0.10	0.20	0.20	0.18
MgO	3.07	7.77	6.73	4.06	4.20	5.70	5.90	8.10	4.93
CaO	5.42	11.24	12.94	5.95	5.66	6.35	7.80	8.10	6.65
Na ₂ O	3.27	3.62	0.45	1.70	3.24	1.75	0.78	2.89	0.84
K ₂ O	3.06	1.43	2.26	2.69	0.12	1.47	3.62	1.75	2.44
P ₂ O ₅	0.20	0.29	0.22	0.15	0.16	0.28	0.22	0.19	0.29
LOI	9.12	3.45	8.45	11.61	9.60	7.28	2.90	3.20	7.07
TOTAL	100.01	99.38	99.76	100.00	98.72	99.47	99.95	100.05	100.02
Nb	7			4	8		9	5	12
Zr	95			52	112		100	68	159
Y	13			12	26		25	21	26
Sr	150			225	548		557	320	367
Rb	92			106	25		21	74	31
Cu	6	156	57	36	38	186	163	111	101
Pb	17	46	42	37	58	37	80	95	82
Zn	20	64	72	85	60	71	109	106	110
Ni	17	46	86	20	25	44	18	42	25
Cr	54	152	119	124	90	85	46	118	43
V	194			273	325		368	422	329
Ba	592			782	1128		1236	1148	351
CO	54	40	49	44	45	72	46	53	40
Th	7			3	4		3	1	3
Sc	22			36	26		28	35	15
Ga	16			12	20		19	16	24
U	3				4				1

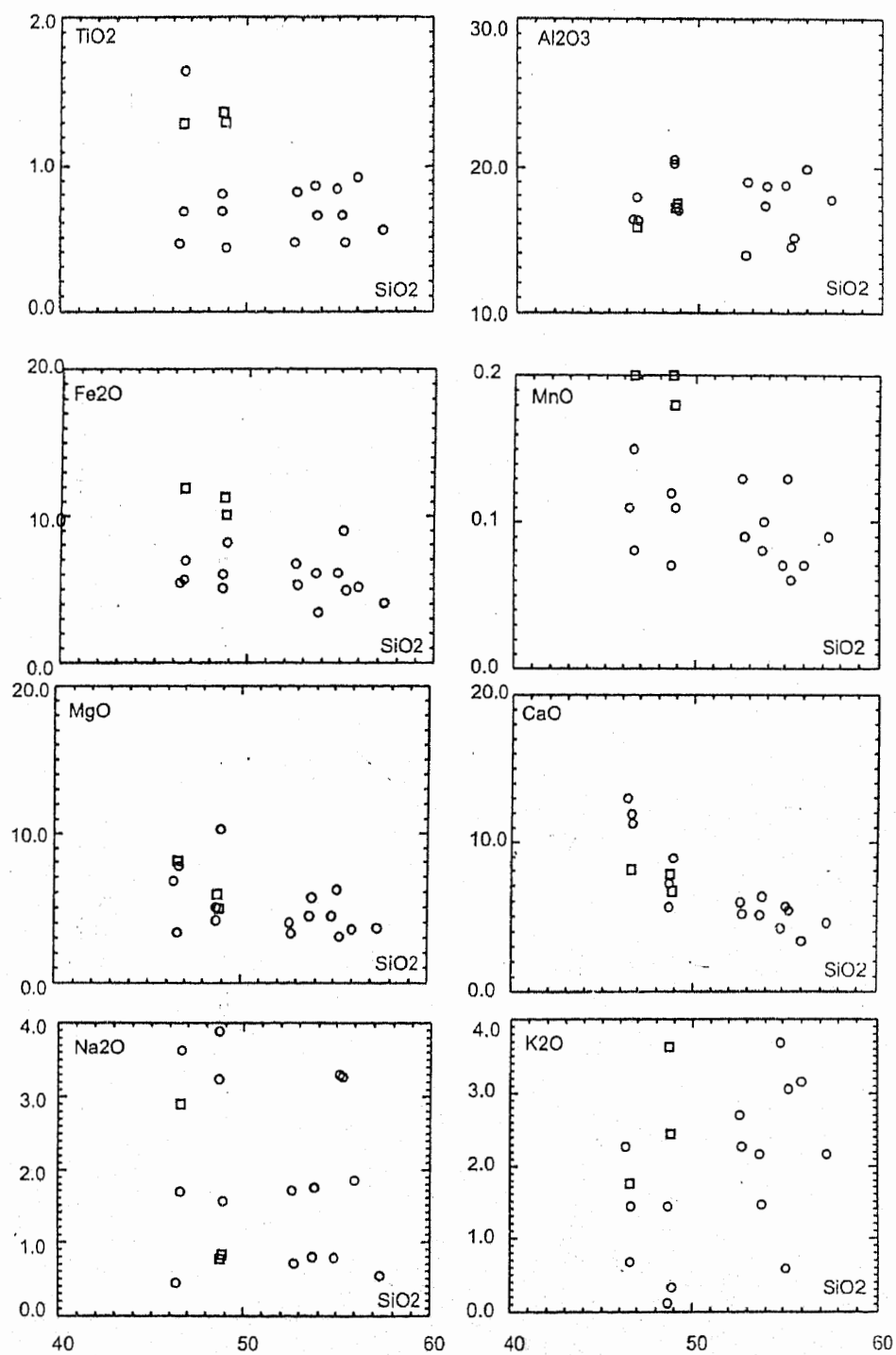


Figure 5.1. Major-element variations in the metavolcanic rocks of the Gawuch (○) and Drosh (◻) formations.

in TiO_2 (>1 wt%) compared to those of Gawuch Formation which are below 1 wt% (except for one sample DR 48). This difference between the two groups of volcanics is also reflected in the MnO vs. SiO_2 and Fe_2O_3 vs. SiO_2 plots; MnO and $\text{Fe}_2\text{O}_{3(t)}$ both are distinctly high in the samples from Drosh Formation. In terms of variations with respect to SiO_2 , samples from Drosh Formation show little variation (SiO_2 ranges between 46 and 49 wt%) and mostly plot as a coherent group. The samples from the Gawuch Formation, on the other hand, show considerable variation in their SiO_2 contents (between 45 and 57 wt%) exhibiting some decent fractionation trends. $\text{Fe}_2\text{O}_{3(t)}$, MnO, MgO and CaO exhibit well defined negative correlation with increasing fractionation. These variations reflect a lack of iron-enrichment for the volcanic rocks of the Gawuch Formation and therefore suggest their calc-alkaline nature. However, TiO_2 shows a slight enrichment with increasing SiO_2 . This could be attributed to magnetite fractionation rather than that of titanomagnetite in the initial stages of fractionation. Strong depletion of MgO with increasing fractionation points to a constant fractionation of olivine and/or orthopyroxene. The variations in CaO and Al_2O_3 are not mutually consistent; Al_2O_3 shows more or less constant levels from primitive to fractionated samples. In comparison CaO shows a strong depletion with fractionation. These variations point to the role of clinopyroxene in the fractionation rather than that of plagioclase. Unlike CaO, MgO and Fe_2O_3 , alkalis ($\text{Na}_2\text{O}+\text{K}_2\text{O}$) show greater spread against SiO_2 suggesting their mobilization due to metasomatism.

The classification of the volcanic rocks of the studied area in terms of alkaline, tholeiite or calc-alkaline compositions is presented in Figure (5.2a,b,c, 3

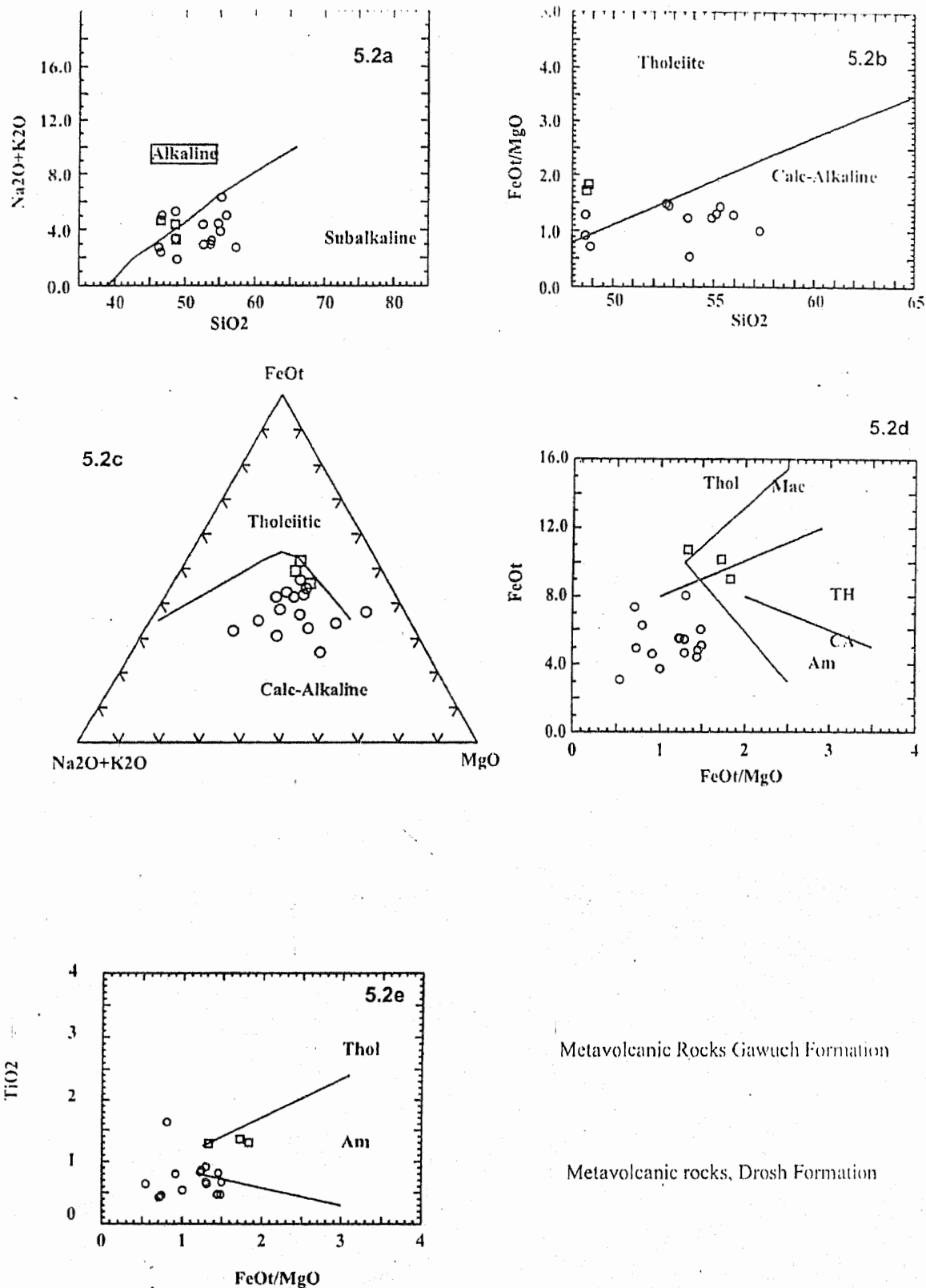


Figure 5.2. Variation highlighting the calc-alkaline character of the volcanic rocks from the Gawuch Formation relative to the tholeiitic composition of the volcanic rocks from the Drosh Formation. a) SiO_2 vs. $\text{Na}_2\text{O} + \text{K}_2\text{O}$, b) SiO_2 vs. FeO/MgO , c) AFM diagram, d) FeOt vs. FeO/MgO , and e) TiO_2 vs. FeO/MgO . Majority of these diagrams are adopted from after Irvine and Baragar (1971).

and 4). The studied volcanic rocks are essentially sub-alkaline although some samples, probably affected by alkali metasomatism, plot in the field of alkaline rocks on the SiO_2 vs. $\text{Na}_2\text{O}+\text{K}_2\text{O}$ plot of Irvine and Baragar (1971). For the same reason the studied rocks show some scatter when plotted on the AFM diagram (Figure 5.2c). This diagram, however, shows that volcanic rocks of the Drosh Formation are more iron-enriched than those of the typical calc-alkaline rocks of the Gawuch Formation. The best discrimination can be obtained using a scheme without involving alkalis e.g., SiO_2 vs. FeO/MgO (Figure 5.2b). In such a diagram, the Drosh volcanics plot as tholeiites while all the samples of the Gawuch Formation (except one) plot in the field of calc-alkaline basalts. A comparable result is achieved for these rocks when plotted in diagrams of $\text{FeO}(\text{t})$ and TiO_2 vs FeO_t/MgO (Figure 5.2d and 5.2e).

Trace-Element Chemistry

Trace-element data of the volcanic rocks from the studied area are presented in the form of spider-diagrams in which the data have been normalized to primordial mantle by using the normalization factors of Sun and McDonough (1989) (Figure 5.3 and 5.4). Both the Drosh tholeiitic volcanics as well as the Gawuch calc-alkaline volcanics do not exhibit major differences in terms of inter-element ratios between the incompatible trace elements. Both have trace element patterns sloping towards right suggesting enrichment in the large-ion lithophile elements (LILE) relative to the high-field strength elements (HFSE). In both cases LILE show a greater scatter compared to HFSE, probably reflecting the greater degree of mobilization in the former due to metasomatism, alteration or metamorphism. The only difference between the two groups of volcanics is in the

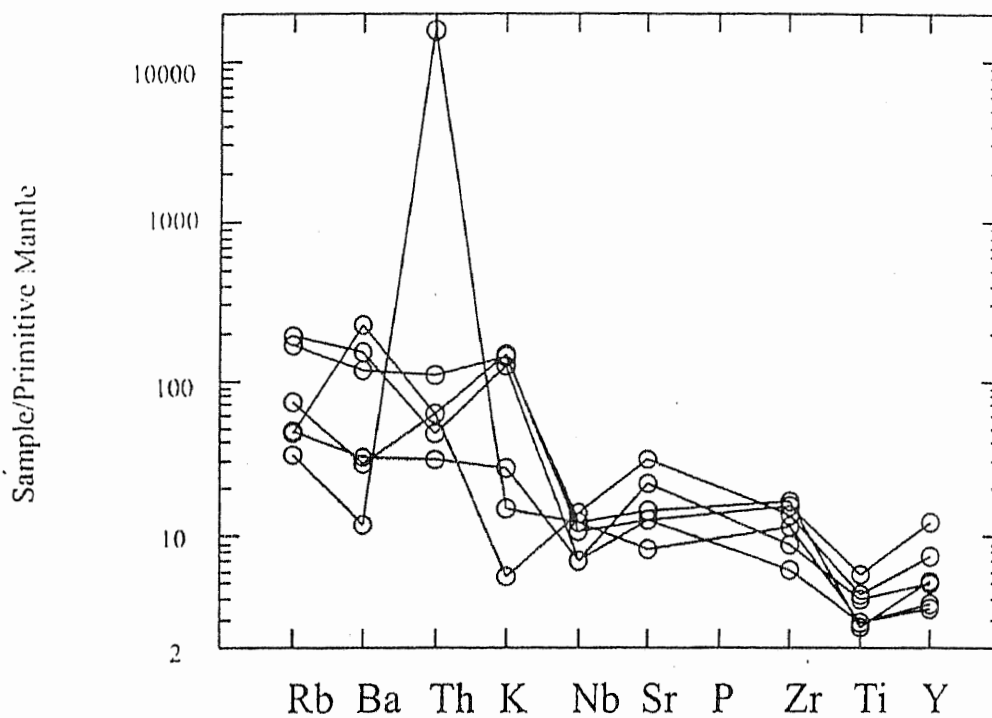


Figure 5.3. Mantle normalized spider diagrams for trace elements of Gawuch calc-alkaline volcanics.

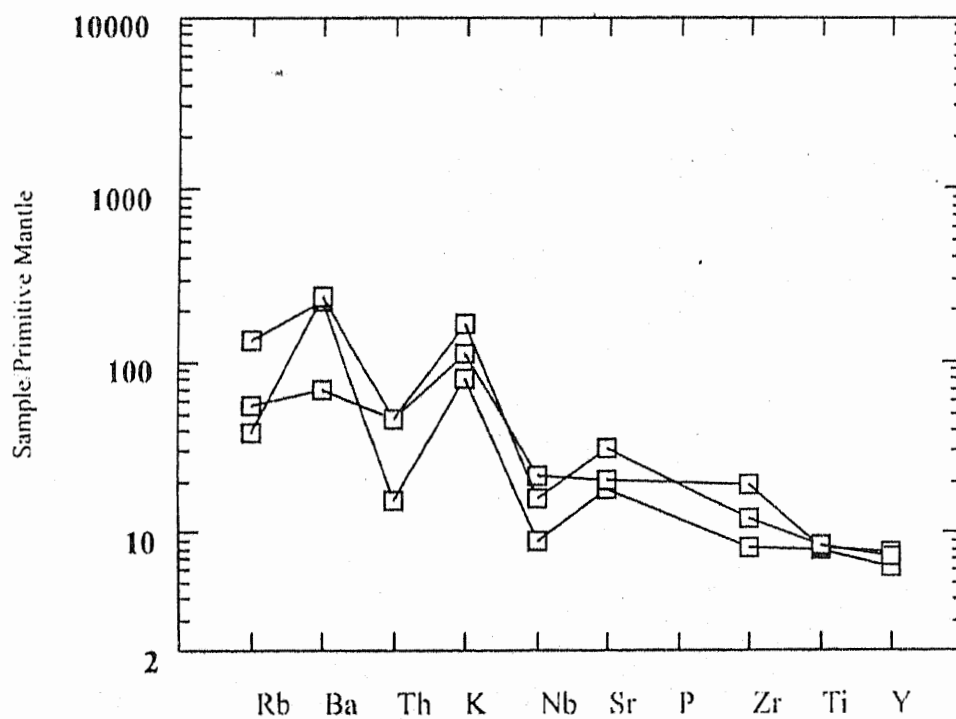


Figure 5.4. Mantle normalized spider diagrams for trace elements of Drosh tholeiitic volcanics.

Ti/Y (Gawuch= $Ti/Y=174.30\text{ppm}$; Drosh = $Ti/Y=331.37\text{ppm}$). This difference is due to higher Ti content in the Drosh volcanics due to their tholeiitic nature.

The transitional elements like Sc, V, Ti, Co, Fe, Mn, Cr, and Ni are also plotted in the form of primordial mantle normalized spidergrams (Figure 5.5). Again the two groups of rocks show broadly similar patterns. The tholeiites of the Drosh Formation are characterized by positive anomalies for Ti compared to absence of such an anomaly in the case of the Gawuch calc-alkaline volcanics. Similarly Fe and Mn peaks are slightly higher in the case of Drosh volcanics compared to those of the Gawuch Formation. Compared to the primordial mantle, Cr and Ni are extensively depleted in the studied volcanics probably due to the role of olivine and clinopyroxene fractionation control. Sc, V and Ti are only slightly enriched compared to the primordial mantle while Fe, Mn and Co are slightly to moderately depleted relative to the primordial mantle.

Tectonic Setting

Whole-rock geochemistry has now emerged as an important tool in identification of petrogenetic and palaeotectonic aspects of igneous rocks (see Wilson, 1989, Rollinson, 1993 for reviews). However, the discrimination diagrams in use are primarily meant for highly fresh rocks devoid of phenocrysts. Unfortunately, volcanic rocks in terranes like Kohistan have little chance of escaping alteration and metamorphism due to their involvement in collision tectonics of Karakoram and Himalayas. It is for this reason that several of the conventional diagrams, especially those involving major elements, when tried for the volcanic rocks of the studied area do not yield an unequivocal tectonic setting of origin for all the samples plotted.

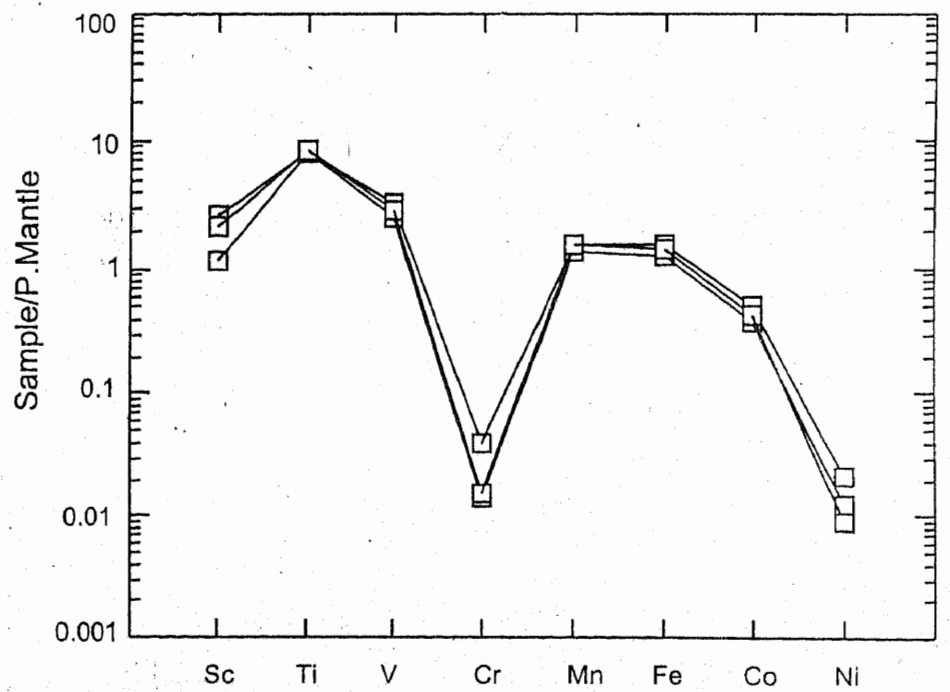
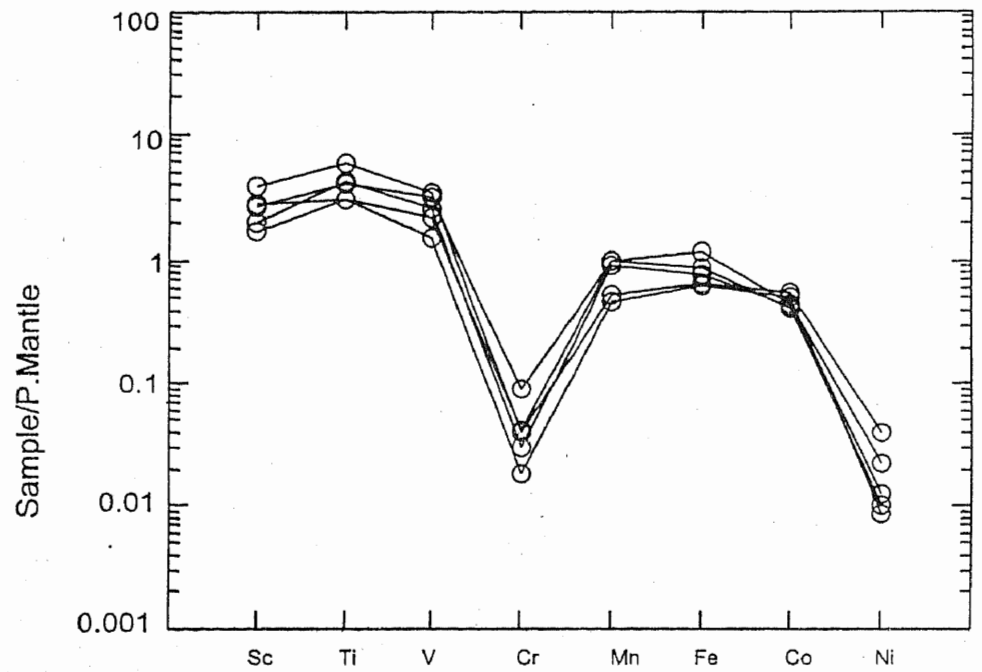


Figure 5.5. Primordial mantle normalised transitional element patterns for the volcanic rocks of the Gawuch (a) and Drosh(b) formations. Note the similarity in the shape of the two set of patterns.

When plotted on triangular plot involving Nb, Zr and Y (Meschede, 1986), most of the studied volcanic rocks from the Drosh-Shishi area plot in the field of volcanic arc basalts, yet one sample plots in the field of within-plate basalts and two in the N-MORB (Figure 5.6a). In the triangular diagram of Pearce and Cann (1973), all the samples plot in the field of calc-alkaline basalts (Figure 5.6b). In the triangular diagram of Pearce and Cann (1973), involving Ti, Zr and Y, all the volcanics from the Gawuch Formation and one sample from the Drosh Formation plot in the field of the calc-alkaline basalts while the remaining two samples of volcanics from the Drosh Formation plot in the combined field of island arc tholeiites and mid-oceanic ridge basalts (Figure 5.6c). In the binary plot of Zr vs. Ti (Pearce and Cann, 1973) all the three samples of the Drosh Formation plot in the field of ocean-floor basalts, while the samples of the Gawuch Formation generally plot in the fields of calc-alkaline basalts (Figure 5.6d).

Almost all the analyzed samples (except one from Drosh Formation) plot within the field of calc-alkaline basalt when plotted in the triangular diagram (Ti-Zr-Sr) of Pearce and Can (1973). In the Zr vs. Zr/Y plot of Pearce and Norry (1979), surprisingly none of the analyzed samples plot as island arc basalts. Rather, two plot as MORB and rest as within-plate basalts (Figure 5.6e). On the Ti vs. V plot of Shervais (1982), samples from the Gawuch Formation have a Ti / V ratio of 10 which classifies them as true island arc basalts. The samples of Drosh Formation, on this plot show a Ti/V ratio of ~20 which is transitional between the island arc and ocean-floor basalts (Fig 5.6f).

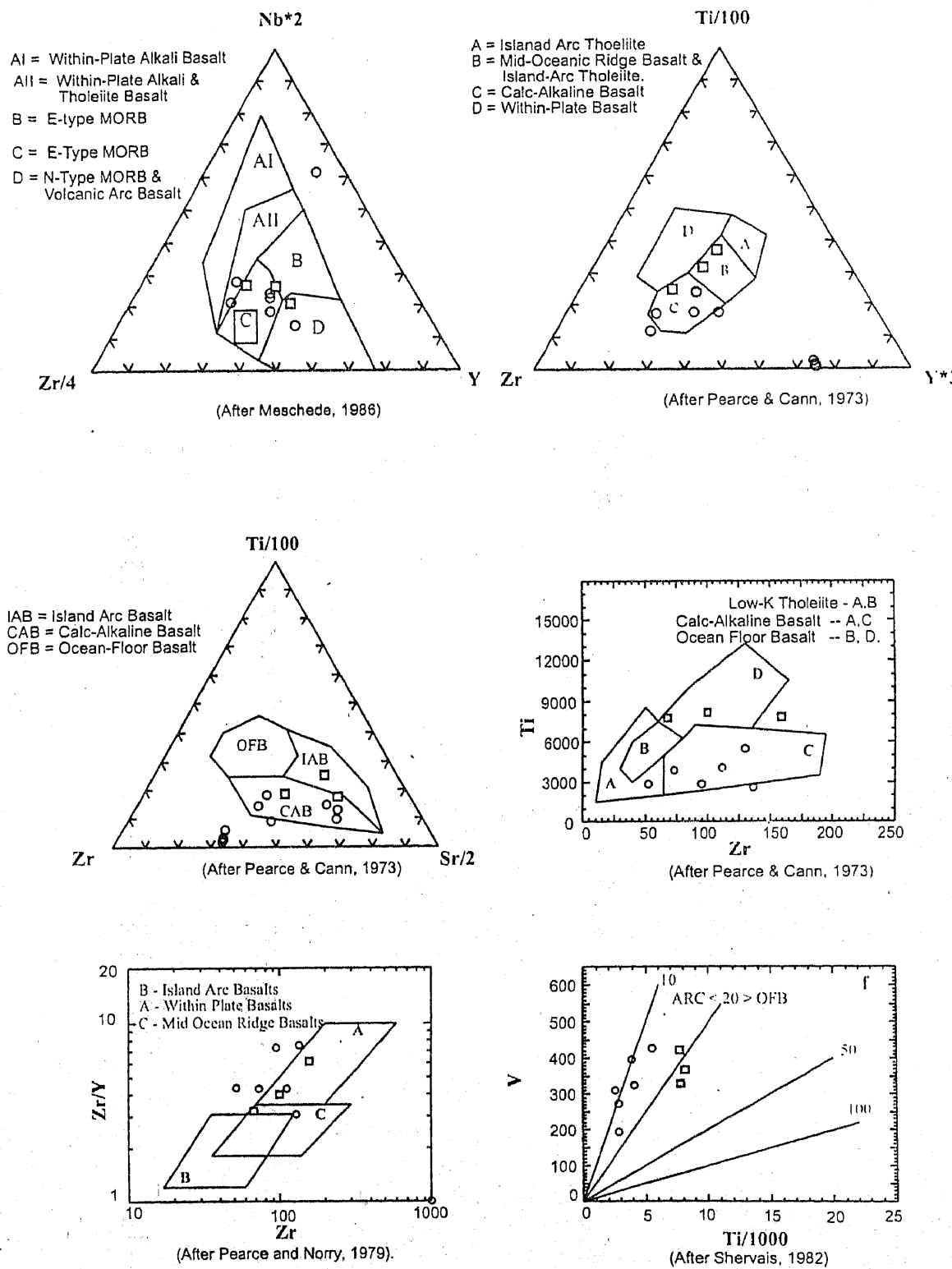


Figure 5.6. Discrimination diagrams showing tectonic setting of origin for the volcanic rocks of the Gawuch (○) and Drosh (◻) formations.

Thus, the volcanic rocks from the studied area, when plotted on conventional discriminatory diagrams yield unequivocal results in terms of their tectonic setting of origin. Majority of the samples from the metavolcanic rocks of the Gawuch Formation yield a calc-alkaline nature formed in an island-arc setup. The volcanic rocks of Drosh Formation, on the other hand, are mostly classified as tholeiites either of an island arc affinity or that of the ocean-floor origin. A more precise assessment of the tectonic setting of igneous rocks can be obtained by using multi-element diagrams (Holms, 1986). Primordial-mantle normalized trace-element patterns of the volcanic rocks both from Gawuch and Drosh formations are compared with each other and with those of MORB, island arc tholeiitic basalt, island-arc calc-alkaline basalt and within plate basalt (Figure 5.7). Firstly, the trace-element patterns of the Drosh and Gawuch volcanics are characterized by certain characteristics (eg., negative Nb anomaly) which are mutually consistent and closely comparable with subduction-related rocks. This characteristic of the trace element pattern of the studied rocks is closely comparable with all other subduction-related rocks from the Kohistan island arc terrane (Pettersson and Windley, 1985, 1991; Khan et al., 1989, 1993; Sullivan et al., 1993; Shah et al., 1994). Trace element patterns of the studied rocks are drastically different from those of MORB and within-plate basalts. Thus, although the conventional discriminatory diagrams do not unequivocally discriminate the studied volcanic rocks, the mantle-normalized trace element patterns clearly classify them as subduction-related, negating the possibility of their origin at mid-oceanic ridge or in a within-plate oceanic setting.

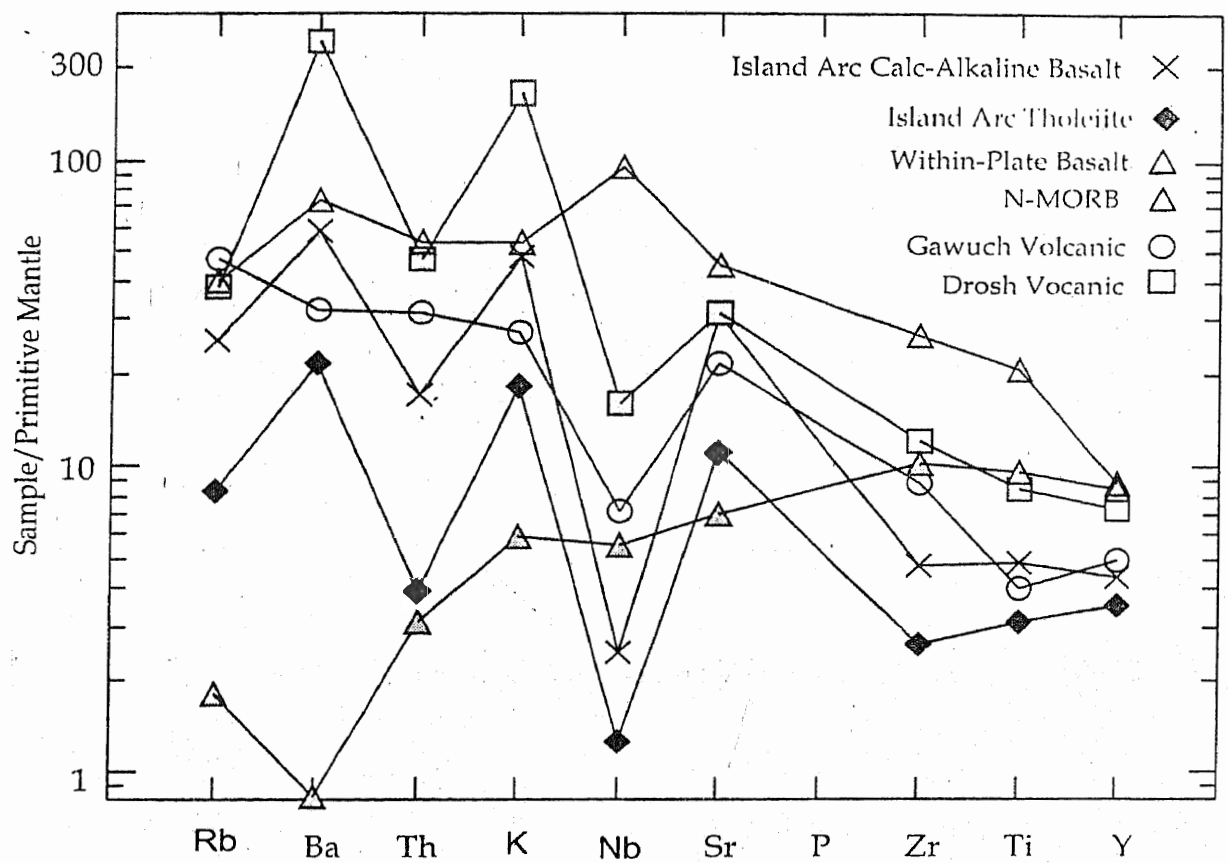


Figure 5.7. Primordial-Mantle normalized trace-element patterns of the representative volcanic rocks from the Gawuch and Drosh formations compared with volcanic rocks from type tectonic settings.

THE DROSH DIORITE COMPLEX

Fifteen samples from the intermediate to felsic plutonic rocks exposed in the studied area were analysed by using atomic absorption spectrophotometer and UV/visible spectrophotometer, while three were analysed by X-ray fluorescence (Table 5.2).

The intermediate plutonic rocks of the studied area are classified using scheme of Cox et al. (1979), adopted for plutonic rocks by Wilson (1989). According to this scheme (Fig 5.8), a great majority of the studied rocks classify as diorites. One sample plots as syeno-diorite, while three others have alkali contents too low to be plotted outside the limits of the diagram. Only one sample has $\text{SiO}_2 > 65$ wt% and classifies close to the field of granites, although it has low total alkali contents.

Major-Element Chemistry

The diorites of the studied area are characterized by intermediate to high SiO_2 content (55-65 wt%), intermediate to low alkali content (< 6 wt%), high Al_2O_3 (avg. 16.6 wt%), and intermediate to low MgO content (1-7 wt%). These compositional characteristics suggest a high aluminium basaltic or more precisely andesitic composition of the crystallizing magma. The analyzed diorites are metaluminous in characteristics, with the exception of three samples which are marginal between metaluminous and peraluminous (Fig 5.9). The diorites are predominantly calc-alkaline (Figures 5.10 and 5.11), although on the AFM diagram (Fig 5.11), two of the analyzed samples have high FeO/MgO ratio. In this diagram the studied diorites show great resemblance with that of the Kohistan batholith (Pettersson and Windley, 1985).

Table 5.2. Major and trace element chemistry of diorites and granodiorites from the Drosh area, Chitral.

SAMPLE	KG10	KG11a	KG11b	KG13	KG189	KG196	GL133	GL135	GL141	GL144	GOG38	GR84	GR95	GR96	GR97
SiO ₂	60.78	55.89	58.98	57.98	58.7	55.13	62.78	63.78	59.04	62.89	58.78	55.67	55.45	56.98	71.6
TiO ₂	0.63	0.55	0.39	0.41	0.85	0.52	0.75	0.51	0.72	0.51	0.44	0.36	0.41	0.41	0.17
Al ₂ O ₃	18.78	16.89	17.67	18.96	17.71	15.23	15.89	18.96	18.76	15.75	14.23	15.23	16.45	16.89	10.81
Fe ₂ O ₃	2.69	3.46	3.53	3.30	7.22	5.17	5.56	5.03	5.46	5.31	3.79	5.88	2.98	2.98	2.08
MnO	0.04	0.05	0.05	0.06	0.06	0.11	0.05	0.14	0.13	0.17	0.05	0.12	0.09	0.09	0.04
MgO	1.72	6.88	2.11	3.12	3.13	3.79	3.36	2.36	3.69	1.66	1.97	3.17	5.53	5.53	1.44
CaO	6.64	5.14	4.88	8.76	2.61	5.96	4.07	6.00	7.69	8.17	4.88	4.69	8.69	8.69	3.52
Na ₂ O	2.84	1.52	1.06	0.26	0.37	3.02	3.02	0.26	2.40	0.57	4.31	2.78	2.33	2.33	4.78
K ₂ O	2.66	4.06	3.84	4.46	3.82	1.43	2.51	0.23	0.91	0.99	2.42	2.71	1.39	1.39	0.42
P ₂ O ₅	0.10	0.02	0.20	0.20	0.15	0.57	0.17	0.16	0.15	0.12	0.54	0.30	0.14	0.14	0.04
LOI	1.63	6.32	6.86	2.14	5.37	8.45	2.42	2.15	0.99	2.94	7.50	8.34	4.93	4.60	5.11
TOTAL	98.51	100.78	99.57	99.65	99.99	99.38	100.58	99.58	99.94	99.08	98.91	99.25	98.39	100.03	100.01
Trace elements (ppm)															
Nb	-	-	-	-	16	-	-	-	-	-	-	-	2	-	3
Zr	-	-	-	-	168	-	-	-	-	-	-	-	31	-	60
Y	-	-	-	-	30	-	-	-	-	-	-	-	9	-	-
Sr	-	-	-	-	88	-	-	-	-	-	-	-	255	-	156
Rb	-	-	-	-	205	-	-	-	-	-	-	-	58	-	20
Cu	69	157	157	98	122	34	276	245	119	140	47	208	209	135	418
Pb	58	42	42	276	36	43	29	34	32	41	71	41	32	40	34
Zn	74	153	65	85	78	47	63	78	69	130	71	49	64	162	51
Ni	37	52	55	125	101	42	85	45	28	23	39	44	16	54	-
Cr	49	43	43	29	188	71	27	54	63	21	42	58	60	41	15
V	-	-	-	-	202	-	-	-	-	-	-	-	218	-	56
Ba	-	-	-	-	364	-	-	-	-	-	-	-	367	-	580
CO	43	24	62	41	17	34	44	46	53	49	45	1	58	58	13
Th	-	-	-	-	14	-	-	-	-	-	-	-	-	-	5
Sc	-	-	-	-	14	-	-	-	-	-	-	-	32	-	9
Ga	-	-	-	-	20	-	-	-	-	-	-	-	8	-	4
U	-	-	-	-	3	-	-	-	-	-	-	-	-	-	1

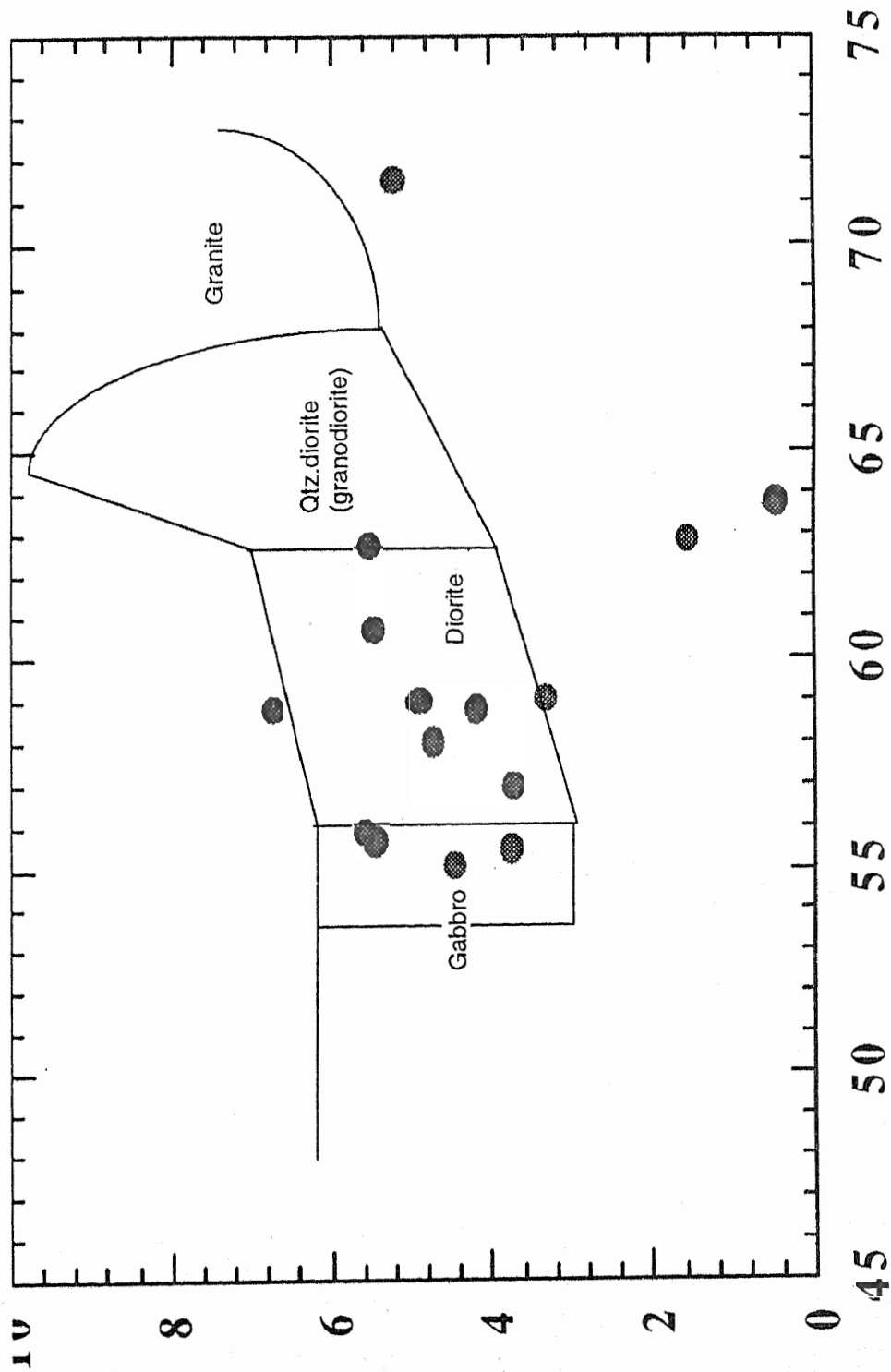


Figure 5.8. Classification of the plutonic rocks intruding the Gawuch Formation using Scheme of Cox et al (1979) adopted for plutonic rocks by Wilson et al.(1989).

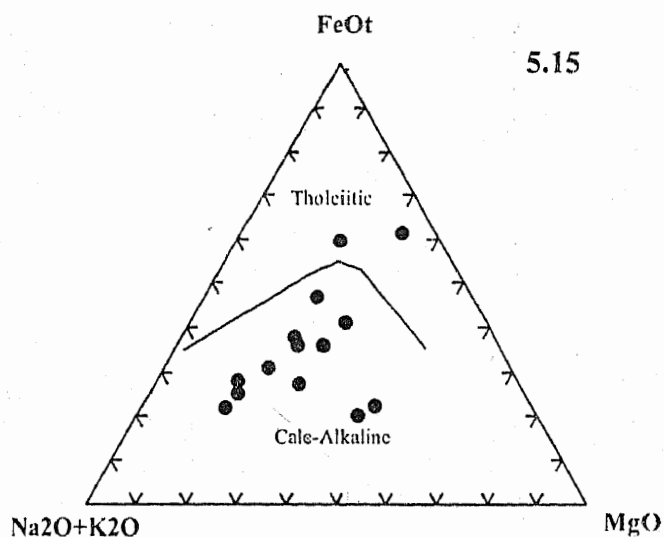
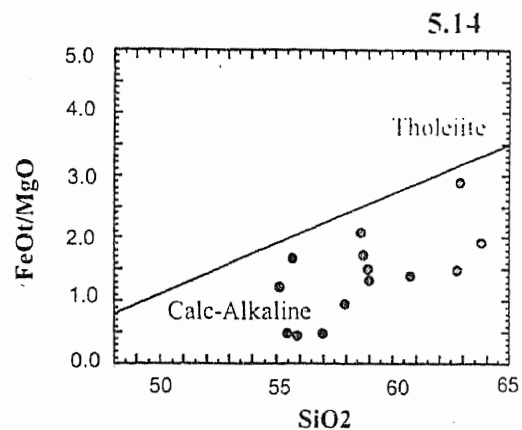
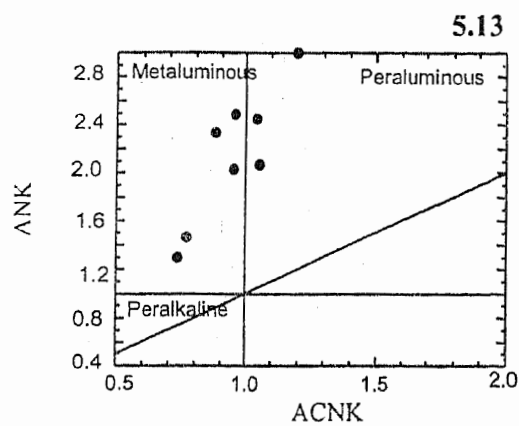


Figure 5.9. Classification of diorites from the Gawuch Formation on the basis of Shands indices (after Maniar and Piccoli, 1989).

Figure 5.10. SiO_2 versus FeO/MgO plot for diorites from the Gawuch Formation. The diagonal lines separates tholeiitic from calc-alkaline rocks (after Miyashiro, 1974).

Figure 5.11. AFM plot of Gawuch diorites. The line demarcating the division between calc-alkaline and tholeiitic after Irvine and Baragar (1971).

When plotted against SiO_2 as a fractionation index, MgO , shows regular depletion (Fig 5.12). TiO_2 and Fe_2O_3 show a slight initial enrichment but then become constant, suggesting attainment of a calc-alkaline trend of fractionation involving iron-bearing minerals. Surprisingly, CaO and $\text{K}_2\text{O}+\text{Na}_2\text{O}$ plots show a wide scatter. Al_2O_3 has vaguely defined positive correlation against SiO_2 . The variations at hand are insufficient to infer the sequence of fractionating minerals.

Trace-Element Chemistry

The variation in the incompatible trace elements is shown in the form of spidergram (Figure 5.13). All the three representative samples have slopes inclined towards right indicating large-ion lithophile elements (LILE) enrichment ($\sim 100 \times$ primordial mantle) compared to high-field strength elements (HFSE). Two of the three samples show distinct negative anomaly for Nb, a characteristic of subduction-related calc-alkaline magmas. The same two samples are rich in Sr and low in Ti. The LIL elements show a broad scatter suggesting post-crystallization remobilization of these elements.

Tectonic Setting of Magma Generation

The high-aluminium or andesitic characteristics of the magma are clearly reflected in the composition of the analyzed diorites. Such magmas are typically produced in subduction-related settings particularly at continental margins (Wilson, 1989). Figure (5.13) shows a multi-element pattern (normalized to primordial mantle) of three diorite samples analyzed by XRF. The patterns for all the three samples slope towards right. This implies that the studied rocks are characterized by high contents of large-ion lithophile elements compared to high-field strength elements. Additionally the patterns are characterized by the

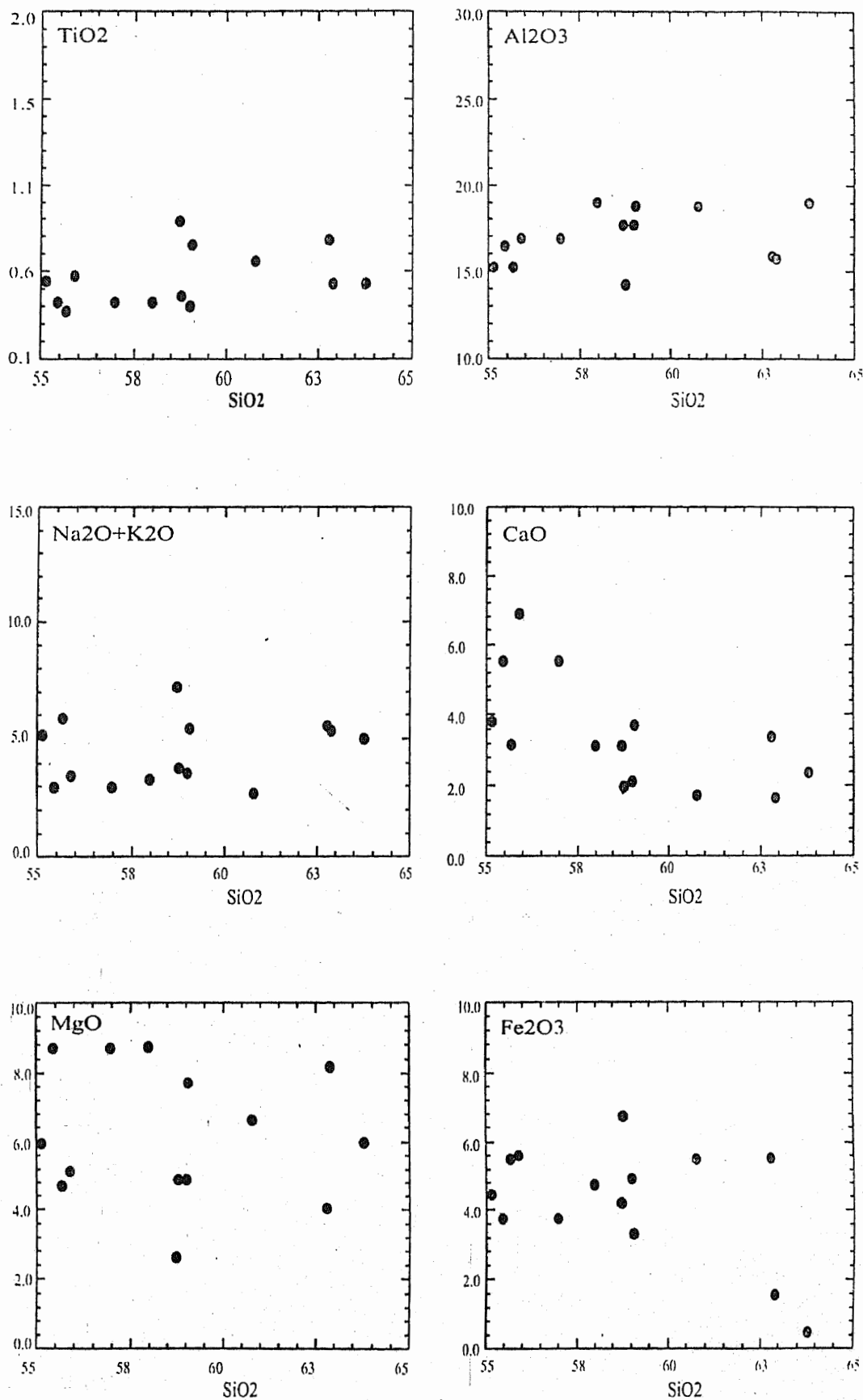


Figure 5.12. Variation in some major elements TiO₂, Al₂O₃, Fe₂O₃, MgO, CaO and Na₂O + K₂O in diorites from the Gawuch Formation with increasing degree of fractionation.

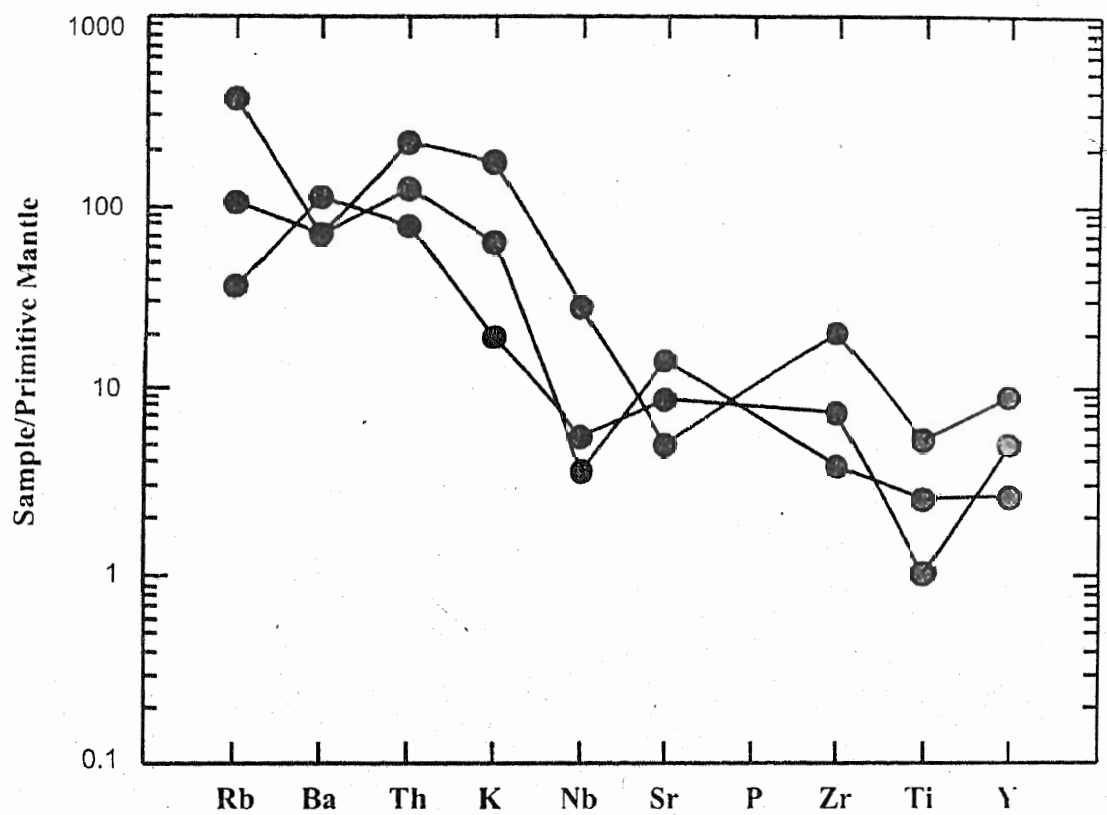


Figure 5.13. Mantle-normalized spider diagrams for the trace elements of dioritic rocks from the Gawuch Formation.

presence of negative Nb anomaly, positive Sr anomaly and low Ti contents. All these characteristics are consistent with a tectonic setting generating subduction-related magmas.

In the major-element based Fe-Mg-Al diagram (Pearce et al, 1977) the studied diorites cluster closely in the combined field of Island arc and continental margin (Fig 5.14a). The binary plot involving CaO and FeO+MgO (Figure 5.14b), all the studied diorites plot in the field covering island arc granitoids, calc-alkaline granitoids and collision-controlled granitoids. A similar tectonic setting is evident from a plot of $\text{FeO}^t / (\text{FeO}^t + \text{MgO})$ vs. Si (Figure 5.14c). Unfortunately, limited samples have been analyzed by using XRF which limit the use of other discrimination diagrams commonly in practice. In the Ti-Zr-Y triangular diagram (Fig 5.14d; Pearce and Cann, 1973), most of diorite samples fall in the fields defined for calc-alkaline basalt.

DISCUSSIONS AND CONCLUSIONS

Geochemical data, involving both major and trace elements, have been used to characterize the petrology and tectonic setting of the igneous rocks of the area. Metavolcanic rocks belonging to Gawuch and Drosh formations show different petrological lineage, the former are calc-alkaline while the latter are clearly tholeiitic. This raised the possibility that the volcanic rocks of the Drosh Formation, which are closely associated with the melange zone, could have tectonically escaped from the oceanic floor closed at the site of the Shyok suture. Detailed treatment in terms of mantle-normalized trace element patterns and discrimination diagrams involving immobile trace elements, however, suggested that the two group of volcanics, despite their different petrological character,

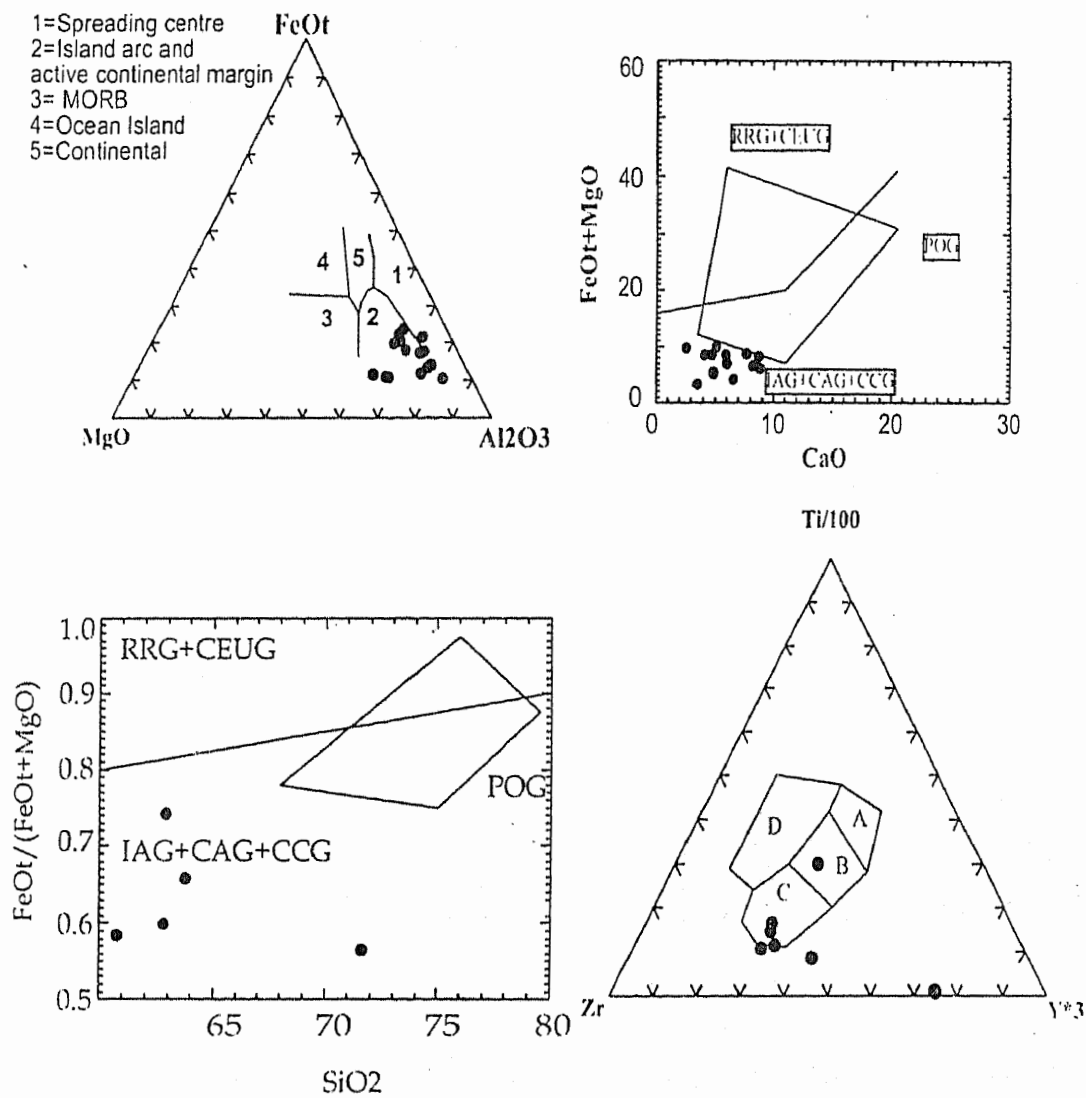


Figure 5.14. Different discrimination diagrams showing the tectonic setting of diorites from the Gawuch Formation. Note that a subduction-related origin is indicated in all the diagrams used.

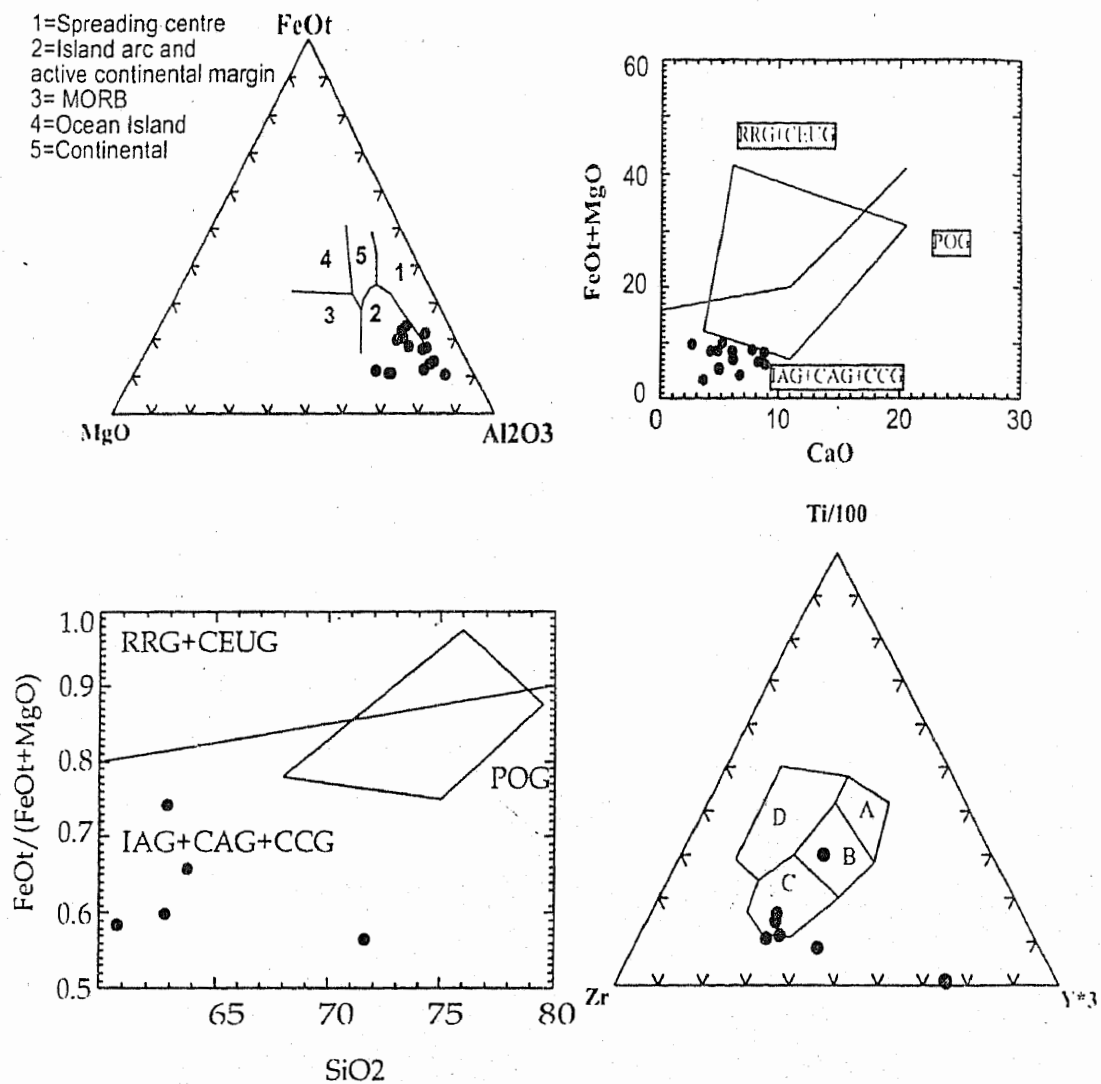


Figure 5.14. Different discrimination diagrams showing the tectonic setting of diorites from the Gawuch Formation. Note that a subduction-related origin is indicated in all the diagrams used.

originated with a strong subduction component. The present data are, however, not sufficient to deduce the exact position of these volcanics within the Kohistan arc system i.e., back arc, volcanic arc or fore arc. It may be noted that calc-alkaline and tholeiitic volcanics occur together in the entire Chalt volcanic belt in north Kohistan (Petterson and Windley, 1985). Sullivan et al (1993), in the context of Shamran part of the Chalt volcanic belt, suggested that calc-alkaline volcanics may be younger than the tholeiitic volcanics, correlatable with the Eocene volcanics of Utror (Kalam) and Dir area. This cannot be applied to the studied area around Drosh, since here the calc-alkaline Gawuch Formation volcanics are more highly metamorphosed than the tholeiitic Drosh volcanics. Precise age determinations using radiometric systems like $Ar_{40}-Ar_{39}$ (amphibole) and U-Pb (zircon) are needed to resolve the relationship between calc-alkaline and tholeiitic volcanics in northern Kohistan.

The suite of analyzed diorites is calc-alkaline in its petrology and contains strong subduction component. It has not been possible to confirm the continental margin setting for these diorites, as opposed to intraoceanic island arc. Since the diorites of the study area are probably related with the pluton at Lowari Pass, for which an age of 40 -45Ma is available (Zeitler et al., 1982), a continental margin tectonic setting of origin can be assigned to the diorites of the study area. The island-arc/continental margin setting of volcanic and dioritic rocks from the studied area constrain a subduction-related origin for the Cu mineralization in the Drosh area.

CHAPTER 6

GEOLOGY OF THE MINERALIZED ROCKS

The mineralized rocks of the study area are divided in to three units on the basis of field and petrographic observations. These are:

1. Sulfide-bearing quartz veins.
2. Sulfide-bearing altered diorites.
3. Sulfide-bearing shear zones.

1. SULFIDE-BEARING QUARTZ VEINS

Numerous quartz veins along fractures and fissures intrude the rocks of the area. These veins are usually one mm to more than 35 cm in length and about 0.5 mm to 15 cm in width. These veins are mainly composed of quartz with small amounts of carbonate, sericite and muscovite. Few grains of feldspars are also seen. Among the ores, tetrahedrite, and at places galena are the dominant phases with small amounts of sphalerite, chalcopyrite and pyrite. Azurite and malachite occur mainly along the mineralized zone (Plate 6.1 and 6.2).

Quartz (up to 90-vol.%) is the dominant mineral phase in these veins. It occurs as subhedral to anhedral, fine- to medium-grained material. The large grains of quartz are strained as suggested by the fractures and undulose extinction. Carbonates, muscovite and sericite mainly occur as fine-grained material along the fractures and interstices of quartz.

Tetrahedrite (5-60 vol.%) occurs as irregular grains within the interstices of quartz. It is massive, highly fractured and has enclosed the anhedral to subrounded grains of quartz. In some thin sections it is present in the form of fine- to medium-grained dissemination. Galena, if present, is usually associated with

CHAPTER 6

GEOLOGY OF THE MINERALIZED ROCKS

The mineralized rocks of the study area are divided into three units on the basis of field and petrographic observations. These are:

1. Sulfide-bearing quartz veins.
2. Sulfide-bearing altered diorites.
3. Sulfide-bearing shear zones.

1. SULFIDE-BEARING QUARTZ VEINS

Numerous quartz veins along fractures and fissures intrude the rocks of the area. These veins are usually one mm to more than 35 cm in length and about 0.5 mm to 15 cm in width. These veins are mainly composed of quartz with small amounts of carbonate, sericite and muscovite. Few grains of feldspars are also seen. Among the ores, tetrahedrite, and at places galena are the dominant phases with small amounts of sphalerite, chalcopyrite and pyrite. Azurite and malachite occur mainly along the mineralized zone (Plate 6.1 and 6.2).

Quartz (up to 90-vol.%) is the dominant mineral phase in these veins. It occurs as subhedral to anhedral, fine- to medium-grained material. The large grains of quartz are strained as suggested by the fractures and undulose extinction. Carbonates, muscovite and sericite mainly occur as fine-grained material along the fractures and interstices of quartz.

Tetrahedrite (5-60 vol.%) occurs as irregular grains within the interstices of quartz. It is massive, highly fractured and has enclosed the anhedral to subrounded grains of quartz. In some thin sections it is present in the form of fine- to medium-grained dissemination. Galena, if present, is usually associated with

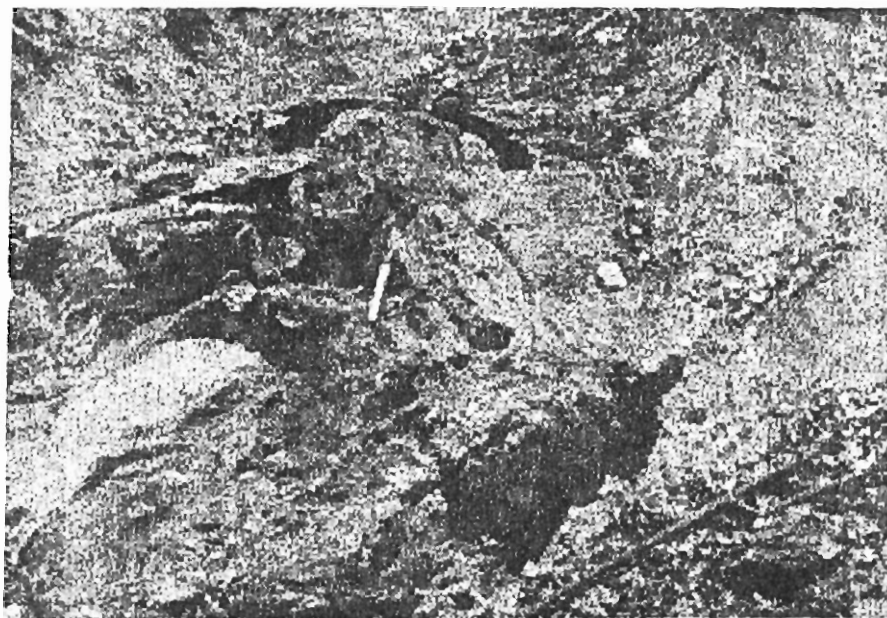


Plate 6.1. Photograph showing a one meter thick mineralised zone associated with a quartz vein. Malachite and azurite (green and bluish green in colour) occur as supergene enrichment along the mineralised zone.

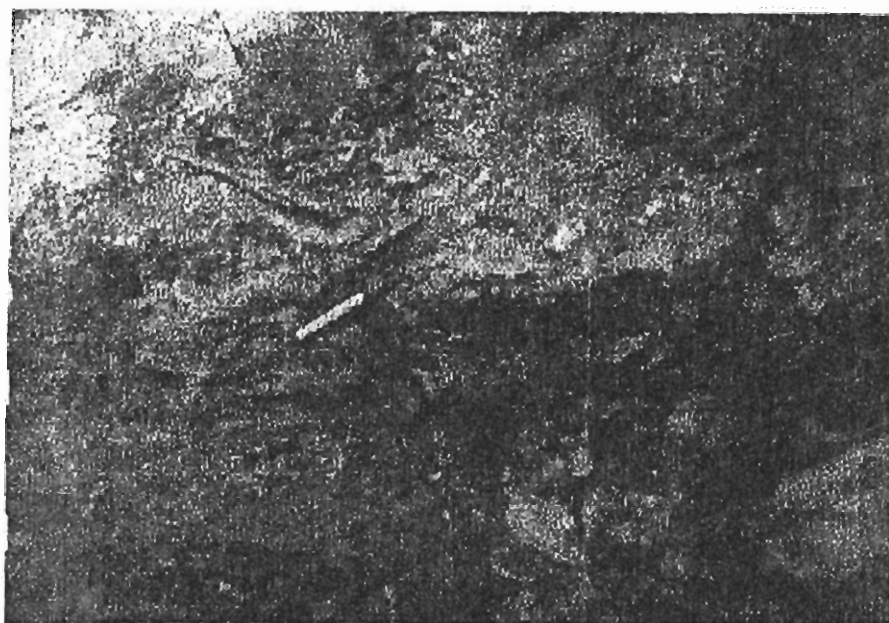


Plate 6.2. Photograph of the same mineralised zone as above which is vanishing as the quartz vein pinches out.

tetrahedrite, (Plate 6.3) and at times has intergrown with it. Tetrahedrite contains small inclusions of chalcopryite. In rare cases, chalcopryite occurs as relicts in large grains of tetrahedrite (Plate 6.4a and 6.4b). The oxidation of tetrahedrite is a common feature of these rocks particularly along the oxidized zones (Plate 6.5). Here, the tetrahedrite is oxidized to magnetite, azurite and malachite along the fractures and at the margins. In some rocks tetrahedrite in the quartz veins shows replacement to chalcocite along the fractures (Plate 6.6).

Galena (5-20 vol.%) is the second dominant ore phase in the quartz veins. It is generally medium- to coarse-grained, anhedral to subhedral and exhibits typical triangular pits at the surface (Plate 6.7a, 6.7b). Galena is usually associated with tetrahedrite and is commonly intergrown with it. However, in some thin sections it exhibits intergrowth with chalcopryite, pyrite and sphalerite. At places galena is precipitated along fractures within the quartz veins (Plate 6.7b).

Chalcopryite (3-5 vol.%) is brass yellow in the reflecting light and is usually disseminated as fine- to medium-grained grains within the quartz veins. Additionally, it occurs as inclusions in the tetrahedrite grains. Rarely, however, it occurs as relicts in the tetrahedrite grains. In some cases, chalcopryite occurs as medium- to coarse-grained irregular masses within the interstices of quartz grains. This type of chalcopryite is mainly altered along fractures and margins to magnetite and limonite. At places the chalcopryite is completely or partially replaced by magnetite and limonite.

Sphalerite (6-10 vol.%) is gray in reflected light and brown in polarized light. It is present as irregular masses within the interstices and fractures of the pre-existing silicate phases. It is mostly associated with or has intergrown with

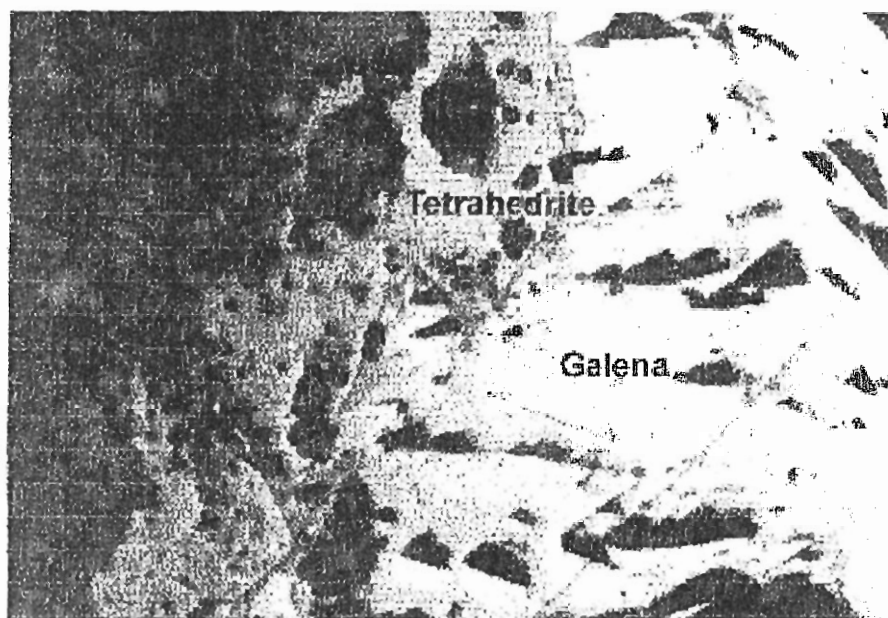


Plate 6.3. Photomicrograph showing a large grain of galena in contact with an irregular grain of tetrahedrite. Note the presence of triangular pits in galena (X4, reflected light).

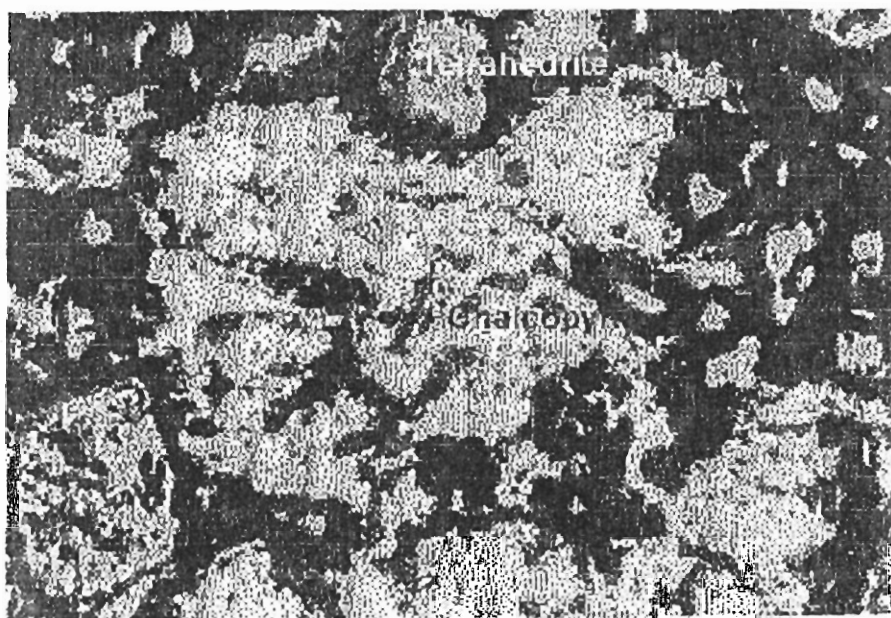


Plate 6.4a. Photomicrograph showing irregular grains of chalcopyrite within the tetrahedrite grains in a quartz vein (reflected light (X4, reflected light)).

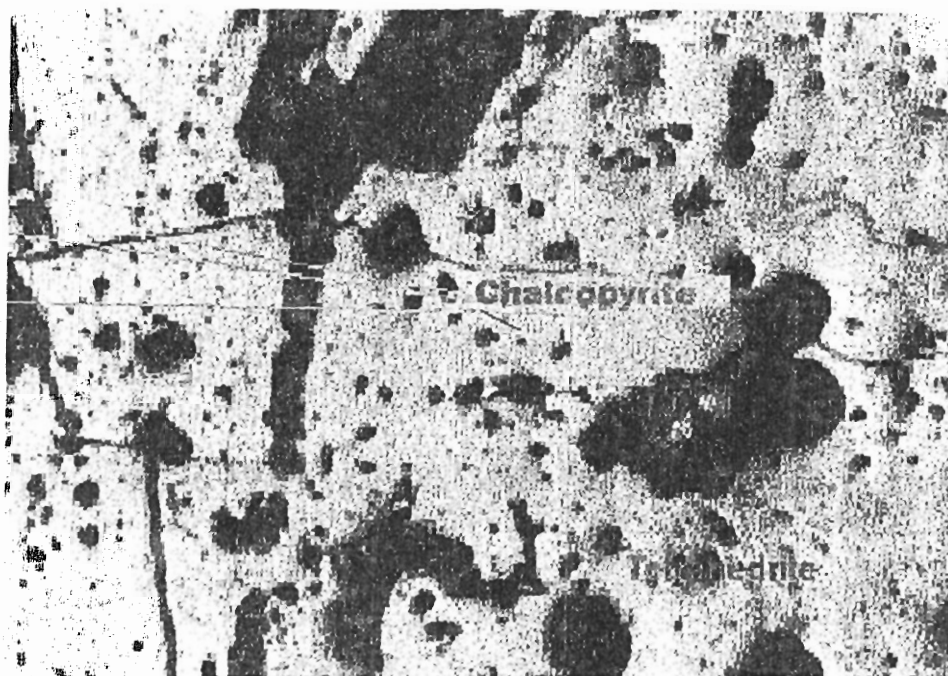


Plate 6.4b. Photomicrograph showing a grain of tetrahedrite as viewed in the reflected light. Note the presence of inclusions of chalcopyrite. The tetrahedrite shows oxidation to limonite material along fractures.

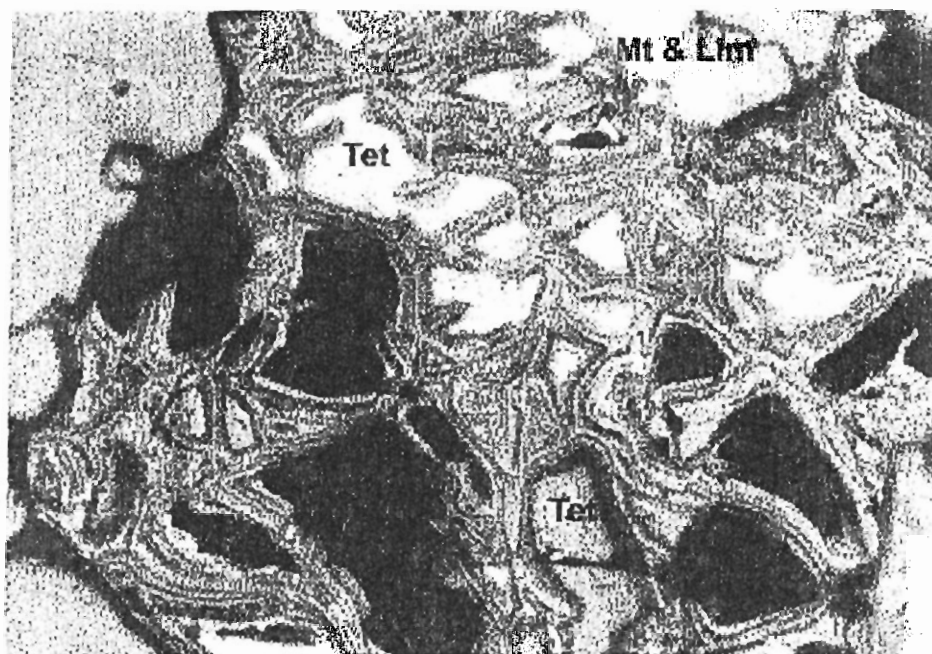


Plate 6.5. Photomicrograph of a tetrahedrite (Tet) grain in the reflected light showing oxidation alteration to magnetite (Mt) and limonite (lm) at the margins and along the fractures. Note that the tetrahedrite host is now left as relics.

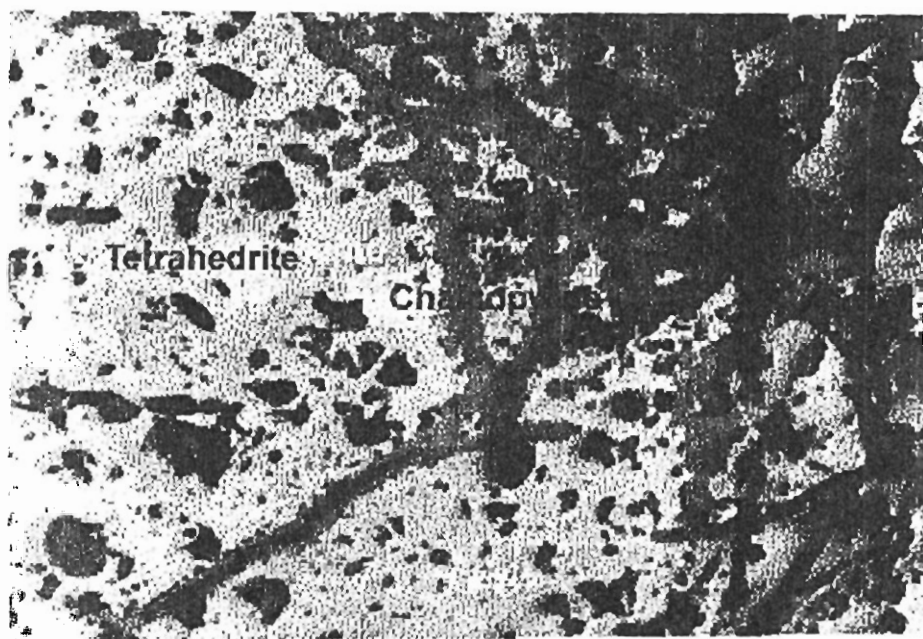


Plate 6.6. Photomicrograph of a tetrahedrite grain in the quartz veins showing replacement to chalcocite along the fractures.

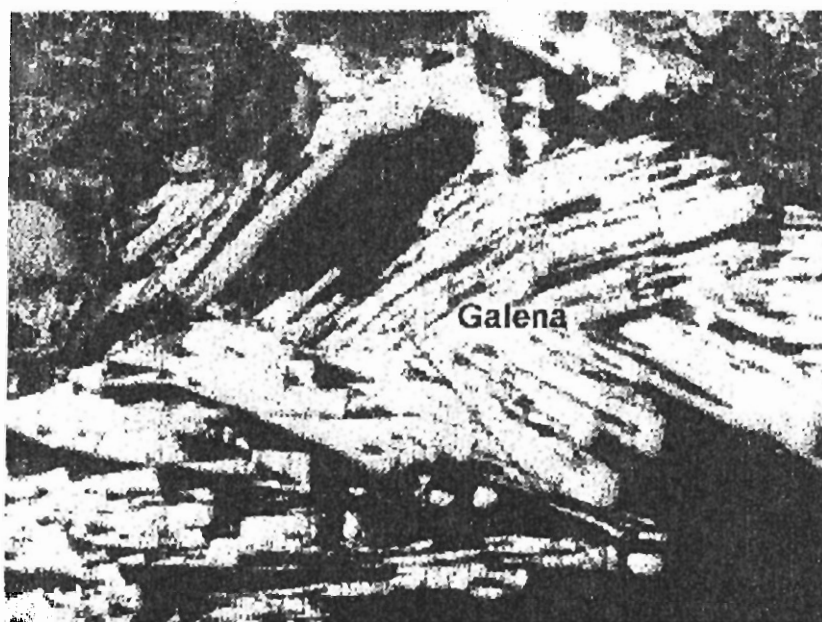


Plate 6.7a. Photomicrograph showing an irregular and fractured grain of galena with typical triangular pits. The abnormal morphology suggests strain post-dating the mineralisation.



Plate 6.7b. Photomicrograph of a galena grain (bright-white reflectance) in a quartz veins. Note the irregular grain boundaries suggesting precipitation in a pre-existing fracture.

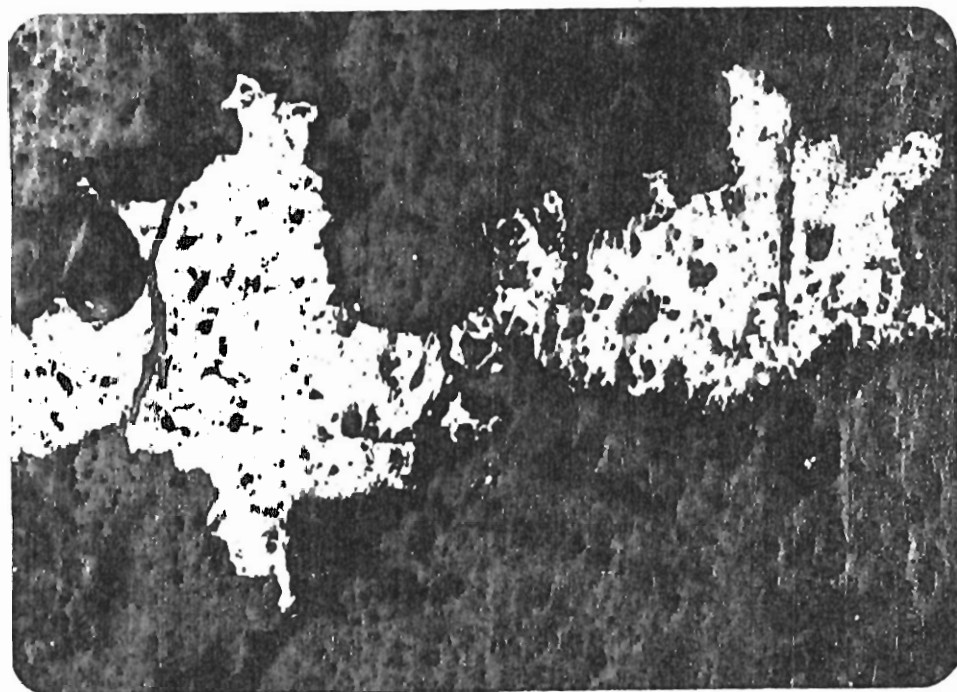


Plate 6.8. Photomicrograph showing irregular grains of pyrite (bright reflectance) in a quartz vein (X4).

chalcopyrite, pyrite and galena, suggesting simultaneous crystallization. In some sections, sphalerite contains small micron-size blebs and rods of chalcopyrite resembling what is termed as the chalcopyrite disease (Eldridge, 1983).

Pyrite (less than 2 vol.%) occurs as cubic to subhedral and irregular disseminated grains (Plate 6.8 and 6.9). Some of the pyrite grains are fractured and contain chalcopyrite as a fracture-filling material.

Azurite and Malachite (<1 vol.%) are usually present as supergene enrichment within the oxidized zones. In thin section, these are observed to be located along the microfractures and along the boundaries of the ore minerals as stained material.

Bornite (traces) is pinkish brown to purplish violet in reflected light. It occurs as anhedral prismatic grain associated with pyrite and chalcopyrite.

The textural characteristics of the silicate and ore phases in the quartz veins suggest that the ore phases precipitated along the interstices and fractures in the pre-existing quartz grains. This could be due to the later remobilization of the ore phases. The intergrowth textures between the various phases, especially tetrahedrite, galena, chalcopyrite and sphalerite suggest a simultaneous crystallization of these phases from the hydrothermal solutions. However, the presence of chalcopyrite as inclusions and some times as relicts in the tetrahedrite grains suggest that the chalcopyrite crystallized earlier than the rest of the ore phases. However, the chalcopyrite is intergrown with the other ore phases (e.g., galena, sphalerite) and in rare cases, as a fracture-filling material (e.g., in pyrite), suggesting several generations of its precipitation.

2. SULFIDE-BEARING ALTERED DIORITES

Both the mineralized and unmineralized diorites have the same silicate mineralogy but the latter contain greater proportions of alteration phases such as carbonate, kaolinite, sericite, epidote and muscovite. The principal difference between these rocks is the development of various ore phases in the mineralized rocks. The petrography of the unmineralized diorites is already discussed in Chapter 4, therefore only the prominent features of the silicate mineralogy are listed below.

Feldspar, including both plagioclase and alkali feldspar, occurs as anhedral grains, commonly altered to carbonate, sericite, kaolinite and epidote furnishing a cloudy appearance to the mineral. Usually the alteration is so intense that the feldspar grains, especially plagioclase, are completely altered and pseudomorphs after plagioclase and relics are well seen in the thin section. The samples collected from the shear zones have a greater proportion of chlorite and epidote with lesser amount of hornblende.

Among the ore minerals, chalcopyrite, tetrahedrite, sphalerite and pyrite are prominent. Magnetite, limonite, azurite and malachite occur only in the oxidized zones.

Chalcopyrite (5-15 vol.%) is the dominant copper-bearing phase in these diorites. It is generally present as irregular grains within the fractures and interstices of the silicate phases. This type of chalcopyrite has common intergrowth textures with tetrahedrite and sphalerite (Plate 6.10). Fine-grained chalcopyrite in the form of aggregates is also found disseminated in the rocks.

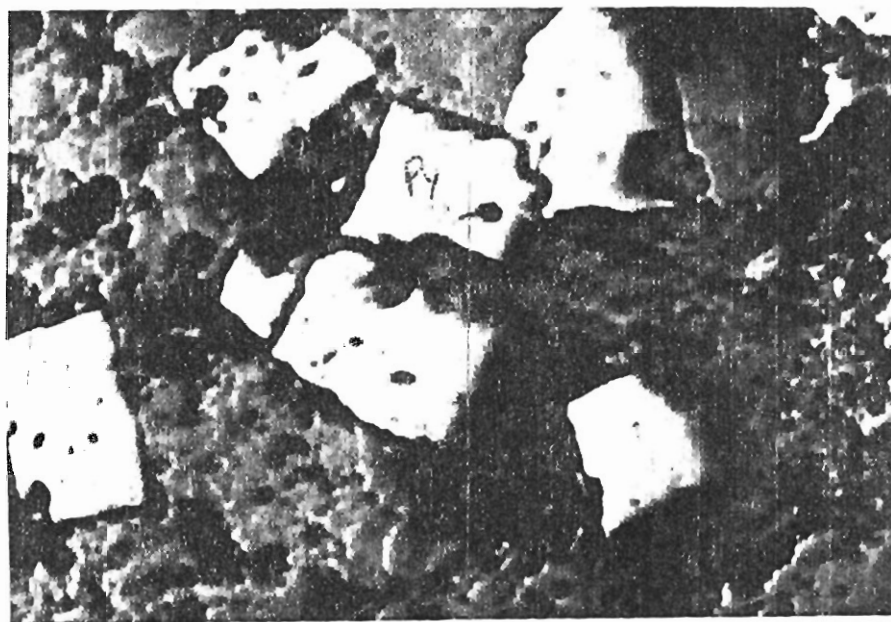


Plate 6.9. Photomicrograph showing cubic to subcubic grains of pyrite (bright reflectance) as observed in reflected light (X4).

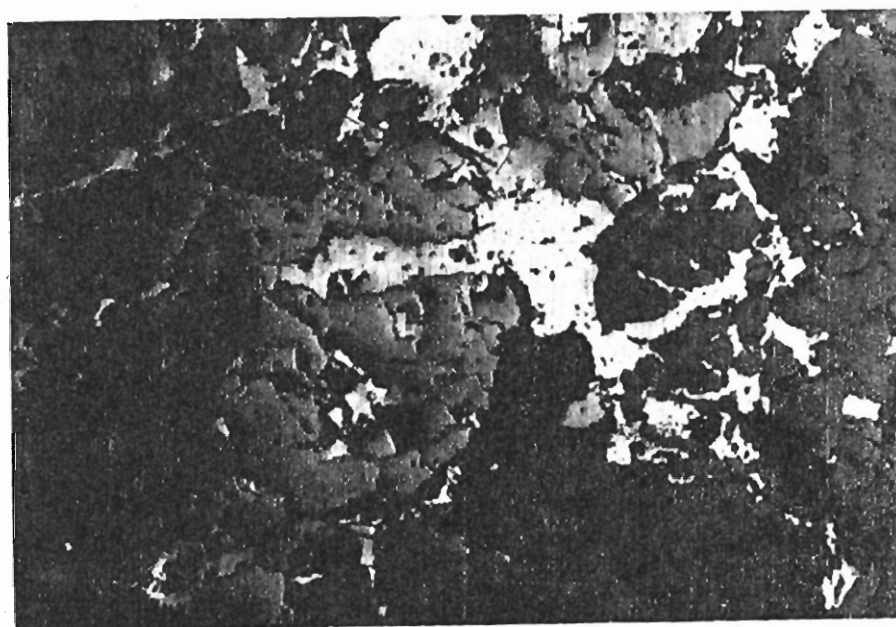


Plate 6.10. Photomicrographs showing intergrowth between tetrahedrite (high relief, pinkish grey) and chalcopyrite (low relief, yellow) suggesting simultaneous crystallization of the two phases.

Pyrite (up to 10 vol.%) is yellowish white in reflected light. It occurs as fine- to medium-grained euhedral to subhedral grains and is cubic in form. It commonly occurs as fracture-fill material along with chalcopryite (Plate 6.11).

Sphalerite (2-8 vol.%) is yellowish brown to reddish brown and forms isolated irregular grains. Occasionally intergrown with chalcopryite. It also occurs in interconnected ameboidal masses.

Tetrahedrite (up to 5 vol.%) is another copper-bearing phase in these diorites. It occurs as fine- to medium-grained irregular mass associated with chalcopryite. In some cases tetrahedrite replaces the chalcopryite along the margins and fractures. In other cases, tetrahedrite itself is altered to azurite.

Magnetite (5-30 vol.%) is gray in reflected light with brownish tint. It is fine- to medium-grained and occurs as an irregular grain as well as fine-grained material disseminated through out the rock. It is also present along the fractures and margins of chalcopryite, tetrahedrite and pyrite as the replacement product and is mainly associated with limonite.

Azurite, malachite and limonite occur as alteration products mostly along the fractures and at the margins of the sulfide phases (Plate 6.12, 6.13).

3. SULFIDE-BEARING SHEAR ZONES

Shearing along local faults is a common feature of the rocks in the studied area. These shear zones are usually up to 5 m in thickness. The rocks in the shear zones are intensively fractured, mylonitized and schistose. Quartz and carbonate veining and the precipitation of the ore phases in these veins and also along the foliation planes is a common feature. The supergene enrichment of azurite,

malachite and limonite at the rock surface is a common feature of this zone (Plate 6.12).

The rock samples collected from these shear zones are dominantly (up to 70 vol.%) composed of carbonates, quartz, sericite, kaolinite, epidote, muscovite, chlorite with relics and pseudomorphs of feldspars. Among the ore minerals, tetrahedrite, magnetite, galena, pyrite, chalcopyrite and chalcocite are identified. Magnetite, azurite, malachite and limonite are common alteration products.

Calcite (30-60 vol.%) is the dominant carbonate phase with lesser amount of siderite. It is fine- to medium-grained in size and occurs as isolated aggregates arranged parallel to the foliation. At places it occurs as a mosaic of equigranular grains surrounded by opaque minerals.

Quartz (up to 30 vol.%) is fine- to medium-grained. No fresh grains of plagioclase and alkali-feldspar are observed in the thin sections. All grains are partially or completely altered to carbonates, sericite, kaolinite and epidote. The relics and pseudomorphs of these feldspar are visible within a mass of these alteration phases.

Magnetite (5-25 vol.%) is gray in reflected light with brownish tint. It is fine-medium grained in size and occurs as euhedral, subhedral and even skeletal crystals and anhedral polycrystalline aggregates. The fine-grained variety occurs in dissemination, and probably represents the primary phase. The medium-grained phase occurs in the form of irregular masses and is commonly the product of pseudomorphic replacement of pyrite and chalcopyrite. In some thin sections, it is present as irregular interstitial phase and enclosing rounded to subrounded quartz grains. It also occurs as elongated blades and form box work

type texture in these rocks. Magnetite is generally associated with pyrite, chalcopyrite, chalcocite but at places it replaces pyrite, chalcopyrite and chalcocite along the fractures and at the margins.

Pyrite (5-15 vol.%) occurs as medium to fine grained crystalline aggregate. The medium-grained pyrite is generally fractured and these fractures are filled with chalcopyrite. In some rocks the pyrite occurs in two types, one as early euhedral phase and the other as a late anhedral phase. The former phase is present as cubes, which are fractured and disseminated throughout the rock. The later phase is usually associated with chalcopyrite and is intergrown with chalcopyrite. At places, pyrite also occurs as small disseminated anhedral grains either alone or intergrown with chalcopyrite. In some samples pyrite appear to have corroded and weathered along margins and at the surface and thus form coliform texture.

Chalcopyrite (5-20 vol.%) is white to brass yellow in colour. it is present as fine- to coarse-grained anhedral to subhedral grains (Plate 6.14) and it is commonly found in association with magnetite and pyrite. In some rocks chalcopyrite is distributed as irregular veinlets and small disseminated grain. At places, chalcopyrite is fractured and precipitated as microveins along the foliation planes. Chalcopyrite is generally oxidized along its margin and fractures to magnetite and limonite.

Limonite, azurite and malachite are the secondary minerals formed due to the oxidation of the sulfide minerals. Limonite is dark red in colour, while azurite and melachite have their typical blue and green colours, respectively. These occur in close association with each other, within the fractures and at the

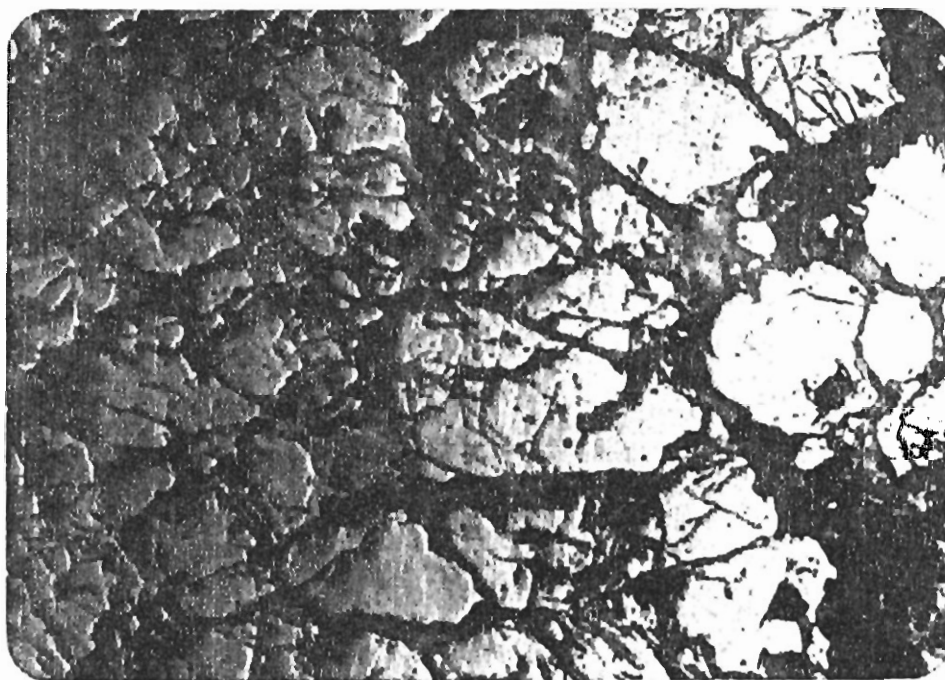


Plate 6.11. Photomicrograph showing fractured pyrite (high relief). The fractures are filled by the chalcopyrite (low relief, yellow) suggesting later crystallization relative to pyrite (X4).



Plate 6.12. A field view of the altered diorites showing surface staining due to the supergene enrichment of azurite and malachite.

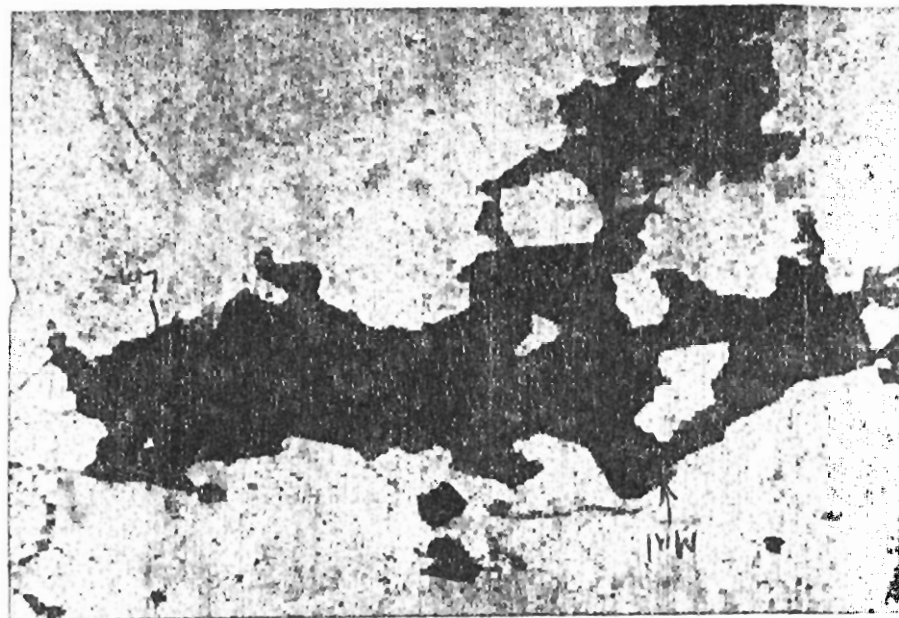


Plate 6.13. Photomicrograph showing the precipitation of malachite (dark bluish-green) and limonite (orange brown) along fractures within the altered diorites (X4).

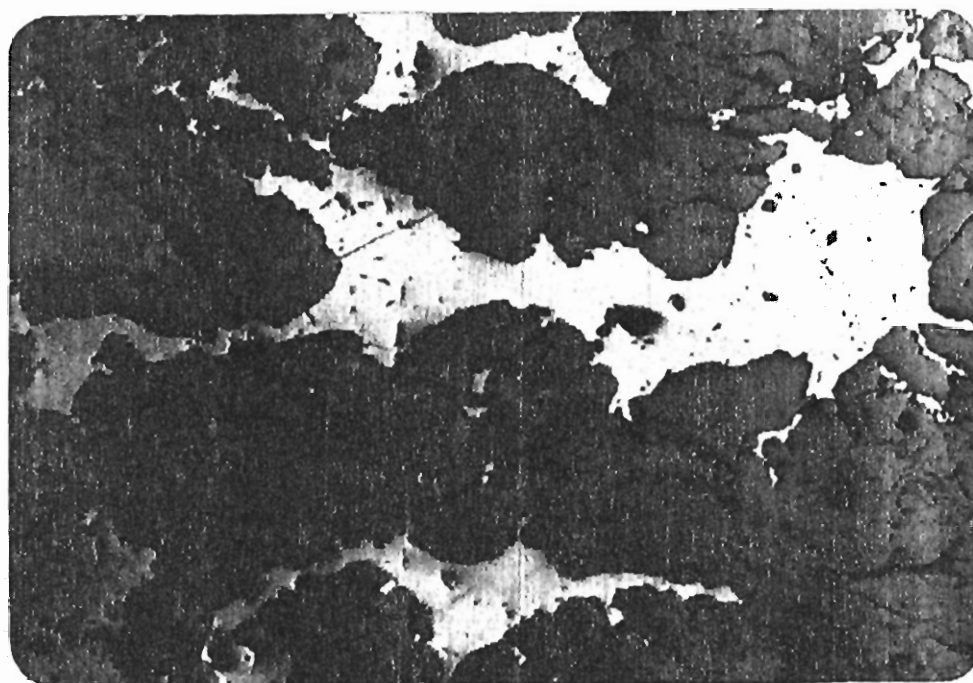


Plate 6.14. Photomicrograph showing irregular grains of chalcopyrite (low-relief, yellow) which are precipitated as interstitial phase to the silicates (high relief, grey).

margins of the sulfide minerals. These minerals form concentric bands and also show staining at the surface.

TYPES OF COPPER MINERALIZATION

Based on field observation four types of copper mineralizations are observed in the area.

1. Copper mineralization along quartz veins.
2. Copper mineralization along foliation planes.
3. Disseminated Copper mineralization.
4. Supergene enrichment of Copper.

1. Copper Mineralization along Quartz Veins

A large number of quartz veins intrude the altered diorites in the Gawuch Formation. Most of these veins are enriched with copper-bearing sulfides and oxides, such as tetrahedrite, galena, chalcopyrite, pyrite, sphalerite and magnetite. These phases occur as coarse-grained irregular masses in the interstices between the quartz grains.

2. Copper Mineralization along the Foliation Planes

Copper mineralization in the form of tetrahedrite and chalcopyrite along with other sulfide phases like galena, sphalerite, chalcocite and pyrite are generally present along foliation planes in the zone of intense shearing. These ore phases are usually precipitated along foliation planes in the form of microveins or thin bands of carbonates and quartz.

3. Disseminated Copper Mineralization

Copper mineralization in the form of chalcopyrite and tetrahedrite is disseminated mainly in the diorites. Chalcopyrite is dominant phase and occurs as

fine- to medium grained interstitial phase. Cubic grains of pyrite are also found in association with chalcopyrite and tetrahedrite.

ORE MINERALOGY

Identification of the ore minerals, in this study, is based on microscopic, electron microprobe and in some cases, X- ray diffraction investigation. The electron microprobe analysis were performed on Cameca automated SX 50 Electron Microprobe at the University of South Carolina, USA, while the X-Ray Diffraction analyses were carried out on a Rigaku XRD at the NCE in Geology, University of Peshawar. The ore minerals observed in the mineralized quartz veins, diorites/ granodiorites are tetrahedrite, chalcopyrite, galena, pyrite, sphalerite, bornite and magnetite.

Tetrahedrite

Tetrahedrite is the most abundant copper-bearing phase, both in the quartz veins as well as in mineralized diorites/granodiorites. It occurs as a coarse grained irregular mass, mostly filling the interspaces of silicate phases and also along their fractures. Occasionally tetrahedrite encloses the silicate phases, especially quartz. It is intimately associated with chalcopyrite and galena. At places tetrahedrite is highly fractured and is generally replaced by chalcocite and bornite along fractures. While in other samples it appears to be replacing chalcopyrite too. In some sections, shows alteration to magnetite at its margin.

Electron microprobe analyses show the tetrahedrite to be stoichiometric $(\text{CuFeZn})_{12}(\text{SbAs})_4\text{S}_{13}$. Rim to core relationship in a single grain does not show any significant compositional variation (Table 6.1). This suggests a homogenous nature of the tetrahedrite. Tetrahedrite shows less variation in Cu (40.10 to 42.84),

Table 6.1 Microprobe analyses of ore minerals from the Gawuch Formation, Drosh, Chitral.

TETRAHEDRITE

Sample	GR 71	GR 71	Gr 71	GR 71	GR 72	GR 72	GOG 19	GOG 19	GOG 19	GOG 19	GR 81
Area	Rim	Core	Rim	Rim	Rim	Core	Rim	Core	Rim	Rim	Core
Cu	40.37	40.28	40.86	40.10	41.68	40.97	41.75	41.42	41.87	42.84	41.12
Zn	6.67	6.67	6.82	6.66	6.97	6.89	5.81	5.58	5.52	5.74	5.35
As	10.51	9.27	9.20	9.86	12.21	10.74	15.73	15.03	16.82	17.48	10.66
Si	0.00	0.00	0.00	0.00	0.00	0.00	0.00	0.00	0.00	0.00	0.00
S	26.31	26.27	26.26	25.96	26.68	26.31	27.16	27.21	27.16	27.33	25.48
Pb	0.00	0.00	0.00	0.00	0.00	0.00	0.00	0.00	0.00	0.00	0.00
Ag	0.19	0.31	0.31	0.32	0.14	0.13	0.11	0.15	0.26	0.11	0.31
Sb	15.68	17.07	17.51	16.51	13.2	14.48	7.56	8.60	5.86	5.23	13.99
Mn	0.00	0.05	0.00	0.02	0.00	0.00	0.00	0.00	0.00	0.00	0.00
Fe	1.20	1.18	1.14	1.08	1.31	1.15	2.28	2.14	2.68	2.60	2.15
Total	100.94	101.11	102.09	100.50	102.10	100.67	100.39	100.13	100.16	101.32	99.05

Atomic Proportions

Sum=29

Cu	9.96	9.97	10.05	9.99	10.06	10.08	9.99	9.96	9.99	10.09	10.30
Zn	1.60	1.61	1.63	1.61	1.64	1.65	1.35	1.31	1.28	1.31	1.30
As	2.20	1.95	1.92	2.08	2.54	2.24	3.19	3.07	3.40	3.49	2.26
S	12.86	12.89	12.80	12.81	12.77	12.83	12.88	12.98	12.84	12.75	12.65
Sb	2.02	2.21	2.25	2.15	1.65	1.86	0.94	1.08	0.73	0.64	1.83
Fe	0.34	0.33	0.32	0.31	0.36	0.32	0.62	0.59	0.73	0.70	0.61

GALENA

Sample	KG 225	KG 225	KG 225	KG 225	GOG 22	GOG 36	GOG 36	GOG 36	GL 54	GL 54
Area	Rim	Core	Rim	Rim	Core	Rim	Core	Rim	Rim	Core
Cu	0.00	0.00	0.00	0.00	0.00	0.00	0.00	0.00	0.00	0.00
Zn	0.00	0.00	0.00	0.04	0.00	0.00	0.00	0.00	0.00	0.00
As	0.00	0.01	0.00	0.00	0.25	0.00	0.00	0.00	0.04	0.00
Si	0.10	0.02	0.11	0.18	0.12	0.00	0.00	0.00	0.12	0.12
S	12.38	12.88	12.20	12.89	12.20	13.36	13.35	12.68	12.55	12.23
Pb	86.37	86.09	86.97	86.85	86.34	87.53	86.09	85.34	86.78	86.76
Ag	0.00	0.01	0.04	0.00	0.00	0.01	0.00	0.00	0.00	0.00
Sb	0.04	0.00	0.06	0.03	0.08	0.09	0.00	0.00	0.01	0.01
Mn	0.02	0.00	0.02	0.00	0.00	0.02	0.00	0.00	0.00	0.00
Fe	0.02	0.02	0.01	0.00	0.00	0.00	0.00	0.00	0.00	0.02
Total	98.94	99.03	99.39	99.98	98.99	101.01	99.45	98.02	99.49	99.13

Atomic Proportions

Sum=2

S	0.96	0.98	0.95	0.98	0.95	0.99	1.00	0.98	0.97	0.95
Pb	1.04	1.02	1.05	1.02	1.05	1.01	1.00	1.02	1.03	1.05

PYRITE

Sample	KG 225	KG 225	KG 225	GOG 36	GOG 36	GOG 36	GOG 24	GOG 24	GOG 24
Area	Rim	Core	Rim	Rim	Core	Rim	Rim	Core	Rim
Cu	0.06	0.08	0.06	0.00	0.05	0.05	0.08	1.00	0.25
Zn	0.05	0.05	0.08	0.01	0.06	0.05	0.04	0.03	0.03
As	0.04	0.04	0.05	0.00	0.00	0.00	0.00	0.01	0.00
Si	0.00	0.00	0.00	0.00	0.00	0.00	0.00	0.00	0.00
S	53.56	52.99	53.50	53.56	53.49	53.53	54.44	53.00	53.10
Pb	0.00	0.00	0.00	0.00	0.00	0.00	0.00	0.00	0.00
Ag	0.00	0.00	0.00	0.00	0.00	0.00	0.00	0.00	0.00
Sb	0.00	0.00	0.00	0.00	0.00	0.00	0.00	0.00	0.00
Mn	0.00	0.00	0.00	0.00	0.00	0.00	0.00	0.00	0.00
Fe	46.94	47.00	46.50	47.10	47.20	47.85	38.59	46.80	50.00
Total	100.65	100.16	100.19	100.67	100.80	101.48	93.15	100.84	103.38

Atomic Proportions

Sum=3

S	1.99	1.98	2.12	2.00	1.95	1.98	2.13	1.99	1.95
Fe	1.01	1.02	0.88	1.00	1.05	1.02	0.87	1.01	1.05

CHALCOPYRITE

Sample	GR 72	GR 72	GOG 24	GOG 24	GOG 24	GR 81b	GR 81b	GR 81b
Area	Rim	Core	Rim	Core	Rim	Rim	Core	Rim
Cu	35.04	34.81	33.05	33.50	33.06	35.73	35.26	35.07
Zn	0.05	0.04	0.00	0.05	0.04	0.05	0.00	0.00
As	0.07	0.06	0.05	0.02	0.05	0.04	0.12	0.08
S	34.80	35.00	34.75	34.75	34.10	34.97	34.87	34.92
Pb	0.00	0.00	0.00	0.00	0.00	0.00	0.00	0.00
Ag	0.00	0.00	0.00	0.08	0.08	0.00	0.02	0.00
Sb	0.01	0.02	0.00	0.03	0.01	0.00	0.00	0.01
Mn	0.02	0.00	0.00	0.00	0.00	0.00	0.00	0.00
Fe	30.00	29.89	30.29	31.09	31.09	30.04	30.28	30.28
Total	99.99	99.82	98.14	99.52	98.43	100.83	100.55	100.36

Atomic Proportions

Sum=4

Cu	1.01	1.01	0.97	0.97	0.97	1.03	1.02	1.01
S	2.00	2.01	2.02	2.00	1.99	1.99	1.99	2.00
Fe	0.99	0.98	1.01	1.03	1.04	0.98	0.99	0.99

SPHELERITE

Sample	KG225	KG225	KG225	GR 74	Gr 74	GR 74	GOG 37	GOG 37
Area	Rim	Core	Rim	Rim	Core	Rim	Rim	Core
Cu	0.35	0.30	0.82	1.00	0.09	1.00	0.80	0.75
Zn	62.90	63.96	62.40	59.00	58.59	60.85	63.20	62.45
As	0.05	0.06	0.06	0.02	0.01	0.00	0.01	0.02
S	31.80	31.50	31.80	32.00	31.85	31.50	32.50	32.50
Pb	0.00	0.00	0.00	0.00	0.00	0.00	0.00	0.00
Ag	0.00	0.00	0.00	0.00	0.00	0.00	0.00	0.00
Sb	0.01	0.04	0.02	0.01	0.01	0.00	0.01	0.00
Mn	0.00	0.00	0.00	0.00	0.00	0.00	0.00	0.00
Fe	2.60	2.64	5.80	5.90	5.80	6.00	5.90	6.00
Total	97.71	98.50	100.90	97.93	96.35	99.35	102.42	101.72

Atomic Proportions

Sum=2

Zn	0.96	0.97	0.93	0.90	0.90	0.92	0.93	0.92
S	0.99	0.98	0.97	0.99	1.00	0.97	0.97	0.98
FE	0.05	0.05	0.10	0.11	0.10	0.11	0.10	0.10
M%FeS	4.66	4.73	10.39	10.57	10.39	10.74	10.57	10.74

Table 6.1.(continued)

BORNITE

Sample	GL 37	GL 37	GL 37
Area	Rim	Core	Rim
Cu	61.89	62.78	63.24
Zn	0.00	0.09	0.05
As	0.00	0.06	0.09
S	26.12	25.98	25.65
Pb	0.00	0.00	0.00
Ag	0.17	0.04	0.00
Sb	0.07	0.03	0.02
Fe	11.48	11.30	11.67
Total	99.73	100.28	100.72

Atomic Proportions

Sum=10

Cu	4.88	4.94	4.97
S	4.09	4.05	3.99
Fe	1.03	1.01	1.04

MAGNETITE

Sample	Ps254	Ps254	Ps254
Area	Rim	Core	Rim
Fe	72.36	71.90	73.36
O	27.64	26.64	23.06
Total	100.00	98.54	96.42

Atomic Proportions

Sum=2

Fe	0.86	0.87	0.95
O	1.14	1.13	1.05

Zn (5.35 to 6.89), S (25.25 to 27.33), Ag (0.11 to 0.32), and Fe (1.08 to 2.68) whereas As (9.20 to 17.48) and Sb (5.23 to 17.51) have greater variation among different grains. The tetrahedrite is also confirmed by XRD studies and pattern is shown in Figure (6.1).

Galena

Galena appears in anhedral- to irregular-shaped patches having triangular pits on the surface. It is commonly intergrown with sphalerite, chalcopyrite and tetrahedrite, however, discrete grains with no intergrowths are also common. Galena is mostly precipitated within the interstices of silicate phases. At places galena exhibits textures reflecting strain. Rim to core analyses do not show any significant compositional variation suggesting a homogeneous nature of the grains. XRD pattern (Figure 6.2.) confirms the presence of galena in the studied rocks. The electron microprobe analyses suggest galena to be nearly stoichiometric PbS (Table 6.1) containing traces of AS (0.0 to 0.25); Sb (0.0 to 0.9) , Fe (0.0 to 0.024), Ag (0.0 to 0.035). Zn is below the detection limit. Pb and S have greater values like Pb (86.09 to 87.53), S (12.19 to 13.36).

Chalcopyrite

Chalcopyrite is the second most abundant copper-bearing phase in both the mineralized quartz veins and the mineralized diorites/granodiorites. It is white to brass yellow in the reflected light, and occurs as medium-grained irregular mass within the interstices of silicates. It generally occurs in three distinct forms: as medium-grained irregular masses, as intergrowth with tetrahedrite and galena, and as small blebs within the sphalerite. At places, chalcopyrite and tetrahedrite enclose the silicate phases. In some sections

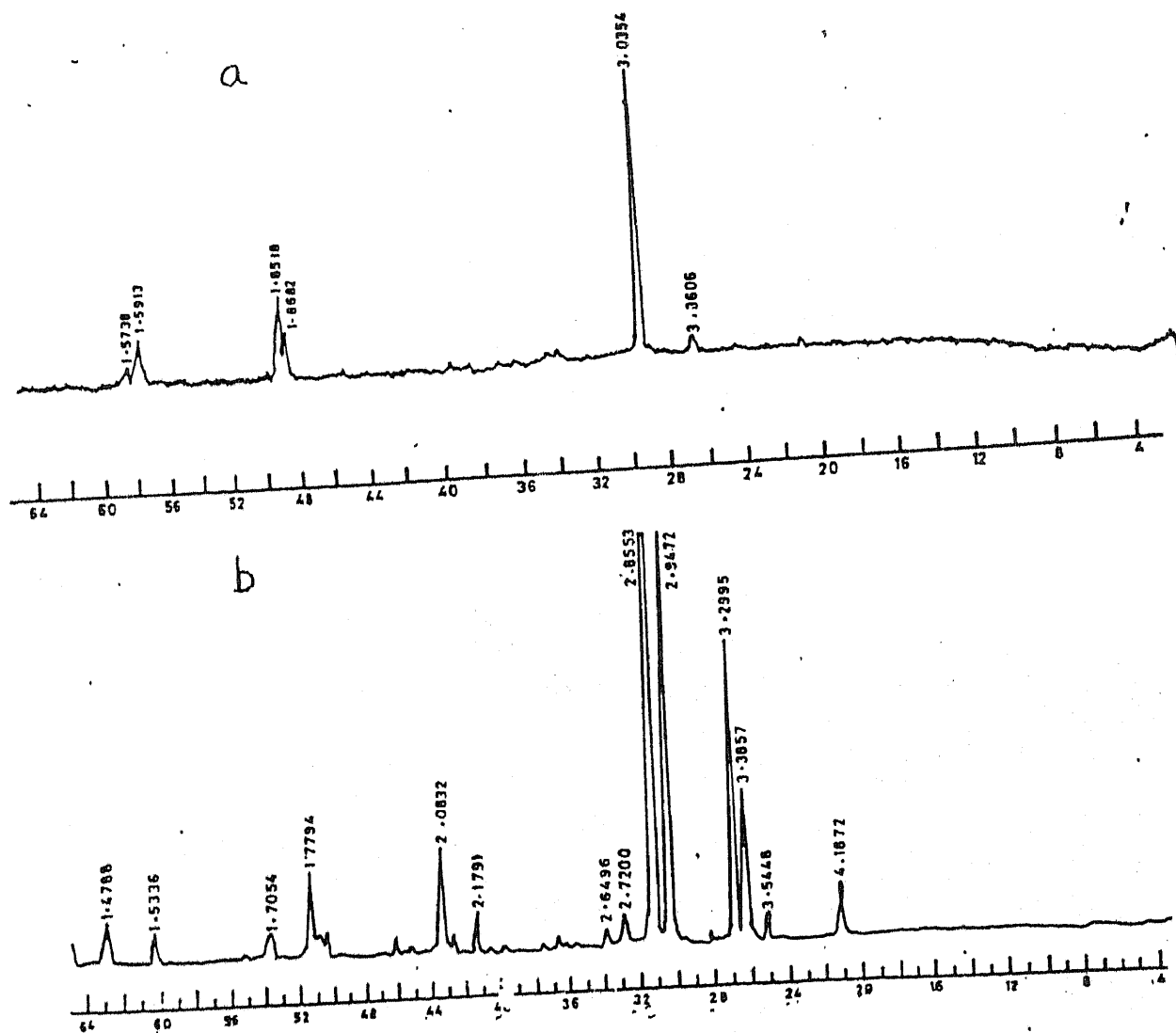


Figure 6.1. X-Ray diffraction pattern of tetrahedrite from the Gawuch Formation.
 Figure 6.2. X-Ray diffraction pattern of galena from the Gawuch Formation.

tetrahedrite grains have chalcopyrite as a core material, suggesting that chalcopyrite could be the main primary phase which has been replaced by the tetrahedrite. Many chalcopyrite veinlets cut the pyrite grains indicating that some of the chalcopyrite formed later than the bulk sulfide deposition. In some cases pyrite is also replaced by chalcopyrite. In oxidized zones, chalcopyrite is extensively replaced by limonite /hematite and magnetite.

Electron microprobe analyses show the chalcopyrite to be stoichiometric CuFeS_2 . Most of the analyses exhibit negligible or undetectable concentration of Pb and Sb, however, the other elements i.e. Zn (up to 0.05 Wt %), As (up to 0.12 wt %) and Ag (up to 0.08wt %) have the detectable concentration in the chalcopyrite (Table 6.1). The chalcopyrite is also confirmed by XRD pattern (Figure 6.3).

Sphalerite

Sphalerite is ameboidal in shape and is generally associated with or intergrown with galena and tetrahedrite. It is generally light brown in colour, however, reddish brown colour grains are also noticed in few cases. Tiny (<1 micron size) disseminated blebs and rods of chalcopyrite within the sphalerite, termed as chalcopyrite disease (Eldridge, 1983), are also noticed. At places, the iron staining along fractures, in association with light brown sphalerite is noticed. This can be attributed to the release of iron from sphalerite during oxidation.

The electron microprobe analyses suggest the sphalerite to be stoichiometric ZnS (Table 6.1). Sphalerite is generally homogenous as rim to core relationships in single grain of sphalerite does not show any compositional variation (Table 6.1). The mole % of FeS in sphalerite ranges from 4.66 to 10.74 and

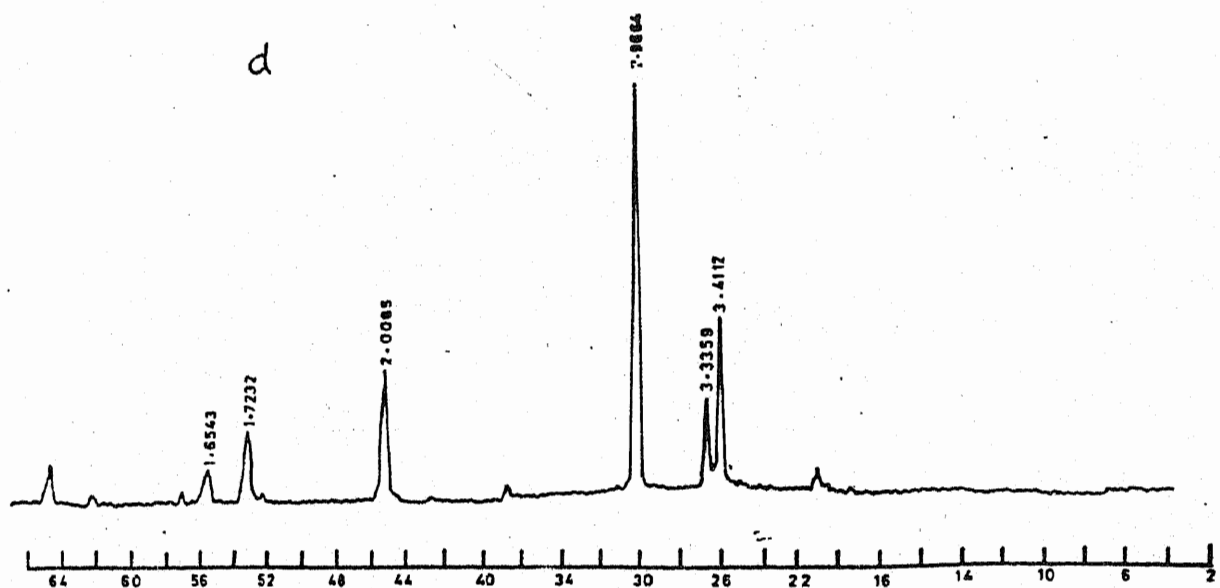
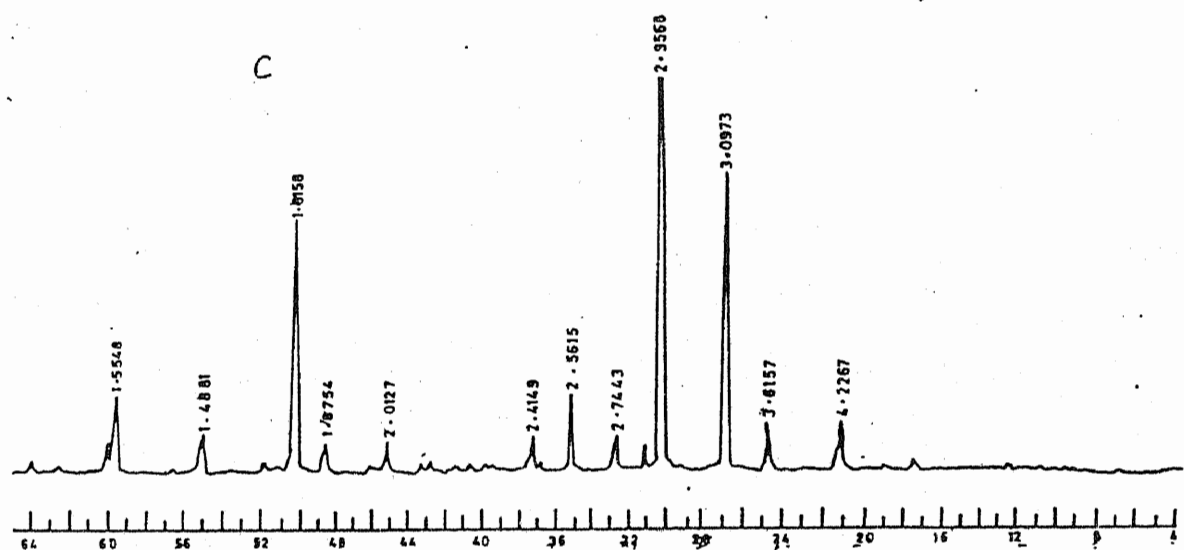


Figure 6.3, X-Ray diffraction pattern of chalcopyrite from the Gawuch Formation.
Figure 6.4, X-Ray diffraction pattern of magnetite from the Gawuch Formation.

is reflected in change in colour in the sphalerite grains from light brown to reddish brown, respectively.

Among the trace elements Cu is ranging from (0.3 to 1.00 wt%), As from (0.01-0.06 wt%) and Sb from (0.01 to 0.04 wt%), while the Pb and Ag are undetectable.

Pyrite

Pyrite is ubiquitous in all the sulfides-bearing phases. It has slightly high reflectivity and has white to light yellow reflecting colour. Two distinct types of pyrite have been identified : 1) the early formed pyrite and 2) the later formed pyrite. The early formed pyrite has smooth surface and is generally present in anhedral, subhedral and rarely in euhedral form . The later formed pyrite (i.e. second generation) is mostly irregular in shape with some crystal outlines or partial crystal surfaces and is generally present along the microfractures of other sulfide and silicate phases.

Electron microprobe analyses suggest pyrite to be nearly stoichiometric FeS_2 (Table 6.1). Minor trace elements i.e.(Cu, As, Pb, Ag, Sb) have also been analyzed. Most of pyrite analyses show negligible or undetectable concentration of these elements. However, Cu is present up to 1.0 wt% . Fe has wide range (38-50wt %) whereas S has narrow range (53-55 wt %) in these pyrites (Table-6.1).

Magnetite

It is gray with brownish tint, and occurs as anhedral, subhedral and even skeletal. It also occurs as anhedral polycrystalline aggregates. Irregular magnetite grains occur as interstitial phase, and enclose rounded to subrounded grains of silicate phases. It also occurs as microveins along the foliation planes. Magnetite

often contains exsolution or oxidation lamellae of hematite. It is mostly associated with pyrite, chalcopyrite, galena and sphalerite.

The electron microprobe analyses show the magnetite to be nearly stoichiometric Fe_3O_4 . Most of the analyses exhibit negligible or undetectable concentration of Cu, Zn, Pb, and Ag. However, Fe has narrow range of variation (71.9 to 73.36 wt %) and oxygen (23.06-27.64 wt %)(Table 6.1) (Fig 6.4).

Bornite

Bornite is pink in colour and occurs as irregular grains. It is generally found in association with tetrahedrite. However, in some samples it is also replacing tetrahedrite along the margins and the fractures. Sometime it has intergrown behaviour with tetrahedrite and chalcopyrite.

Electron microprobe analyses show the bornite to be nearly Cu_5FeS_4 (Table 6.1). Traces of Zn (0.0 to 0.9 wt %), Ag (0.0 to 0.17 wt %) and Sb (0.02 to 0.07 wt %) are present . However, Pb is undetectable.

WHOLE-ROCK GEOCHEMISTRY

The mineralized rocks of the studied area have been analyzed for major and trace elements and the results are given in (Table 6.2). These rocks, as already mentioned in the petrography section in Chapter (6), are highly altered therefore cannot be treated using conventional classification schemes and tectonic discrimination diagrams.

There is a great variation in both major and trace elements of these rocks (Table 6.2). SiO_2 ranges from 42.67 to 69.45 wt%, Al_2O_3 from 8.23 to 18.94 wt%, TiO_2 0.19 to 1.05 wt%, Fe_2O_3 from 2.29 to 9.38 wt%, MnO from 0.03 to 0.14 wt%, MgO from 0.58 to 4.80 wt%, CaO from 0.33 to 12.87 wt%, Na_2O from 0.40

Table 6.2. Major and trace element concentration of mineralized diorites from the Gawuch Formation, Drosh, Chitral.

Sample	KG14	KG195	KG205	KG209	GG17	GG18	GG19	GG22	GG24
SiO ₂	58.67	55.34	56.41	61.89	69.45	65.78	54.78	54.34	52.23
TiO ₂	0.53	0.45	0.55	0.63	0.19	0.38	0.24	0.34	0.52
Al ₂ O ₃	18.94	15.67	16.89	15.34	8.23	13.45	16.45	15.78	11.78
Fe ₂ O ₃	2.29	3.40	4.99	9.38	2.82	3.86	9.60	3.16	4.50
MnO	0.03	0.05	0.07	0.12	0.09	0.05	0.05	0.07	0.09
MgO	1.76	1.58	2.55	0.58	1.08	1.08	2.56	4.27	4.80
CaO	4.37	5.46	3.32	0.33	7.27	3.11	5.85	8.18	9.80
Na ₂ O	2.89	4.85	0.37	0.40	0.56	3.00	2.01	5.63	2.73
K ₂ O	2.41	0.98	4.26	2.14	0.84	0.72	0.50	0.65	1.73
P ₂ O ₅	0.22	0.08	0.35	0.63	0.05	0.54	0.16	0.07	0.29
LOI	6.52	8.80	9.04	6.56	7.78	5.03	6.54	5.78	7.23
TOTAL	98.63	96.66	98.80	98.00	98.36	97.00	98.74	98.27	98.70

Trace elements (ppm)

Ni	43	26	83	59	97	76	48	53	50
Zn	86	414	45	288	903	146	59	48	561
Cu	3408	27525	720	7740	5475	23700	5370	1035	2655
Pb	42	137	54	98	67	208	39	36	924
Cr	53	30	87	71	48	58	45	98	108
Co	54	37	62	74	41	73	85	59	41
Ag	0	49		15	64	0	38	0	35
Au	10	0	4	340	15	18	58	18	10

Table 6.2. (continued)

Sample	GG25	LG43	LG45	LG57	GR81	GR83
SiO ₂	57.34	58.98	55.67	42.67	55.45	54.52
TiO ₂	0.46	0.39	0.36	1.05	0.46	0.41
Al ₂ O ₃	17.89	17.67	15.23	16.45	15.89	15.32
Fe ₂ O ₃	2.89	3.53	5.88	8.34	5.65	5.36
MnO	0.06	0.05	0.12	0.14	0.10	0.09
MgO	2.14	2.11	3.17	4.08	2.95	3.34
CaO	4.51	4.88	4.69	12.87	3.11	4.23
Na ₂ O	3.38	1.06	2.78	0.29	2.71	2.95
K ₂ O	2.05	1.45	1.71	1.23	2.92	2.47
P ₂ O ₅	0.64	0.20	0.30	0.45	0.10	0.46
LOI	7.07	5.78	5.25	8.78	9.52	9.34
TOTAL	98.43	96.10	95.16	96.35	98.86	98.49

Trace elements (ppm)

Ni	41	55	44	753	45	40
Zn	39	65	49	24	56	44
Cu	705	157	208	48600	3018	3356
Pb	39	42	41	62	42	116
Cr	70	43	58	64	86	41
Co	62	62	1	546	2	2
Ag	0	0	0	0	0	0
Au	22	3	2	7	13	23

to 5.63 wt%, K₂O from 0.50 to 4.26 wt% and P₂O₅ from 0.05 to 0.64 wt%. These rocks also have very high (up to 9 wt%) loss on ignition (Table 6.2).

Among the trace elements Cu has very high concentration (ore grade) in almost all the samples (0.02 -4.86 wt%). Zn and Pb are generally high in mostly samples, however, four samples have >250 ppm Zn and >100 ppm Pb with maximum of 903 ppm of Zn and 924 ppm of Pb. Most of these rocks have Cr in the range of 30 to 108 ppm, Ni, 26 to 97 ppm, Co, 2 to 85ppm, Ag, 0 to 30 ppb and Au, 0 to 34 ppb in the normal range. However, One sample has high Ni (753 ppm) and other four have high Ag (> 30 ppm) contents.

Major elements of these rocks when plotted against silica (Fig 6.5), show wide variations resulting in considerable scatter. Despite this scatter, variations in the contents of various elements do have some characteristics. For example CaO, MgO, MnO, Fe₂O₃ all show a scatter but continuous depletion with increasing contents of SiO₂ suggesting a role of fractionation of ferromagnesian minerals. It is, however, difficult to infer the order in which various ferromagnesian minerals crystallized from the present data-set. Samples with intermediate SiO₂ contents i.e., between 50-60 w% show an increase in Al₂O₃, TiO₂, and Na₂O that may imply the plagioclase and amphibole crystallization.

The lack of data for incompatible trace elements like Rb, Sr, Nb, Y, Zr, Sm, Nd etc. inhibit further evaluation of the analyzed rocks in terms of their tectonic setting of origin. The analyzed set of trace elements is compatible to metallic minerals and is thus indicative of modal proportions of certain metallic minerals in a sample rather than petrological character of that rock. When these trace elements are plotted on various binary diagrams they do not show any

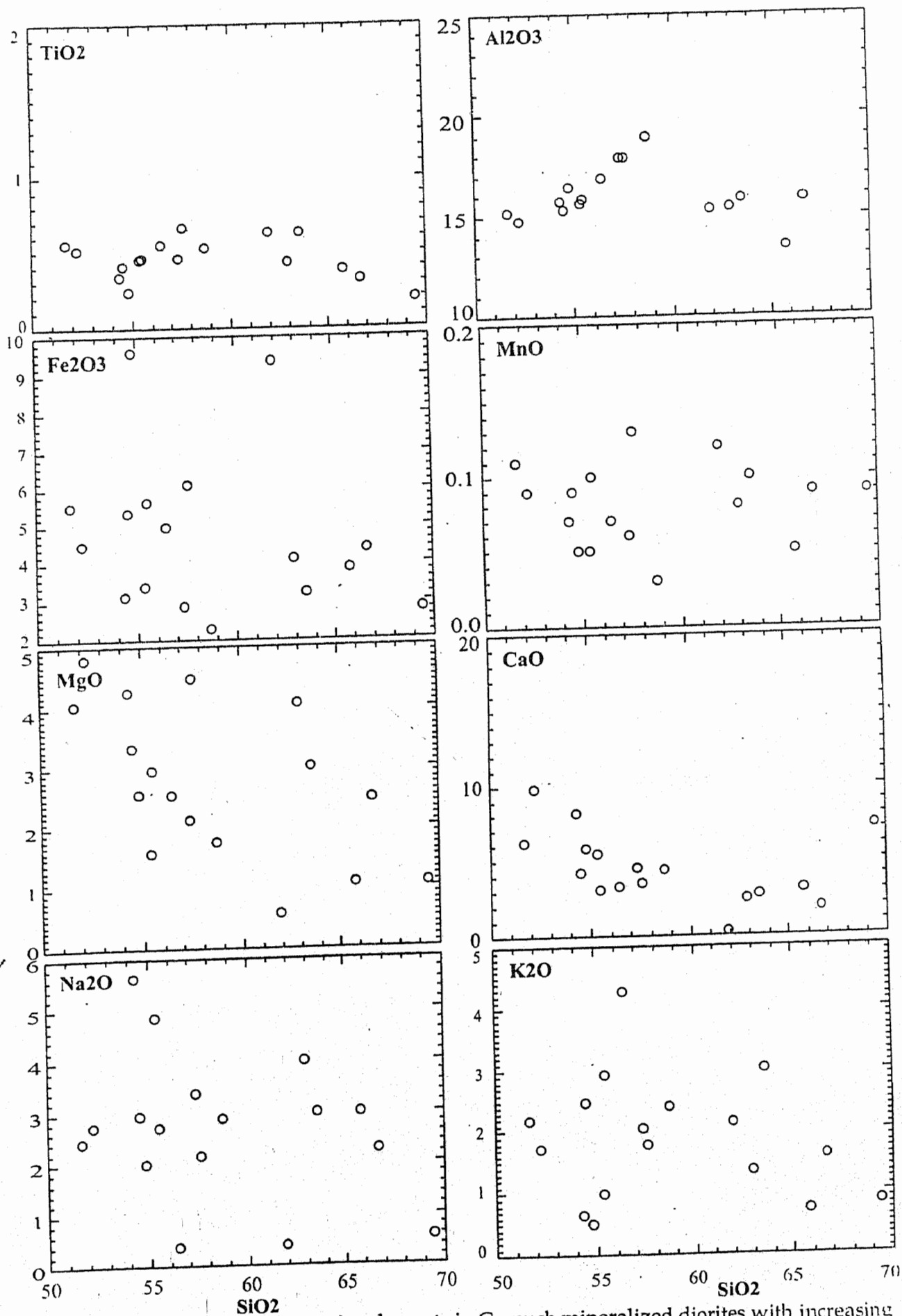


Figure 6.5. Variation in some major elements in Gawuch mineralized diorites with increasing degree of fractionation as depicted by increasing Wt% of SiO₂.

systematic trends. This suggests that samples have varying modal proportions of metallic minerals. There is, however, some mutual compatibility indicated by some trace elements like Ag and Zn, Ni and Co, Zn and Cr and Ni and Cr (Fig. 6.6).

CHEMICAL GAIN / LOSS ACCOMPANYING MINERALIZATION

The hydrothermal mineralization is capable of greatly modifying the original chemical composition of the host rocks. The process involves addition of certain metallic elements to the original chemical composition. This may or may not necessarily involve removal of any other element(s) from the protolith composition. However, since the chemical composition of rocks is expressed in wt %, the net effect is that rest of the elements have a lower percentage than that prior to modification by the hydrothermal mineralization.

In order to determine the chemical changes during mineralization, mineralized rocks from four separate locations i.e., Kaldom Gol, Gawuch Gol, Gorin Gol and Langer Gol are compared with each other (Fig 6.7) and also compared with unmineralized diorites collected from the same locations, computing the enrichment and depletion factors (mineralized-unmineralized/unmineralized)*100) (Table 6.3; Fig. 6.8-11). This involves assumption that the mineralized and unmineralized diorites had identical composition prior to mineralization. Since there is no direct method to ascertain this requirement, care has been taken to select the mineralized and unmineralized diorites from the same body yet with a safe mutual distance to avoid any hydrothermal effect.

Table 6.3 Average major and trace element data of mineralized and unmineralized rocks from Gawuch Formation and their enrichment and depletion factor.

Kaldam Gol

Mineralized Rocks															
Samp. No.	SiO ₂	TiO ₂	Al ₂ O ₃	Fe ₂ O ₃	MnO	MgO	CaO	Na ₂ O	K ₂ O	P ₂ O ₅	Ni	Zn	Cu	Pb	Au
KG 14	58.67	0.53	18.94	2.29	0.03	1.76	4.37	2.89	4.41	0.22	43	86	3408	42.22	53.4
KG 195	55.34	0.45	15.67	3.4	0.05	1.58	5.46	2.85	2.98	0.08	26	414	27525	137	30
KG 205	56.41	0.55	16.89	4.99	0.07	2.55	3.32	0.37	4.26	0.35	83	45	720	54	87
KG 209	60.89	0.63	15.34	9.38	0.12	0.58	0.33	0.4	3.14	0.63	59	288	7740	98	71
Average	57.83	0.54	16.71	5.02	0.07	1.62	3.37	1.63	3.70	0.32	53	208	0	83	60

Unmineralized Rocks															
Samp. No.	SiO ₂	TiO ₂	Al ₂ O ₃	Fe ₂ O ₃	MnO	MgO	CaO	Na ₂ O	K ₂ O	P ₂ O ₅	Ni	Zn	Cu	Pb	Au
KG 10	60.78	0.63	18.78	2.69	0.04	1.72	6.64	2.84	2.66	0.1	39	74	69	58	49
KG 11a	55.89	0.55	16.89	3.46	0.05	6.88	5.14	1.52	4.06	0.02	52	153	157	42	43
KG 11b	58.98	0.39	17.67	3.53	0.05	2.11	4.88	1.06	3.84	0.2	55	65	157	42	43
KG 13	58.98	0.39	17.67	3.53	0.05	2.11	4.88	1.06	3.84	0.2	55	65	157	42	43
KG 189	58.7	0.85	17.71	7.22	0.06	3.13	2.61	0.37	3.82	0.15	101	78	122	36	188
KG 196	55.13	0.52	15.23	5.17	0.11	3.79	5.96	3.02	1.43	0.57	42	47	34	43	71
Average	58.08	0.56	17.33	4.27	0.06	3.29	5.02	1.65	3.28	0.21	57	80	116	44	73

Average Mineralized Rock															
Average Mineralized Rock	57.83	0.54	16.71	5.02	0.07	1.62	3.37	1.63	3.70	0.32	53	208	9848	83	60
Average Unmineralized Ro	58.08	0.56	17.33	4.27	0.06	3.29	5.02	1.65	3.28	0.21	57	80	116	44	73
Depletion/Enrichment Fact	-0.43	-2.70	-3.55	17.54	12.50	-50.84	-32.85	-1.06	12.90	54.84	-8	159	8385	88	-17

Table 6.3. (Continued)

Gawuch Gol

Unmineralized Rocks

Samp. No.	SiO ₂	TiO ₂	Al ₂ O ₃	Fe ₂ O ₃	MnO	MgO	CaO	Na ₂ O	K ₂ O	P ₂ O ₅	Ni	Zn	Cu	Pb	Cr	Co	Ag	Au
GOG17	61.89	0.63	15.34	9.38	0.12	0.58	0.33	0.4	3.84	0.63	59	288	7740	98	71	74	64	15
GOG18	69.45	0.19	8.23	2.82	0.09	1.08	7.27	0.56	2.72	0.05	97	903	5475	67	48	41	0	18
GOG19	65.78	0.38	13.45	3.86	0.05	1.08	3.11	3	3.5	0.54	76	146	23700	208	58	73	38	58
GOG22	54.78	0.24	16.45	9.6	0.05	2.56	5.85	2.01	2.65	0.16	48	59	5370	39	45	85	0	18
GOG24	54.34	0.34	15.78	3.16	0.07	4.27	8.18	5.63	2.73	0.07	53	48	1035	36	98	59	35	10
GOG25	52.23	0.52	14.78	4.5	0.09	4.8	9.8	2.73	2.05	0.29	50	561	2655	924	108	41	0	22
Average	59.75	0.38	14.01	5.55	0.08	2.40	5.76	2.39	2.92	0.29	64	334	7663	229	71	62	23	24

Unmineralized Rocks

Samp. No.	SiO ₂	TiO ₂	Al ₂ O ₃	Fe ₂ O ₃	MnO	MgO	CaO	Na ₂ O	K ₂ O	P ₂ O ₅	Ni	Zn	Cu	Pb	Cr	Co	Ag	Au
GOG38	58.78	0.44	14.23	3.79	0.05	1.97	4.88	4.31	2.42	0.54	39	71	46.8	71	42	45	0	6

Samp. No.	SiO ₂	TiO ₂	Al ₂ O ₃	Fe ₂ O ₃	MnO	MgO	CaO	Na ₂ O	K ₂ O	P ₂ O ₅	Ni	Zn	Cu	Pb	Cr	Co	Ag	Au
Average Mineralized Rock	59.75	0.38	14.01	5.55	0.08	2.40	5.76	2.39	2.90	0.29	64	334	7663	229	71	62	23	24
Average Unmineralized Ro	58.78	0.44	14.23	3.79	0.05	1.97	4.88	4.31	2.42	0.54	39	71	47	71	42	45	0	6
Depletion/Enrichment Fact	1.64	-12.88	-1.58	46.53	56.67	21.57	17.96	-44.59	19.83	-46.30	64	371	16273	222	70	38	0	292

Langer Gol

Mineralized Rocks

Samp. No.	SiO ₂	TiO ₂	Al ₂ O ₃	Fe ₂ O ₃	MnO	MgO	CaO	Na ₂ O	K ₂ O	P ₂ O ₅	Ni	Zn	Cu	Pb	Cr	Co	Ag	Au
GL57	42.7	1.1	16.5	8.3	0.1	4.1	12.9	0.3	4.8	0.5	753	24	48600	62	64	546	0	7

Unmineralized Rocks

Samp. No.	SiO ₂	TiO ₂	Al ₂ O ₃	Fe ₂ O ₃	MnO	MgO	CaO	Na ₂ O	K ₂ O	P ₂ O ₅	Ni	Zn	Cu	Pb	Cr	Co	Ag	Au
GL43	58.98	0.39	17.67	3.53	0.05	2.11	4.88	1.06	1.45	0.2	55	65	157	42	43	62	0	3
GL45	55.67	0.36	15.23	5.88	0.12	3.17	4.69	2.78	1.71	0.3	44	49	208	41	58	1	0	2
Average	57.3	0.4	16.5	4.7	0.1	2.6	4.8	1.9	1.6	0.3	50	57	183	42	51	31	0	3

Samp. No.	SiO ₂	TiO ₂	Al ₂ O ₃	Fe ₂ O ₃	MnO	MgO	CaO	Na ₂ O	K ₂ O	P ₂ O ₅	Ni	Zn	Cu	Pb	Cr	Co	Ag	Au
Average Mineralized Rock	42.7	1.1	16.5	8.3	0.1	4.1	12.9	0.3	4.8	0.5	753	24	48600	62	64	546	0	7
Average Unmineralized Ro	57.3	0.4	16.5	4.7	0.1	2.6	4.8	1.9	1.6	0.3	50	57	183	42	51	31	0	6
Depletion/Enrichment Fact	-25.53	162.50	0.00	77.45	0.00	56.92	168.13	-84.74	200.00	50.00	0	-58	26516	49	20	1644	0	27

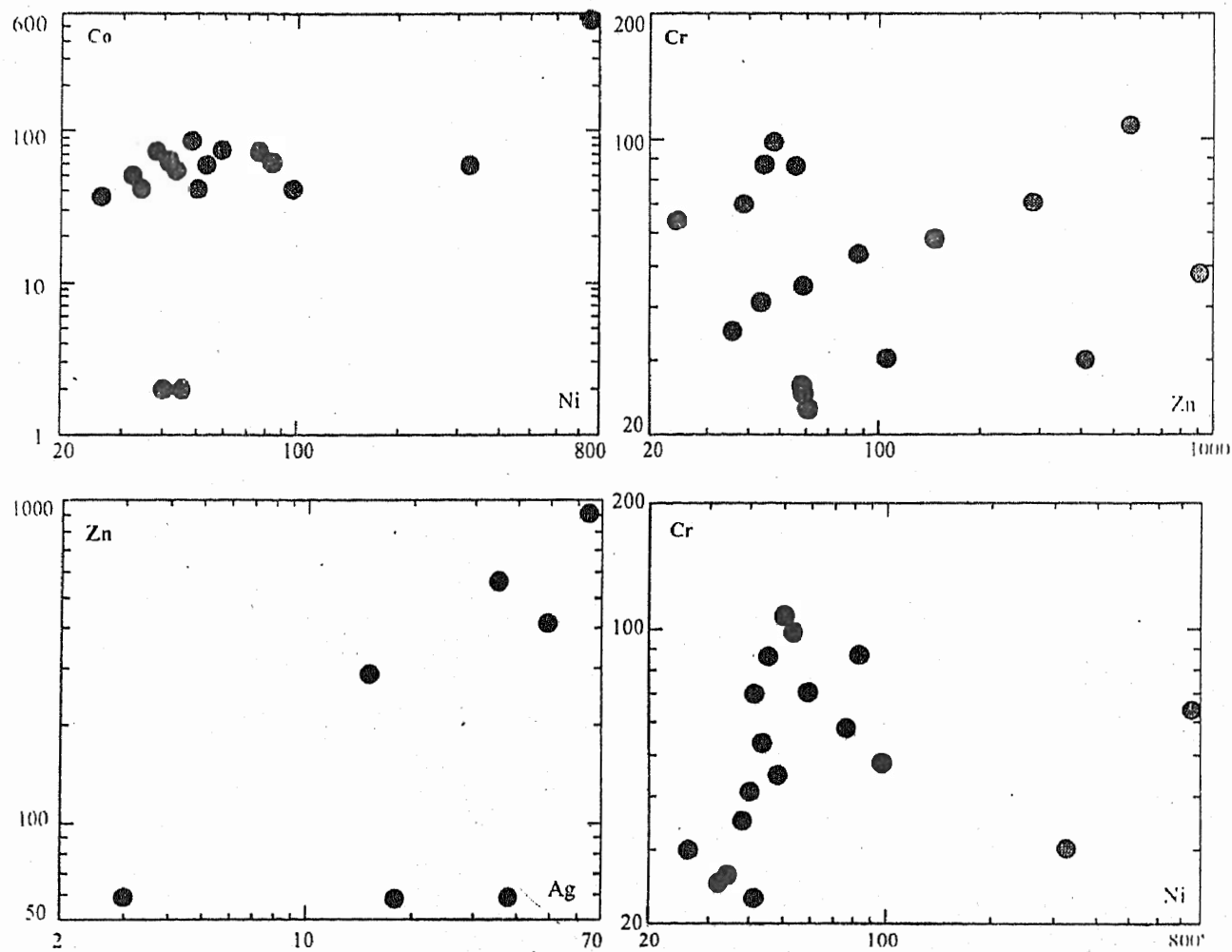


Figure 6.6. Mutual variations in transitional elements in Gawuch mineralized diorites.

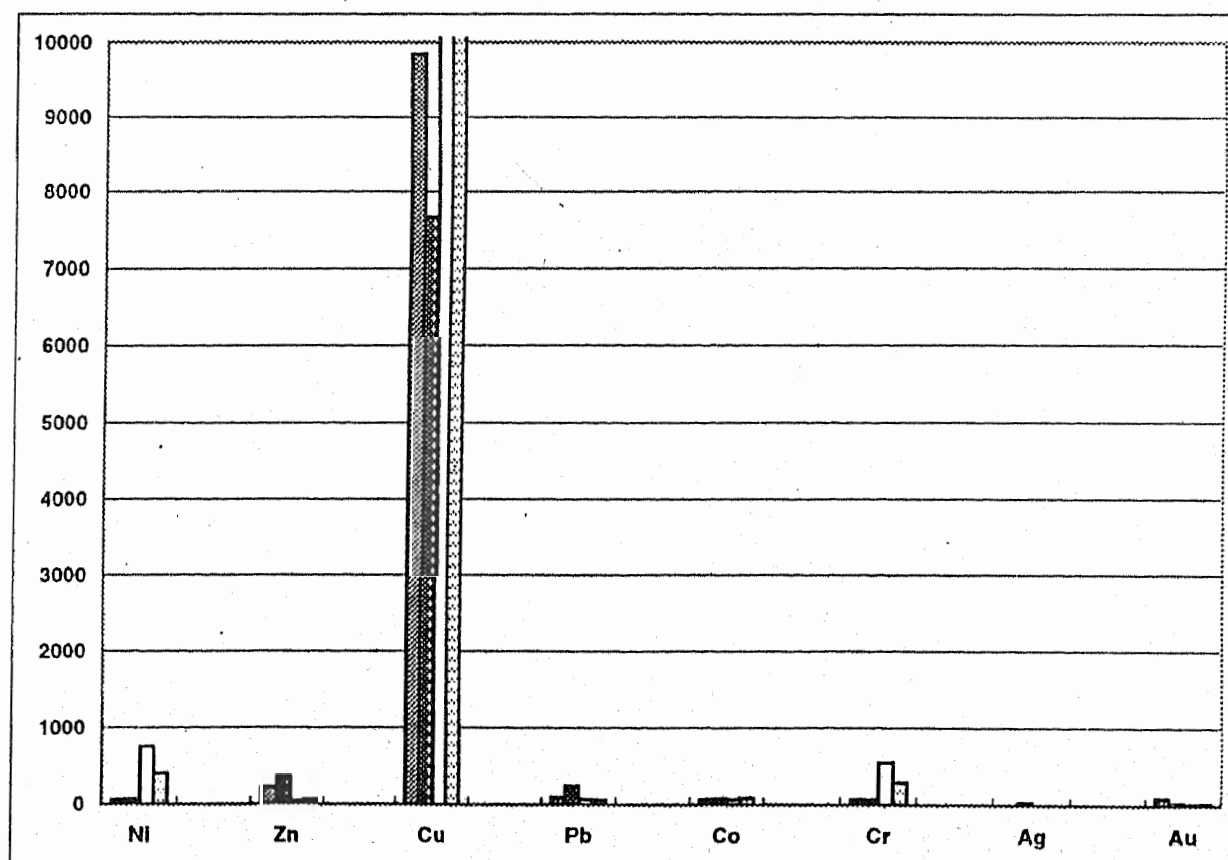
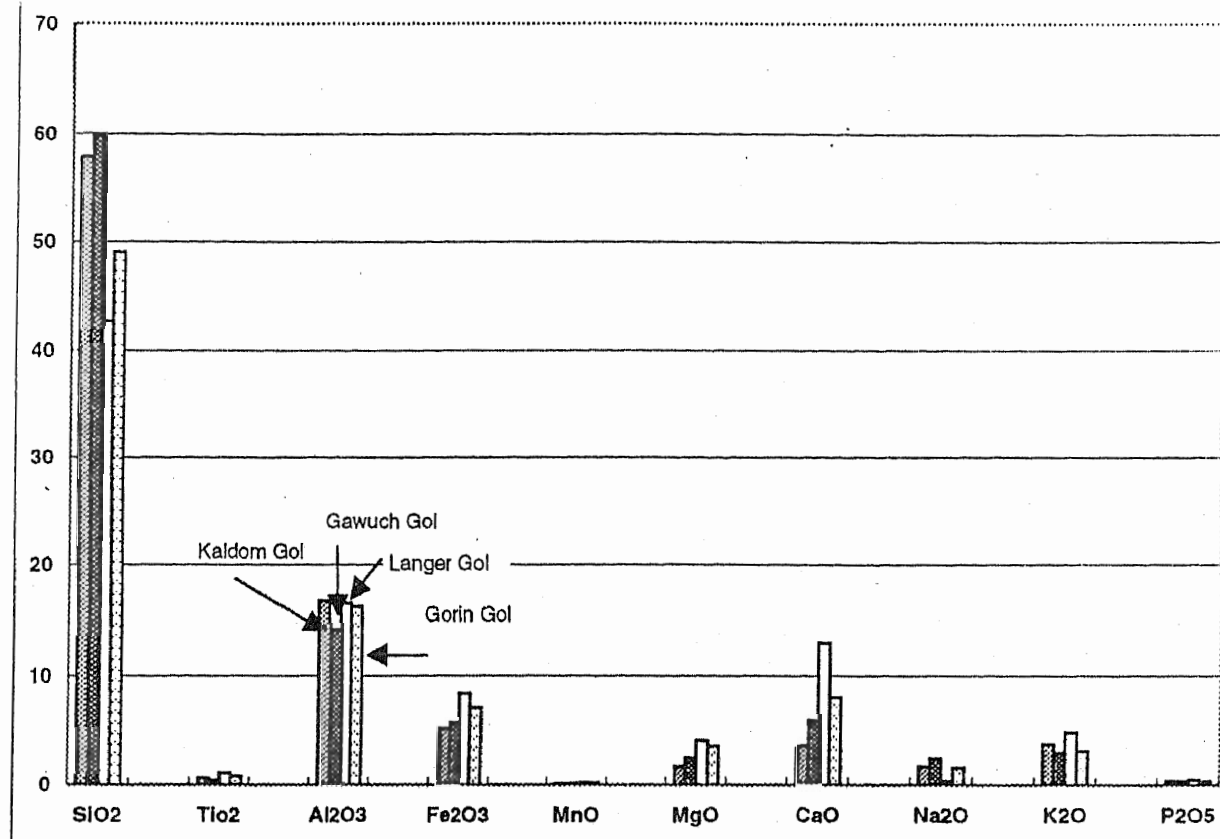


Figure 6.7. Comparison of the relative concentration of various major and trace elements in the outcrops of the Gawuch Formation in four principal streams (i.e., Kaldom Gol, Gawuch Gol, Langer Gol and Gorin Gol).

An average of four mineralized diorites has been normalized against an average of five unmineralized diorites to assess the chemical gain and loss in the Kaldom Gol part of the studied mineralized zone (Fig. 6.8). Amongst the major elements, SiO_2 , TiO_2 , Al_2O_3 and Na_2O show negligible difference between the mineralized and unmineralized diorites. Fe_2O_3 , MnO , K_2O and P_2O_5 are enriched in the mineralized rocks while MgO , and CaO are depleted. All the trace elements are enriched in the mineralized diorites relative to the unmineralized ones. In particular, enrichment in the trace elements like Cu , Au and Ag is significant.

Gawuch Gol

The major elements in the average mineralized rock from the Gawuch Gol show enrichment in major elements like Fe_2O_3 , MnO , MgO , CaO and K_2O and depletion in TiO_2 , Al_2O_3 , Na_2O and P_2O_5 . Like in the Kaldom Gol, all the trace elements show enrichment, particularly being significant in Cu . Enrichment in Ag and Au in the Gawuch Gol is not as significant as in the Kaldom Gol (Fig 6.9).

Gorin Gol

At Gorin Gol, the mineralized diorites are enriched in major elements like TiO_2 , Fe_2O_3 , MnO , CaO , K_2O and P_2O_5 and are depleted in SiO_2 , MgO and Na_2O (Fig. 6.10). Amongst the metallic trace elements, Cu is strongly enriched followed by Ni and Co .

Langer Gol

At Langer Gol, major elements like Al_2O_3 and MnO do not show any significant difference between the mineralized and unmineralized diorites,

rocks while SiO_2 , Na_2O are depleted. (Fig. 6.11). In the trace elements, Cu mineralization is accompanied by enrichment in Co and Ni.

Summary

Figures 6.8-6.11 present chemical gain/loss budget for the entire mineralized zone. Amongst the major elements, Fe_2O_3 , and K_2O are consistently enriched in the mineralized rocks from all the four sections i.e., Kaldom Gol, Gawuch Gol, Langer Gol and Gorin Gol, while Na_2O is consistently depleted everywhere in the mineralized diorites compared to the unmineralized diorites. P_2O_5 and MnO shows considerable enrichment in the mineralized diorites everywhere except for the P_2O_5 in Gawuch Gol and MnO in Langer suggesting that it formed an important component of the mineralizing fluids. SiO_2 has either remained unchanged or only slightly depleted compared to the unmineralized diorites. Similarly Al_2O_3 has not been added or removed to the mineralized rocks to a great extent. TiO_2 , CaO and MgO show mixed characters, at places these are enriched relative to the unmineralized diorites while elsewhere these are depleted. Amongst the trace elements, Cu is strongly enriched everywhere in the mineralized rocks. None of the rest of the trace elements analyzed show depletion in the mineralized rocks relative to the unmineralized diorites.

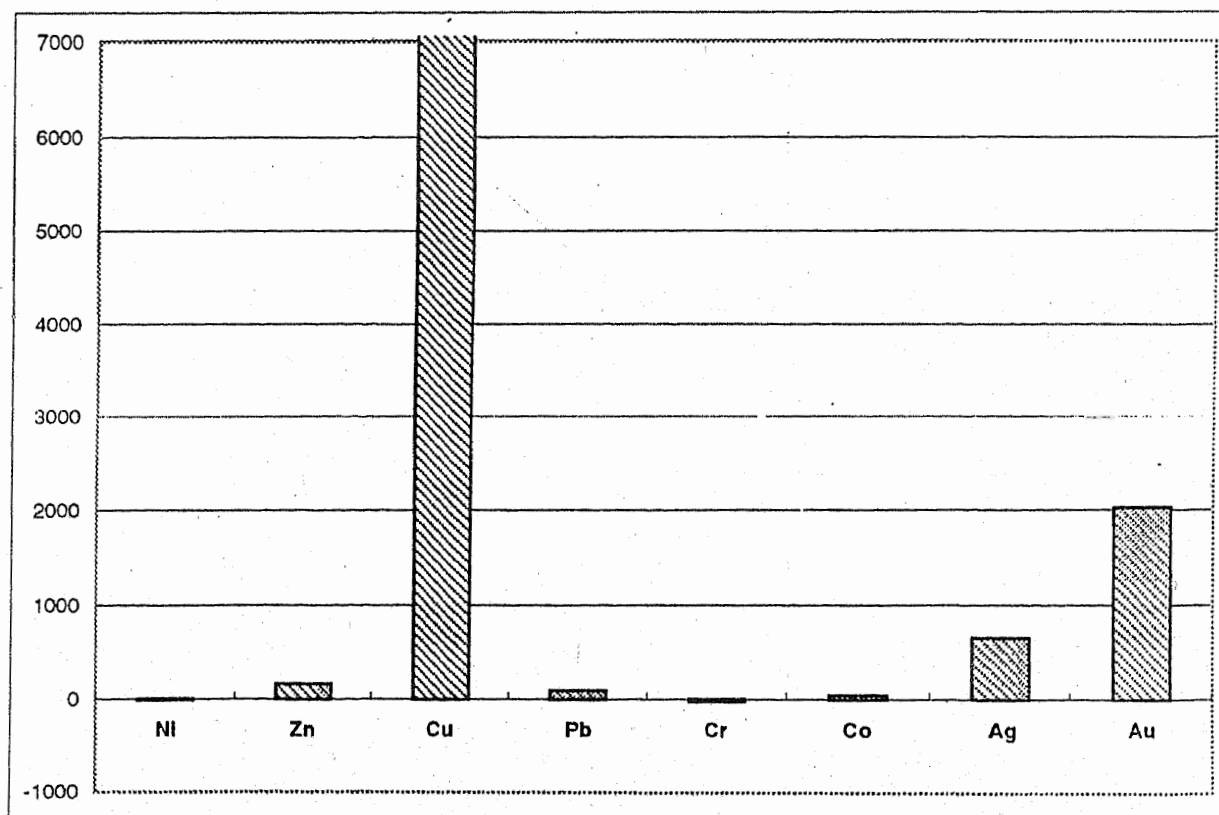
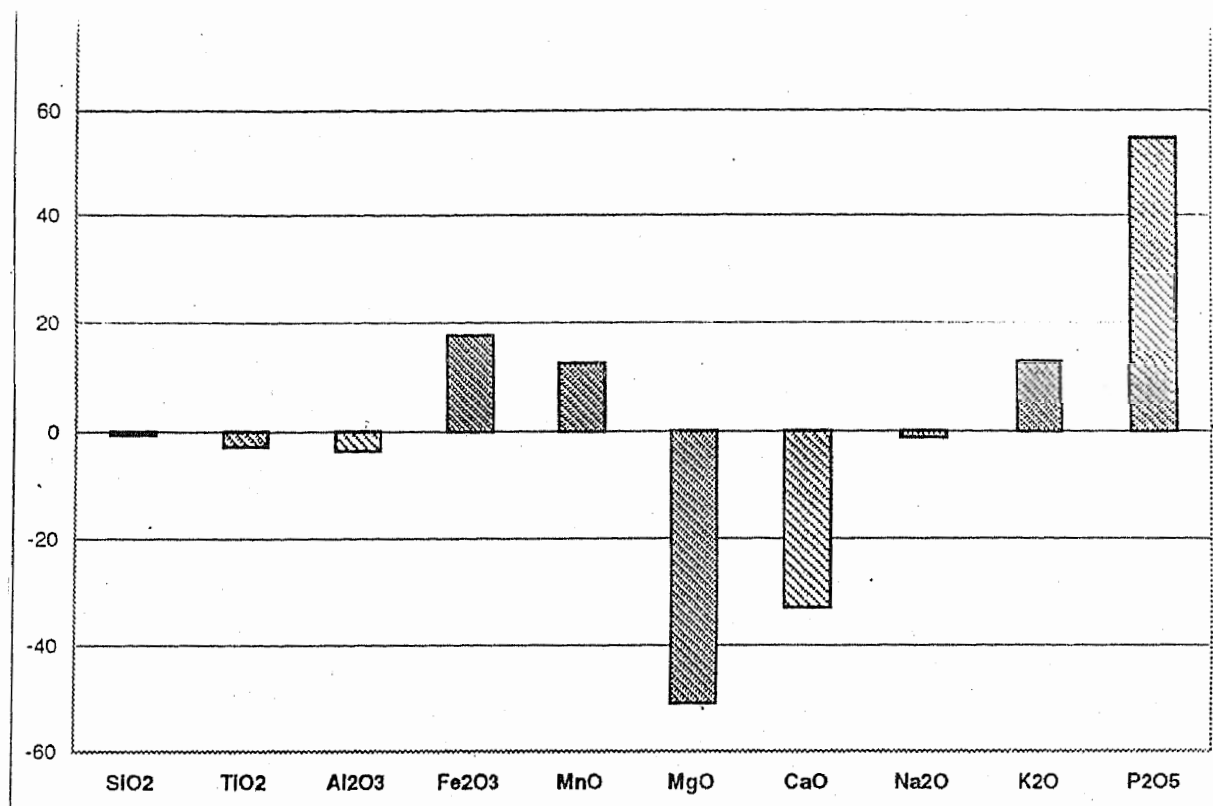


Figure 6.8 Enrichment and depletion in major and trace element abundances in mineralized dioritic rocks in the Gawuch Formation exposed at the Kaldom Gol during alteration and mineralization.

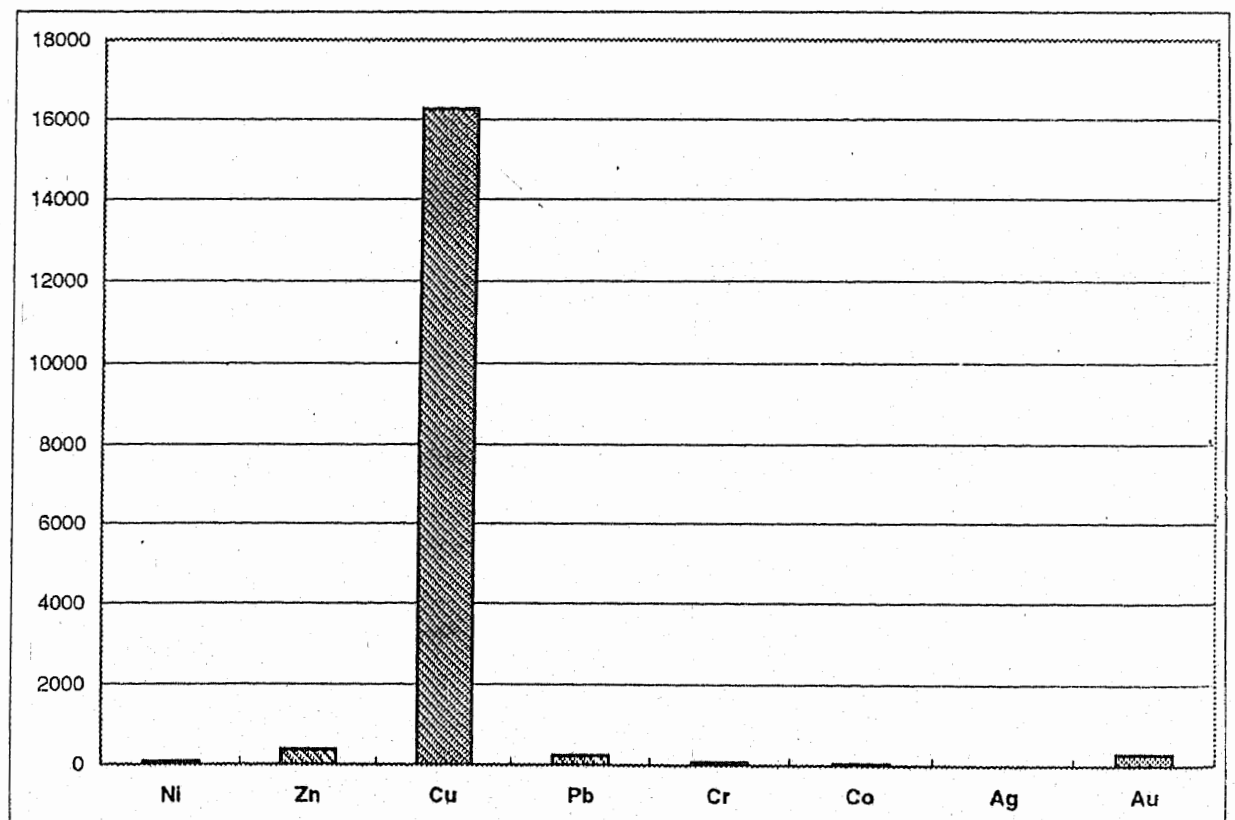
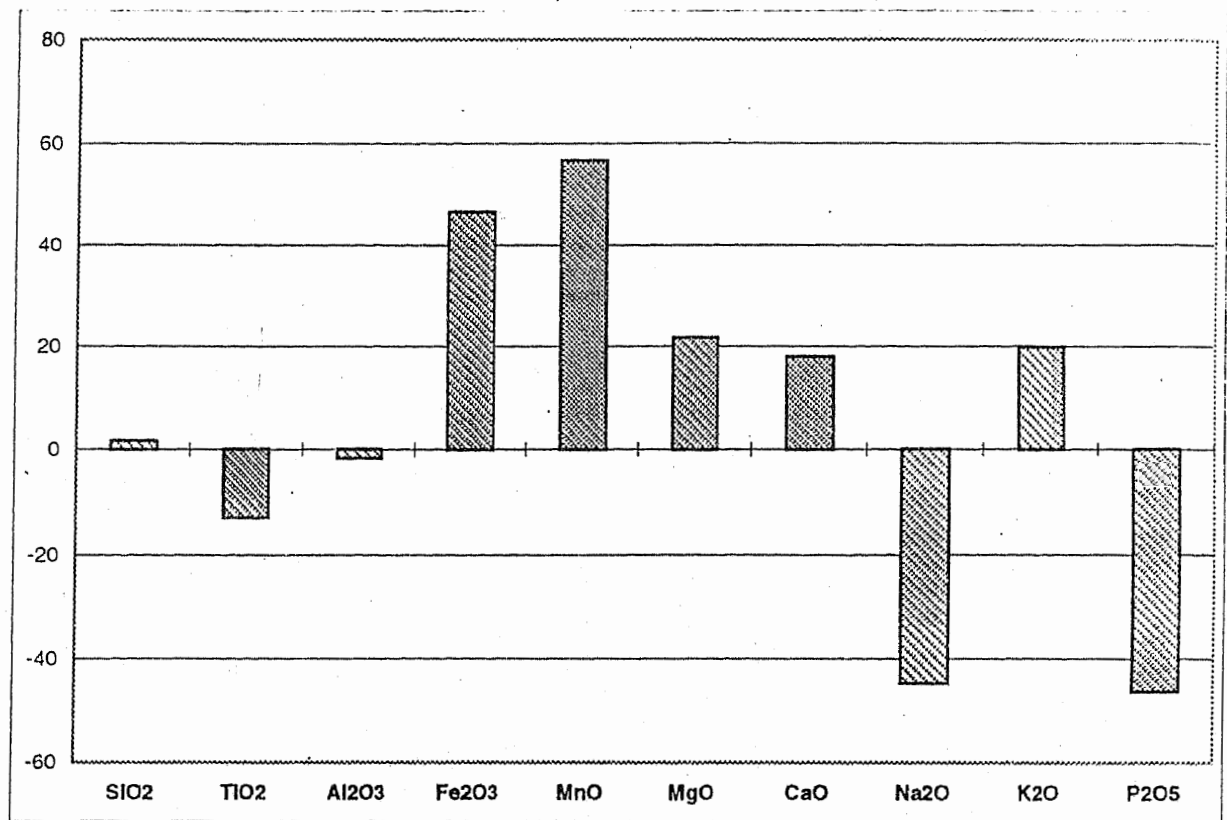


Figure 6.9. Enrichment and depletion in major and trace element abundances during alteration and mineralization in diorites in the outcrops of Gawuch Formation at Gawuch Gol.

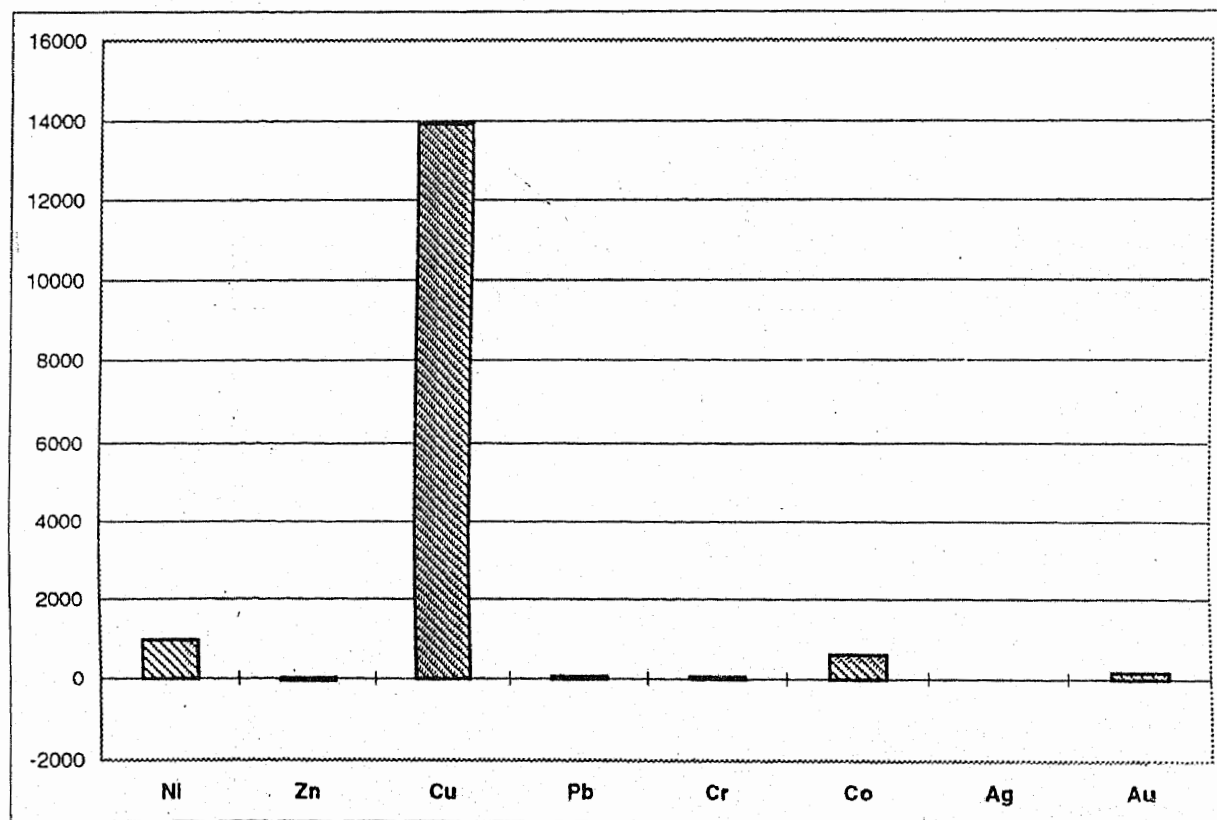
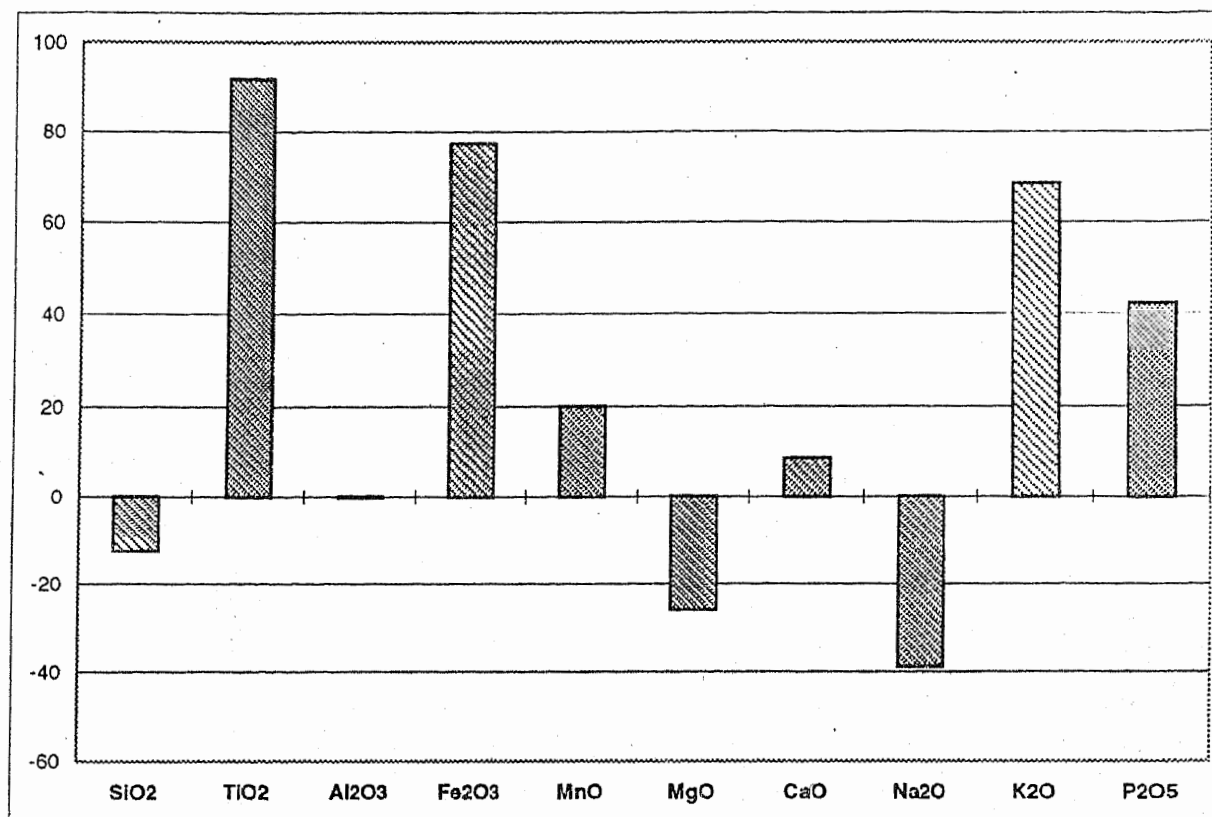


Figure 6.10 Enrichment and depletion in major and trace element abundances during alteration and mineralization of diorites from Gawuch Formation exposed at Gorin Gol.

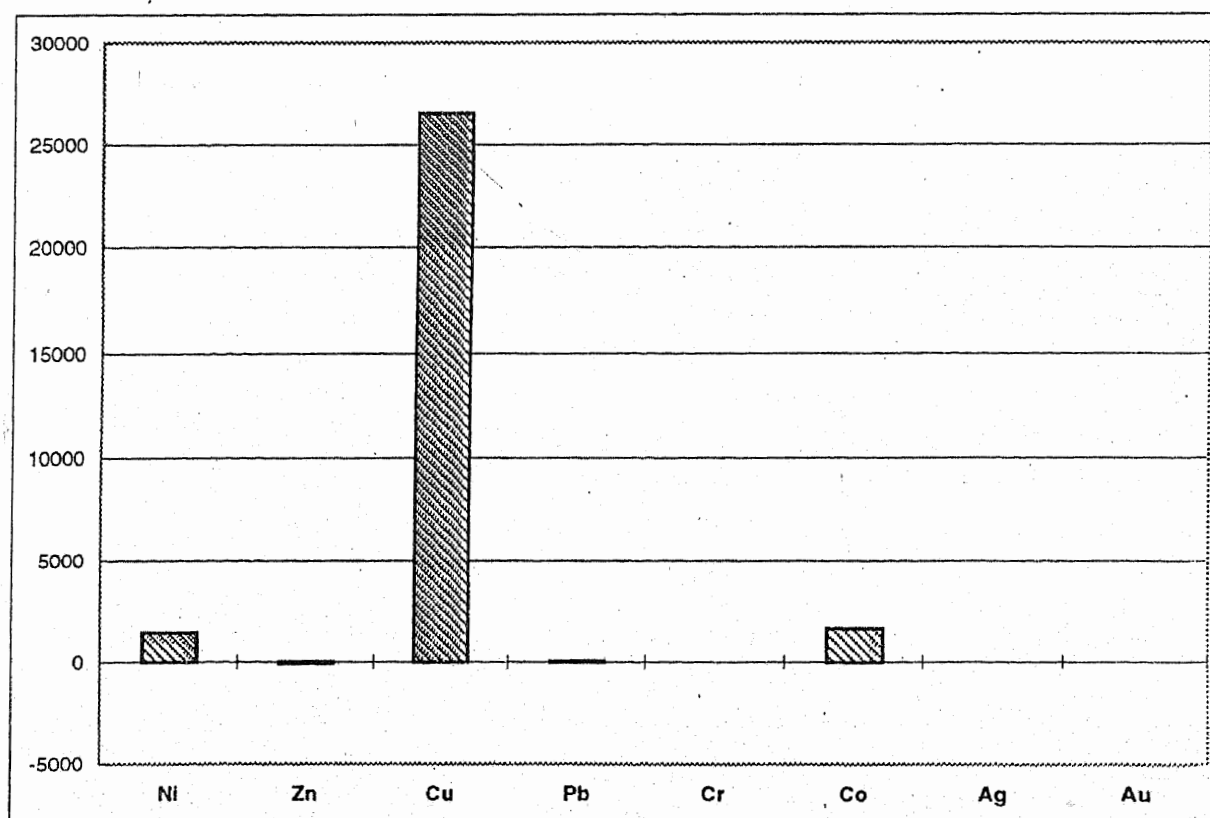
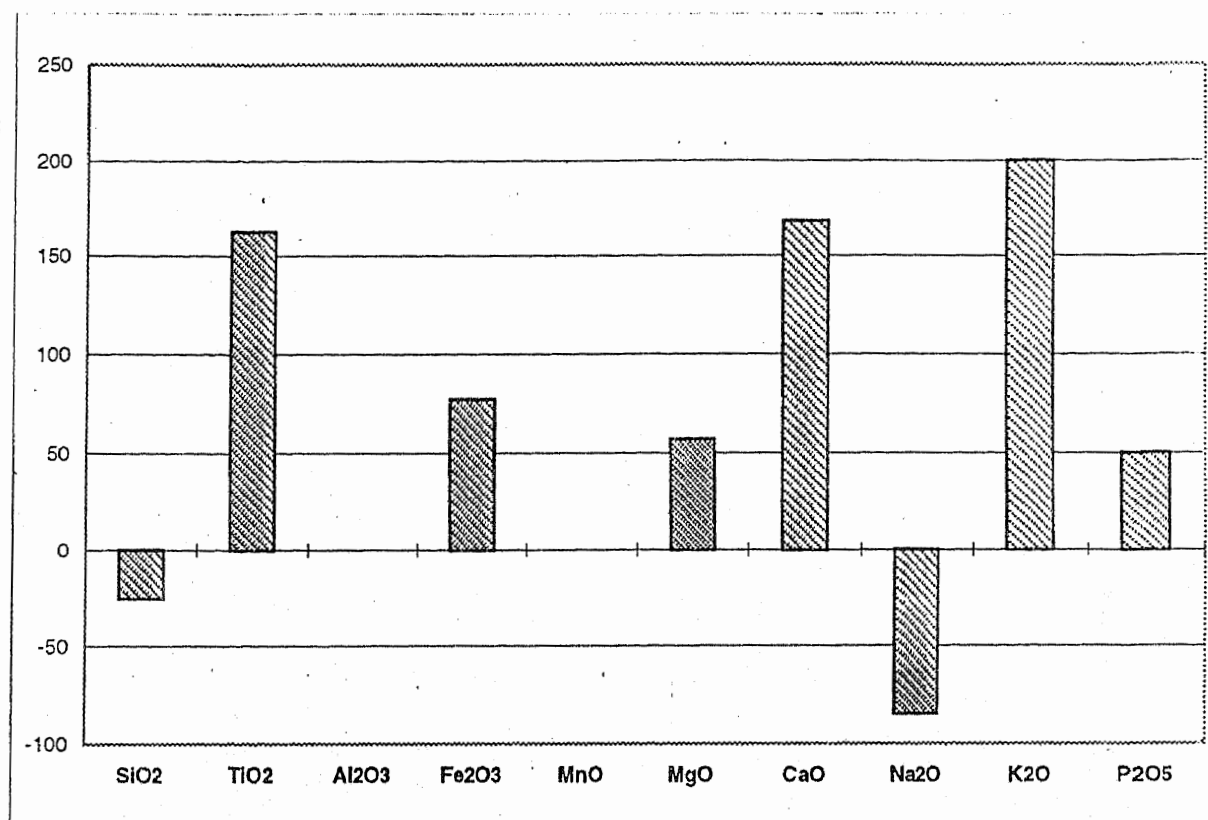


Figure 6.11. Enrichment and depletion in major and trace element abundances during alteration and mineralization of diorites from Gawuch Formation exposed at Langer Gol.

FLUID-INCLUSION STUDIES

INTRODUCTION

Small volumes of fluid are trapped within crystals as inclusions by any of several mechanisms either during their growth or by later processes. They are generally representative of the fluids present during crystal growth or in which it was later bathed (Roedder, 1977; Bodnar, 1994; Bodnar and Vityk, 1994). The fluid inclusions occur in almost all ore and gangue minerals, sometimes as many as a billion per cubic centimeter but are seldom >1mm in size and most are <10 μ m. They are usually studied under the microscope in doubly polished plates of the host mineral, but small ones can be examined in ordinary petrographic thin sections and larger ones can be seen with a hand lens. The fluid inclusions trapped during the growth of host crystals in an ore (i.e. primary inclusions) are samples of the ore fluids, and hence may reveal much about the conditions of ore transport and deposition. There are also secondary fluid inclusions which develop due to shearing and rehealing of fractures, and provide information on fluids that were present around the host crystal at some unspecified time after the original growth (Roedder, 1977). The fluid inclusions can be classified as two-phase or poly-phase inclusions depending upon the nature of the fluid. It can be heterogeneous or homogeneous. Examples include the trapping of two immiscible liquids, such as oil and water or CO₂ and water, liquids and gases, such as boiling water and steam, and liquids and solids. Most fluid inclusions ore deposits are trapped from a single, homogeneous fluid, and because of thermal contraction

vapor bubbles (Roedder, 1977).

The fluid-inclusion research is widely used for the search of blind ore bodies, environment of ore deposition, evaluation of altered and weathered materials in outcrop and sediments, oil exploration, metamorphic petrology and gemology. The microthermometric investigations, i.e. the homogenizing temperature (T_h) and the melting temperature (T_m) reflect the observation of various phase changes in the fluid inclusions under controlled conditions of heating and cooling (Belkin, 1994). The microthermometry is a non-destructive method. In the temperature of homogenization which is also the temperature of trapping, by heating the sample to the point at which the bubble disappears (Hollister and Crawford, 1981; Roedder, 1984; Shepherd et al., 1985; Goldstein and Reynolds, 1994). The temperature of melting for ordinary water rich inclusions refer to the melting of ice. The quantity of NaCl would yield the melting temperature (T_m) value of ice, and thus the salinity is determined by plotting the melting temperature against the weight percentage of the NaCl (Belkin 1994). Freezing the inclusion can determine salinity as the depression of the freezing point of the pure water which is directly proportional to the amount of salt in the solution. Salinity is usually reported as the weight % NaCl equivalent unless melting behaviour or the presence of daughter phase identifies additional cations (Belkin, 1994).

The present fluid inclusion study has been conducted on the ore-bearing quartz veins which transact the diorites of the Kohistan arc in Drosh area, Chitral.

composition of the ore forming fluids and the environment of ore deposition.

PREPARATION AND PROCEDURES

The analytical work for the fluid inclusion research has been carried out in the Geological Survey of Japan, Tsukuba, Japan. A total of 8 samples of copper-bearing quartz veins were selected for doubly polished section of 100-150 μ m. These polished sections were studied under the petrographic microscope to observe the morphology of the inclusions and to select them for microthermometry measurements.

TYPES OF FLUID INCLUSIONS

Fluid inclusions are classified as primary, secondary or pseudosecondary depending upon when the inclusions were trapped relative to the formation of bulk of the enclosing mineral. All the quartz veins examined in this study experienced repeated fracturing in the presence of aqueous fluids as is evidenced by the abundant planes of secondary inclusions observed at low magnification. Generally, high density of randomly oriented fractures decorated with fluid inclusions made it difficult to determine with confidence whether a given inclusion was along one of these fractures (secondary or pseudosecondary) or was trapped during crystal growth (primary). Therefore, it is avoided to classify the fluid inclusion as primary, secondary or pseudosecondary but, rather, have related groups of inclusions to various stages of vein filling.

These fluid inclusions are mainly two-phase (liquid + vapor), but too small (<5 μ m), and make trails occurring across the quartz grain boundaries. It may be noted that the quartz grains are the fine-grained aggregated stuff

the measurement. The fluid inclusions present in this sample are fairly large > 10 μ m. Two phase (liquid + vapor) liquid rich inclusions and poly-phase (liquid+CO₂+ vapor) liquid rich inclusions were the only inclusion types identified. They commonly occurred together in quartz. No daughter crystals were seen. The co-existence of these two types of inclusions is the strong evidence for the presence of two or more immiscible phases, (i.e. liquid, vapor and CO₂) due to boiling at the time of inclusion formation.

A USGS-type Gas-flow Heating/Freezing Stage was used for the measurement of T_h and T_m . This equipment includes i) Heating/Freezing Stage, ii) Electric Gas Heating Element, iii) Doric Trendicator, and iv) Microscopic Objectives. Air compressor, thermocouple, cylinder containing dry nitrogen and Dewar containing liquid nitrogen are also included in the Heating/Freezing Stage.

Calibration of the thermocouple and the whole system has been done. For the thermocouple calibration pure water and pure ice was used. Both the thermocouple and the system were calibrated to 0°C. A number of inorganic, organic and pure metals were used for the calibration of the instrument, and accuracy and precision of the instrument was thus obtained (Table 7.1). During the operation the gas flow rate was maintained as 20 SCFH at $T > 0^\circ\text{C}$ and 10 SCFH at $T < 0^\circ\text{C}$.

DISCUSSIONS

A total number of 6 two-phase (liquid+vapor) fluid inclusions were subjected for freezing measurement. The freezing temperature was measured up

Table 7.1. Melting temperature of the standard materials used for the calibration of the USGS-type Gas-Flow Heating/Freezing system.

Materials	Melting Point
Hg	-38.9 °C
Pure Water	0 °C
Phneoxybenzen (NPL triple-point cell)	26.867 °C
In	156.5 °C
Sn	231.97 °C
Bi	271.3 °C
Pb	327.43 °C
Zn	419.58 °C
NaNO ₃	306.8 °C
KNO ₃	333 °C
K ₂ Cr ₂ O ₇	398 °C
Organic Materials (e.g., anthraquinone etc)	Various
Synthetic Fluid Inclusions (e.g., NaCl-H ₂ O etc)	Various

The material used in the calibration is 99.999% pure. For the organic materials capillaries of 0.5 mm diameter are used.

have been calculated from final melting measurements (Figure 7.1, Table 7.2) and are reported as equivalent concentrations of NaCl. The low T_m affinity advocates 12.28 to 13.40 equivalent wt.% NaCl within the inclusions (Bodnar, 1992; Goldstein and Reynolds, 1994). This salinity (<26 equivalent wt % NaCl) is inferred from the absence of cubic salt daughter minerals (Nash and Cunningham, 1974). The homogenizing (T_h) temperatures recorded ranges from 160 to 350°C. However, it is assumed that the mean temperature (255°C) represents true trapping temperature. There is a wide range of homogenization temperatures occurs in the sample studied. Ahmad and Rose (1980) have proposed various reasons for this kind of wide range of homogenization temperature. The important one are as follows:

- a. Leakage: This could be natural or at the time of heating measurement.
- b. Trapping of both steam and liquid: This would give anomalously high homogenization temperature.
- c. Low homogenization temperature: this might result from inadvertent examination of secondary and/or pseudosecondary inclusions.
- d. Fluctuations in both pressure and salinity at the time of fluid trapping: These would affect the filling temperature.

The wide range in temperature, as observed in the studied samples, could be resulted from any or all of the above reasons. It is therefore, very difficult to draw conclusion about the nature of the mineralizing fluid at this stage, however, we can at least know the high temperature range of mineralizing fluid which will help in determining the composition of fluid

Table 7.2. Table of salinities (wt.% NaCl) that correspond to freezing point depressions (T_m ice) for fluid inclusions melting in the presence of a vapour bubble. Data from Bodnar (1992), adopted from Goldstein and Reynolds (1994).

FPD	.0	.1	.2	.3	.4	.5	.6	.7	.8	.9
0.	0.00	0.18	0.35	0.53	0.71	0.88	1.05	1.23	1.40	1.57
1.	1.74	1.91	2.07	2.24	2.41	2.57	2.74	2.90	3.06	3.23
2.	3.39	3.55	3.71	3.87	4.03	4.18	4.34	4.49	4.65	4.80
3.	4.96	5.11	5.26	5.41	5.56	5.71	5.86	6.01	6.16	6.30
4.	6.45	6.59	6.74	6.88	7.02	7.17	7.31	7.45	7.59	7.73
5.	7.86	8.00	8.14	8.28	8.41	8.55	8.68	8.81	8.95	9.08
6.	9.21	9.34	9.47	9.60	9.73	9.86	9.98	10.11	10.24	10.36
7.	10.49	10.61	10.73	10.86	10.98	11.10	11.22	11.34	11.46	11.58
8.	11.70	11.81	11.93	12.05	12.16	12.28	12.39	12.51	12.62	12.73
9.	12.85	12.96	13.07	13.18	13.29	13.40	13.51	13.62	13.72	13.83
10.	13.94	14.04	14.15	14.25	14.36	14.46	14.57	14.67	14.77	14.87
11.	14.97	15.07	15.17	15.27	15.37	15.47	15.57	15.67	15.76	15.86
12.	15.96	16.05	16.15	16.24	16.34	16.43	16.53	16.62	16.71	16.80
13.	16.89	16.99	17.08	17.17	17.26	17.34	17.43	17.52	17.61	17.70
14.	17.79	17.87	17.96	18.04	18.13	18.22	18.30	18.38	18.47	18.55
15.	18.63	18.72	18.80	18.88	18.96	19.05	19.13	19.21	19.29	19.37
16.	19.45	19.53	19.60	19.68	19.76	19.84	19.92	19.99	20.07	20.15
17.	20.22	20.30	20.37	20.45	20.52	20.60	20.67	20.75	20.82	20.89
18.	20.97	21.04	21.11	21.19	21.26	21.33	21.40	21.47	21.54	21.61
19.	21.68	21.75	21.82	21.89	21.96	22.03	22.10	22.17	22.24	22.31
20.	22.38	22.44	22.51	22.58	22.65	22.71	22.78	22.85	22.91	22.98
21.	23.05	23.11	23.18							

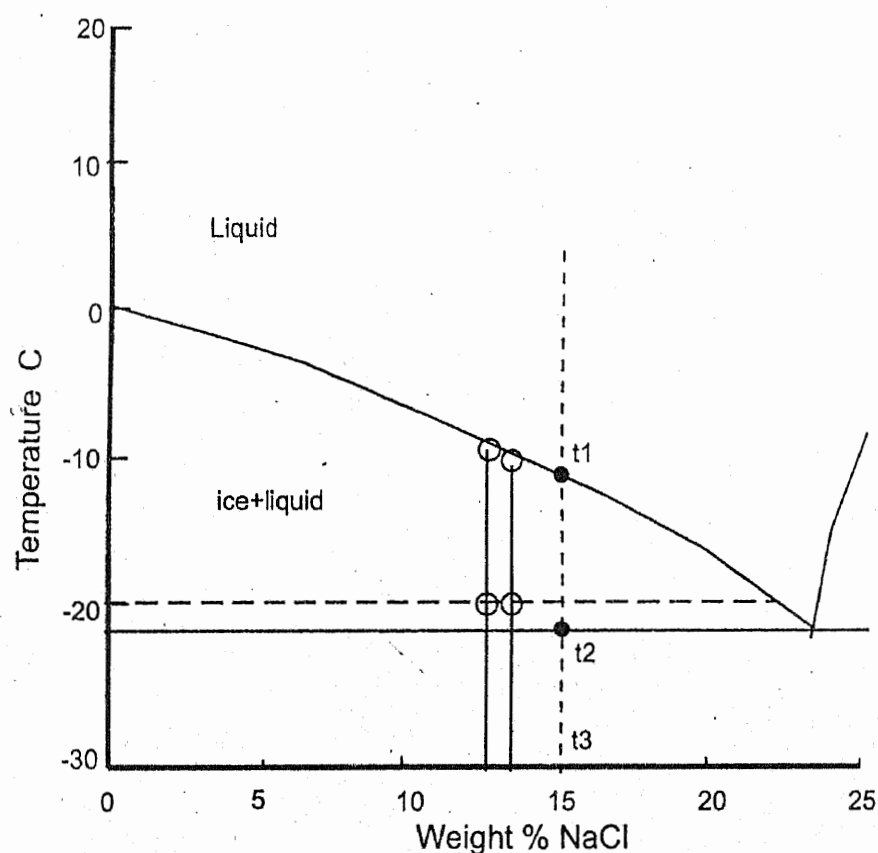


Figure 7.1. Portion of the NaCl-H₂O phase diagram to show the temperatures at which phase changes occur in an inclusion containing 15 wt% NaCl (after Shepherd et al., 1985), $t_1 = -10^\circ\text{C}$ (ice forms and continues to crystallize), $t_2 = \text{eutectic } -21.2^\circ\text{C}$; $t_3 = -20^\circ\text{C}$ (supercooled temperature). On warming the inclusion follows the same path as taken upon freezing until at t_2 the first liquid forms from melting of solid phases. For 13.40 to 12.28 equivalent wt% NaCl: $t_1 = -9.5 - -8.5^\circ\text{C}$; $t_2 = \text{eutectic, } -19.2^\circ\text{C}$; $t_3 = -45^\circ\text{C}$ (super-cool temperature).

the fluid inclusions are the late stage hydrothermal veins formed as a result of dioritic or granodioritic intrusions. The high saline affinity corroborate shallow depositional environment for these veins. The evidences such as the daughter minerals (NaCl: KCl) in the fluid inclusions, high homogenization temperature (Th) and high salinity (>50 equiv. wt.%) as commonly reported in the porphyry Cu deposits are absent in to the ore-bearing quartz veins of Drosh area.

CHAPTER 8

OXYGEN ISOTOPE GEOCHEMISTRY

INTRODUCTION

The isotopic composition of rock-forming minerals is of great importance regarding their origin and conditions of formation. Oxygen isotope data have become an important tool in igneous and metamorphic petrology and in the study of ore deposits. In the recent years, the application of oxygen and hydrogen isotopes played an important role in solving the problems of hydrothermal alteration and ore deposition.

Oxygen has three isotopes whose approximate abundances are: $^{16}\text{O} = 99.766$, $^{17}\text{O} = 0.039 \text{ ‰}$ and $^{18}\text{O} = 0.205 \text{ ‰}$. Its isotopic composition in rocks and minerals is reported in terms of the delta notation ($\delta^{18}\text{O}$) which is the difference between the $^{18}\text{O}/^{16}\text{O}$ ratio of the sample and that of a standard called SMOW (Standard Mean Ocean Water). $\delta^{18}\text{O}$ is expressed as per mil (‰) difference relative to SMOW.

$$\delta^{18}\text{O} = [(^{18}\text{O}/^{16}\text{O})_{\text{sample}} - (^{18}\text{O}/^{16}\text{O})_{\text{SMOW}} / (^{18}\text{O}/^{16}\text{O})_{\text{SMOW}}] * 10^3$$

Thus an increase in $\delta^{18}\text{O}$ represents a relative enrichment in the heavier isotopes. Consequently, positive $\delta^{18}\text{O}$ values indicate enrichment in heavy oxygen while negative $\delta^{18}\text{O}$ values suggest the depletion of ^{18}O in the rock compared to the standard (SMOW). Igneous, metamorphic and sedimentary rocks display systematic variations in their isotopic composition of oxygen that provide insight into the origin of such rocks. These data reflect the temperature of final oxygen-isotope equilibrium and the oxygen-isotope composition of the fluid phase.

The per mil fractionation, $10^3 \ln \alpha$ between two substances (A and B) can be very well approximated by the - value:

$$\Delta_{A-B} = S_{A-B} = 10^3 \ln \alpha_{A-B}$$

The temperature of formation of the minerals can be determined from the measured $\delta^{18}\text{O}$ values, if the equilibrium $\delta^{18}\text{O}$ relation among the minerals is known. Various factors that affect the isotopic composition of the minerals have been discusses in detail by O'Neil (1977). The $\delta^{18}\text{O}$ values of the water in which the mineral formed can be calculated from the $\delta^{18}\text{O}$ values of the minerals if the temperature can be measured by any other means.

TYPES OF WATER IN HYDROTHERMAL SYSTEM

There are five basic types of water in the hydrothermal system:

1. Sea Water

The sea water has constant isotopic composition ($\delta^{18}\text{O} = 0 \pm 1 \text{ ‰}$) in most parts of the oceans. This is the reason that it represents a useful isotopic standard (SMOW). Its values are variable where strong evaporation occurs (e.g. Red Sea) or where sea water is mixed with water of other origin (e.g., rivers).

2. Meteoric Water

Water derived from the atmosphere is called meteoric water. Where this water sinks in to the earth, it assumes the temperature of enclosing rocks, and as a result the water temperature generally increases with depth of circulation. Meteoric water contains major crustal elements, such as sodium, calcium, magnesium and sulfate and carbonate radicals. The δD and $\delta^{18}\text{O}$ values for meteoric water are negative in most places. The average δD and $\delta^{18}\text{O}$ of almost all meteoric water is

close to -70 ‰ and 0 -10 ‰ respectively. These values vary with geographic locations. The higher the latitude or elevation, the lower are δD and $\delta^{18}O$ values of waters.

3. Juvenile Water

Juvenile water is derived from the mantle and never exists on the surface. The range in isotopic composition of $\delta^{18}O$ is 7 to 8 ‰ (Shepherd and Epstein, 1970). It is also defined as water in isotopic equilibrium with normal mafic magma $\delta D = 75 \pm 10$ ‰, $\delta^{18}O = 6 \pm 0.5$ ‰ (Taylor, 1979) at temperature around 1200°C.

4. Magmatic Water

This is the water which is involved in magmatic system. This water is exsolved in magmatic system regardless of the origin or the ultimate nature of water. The magmatic water would presumably consist of juvenile, metamorphic and/or subduction components. These waters have isotopic compositions that have equilibrated with magmas at higher temperatures ranging from 700 to 1000°C. The typical range for the isotopic composition calculated for the magmatic water is $\delta D = -50$ to -85 ‰ and $\delta^{18}O = +5$ to $+9$ ‰ (Taylor, 1974).

5. Connate or Metamorphic water

This is the water generated by the dehydration of the rocks/minerals during regional metamorphism and connate formational interstitial burial water driven off during compaction and early metamorphism. The isotopic composition of metamorphic waters has been modified by equilibrium with oxygen- and hydrogen-bearing minerals during metamorphism at temperatures from 300 - 600°C. The δD and $\delta^{18}O$ values for metamorphic waters are estimated as -20 to -65 ‰ and +5 to +25 ‰.

‰ respectively. The isotopic composition of this kind of water varies from one area to other and is dependent on the initial rock types and their history of water-rock interaction.

There are certain processes that change the isotopic composition of hydrothermal water which should be considered during interpretation. These processes are 1) variation at the source; 2) isotopic fractionation between water and other solid, liquids or vapors, any or all of which can be later separated or isolated from the system; 3) exchange with a large isotopic reservoir; and 4) mixing of waters derived from different and isotopically distinct sources. Independent or combination of two or more of these mechanisms can produce very complex hydrothermal water isotopic data.

$\delta^{18}\text{O}$ IN MINERALIZED QUARTZ VEINS

A reconnaissance study of the oxygen isotope composition of quartz from the mineralized quartz vein in Gawuch area was undertaken to investigate possible origin of the fluid component involved in the vein formation and associated alteration and cu-mineralization.

Quartz in 9 samples of the mineralized quartz veins, having mainly tetrahedrite with subordinate galena, chalcopryite, bornite, pyrite and magnetite, were analyzed for oxygen isotope composition. The ^{18}O values of quartz veins range from 14.49 to 18.32 ‰ with a mean of 16.63 ‰ (Table 7.3). The oxygen isotope composition of the quartz from the studied quartz veins suggests that the mineralization in the area is related with a hydrothermal event which has produced a

high $\delta^{18}\text{O}$ signature in the mineralized quartz veins and most probably also in the associated altered host rocks.

$\delta^{18}\text{O}$ VALUES OF THE HYDROTHERMAL FLUID

The oxygen isotopic composition of the mineralizing fluids can be calculated from the measured mineral isotopic composition and the mineral-water isotopic fractionation factors. These studies involved the experimentally and/or empirically determined mineral-water fractionation equations for quartz, plagioclase and feldspar (see Taylor, 1974; Clayton et al., 1972; Bottinga and Javoy, 1973; Friedman and O'Neil, 1977; Kulla, 1979; Matsuhisa et al. 1979 and Matthews et al., 1983). Since Matsuhisa et al. (1979) offer the best calibration for quartz-water oxygen isotopic fractionation factor, their calibration curve is used here.

The $\delta^{18}\text{O}$ value of the mineralizing fluid of the Gawuch Formation can be calculated from the $\delta^{18}\text{O}$ measurement of quartz in the quartz vein, if the temperature of formation of the quartz veins or temperature of alteration of adjacent rocks is known. Appropriate formation temperatures (homogenization temperature) were calculated from the fluid inclusion data for the quartz veins which is varying from 160-350 °C with a mean value of 255°C (Chapter 7). The isotopic composition of water in equilibrium with the quartz veins was calculated at this mean temperature (255°C) using the empirically determined quartz-water fractionation equation $1000 \ln \alpha = 3.34 (10^6 T^{-2}) - 3.31$ or the curve of Matsuhisa et al. (1979). This temperature yields the average $\Delta^{18}\text{O}$ (quartz-water) value of 8.70 for the mineralized quartz veins. The estimated δO^{18} value of the mineralizing fluid, therefore, ranges from 5.79 to 9.62 ‰ with a mean value of 7.98 ‰ (Table 8.1). These values are falling within the range of

Table 8.1. Oxygen isotope composition of quartz from the mineralized quartz veins from the Drosh area, Chitral, and $\delta^{18}\text{O}$ value of the mineralizing fluids.

Sample No.	^{18}O quartz	$\delta^{18}\text{O}$ fluid %
GR73	16.84	8.14
KG168	17.17	8.47
KG203	16.83	8.13
KG12	14.49	5.79
KG17b	16.72	8.02
GR74	17.78	9.08
GR75	18.32	9.62
GR76	14.61	5.91
GR81 b	17.36	8.66
Average	16.68	7.98

Average $\delta^{18}\text{O}$ (fluid) = 7.98 % at temperature = 255 °C

values accepted for waters of metamorphic (4-25‰) and magmatic (5-9‰) origin (Taylor 1974) (Figure 8.1). The lack of negative values for the mineralizing fluids strongly disprove the involvement of meteoric waters. This suggests that the mineralized quartz veins and the associated copper mineralization in the Gawuch Formation would be in equilibrium at geologically reasonable temperatures of $255 \pm 95^\circ\text{C}$ with fluids having an average $\delta^{18}\text{O}$ values of 7.98 ‰ based on the quartz-water fractionation curve of Matsuhisa et al. (1979).

THE ORE-FORMING FLUID

The most distinctive feature of the isotopic data of the studied quartz veins is the ^{18}O enrichment of quartz. This pattern is in strong contrast to those in many recently investigated hydrothermal systems in which ^{18}O depletion is due to the involvement of low ^{18}O fluid of meteoric origin (O'Neil et al., 1973; Taylor, 1974; Klein and Criss, 1988). The high oxygen isotopic signature of the studied quartz veins, however, rules out the possibility of involvement of meteoric water and shows that some of heavy fluids (much higher than the present-day sea water) played an important role in the formation of quartz veins and associated Cu-mineralization and alteration.

There are, however, certain examples of ^{18}O enrichment in hydrothermal systems which result in the high $\delta^{18}\text{O}$ values (Kerrick and Fryer, 1979; Taylor, 1971; Magaritz and Taylor, 1976; Paterson, 1982; Beaty and Taylor, 1988 and Constantopoulos, 1994). High $\delta^{18}\text{O}$ hydrothermal fluids can be originated by various processes namely; evaporation in a closed basin, exchange with high $\delta^{18}\text{O}$ of country

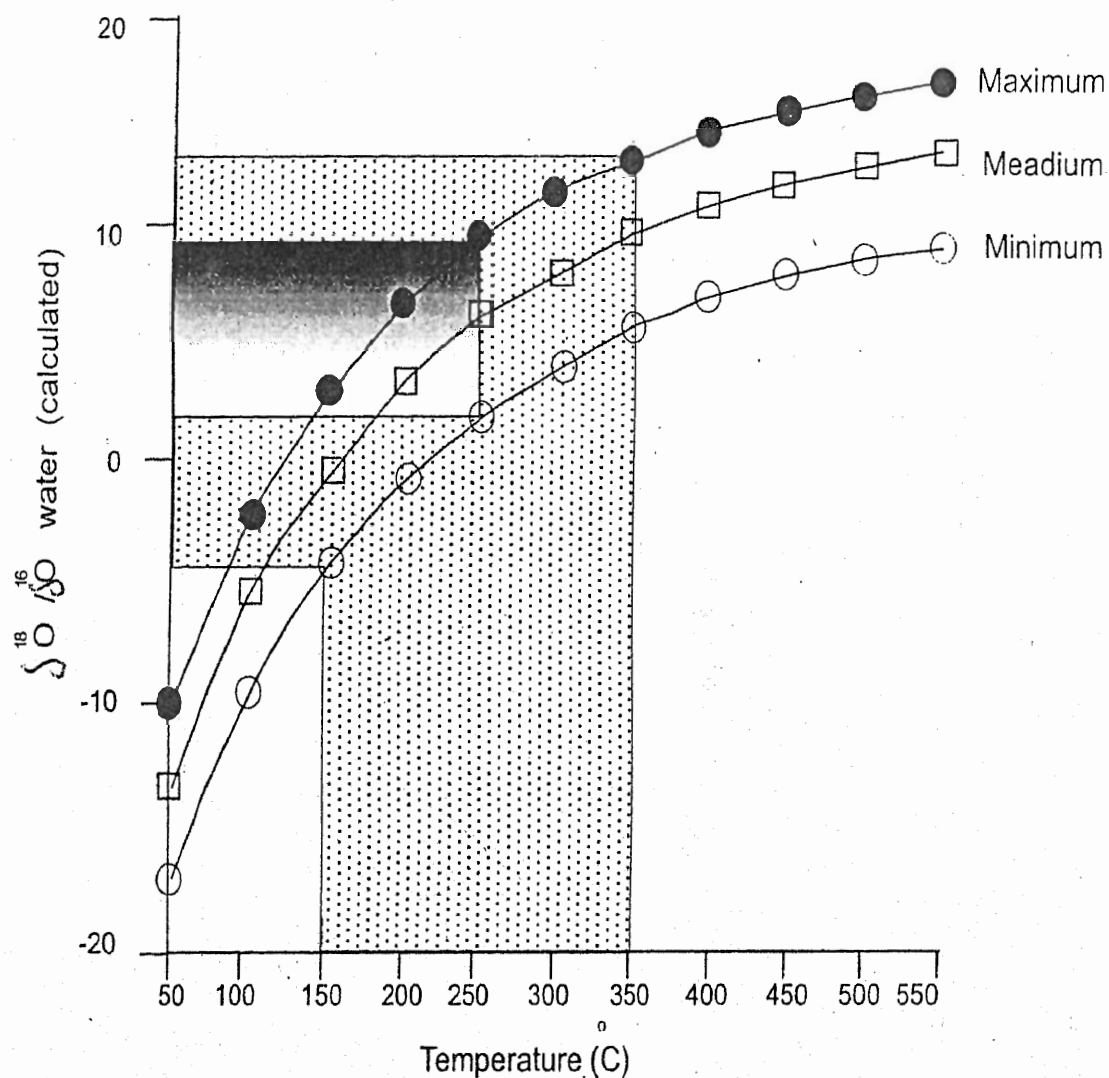


Figure 8.1. Oxygen isotope composition of parental water calculated at a series of temperatures from the measured oxygen isotope composition of quartz from the Gawuch Formation. The lightly shaded area represents the range of the fluid inclusion homogenization temperature (160-350 °C) and the range of corresponding oxygen-isotope composition (calculated) of parental waters. The inset with darker shades represents the range of oxygen-isotope composition of the magmatic water. similarity in the

rocks, boiling in the ore fluids, metamorphic and magmatic water (Beatty and Taylor, 1988).

A single or combined effect of all these processes can be evaluated for the possible high $\delta^{18}\text{O}$ of the ore-forming fluids of the Gawuch Formation. Because of the limited data one can not prove or disprove any of the above mentioned processes. However, it can be suggested that an isotopically heavy fluid ($\delta^{18}\text{O} = 5$ to 9‰) of some type, probably of acidic nature having chlorine to form complexes with metal, can be the ore-metal transporting agent in the rocks of the area. The more probable fluid in this case can be either metamorphic or magmatic or even mixture of both.

It is already mentioned that the rocks of the area are metamorphosed to greenschist- and at places, to epidote-amphibolite facies metamorphism. These rocks have well developed fabrics, faulting and shearing. Moreover the Cu-mineralization (both in the quartz veins and the associated rocks) occurs within the granodiorite sills, dikes and plugs in the Gawuch Formation. The involvement of either metamorphic or magmatic water in the development of higher $\delta^{18}\text{O}$ values in the Gawuch Formation is, therefore, evaluated here.

The development of high ^{18}O values, in the mineralizing fluids, in the region affected by low-grade regional metamorphism can be attributed to the metamorphic dehydration (Spooner et al., 1974; Paterson, 1982). During this process the metals leach out of the host rocks and concentrate in the metamorphic dehydration fluids (Paterson, 1982). The higher $\delta^{18}\text{O}$ signature of the mineralizing fluids in Gawuch Formation can be related to this type of dehydration phenomenon. However, the development of hydrous mineral phases and the higher amount of H_2O in the

mineralized rocks of the Gawuch Formation do not favor the possibility that the metamorphic dehydration or dewatering can be the cause of ore-forming fluid in the area. Moreover, the restriction of the mineralization to the plutonic igneous rocks (diorites and granodiorites) and the quartz veins closely associated with them and absence from the metavolcanic rocks negate a role of metamorphic fluids as a carrier of the mineralization.

The persistence of igneous activity in the form of diorite-granodioritic plugs, sills and dikes (as appophyses of the Lowari pluton) hosting the mineralization suggests a role of magma in the generation of hydrothermal system rather than metamorphism. It is, therefore, hypothesized that the diorite -granodiorite plutons existing at depth beneath the mineralization in Gawuch Formation could have been sources of brine metalliferous fluids. These types of brine fluids related to porphyry copper mineralization are well documented in literature (Beane and Titley, 1981) and are thought to have evolved from magmas (e.g. Henley and McNabb, 1978; Burnham, 1979; Dilles et al., 1992). These fluids have precipitated the cu-sulphide phases along with silica mainly in the form of quartz veins in shallow level. However, for some reason the meteoric water did not have excess to the hydrothermal system of the area. The magmatic signature of the ore fluids could either reflect direct magmatic association or the extensive isotopic exchange between the hydrothermal water and the wall rocks, perhaps in response to the intrusive activity.

It is not possible at this stage to distinguish firmly between these possibilities with available data, but it is considered that the oxygen isotope data are supportive

of at least an indirect relationship with magmatism. Further detailed studies are required to confirm the oxygen isotope observations regarding the evolution of ore-forming fluid in the Drosh area.

CHAPTER 9

LEAD ISOTOPE GEOCHEMISTRY

INTRODUCTION

Lead, in the form of 1) radiogenic daughter of U and Th, 2) Lead-bearing minerals and 3) a trace element in all kinds of rocks, is widely distributed throughout the Earth. It occurs in three isotopic forms such as ^{206}Pb , ^{207}Pb and ^{208}Pb . ^{206}Pb , ^{207}Pb are known as radiogenic isotopes and are forming due to the radioactive decay of ^{238}U and ^{235}U respectively while the ^{208}Pb is known as thorogenic lead and is forming due to the decay of ^{232}Th . This decay causes variation in lead isotope composition which is considered a powerful tool in solving problems of petrogenesis and metallogenesis. The isotopic composition of lead has a wide range of variation from highly radiogenic Pb in very old U and Th-bearing minerals to common Pb in galena and other minerals. The isotopic composition of lead in galena remains unchanged after its initial crystallization because of its extremely low U/Pb and Th/Pb ratios. The lead isotope ratios in galena are, therefore, used to estimate the model ages of the deposits in which galena crystallized.

Various lead isotope models were proposed in the past among which the Holmes-Houterman model (based on single-stage history) of Holmes and Houterman (1946); Stacey and Kramers (1975) two stage model; Wisconsin model (Afifi et al., 1984) and Proterozoic model (Deb et al., 1989) are of importance. Stacey and Kramers (1975) two stage model is mostly used in the lead isotope system. The processes evolved in lead evaluation in the earth are also discussed by Gancarz and Wasserburg (1979), Tera (1981) and Abarede and Juteau (1984).

One of the fundamental problems in metallogenesis is that of the origin of the chemical elements that make up mineralization. This problem of origin of metal can become very complex indeed since the metallogenesis is directly related to the complexity of the regional geologic and metallogenic history. The lead isotope geochemistry is considered to be the most useful approach available in dealing with these kinds of problems. The lead isotope geochemistry is useful in many ways: 1) It provides a correlation between isotopic composition of lead in a minerals deposit and that of the rock units in their regional setting (see Doe, 1977; Doe and Delevaux, 1972; Wedepohl et al., 1978; Keopped, 1984; Marcoux and Jebrak, 1987); 2) It may provide a better understanding of ore forming processes and an explanation for the origin of lead (and probably other base metals) in ores; 3) It has made it possible to re-examine the question of the role played by old mineralization as a source of new mineralization. This re-generation theory was first advanced by Schneiderhohn (1952) and later further development by Routhier (1969; 1980); 4) It could lead to the dating of certain deposits formed by hydrothermal sedimentary origin thus determining whether they are syngenetic or epigenetic and 5) It provides a perfect separation of paragenesis belonging to distinct metallogenic processes. This is due to the fact that a great stability in lead isotope composition exists for each metallogenic process.

The provenance of metals in ore deposits is a matter of considerable interest and economic importance. The plumbotectonic model is another important contribution by Doe and Zartman (1979) and Zartman and Doe (1981) in this regard. In this model the specific isotopic characteristics of lead reflect the characters of source

areas, which can in turn reflect major reservoirs of lead, such as the mantle, lower and upper continental crust.

Keeping in view the above mentioned characteristics of lead isotope, the lead isotopic composition in the galena of the Cu-mineralization of Gawuch Formation is evaluated and discussed in the following section.

RESULTS AND DISCUSSIONS

Three samples of galenas from the quartz veins of Gawuch Formation were sent to Dr. Robert Stern for the Pb-isotope analyses. These analyses were performed at University of Texas, Dallas by using mass spectrometer. The ratios are normalized to National Bureau of Standard 1981 common lead standard.

The lead isotopic compositions of three galena specimens from Cu-bearing quartz veins of Gawuch Formation along with, computed model ages and their μ values are presented in Table 9.1 and are plotted in conventional diagrams of $^{206}\text{Pb}/^{204}\text{Pb}$ and $^{206}\text{Pb}/^{204}\text{Pb}$ vs. $^{208}\text{Pb}/^{204}\text{Pb}$ (Figure 9.1a and 9.1b). The data plot very close to the evolutionary growth curve of Stacey and Kramers (1975) in $^{207}\text{Pb}/^{204}\text{Pb}$ vs. $^{206}\text{Pb}/^{208}\text{Pb}$ diagram (Figure 9.1a) and plot above the evolution curve in $^{208}\text{Pb}/^{204}\text{Pb}$ vs. $^{206}\text{Pb}/^{204}\text{Pb}$ diagram (Figure 9.1a, b). There is very little or negligible variation in the lead isotopic composition of $^{206}\text{Pb}/^{204}\text{Pb}$ (ranging from 18.73 to 18.79), $^{207}\text{Pb}/^{204}\text{Pb}$ (ranging from 15.66 to 15.73) and that of $^{208}\text{Pb}/^{204}\text{Pb}$ (ranging from 39.04 to 39.28). These leads are considered to be radiogenic.

By considering the Pb-isotope data in regard to single-stage model of Holms-Houterman (1946) it is concluded that the Pb in studied galena is anomalous lead as it does not fit in the single-stage model. It is, therefore, suggested that the single-

Table 9.1. Lead-isotope composition computed model ages of Galena from Cu-bearing quartz veins.

Sample	$^{206}\text{Pb}/^{204}\text{Pb}$	$^{207}\text{Pb}/^{204}\text{Pb}$	$^{208}\text{Pb}/^{204}\text{Pb}$	Model age (Ma)	μ
Tz 5	17.79	15.79	39.29	140	10.01
Tz 8	18.77	15.69	39.14	66	9.98
Tz 203	18.77	15.66	39.04	42	9.86
Average	18.77	15.69	39.15	83	9.95

Model ages and μ values according to Stacey and Kramers (1975) model.

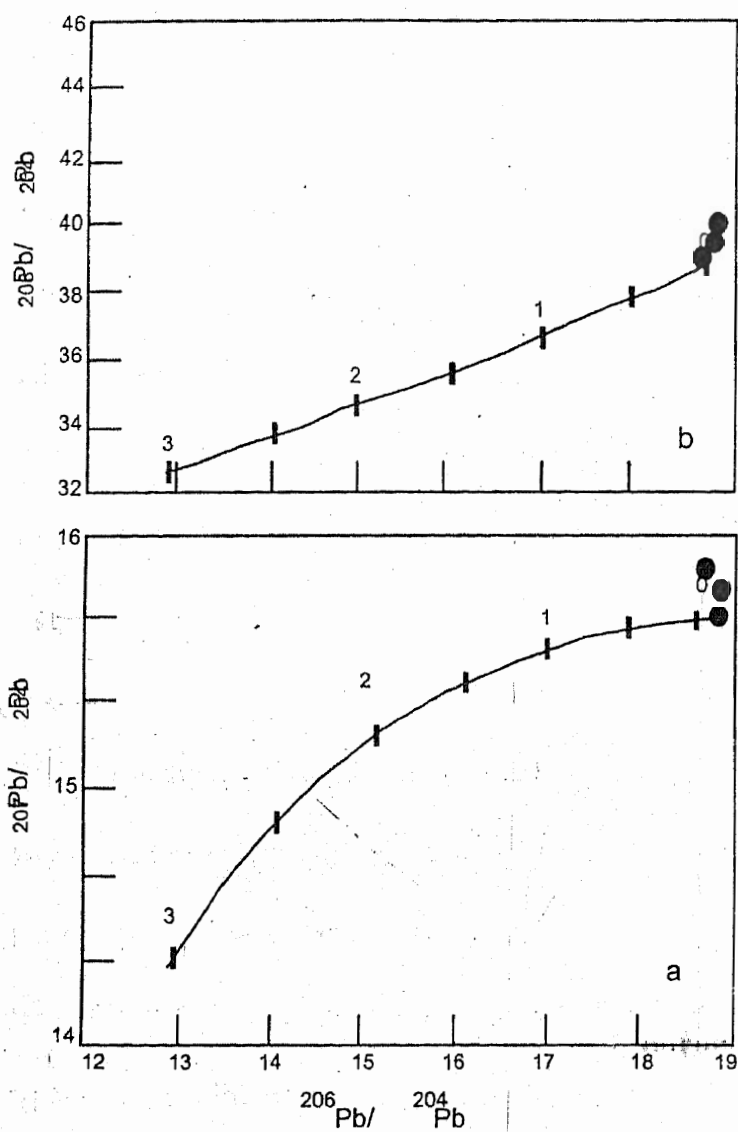


Figure 9.1. Lead isotope ratio diagrams showing growth curve of Stacey and Kramers (1975). The data from Gawuch Cu-mineralization plot very close to the evolutionary curve in $^{207}\text{Pb}/^{204}\text{Pb}$ vs. $^{206}\text{Pb}/^{204}\text{Pb}$ and Pb diagram (a) and above the evolution curve in $^{208}\text{Pb}/^{204}\text{Pb}$ vs. $^{206}\text{Pb}/^{204}\text{Pb}$ (b).

stage model of Holmes and Houterman (1946) is not applicable for the age determination of the studied mineralization. It is, therefore, appropriate to use the two-stage models of lead evolution. In the present study the two-stage model equation (i.e. $m = \frac{{}^{207}\text{Pb}}{{}^{204}\text{Pb}} - b_0 / \frac{{}^{206}\text{Pb}}{{}^{204}\text{Pb}} - a_0$) of Stacey and Karamers (1975) has been used for the calculation of model ages of the Gawuch cu-mineralization. This model yields a wide range of age (42 to 140 Ma) with μ values of 9.86 to 10.01 (Table 9.1). This could be assigned as model date for the mineralization and could be considered as the upper limit of age of the Gawuch cu-mineralization. The time span (t_1) ranging from 42-140 Ma (average 83 Ma) is the time when Pb for the Gawuch Formation cu-mineralization was separated from its source. No isotopic age determination of the host dioritic pluton and the associated metasediments are made yet. However, an age of 42-48 Ma; Ar/Ar basis has been reported by Zeitler (1985); Treloar et al. (1980); for the Lowari pluton, of which the host diorites are related. This age of the Lowari pluton could vary considerably as it is a complex of intrusions during different episodes. Therefore, the correlation of the age of mineralization and the host diorites could be possible. As we have three isotopic compositions and these are not plotting on a single line, therefore, the best fit line with a slope (R) of 0.802 has been determined in a plot of ${}^{206}\text{Pb}/{}^{204}\text{Pb}$ vs. ${}^{207}\text{Pb}/{}^{204}\text{Pb}$ (Figure 9.2). This anomalous line (slope) can be caused by the addition of varying amounts of radiogenic Pb, derived from U-Th bearing minerals in the crust, to ordinary lead (Faure, 1986). If it is assumed that this line is the true secondary Isochron and anomalous lead is not the mixture of two common leads of differing isotopic compositions then the slope of this isochron of anomalous lead can be used to derive information about the age and

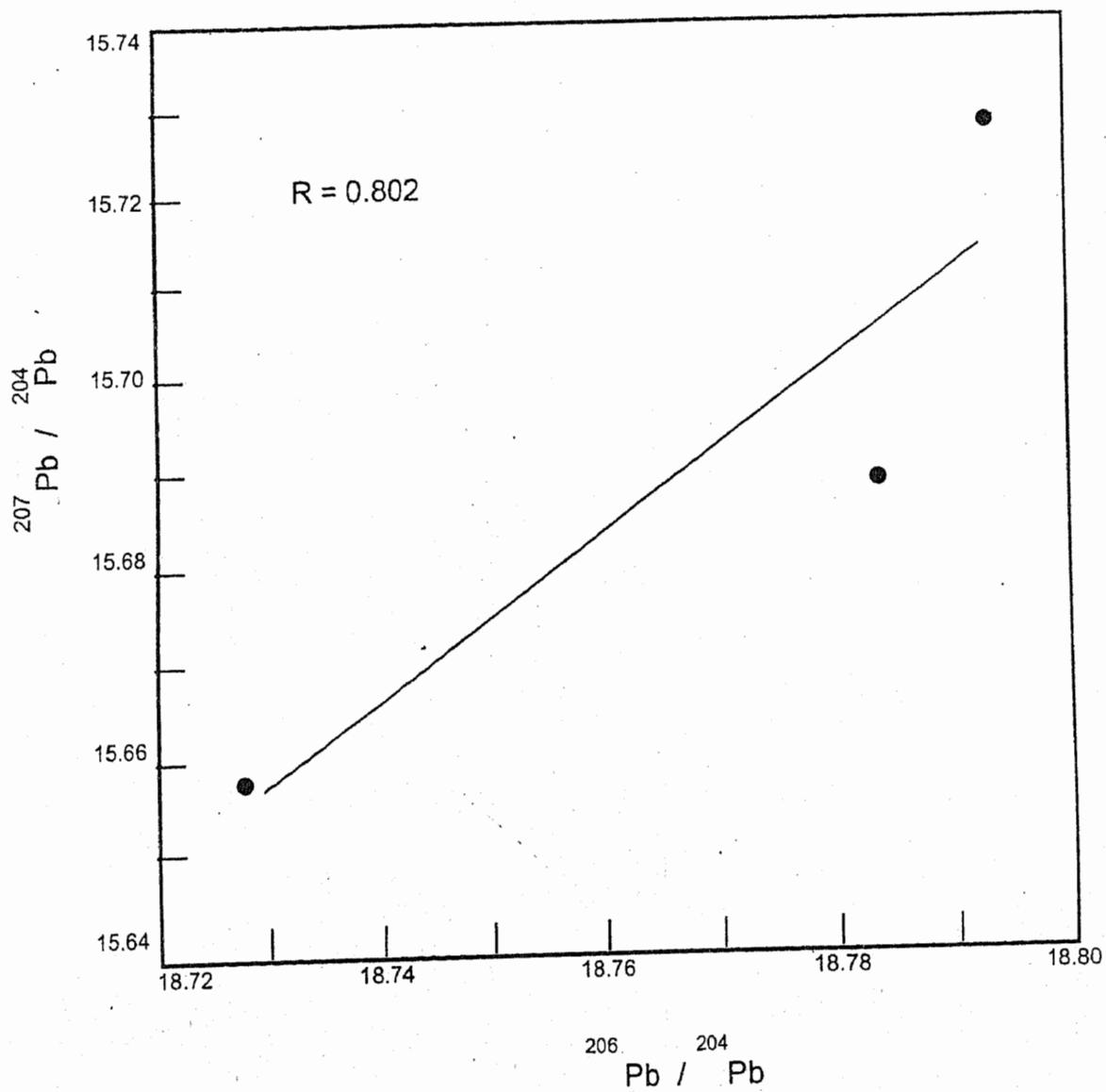


Figure 9.2. $^{206}\text{Pb}/^{204}\text{Pb}$ vs. $^{207}\text{Pb}/^{204}\text{Pb}$ diagram for isotopic composition of galena from quartz veins in Cu-mineralization from the Gawuch Formation.

Th/U ratio of the source rock that have provided the radiogenic lead in the past. By considering the slope R (0.802), a date (t_2) of 3443 Ma has been calculated by using the equation $t = 1/(\lambda_2 - \lambda_1) \ln 137.88 R$. This date (t_2) could be the instant in the past when the decay of U isotope produced radiogenic Pb having the $^{207}\text{Pb}/^{206}\text{Pb}$ ratio equal to the slope of anomalous Pb line. Zartman and Doe (1981) in version I of plumbotectonics has given the summary plots (Figure 9.3a & b) of isotopic ratios which show the various fields defining the present day lead isotopic composition for major reservoirs such as mantle, orogeny^e, upper and lower continental crust. The lead isotopic composition of the studied galena when plotted in these diagrams (Figure 9.3a & b), fall within the intersection of fields for upper and lower crust.

The lead isotope compositions of the studied galena contain significant radiogenic lead and, therefore, one sample fall above the upper continental crust and the other two fall in a field intermediate between the Orogeny and upper crust curve of Zartman and Doe (1981) in $^{206}\text{Pb}/^{204}\text{Pb}$ - $^{207}\text{Pb}/^{204}\text{Pb}$ diagram (Figure 9.4a). However, in $^{208}\text{Pb}/^{204}\text{Pb}$ - $^{206}\text{Pb}/^{204}\text{Pb}$ diagram (Figure 9.4b) the data fall to the left of the orogeny evolutionary curve (i.e. less radiogenic field). This diagram is, however, not informative because of the close spacing between mantle, orogeny, and upper crust curves. The plotting of Pb-isotope data above the orogeny Pb curve of Zartman and Doe (1981), indicate that the studied galena may be characterized as containing an important contribution of lead from radiogenic source (i.e. upper continental-crust-component) and may also have relation with orogeny. However, there could be the possibility of involvement of small mantle derived component. So the lead isotope data is suggestive of crustal provenance to the base metal mineralization in

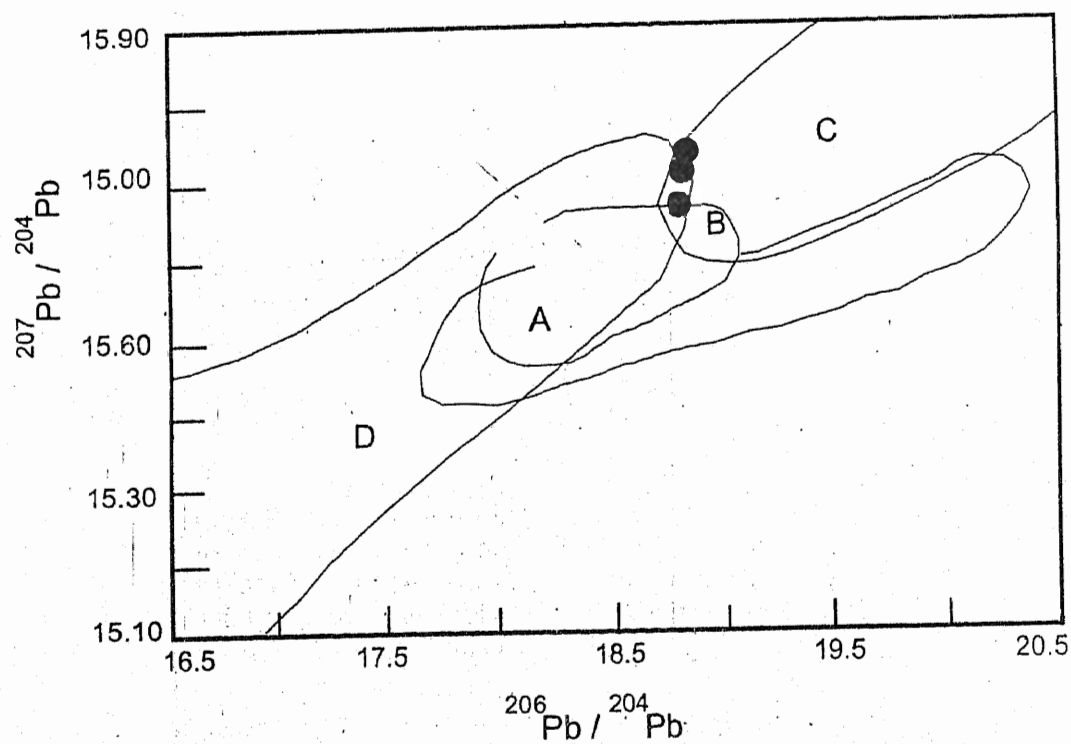
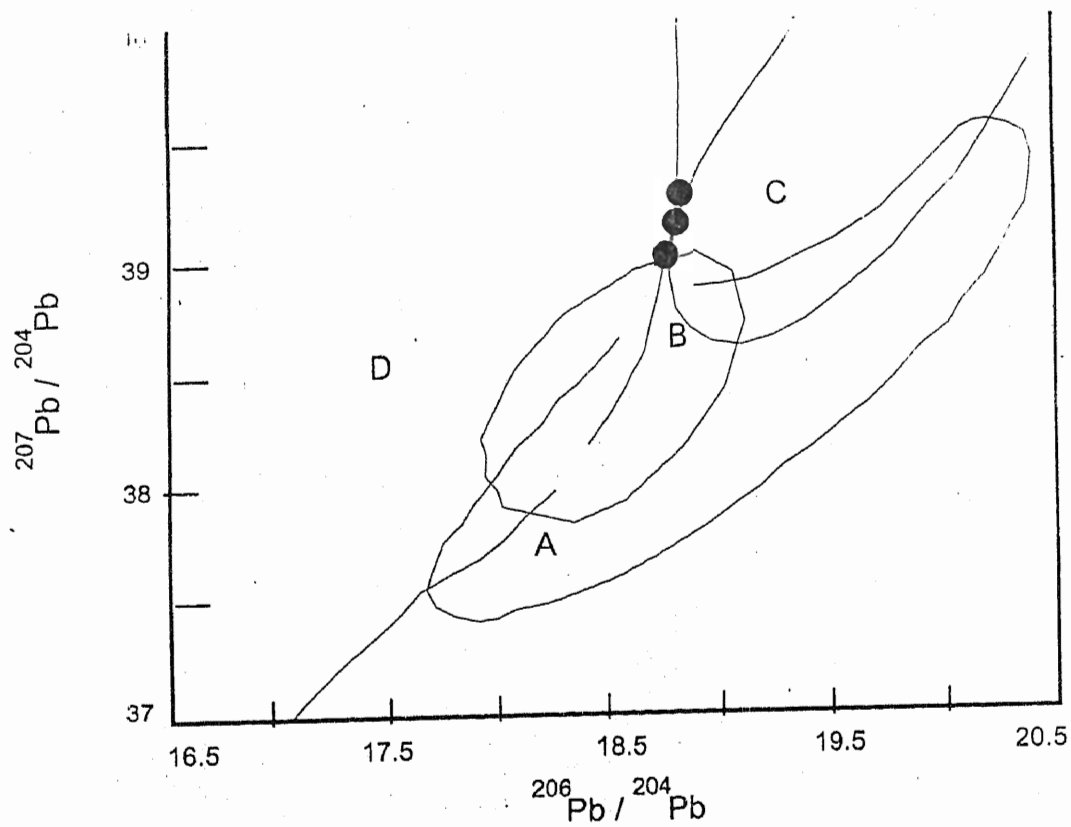


Figure 9.3 a, b. Plots of lead-isotopic ratios used to define the modern fields for mantle, upper crust, lower crust, and orogene (after plumbotectonic model of Zartman and Doe, 1981). A = mantle. B = orogene. C = upper crust. D = lower crust. The lead isotopic data from Gowuch Cu-mineralization g plots within the intersection of fields for upper crust and orogeny curve.

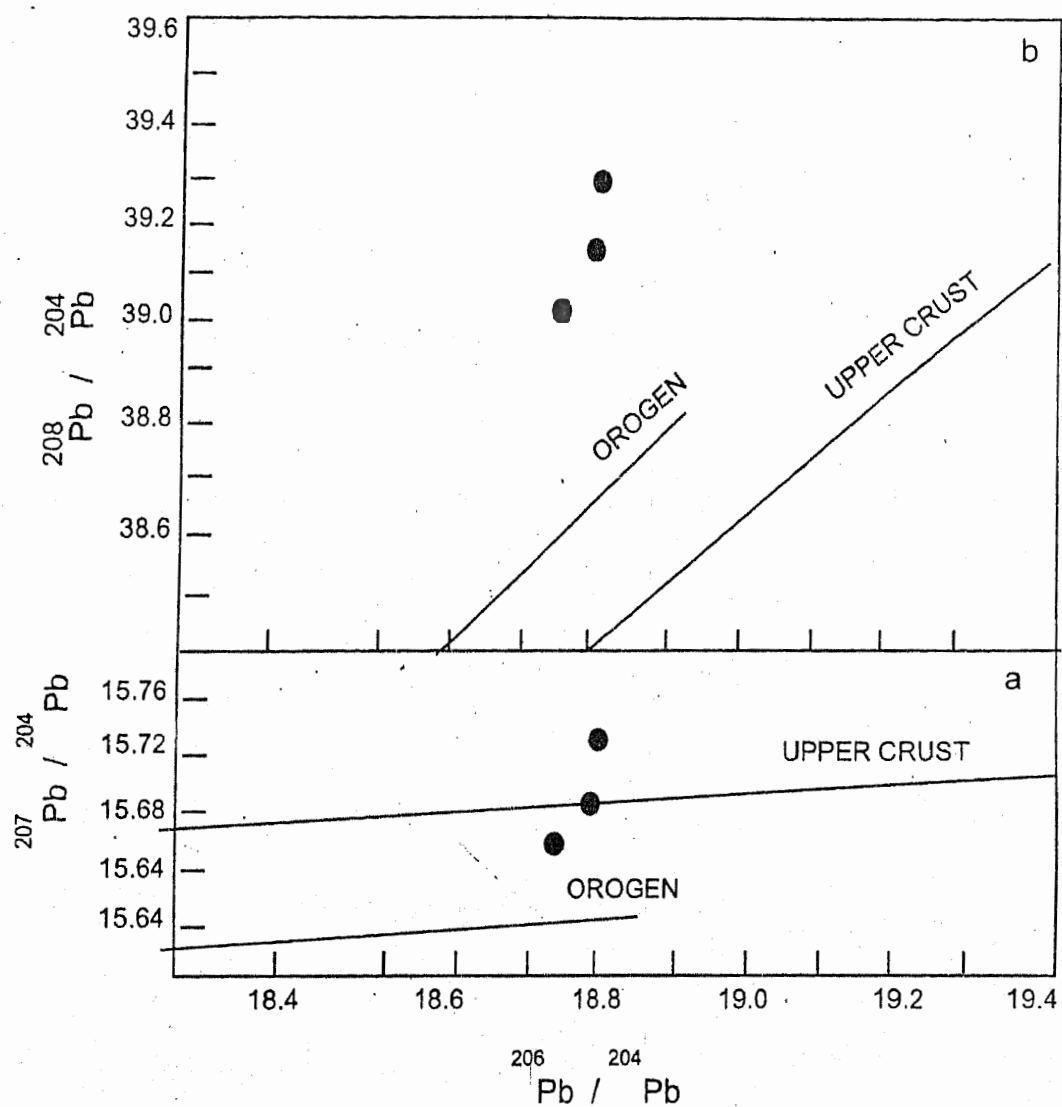


Figure 9.4a,b. The lead isotope ratio diagram showing growth curve of upper crust and orogene of Doe and Zartman (1979). One sample from the Gawuch copper mineralization plots above the upper continental crust and two other between the orogeny and upper crust (a). All the samples plot to the left of the orogeny curve (b).

the area. The role of the mantle could be mainly confined to providing heat for anatexis of the crustal material.

The Pb-isotope composition of galena from the Cu-mineralized quartz vein in the Gawuch Formation are compared with various types of veins and other deposits elsewhere in the world (Figure 9.5a & b). These diagrams also show the average growth curves of plumbotectonic model of Doe and Zartman (1979) for the most significant reservoirs including the mantle, orogene, lower and upper crust. There is very close association of the studied galena isotopic composition with the Rossie-type veins of New York (Ayuso et al., 1987) and Ontario (Fletcher and Farquhar, 1982) in both the $^{207}\text{Pb}/^{204}\text{Pb}$ vs. $^{206}\text{Pb}/^{204}\text{Pb}$ and $^{208}\text{Pb}/^{204}\text{Pb}$ vs. $^{206}\text{Pb}/^{204}\text{Pb}$ diagram (Figure 9.5a & b). Compared to the lead isotope composition of galena from Balmat^a-Edwards district (Doe, 1962; Fletcher and Farquhar, 1982), the studied galena from quartz veins are clearly more radiogenic. The studied galena are, however, less radiogenic than the Mississippi Valley-type deposits (Doe and Delévaux, 1972; Heyl et al., 1966) and the Laisvall-type sandstone-hosted lead-zinc deposits of Sweden (Figure 9.5). The studied galena are also more radiogenic relative to the conformable massive sulfide deposits elsewhere (Gulson et al., 1983, 1984, 1985; LeCoutenr, 1973; Fletcher, 1979; Fletcher and Farquhar, 1981; Koeppel, 1980; Deb et al., 1989; Shah et al., 1992). It is clear from these diagrams (Figure 9.5a & b) that the galena from Gawuch quartz veins have similar isotopic composition as that of Rossie-type veins of USA and Canada.

If we assume 42-140 Ma (average 83 Ma) as the time span for the Gawuch Cu-mineralization. This could be assigned as the model date for mineralization and

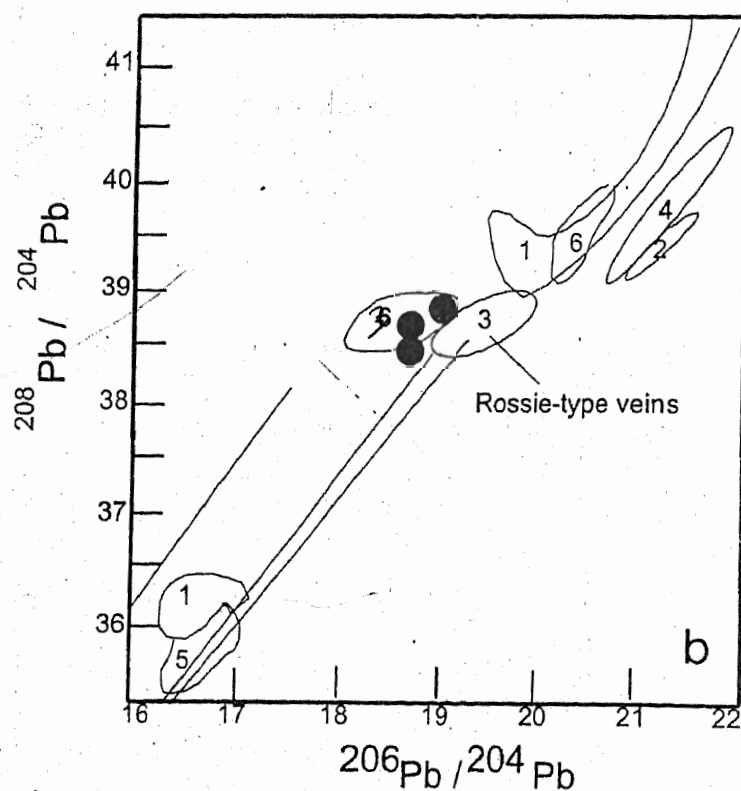
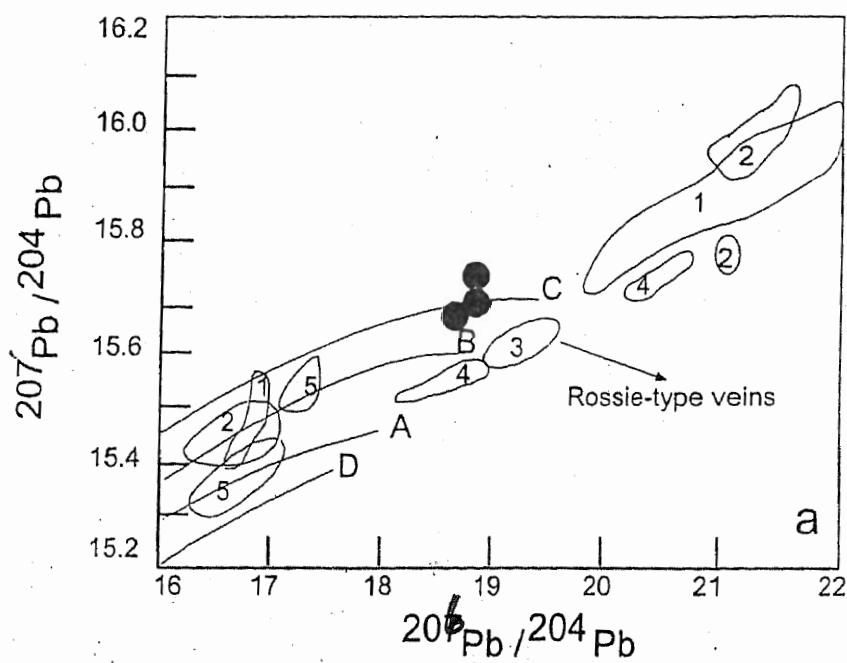


Figure 9.5 a,b. Comparison of plot of $^{207}\text{Pb}/^{204}\text{Pb}$ vs. $^{206}\text{Pb}/^{204}\text{Pb}$ and $^{208}\text{Pb}/^{204}\text{Pb}$ vs. $^{206}\text{Pb}/^{204}\text{Pb}$ for galena from quartz veins of the Gawuch Formation with lead isotope field of 1. Mississippi-valley type deposits (Central Missouri, USA): Doe and Delevaux (1972); 2. Laisvall-type (Sweden) deposits: Richarad et al. (1981); 3. Rossie-type veins: Flecher and Farquhar (1982); 4. Central Metasedimentaries: Flecher and Farquhar (1982); 5. Balmat-Edwards galena: (Flecher and Farquhar (1982).

could be considered as the upper limit of the age of copper mineralization in the Gawuch Formation. This time span is the time when Pb for the studied galenas was separated from its source. According to plumbotectonic model, the studied galenas are characterized as containing an important contribution of lead from a radiogenic source. The minimum age (i.e., 42 Ma) is in close agreement with Ar-Ar age (40-48 Ma Zeitler 1985; Treloar et al., 1989) of the Lowari Pluton which is considered to be the source of the hydrothermal solutions responsible for the copper mineralization in the Gawuch Formation. The model ages of 80 and 140 Ma, however, indicate that the galenas from the Gawuch Formation have also incorporated Pb from an older source. There could be two possibilities for the origin of old age of Pb, first if we consider that much of the Kohistan batholith would have itself formed from partial melting of the early arc lithologies in Kohistan, the older component in studied galenas might be from early arc volcanics or the pelagic sediments of ocean crust of Neotethys (Jurassic age). The other possibility is that radiogenic Pb component of the studied galenas might have been contributed from Pb source in the Indian plate. They were formed during the decay of U in the basement rocks of the Indian plate and later on it was homogenized at the time when the Lowari pluton of 42-48 Ma (Zeitler 1985, Treloar et al. 1989) has started crystallizing from the magma generated by the partial melting of upper continental crust during the subduction of Indian plate underneath the Kohistan-Island arc. Some of the lead may have been extracted in the hydrothermal solution from the resulting magma at the time when probably the dioritic-granodiorite sill have started crystallizing. The lead may have been transported by hydrothermal fluid from cooling pluton in to the country rocks for

deposition in the form of quartz veins. However, because of the limited data and a wider range of time span as calculated from three lead isotope composition, it can be concluded that the age of Lowari pluton (42-48 Ma; Ar/Ar basis, Zeitler 1985, Treloar et al. 1989) falls within the model age limit of the galena of Gawuch copper mineralization and, therefore, must have played an important role in the formation of these galena.

To identify the role of younger magmatism of the Kohistan island arc in the contribution of radiogenic Pb to the hydrothermal system and the formation of galena and other ore phases in the Gawuch Formation, further detail Pb-isotope, Oxygen Isotope and trace element studies of these plutons are necessary.

CHAPTER 10

SUMMARY AND CONCLUSIONS

This study deals with investigations about the nature and petrogenesis of the copper mineralization in Drosh-Shishi area, located in the NW part of the Kohistan arc terrane in the Chitral area of Northern Pakistan. The studied mineralization is restricted to a linear belt of a width of about 4-45 meters stretching for a distance of 40 km between Kaldam Gol in the south-west to Langer in the north-east. The mineralization is generally associated with minor intrusions off-shooting from the Kohistan batholith, intrusive into an upper Cretaceous volcano-sedimentary cover of the Kohistan arc terrane.

Geology of the studied area near Drosh, Chitral, is characterized by a tectonic interaction between the Kohistan arc terrane and the Karakoram plate forming the southern margin of Eurasia. The two tectonic blocks are juxtaposed with each other along the Northern Suture, which, in the study area, comprise a melange zone of about 3 km width. The Northern Suture melange is principally composed of cleaved slate with interbedded clastic sediments, which contain blocks of volcanic greenstone, limestone, red shale and serpentinites. Pudsey (1986) interpreted the Northern Suture melange as an olistostrome, on the basis of predominance of depositional structures over tectonic mixing.

The Kohistan terrane, in this area, comprises a volcano-sedimentary succession of a probable upper Cretaceous age, divided into three formations by Pudsey et al. (1985); Gawuch Formation, Purit Formation, Drosh Formation. The Gawuch Formation occupies the basal part of the sequence and consists of

metavolcanics, with intercalations of metasediments like marbles and quartzites in its upper part. A laterally persistent, five-meter thick bed of marble defines the top of the Gawuch Formation, separating it from the overlying Purit Formation. Unlike the Gawuch Formation, the Purit Formation is fluvial in origin and comprises conglomerate, sandstone, siltstone and shale. Red shale is the most abundant rock type in the Purit Formation. Conformably overlying the Purit Formation, the Drosh Formation is a sequence of thickly bedded porphyritic andesites with phenocrysts of plagioclase, hornblende, and pyroxene. The Northern Suture melange is in direct tectonic contact with the Drosh Formation.

The Gawuch Formation, forming the basal part of the Kohistan sequence, is of principal interest from the point of view of sulfide mineralization. The lower contact of the Gawuch Formation, at present, is faulted against the underlying Lowari pluton of the Kohistan batholith. Initially these two units are believed to have an intrusive relation as suggested by the Early Tertiary age of the Lowari pluton and Early Cretaceous age of the Gawuch Formation. The Gawuch Formation, during this study, is divided into two units; a lower unit comprising predominantly of metavolcanics of basalt to andesite composition, often sheared into phyllites, and an upper unit comprising complex intercalation of metabasalts, and metasediments (quartzites and limestone). This upper unit is commonly intruded by minor intrusions of diorites and granodiorites in the form of sills and dykes. Mineralization is restricted to the upper part of the Gawuch Formation and is characteristically associated with the diorites, granodiorites and associated quartz veins. The five-meter thick marble bed at the top of the Gawuch Formation, is also extensively

mineralized. The confinement of the copper mineralization to the upper parts of the Gawuch Formation is probably related to the fact that the overlying shales of the Purit Formation served to seal the upward migration of hydrothermal solutions, developing a trap in the upper parts of the Gawuch Formation.

The metavolcanics of the Gawuch Formation are divisible into two types; porphyritic and fine-grained. Porphyritic volcanics are fine- to medium-grained, characteristically porphyritic to poikilitic, with less commonly aphyric seriate texture. These vary from fresh to highly altered and are commonly dissected by quartz and calcite veins. Amphibole, pyroxene, feldspar and chlorite form the predominate constituents, and quartz, epidote, clay and ore occur as minor constituents. The second variety is fine-grained to glassy, composed of chlorite, epidote, carbonate, clay, quartz, feldspar, ore and glass. Chlorite and epidote are secondary and are formed by the alteration of amphibole and feldspars. Quartz is very fine and intermixed with chlorite and epidote. Feldspar is mostly altered but some rocks show the pseudomorph of feldspar, replaced by epidote, carbonate and clay.

Volcanic rocks belonging to the Drosh Formation are massive to weakly foliated, fine-grained and commonly altered. Compositionally, they are mostly andesites. In terms of mineral composition, feldspars, amphibole, clinopyroxene, quartz and ore are the principal primary constituents with chlorite, sericite, epidote, clay and sphene as the secondary minerals. The only difference from those of the Gawuch Formation is the presence of fresh grains of pyroxene in the volcanics of the Drosh Formation.

Three varieties of diorites are distinguished in the studied area on the basis of texture and degree of alteration. These include 1) diorites, 2) altered diorites and 3) gneissose diorites. The diorites of the studied area are medium- to coarse-grained, equigranular to inequigranular, subhedral characterized by a common hypidiomorphic granular texture. The major constituent minerals are plagioclase, orthoclase, amphibole and quartz. Calcite, chlorite, epidote occur as minor constituents, muscovite, biotite and ore are accessory minerals. All rocks are slightly foliated. Granulation is developed along margins.

Altered diorites are mineralogically similar to the fresh diorites and granodiorites, but are different in texture. The principal difference, however, is the degree of alteration. The altered diorites are fine- to coarse-grained, inequigranular and are characteristically porphyritic, but some rocks show typically idiomorphic porphyritic and poikilitic textures. Feldspar and quartz occur as primary minerals, sphene and ore as accessory while chlorite, epidote, sericite and calcite occur as secondary minerals. At places relicts of hornblende are also present in the aggregate of chlorite.

Most of the diorites are strongly foliated and have a banded appearance in the hand specimen. Some of the samples are porphyroclastic with eye-shape appearance of feldspar grains set in a matrix of fine-grained dynamically recrystallized matrix. As far as the mineral composition is concerned, there are only subtle differences between these and non-foliated diorites described above. The major constituents of diorite gneisses are plagioclase and quartz. Amphibole, chlorite, epidote, sericite, clay and ore are accessories. Plagioclase and quartz are

coarse-grained and are enclosed by fine groundmass of quartz, feldspar, hornblende, chlorite, muscovite, biotite and ore. Quartz, plagioclase, perthite and hornblende are the primary minerals while epidote, chlorite, biotite and muscovite are secondary minerals formed by alteration of feldspar and amphibole.

Geochemistry, involving both major and trace elements, have been used to characterize the petrology and tectonic setting of igneous rocks of the area. Metavolcanic rocks belonging to Gawuch and Drosh Formations show different petrology, the former are calc-alkaline while the latter are clearly tholeiitic. Detailed treatment in terms of mantle-normalized trace elements patterns and discrimination diagrams involving immobile trace elements, however, suggest that the two groups of volcanics, despite differences in their petrological character, originated with a strong subduction component.

Copper mineralization in the Gawuch Formation is related with hydrothermal activity, which is mainly confined to the quartz veins and altered diorites. This mineralization occurs in four different forms 1) in quartz veins 2) along foliation planes 3) disseminated mineralization and 4) supergene enrichment.

- 1) The upper part of the Gawuch Formation is studded with quartz veins along fractures and fissures. Most of these veins are generally enriched in copper-bearing sulfides, such as tetrahedrite, chalcopyrite, bornite and chalcocite. Galena, pyrite and sphalerite also occur at places. Magnetite and limonite are important oxides. Tetrahedrite occurs as coarse-grained irregular mass in the interstices of quartz grains. It is massive, highly fractured at places, and encloses anhedral to sub-rounded grains of quartz. Galena is second dominant ore phase, medium in

grain size and exhibits typical triangular pits at surface. Chalcopyrite is brass yellow and usually disseminated as fine- to medium-grained crystals. Sphalerite is present as irregular mass of ameboidal shape within the interstices and fractures. Pyrite occurs as cubic to subhedral disseminated grains.

2. Shearing along local faults is a common feature in the upper part of the Gawuch Formation. The rocks involved in these shear zones are commonly fractured, mylonitized and turned into phyllites or schists. In such rocks quartz and carbonate veining and precipitation of ore phases along the foliation planes is very common. Copper mineralization in the form of tetrahedrite, chalcocite and chalcopyrite along with other sulfide phases like galena, sphalerite and pyrite are generally present along foliation planes in the zones of intense shearing. These ore phases are usually precipitated along foliation planes in the form of microveins or thin bands of carbonates and quartz.
3. Copper mineralization in the form of chalcopyrite and tetrahedrite is disseminated mainly in the diorites. Chalcopyrite is the dominant phase and occurs as fine- to medium grained, irregular in shape and also occurs as interstitial phase. Cubic grains of pyrite are also found in association with chalcopyrite and tetrahedrite.
4. Azurite and malachite are the secondary minerals along with limonite, formed due to oxidation of sulfide minerals. Limonite is dark red and reddish brown in color. Azurite and malachite have thin patches of typical blue and green color, respectively. They generally occur along fractures and at the margins of the sulfide minerals.

Electron microprobe studies show that the tetrahedrite, to be stoichiometric $(\text{Cu Fe Zn})_{12} (\text{Sb As})_4 \text{Si}_3$. It shows less variation in Cu (40.10 to 42.84 wt%), Zn (5.55 to 6.89 wt%), S (25.48 to 27.33 wt%), As (9.20 to 17.48 wt%). Microprobe analyses of galena indicate that all galena in general has traces of Ag (0.0 to 0.04 wt%), Fe ranges from (0.00 to 0.24 wt%). The rest of the elements are generally below detection limit. The analyses suggest the galena to be stoichiometric PbS . Chalcopyrite is stoichiometric CuFeS_2 . Most of analyses exhibit undetectable concentration of Pb and Sb, however, up to 0.05 wt% of Zn, and up to 0.12 wt% of As has been noticed. Sphalerite is stoichiometric ZnS . The mole % of FeS in sphalerite is ranging from 4.66 to 10.74 and is indicative of change in colour of sphalerite from light brown to reddish brown respectively. Electron microprobe analyses of pyrite suggest that the pyrite to be stoichiometric FeS_2 . It shows that Cu is present up to 1.0 wt%. Fe has wide range (38-50 wt%) whereas S has narrow range (53-55 wt%). Magnetite to be nearly stoichiometric Fe_3O_4 . Bornite to be nearly Cu_5FeS_4 . Traces of Zn (0.0 to 0.9 wt%), Ag (0.0 to 17 wt%) are present. However Pb is undetectable.

Fluid inclusion studies indicate that the salinity of the hydrothermal solutions involved in the genesis of Cu-mineralization is <26 equivalent wt% NaCl and homogenization temperature ranges from 160-350° C, with a mean temperature of 255° C.

The oxygen isotope composition of quartz from quartz veins shows $\delta^{18}\text{O}$ values ranging from 14.49 to 18.32 ‰ with a mean value of 16.63 ‰. The $\delta^{18}\text{O}$ value of the mineralizing fluid of the area has been calculated at the mean temperature (255° C) as determined by fluid inclusion studies. The estimated $\delta^{18}\text{O}$ value of the

mineralizing fluid ranges from 5.79 to 9.62 ‰ with a mean value of 7.98 ‰. This indicates the involvement of magmatic fluids in the formation of quartz veins and associated copper mineralization in the investigated area.

The Pb isotopic compositions for galena from copper-bearing quartz veins in Gawuch Formation yield wide a range of age (42 to 140 Ma) with μ values of 9.86 to 10.01. This could be assigned as the model age for mineralization and could be considered as the upper limit of the age of copper mineralization in Gawuch Formation. This time span (42-140 Ma; mean 83 Ma) is the time when lead for the studied galena was separated from its source. According to plumbotectonic model, the studied galena are characterized as containing an important contribution of lead from a radiogenic source. The minimum age (i.e. 40 Ma) is in close agreement with Ar-Ar age (40-48 Ma Zeitler 1985; Treloar et al., 1989) of the Lowari pluton which is considered to be the source of the hydrothermal solutions responsible for the copper mineralization in Gawuch Formation. The model ages of 80 and 140 Ma, however, indicate that the galena from Gawuch Formation have also incorporated Pb from an older source. There could be two possibilities for the origin of old age of Pb; first if we consider that much of the Kohistan batholith would have itself formed from partial melting of the early arc lithologies in Kohistan, the older Pb component in studied galena might be from early arc volcanics or the pelagic sediments of ocean crust of the Neotethys (Jurassic age). The other possibility is that the radiogenic Pb component of the studied galena might have been contributed from Pb source in the Indian plate. The magma generated at the time of 40-48 Ma for Lowari pluton at least

had some contributions from the subducting Indian-plate continental crust, even if in the form of dehydration fluids.

Several lines of investigations have been adopted during the course of this study to ascertain the nature and petrogenesis of the copper mineralization in the Drosh-Shishi area in the NW part of the Kohistan terrane, including field observations, petrography, geochemistry, mineral chemistry and measurement of isotope ratios for Pb in Galena and oxygen in quartz veins. The principal attributes constraining the nature and origin of the studied mineralization include:

- 1) The mineralization is spatially restricted to a narrow belt of a width of 5-45 meters.
- 2) The locale of the mineralization is apparently controlled by stratigraphy i.e., it is confined to the upper parts of the Gawuch Formation.
- 3) The stratigraphic control, confining the mineralization to the upper parts of the Gawuch Formation is itself controlled by a selective locale of the diorite-granodiorite sills intruding into the upper parts of the Gawuch Formation. It may be noted that the basal part of the Gawuch Formation, immediately adjacent to the Lowari pluton is devoid of mineralization.
- 4) The stratigraphic control, confining the mineralization to the upper parts of the Gawuch Formation is further controlled by the presence of impervious lithologies of the Purit Formation on top of the Gawuch Formation. The red shales of the Purit Formation serve as a cap rock sealing the upward migration of hydrothermal solutions from the upper parts of the Gawuch Formation, resulting in their entrapment and concentration at this stratigraphic locale.

5) Presence of fractures and fissures, commonly associated with mineralization, together with common presence of quartz veining imply a structural control on studied mineralization in the Drosh-Shishi area.

These attributes derived from geological field observations, point to a hydrothermal origin for the mineralization in the Drosh-Shishi area. The close association of the mineralization with diorite-granodiorite minor intrusions suggests that the primary source for the solutions responsible for the mineralization rests with the igneous intrusions rather than with the volcanics. Absence of mineralization at the upper contact of the Lowari pluton with the basal parts of the Gawuch Formation, points out that it is only the relatively higher level intrusions which carried mineralization. These higher-level minor intrusions in the upper parts of the Gawuch Formation, however, may not necessarily be unrelated with the Lowari pluton, rather there is a greater possibility that they are fractionation product of the later.

Results from the fluid inclusion studies are combined with the oxygen isotope studies to ascertain the nature of the fluids responsible for mineralization. The measured $\delta^{18}\text{O}$ value of the parental fluids (ranging from +5.79 to + 9.62 ‰; mean= +7.98‰ SMOW) suggest strong enrichment in ^{18}O . This, when combined with homogenization temperatures of approximately 250 °C, suggests a role of heavy liquid of either metamorphic or magmatic origin. As pointed out above, the field observations suggesting a close association of minor intrusions of diorite-granodiorite composition with the mineralization, favour a magmatic origin for the mineralizing fluids rather a metamorphic origin.

The age of the studied mineralization in Drosh-Shishi area remains to be fully understood. The geological evidence relating the mineralization with the Kohistan batholith points to an Early Tertiary age i.e., same as that of the Lowari pluton (Zeitler et al., 1985). The Pb isotope ratios for the three samples of Galena from the studied mineralization yield model ages between 140 and 45 Ma. Of these, the minimum age is probably closer to the actual age of mineralization as ascertained on the basis of geological evidence. The older ages probably reflect a contamination from an older source such as that of the subducted crust of the Neotethys or even that of the Indian-plate continental crust.

REFERENCES

- Abarede, F. & Juteau, M., 1984. Unscrambling the lead model ages. *Geochemica et Cosmochimica acta*, v.48, pp.207-212.
- Afifi, A., Doe, B. R., Sim, P. K. & Delevaux, M. H., 1984. U-Th- Pb isotope chronology of sulfide ores and rocks in the early Proterozoic metavolcanic belt of northern Wisconsin. *Economic Geology*, v.79, pp.338-353.
- Ahmad, S. N. & Rose, A. W., 1980. Fluid inclusion in porphyry and skarnore at Santa Rita, New Mexico. *Economic Geology*, v.75, pp.229-250.
- Ahmed, Z. & Chaudhry, M. N., 1976. Petrology of the Babusar area, Diamir district, Gilgit, Pakistan. *Geological Bulletin. Punjab University*, v.12, pp.67-78.
- Albertson, A. H. F. & Degnan, P. J. 1993. Sedimentology and tectonic implications of the Lamayuru Complex: deep-water facies of the Indian passive margin, Indus Suture Zone, Ladakh Himalaya. In: *Himalayan Tectonics* (Treloar, P. J. & Searle, M. P.: Editors). Geological Society of London, Special Publication, v.74, pp.299-321.
- Arif, M. & Jan, M. Q., 1993. Chemistry of chromite and associated phases from the Shangla ultramafic body in the Indus suture zone of Pakistan. In: *Himalayan Tectonics* (Treloar, P. J. & Searle, M. P.: Editors). Geological Society of London, Special Publication, v.74, pp.101-112.
- Ayuso, R. A., 1986. Lead-Isotope evidence for distinct source of Granite and for distinct basement in the northern Appalachians, Mains. *Geology*, v.14(4), pp.332-325.
- Bard, J. P., Maluski, H., Matte, P. H. & Proust, F., 1980. The Kohistan sequence; Crust and mantle of an obducted island arc. *Geological Bulletin University of Peshawar*, v.13, pp.87-93.
- Beane, R. E. & Titley, S. R., 1981. Porphyry copper deposits: part II. Hydrothermal alteration and mineralization. *Economic Geology*, pp.235-269.
- Beaty, D. W. & Taylor, H. P., Jr., 1988. An oxygen isotope study of the Kidd Creek, Ontario, volcanogenic massive Sulfide Deposit: Evidence for a High ^{18}O ore Fluid. *Economic Geology*, v.83, pp.1-17.
- Belkin, H. E., 1994. Microthermometric investigations: Th and Tm. Practical and Theoretical Aspects. In: *Fluid Inclusions in Minerals: Methods and Applications* (Benedetto De Vivo & Maria Luce Frezzotti: Editors), pp.7-23.

- Bodnar, R. J. & Vityk, M. O., 1994. Interpretation of Microthermometric Data for H₂O-Na-Cl Fluid Inclusions. In: Fluid Inclusions in Minerals: Methods and Applications (Benedetto De Vivo & Maria Luce Frezzotti: Editors), pp.117-130.
- Bodnar, R. J., 1978. Fluid-inclusion study of the porphyry copper prospects at Red Mountain, Arizona: Unpubl. M.S. thesis, University of Arizona, 70p.
- Bodnar, R. J., 1992. Revise equation and table for freezing point depressions of H₂O-salt fluid inclusions (abst.) PACROFI, Fourth Biennial Pan-American Conference on Research on Fluid Inclusions, Program and Abstracts, Lake Arrowhead, Ca, v.4, 15p.
- Bossart, P., Dietrich, D., Greco, A., Ottiger, & Ramsay, J. G., 1988. The tectonic structure of the Hazara-Kashmir syntaxis, (Southern Himalaya) Pakistan. *Tectonics*, v.7/2 pp.273-297.
- Bottinga, Y. & Javoy, M., 1973. Comments on oxygen isotope geothermometry. *Earth and Planetary Science Letters*, v.20, pp.250-265.
- Burnham, G. W., 1979. Magmas and hydrothermal fluids. In: *Geochemistry of hydrothermal ore deposits* (Barnes, H. L.: Editor): New York, Wiley Intersciences., pp.71-133.
- Calkins, J. A., Jamiluddin, S., Bhuyan, K. & Hussain, A., 1981. Geology and mineral resources of the Chitral-Partisan area, Hindu Kush Range, northern Pakistan. U. S. Geological Survey, Professional Paper 716-G, pp.G1-G33.
- Clayton, R. N. O., Neil, J. R. & Mayeda, T. K., 1972. Oxygen isotope exchange between Quartz and water. *Journal of Geophysical Research*, v.77, pp.3057-3067.
- Constantopoulos, J., 1994. Oxygen isotope geochemistry of the Coeur D'Alene mining district, Idaho. *Economic Geology*. v.89, pp.944-951.
- Coward, M. P., Windley, B. F., Broughton, R. D., Luff, I. W., Petterson, M. G., Pudsey, C. J., Rex, D. C. & Khan, M. A., 1986. Collision tectonics in the NW Himalayas. In: *Collision Tectonics* (Coward, M.P. & Ries, A.C. : Editors). Geological Society of London, Special Publication, v.19, pp.203-219.
- Coward, M. P., Butler, R. W. H., Chamberlain, A. F., Graham, R. H., Izatt, C. N., Khan, M. A., Knipe, R. J., Prior, D. J., Treloar, P. J. & Williams, M. P., 1988. Folding and imbrication of the Indian crust during Himalayan collision. *Philosophical Transactions of the Royal Society of London*, v.A326, pp.89-116.

- Coward, M. P., Jan, M. Q., Rex, D., Tarney, J., Thirlwall, M. & Windley, B. F., 1982. Geotectonic framework of the Himalaya of N. Pakistan. Geological Society of London, v.139, pp.299-303.
- Cox, K. G., Bell, J. D. & Pankhurst, R. J., 1979. The interpretation of igneous rocks. Allen and Unwin, London, 450p.
- Deb, M., Thorpe, R. I., Cumming, G. L. & Wagner, P., 1989. Age, source and stratigraphic implications of Pb isotope Data for Conformable, sediment hosted, Base metal Deposits in the Proterozoic Aravalli-Delhi Orogenic belt, Northwestern India. Precambrian Research, v.43, pp.1-22.
- Desio, A., 1963. Review of the geological "formations" of the western Karakorum (Central Asia). Riv. Ital. Pal. Strat., v.69, pp.475-501.
- Desio, A., 1964. Geological tentative map of the western Karakorum. Scale 1:500,000. Istituto Geologico, University of Milano.
- Desio, A., 1964. Tectonic relationship between the Karakorum, Pamir and Hindu Kush, Central Asia. Proc. 22nd International Geological Congress., New Delhi, v.11, pp.192-213.
- Desio, A., 1959. Cretaceous beds between Karakorum and Hindukush ranges (Central Asia). Riv. Ital. Pal. Strat., v.65, pp.221-229.
- Desio, A., 1966. The Devonian sequence in Mastuj valley (Chitral), NW Pakistan. Riv. Ital. Pal. Strat., v.72, pp.293-32
- Desio, A., 1975. Some geological notes and problems on the Chitral valley (NW Pakistan). Rend. Naz. Lincei, v.58, pp.1-7.
- Dilles, J. H., Solomon, G. C., Taylor, H. P. Jr. & Einandi, M. T., 1992. Oxygen and hydrogen isotope characteristics of hydrothermal alteration at the Ann-Mason porphyry copper deposit, Yerington, Nevada. Economic Geology. v.87, pp.44-63.
- Doe, B. R. & Delevaux, M. H., 1972. Source of lead in South east Missouri galena ores. Economic Geology, v.67, pp.409-425.
- Doe, B. R. & Zartman, R. E., 1979. Plumbotectonics 1, the phanerozoic. In: Geochemistry of hydrothermal ore deposits (Barnes, H. L. :Editor), Holt, Rinehart and Winston, New York (2nd Edition).

Eldridge, C. S., Bourcier, W. L., Ohmat, O. H. & Barnes, H. L., 1988, Hydrothermal inocndation and incubation of the chalcopyrite Disease in Sphalerite: Economic Geology, v.83, pp. 97-989.

✓ Faure, G., 1986. Principles of Isotope Geology (second edition). John Wiley & Sons New York. pp.0-589.

✓ Fletcher, I. R. & Farquhar, R. M., 1982. The protocontinental nature and regional variability of central metasedimentary belt of the Grenville province: Lead isotope evidence. Canadian Journal of Earth Sciences, v.19, pp.239-253.

✓ Fletcher, I. R., 1979. A Lead isotope study of Lead-Zinc mineralization associated with the Central Metasedimentary belt of Grenville Province: Ph.D. Thesis, University of Toronto, 165p.

Freidman, I. O. & Neil, J. R., 1977. Compilation of stable isotope fractionation factors of geochemical interest: U. S. Geological Survey, Professional Paper, 440-K, 12p.

Gancarz, A. J. & Wasserburg, G., 1979. Initial lead of the Amitsoq gneiss, West Greenland and implications for the age of the Earth. Geochimica et Conmochimica Acta, v.41, pp.1283-1301.

Gansser, A., 1964. Geology of the Himalayas. Wiley, New York, 289p.

Gill, R. C. O., 1980. Comparative petrogenesis of Archean and Modern Low K-Tholeiites. A periodical review of some geological aspects. Physics and Chemistry of Earth, v.11, pp.431-332.

Goldstein, R. H. & Reynolds, T. J., 1994. Systematic of fluid inclusions in diagenetic minerals. Society for Sedimentary Geology, Short Course 31, 199p.

✓ Gulson, B. L, Perkins, W. G. & Mizon, K. J., 1983. Lead isotope studies bearing on genesis of copper ore bodies at Mount Isa, Queenland. Economic Geology, v.78, pp.1466-1504.

✓ Gulson, B. L., 1984. Uranium-lead and lead investigations of minerals from the Broken Hill lodes and mine sequence rocks. Economic Geology , v.79, pp.476-490.

✓ Gulson, B. L., 1985. Shale-hosted lead-Zinc deposits in Northern Australia: Lead isotope variations. Economic Geology, v. 80, pp.2001-2012.

- Harris, N. B. W., Pearce, J. A. & Tindle, A. G., 1986. Geochemical characteristics of collision zone magmatism. In : Collision Tectonics (M. P. Coward & A.C. Ries: Editors). Geological Society of London, Special Publication, v.19, pp.67-81.
- Hayden, H.H., 1916. Notes on the geology of Chitral, Gilgit and Pamirs. Records Geological Survey of India, v.45, pp.271-335.
- Henley, R. W. & McNabb, A., 1978. Magmatic vapor plumes and groundwater interaction in porphyry copper emplacement. *Economic Geology*, v.73, pp.1-20.
- Heyl, A. V., Delevaux, M. H., Zartman, R. E. & Brock, M. R., 1966. Isotopic study of galena from upper Mississippi Valley, The Illinois-Kentucky and some Appalachian Valley mineral districts. *Economic Geology*, v.69, pp. 992-1006.
- Hollister, L. S. & Crawford, M. L., 1981. Fluid inclusions: Applications to petrology. Mineralogical Association of Canada, Short Course Handbook, v.6, 304p.
- Holm, P. E., 1986. The geochemical finger prints of different tectonomagmatic environments using hydromagmatophile element abundances of tholeiitic basalts and basaltic andesites. *Chemical Geology*, v. 51, pp.303-323.
- Houtermans, F. G., 1946. Die Isotopenhäufigkeiten im natürlichen Blei und Das Alter des Urans. *Naturwissenschaften*, v.33, pp.185-186.
- Irvine, T. N. & Baragar, W. R. A., 1971. A guide to the chemical classification of the common volcanic rocks. *Canadian Journal of Sciences*, v.8, pp.523-548.
- Ivanac, J. F., Traves, D. M. & King, D., 1956. The geology of the N.W. portion of the Gilgit Agency. Records, Geological Survey of Pakistan., v.3, pp.1-27.
- Jan, M. Q., 1979. Petrography of the amphibolites of Swat and Kohistan. *Geological Bulletin University of Peshawar*, v.11, pp.51-64.
- Jan, M. Q. & Tahirkheli, R. A. K., 1969. The geology of the lower part of Indus Kohistan, Swat. *Geological Bulletin University of Peshawar*, v.4, pp.1-13.
- Jan, M. Q. & Kempe, D. R. C., 1973. The petrology of the basic and intermediate rocks of Upper Swat, Pakistan. *Geological Magazine*, v.110, pp.285-300.
- Jan, M. Q. & Howie, R. A., 1981. The mineralogy and geochemistry of the metamorphosed basic and ultrabasic rocks of the Jijal complex, Kohistan, NW Pakistan. *Journal of Petrology*, v.22, pp.85-126.

- Jan, M. Q. & Windley, B.F. 1990. Chromian spinel-silicate chemistry in ultramafic rocks of the Jijal complex, Kohistan, north-west Pakistan. *J. Petrology*, v 31, pp 667-715.
- Jan, M. Q., Banaras, M., Ghani, A., Asif, M. 1983. The Tora-Tigga ultramafic complex, southern Dir district. *Geological Bulletin University of Peshawar*, v.16, pp.11-29.
- Jan, M. Q., Parvez, M. K. & Khattak, M. U. K., 1984. Coronites from the Chilas and Jijal-Pattan complexes of Kohistan. *Geological Bulletin University of Peshawar*, v.17, pp.75-85.
- Jan, M. Q., Khan, M. A. & Qazi, M. S., 1993. The Sapat mafic- ultramafic complex, Kohistan arc, North Pakistan. In: *Himalayan Tectonics* (Treloar, P.J. & Searle, M.P.: Editors). Geological Society of London, Special Publication, v.74, pp.113-121.
- Jan, M. Q., Khan, M. A. & Windley, B. F., 1991. Exsolution in Al-Cr-Fe³⁺-rich spinels from the Chilas mafic-ultramafic complex, Pakistan. *American Mineralogist*, v.77, pp.1074-1079.
- Kamilli, R. J. & Ohmoto, H., 1977. Paragenesis, zoning, fluid inclusion and isotopic studies of the Finlandia vein, Colqui district, Central Peru. *Economic Geology*, v.72, pp.950-982.
- Kaneda, H., Karim, T, Ahmad, M. N., Yoshida, M. & Ali, M. 1996. Ore Mineralogy and Geomagnetic Anomaly of Kaldam Gol Skarn-type Copper Ore, Chitral, Northern Pakistan. *International Seminar on Paleomagnetic Studies in Himalaya-Karakoram Collision Belt and Surrounding Continents*. Geoscience Lab., Geological Survey of Pakistan, pp.125-128
- Kazmi, A. H., Lawrence, R. D., Dawood, H., Snee, L. W. & Hussain, S. S., 1984. Geology of the Indus suture zone in the Mingora-Shangla area of Swat, northern Pakistan. *Geological Bulletin University of Peshawar*, v.17, pp.127-144.
- Kerrick, R. & Freyer, B. J., 1979. Archean precious-metal hydrothermal system, Dome mine, Abitibi greenstone belt. 11. REE and oxygen Isotope relations. *Canadian journal of Earth Science*, v.16, pp. 440-458.
- Khan, M. A. & Searle, M. P., 1996. Geological Map of North Pakistan and adjacent areas of northern Ladakh and western Tibet. Spec. Publ. Sponsored by BPIL, Shell and Amoco.

- Khan, M. A., Jan, M. Q. & Weaver, B. L., 1993. Evolution of the lower arc crust in Kohistan, N. Pakistan: temporal arc magmatism through early, mature and intra-arc rift stages. In: Himalayan Tectonics (Treloar, P.J. and Searle, M.P. :Editors). Geological Society of London, Special Publication, v.74, pp.123-138.
- Khan, M. A., Stern, R. J., Gribble, R. F. & Windley, B. F., 1997. Geochemical and isotopic constraints on subduction polarity, magma source and paleogeography of Kohistan intra-oceanic arc, northern Pakistan Himalaya. Geological Society of London, (in press).
- Khan, M. A. Jan, M. Q., Windley, B. F., Tarney, J. & Thirlwall, 1989. The Chilas mafic-ultramafic igneous complex; the root of the Kohistan island arc in the Himalaya of northern Pakistan. Geological Society of America, Special. Paper., v.232, pp.75-94.
- Khan, T., Khan, M. A. & Jan, M. Q., 1994. Geology of a part of the Kohistan terrane between Gilgit and Chilas, northern areas, Pakistan. Geological Bulletin University of Peshawar, v.27, pp.99-112.
- Klein, T. L. & Criss, R. E., 1988. An Oxygen, isotope and geochemical study of meteoric hydrothermal system at Pilot mountain and selected other localities, Carolina State belt, Economic Geology, v.83, pp.801-821.
- Klootwijk, C. T., Gee, J. S., Peirce, J. W., Smith, G. W. & McFadden, P. L., 1992. An early India-Eurasia contact; Palaeomagnetic constraints from the Ninetyeast Ridge, ODP Leg 121. Geology, v.20, pp.395-398.
- Klootwijk, C., Sharma, M. L., Gergan, J., Tirkey, B., Shah, S. K. & Agarwal, V., 1979, The Extent of Greater India, II. Palaeomagnetic data from the Ladakh Intrusives at Kargil, Northwestern Himalayas. Earth & Planetary Science Letters, v.44, pp.47-64.
- Koeppel, V., 1980. Lead-isotope studies of stratiform ore deposits of Namaqualand, NW Cape Province, South Africa and their implications on the age of the Bushmanland sequence. Proceedings of the fifth quadrennial International Association on the Genesis of ore deposits Symposium, Schweizerbart, sche Verlagsbuch-handling Stuttgart, pp.195-207.
- Koppel, V., 1984. Lead isotope as tracers of the origin of metals in ore deposits and of the evolution of continental crust: Example from western and central Europe. 27th International Geologic Congress, Moscow, 1984, Proceedings, v.12, pp.53-82.

Kulla, J. B., 1979. Oxygen and hydrogen isotopic factors determined in experimental clay-water system. Unpublished Ph.D. thesis, University of Illinois, Urbana, 106p.

✓
LeCouteur, P.C., 1973. A study of lead isotope from mineral deposits of Southeastern British Columbia and in the Anvil Range, Yukon Territory. Unpublished Ph.D. thesis. University of South Carolina, Columbia.

Lindgren, W., 1933. Ore deposits: New York, Mc Graw Hill, 644p.

Magaritz, M. & Taylor, H. P., 1976. Oxygen, hydrogen and carbon isotope studies of the Franciscan formation, Coast Ranges, California, *Geochimica et Cosmochimica acta*, v. 40, pp.215-234.

Maluski, H. & Matte, P., 1984. Ages of alpine tectono-metamorphic events in northwestern Himalaya (north Pakistan) by $^{39}\text{Ar}/^{40}\text{Ar}$ method. *Tectonics*, v.3, pp.1-18.

Maniar, P.D. & Piccoli, P.M. 1989. *Bulletin Geological Society of America*, v 101, 635-643.

Marcoux, E. & Jebrak, M., 1987. Approche geochemique de l'origin et de la duree des depots hydrothermaux dans le district d Ussel (Massif Central, France): *Acad. Sci. Paris, Competes Rendus*, v.305, Ser.11, pp.377-381.

Matsuhisa, Y., Goldsmith, J. R. & Clayton, R. N., 1979. Oxygen isotopic fractionation in system quartz-albite-anorthite-water. *Geochim Cosmochim Acta*, v.43, pp.1131-1140.

Matsushita, S. & Huzita, K. (eds.) 1965. *Geology of the Karakoram and Hindukush; Results of the Kyoto University Scientific Expedition (1955)*, Kyoto University of Japan. v.7, 160p.

Matthews, A., Goldsmith, J. R. & clayton, R. N., 1983. Oxygen isotope fractionation between Zoisite and water. *Geochimica et Cosmochimica acta*, v.47, pp.645-654.

McMahon, H., 1900. Notes on the geology of Gilgit. *Quaternary Journal of Geological Society, London*, v.56, pp.337-369.

Meschede, M., 1986. A method of discriminating between different type of mid-Ocean ridge basalts and continental tholeiites with the Nb-Zr-Y diagram. *Chemical Geology*, v.56, pp.207-218.

- Miller, D. J., Loucks, R. R. & Ashraf, M., 1991. Platinum-group element mineralization in the Jijal layered ultramafic-mafic complex, Pakistani Himalaya. *Economic Geology*, v.86, pp.1093-1102.
- Misch, P., 1949. Metasomatic granitization of batholithic dimensions, Part I: syntectonic granitization in Nanga Parbat area, North West Himalaya. *American Journal Science*, v.247, pp.209-245.
- Miyashiro, A. 1974. Volcanic rock series in island arc and active continental margins. *American Journal of Sciences*, v.274, pp.321-355.
- Molnar, P. & Tapponier, P., 1977. The collision between India and Eurasia. *Science*, v.236, pp.30-41.
- Mullen, E. D., 1983. MnO/TiO₂/P₂O₅: a minor element discriminant for basaltic rocks of oceanic environments and its implications for petrogenesis. *Earth and Planetary Science Letters*, v.62, pp.53-62.
- Nash, J. T. & Cunningham, C. G, Jr., 1973. Fluid-inclusion studies of the flourspar and Gold deposits. Jamstone district, Colorado. *Economic Geology*, v.68, pp.1247-1262.
- O'Neil, J. R., 1977. Stable isotopes in mineralogy: *Physical Mineralogy*, v.2, pp.105-123.
- O'Neil, J. R., Silberman, M. L., Fabbi, B. P. & Chesterman, C. W., 1973. Stable isotope and chemical relations during mineralization in the Bodie mining district, Mono County California, *Economic Geology*, v.68, pp.765-784.
- Pascoe, E. H., 1923. General report for the year 1922. *Geological Survey of India*, 55, 1: pp.1-51.
- Pascoe, E. H., 1924. General report for the 1923. *Records, Geological Survey of India*, 56, 1: pp.44-48.
- Paterson, C. J., 1982. Oxygen isotopic evidence for the origin and evolution of a scheelite ore forming fluid, Glenorchy, New Zealand. *Economic Geology*, v.77, pp.1672-1687.
- Patriat, P. & Achache, J., 1984. India-Eurasia collision: chronology and its implications for crustal shortening and driving mechanisms of plates. *Nature*, v.311, pp.615-621.

- Pearce, J. A. & Cann, J. R., 1973. Tectonic setting of basic volcanic rocks determined using trace element analyses. *Earth & Planetary Science Letters*, v.19, pp.291-300.
- Pearce, J. A. & Norry, M. J., 1979. Petrogenetic implications of Ti, Zr, Y and Nb variations in volcanic rocks. *Contribution to Mineralogy Petrology*, v.69, pp.33-47.
- Pearce T. H., Gorman B. E. & Birkelt T. C., 1977. The relationship between major element chemistry and tectonic environment of basic and intermediate volcanic rocks. *Earth & Planetary Science Letters*, v.36, pp.121-132.
- Pearce, J. A., Harris, N. B. & Tindle, A. G., 1984. Trace element discrimination diagrams for tectonic interpretation of Granitic rocks. *Journal of Petrology*, v.25, pp.956-983.
- Petterson, M. G. & Windley, B. F., 1985. Rb-Sr dating of the Kohistan arc batholith in the Trans Himalaya of N. Pakistan and tectonic implications. *Earth and Planetary Science Letters*, v.74, pp.54-75.
- Petterson, M. G. & Windley, B. F., 1991. Changing source regions of magmas and crustal growth in the Trans-Himalayas: Evidence from the Chalt volcanics and Kohistan batholith, Kohistan, N. Pakistan. *Earth and Planetary Science Letters*, 102, 326-346.
- Powell, C. McA., 1979. A speculative tectonic history of Pakistan and surroundings: Some constraints from the Indian Ocean. In: Farah, A. and DeJong, K. A. (eds.) *Geodynamics of Pakistan*. Geological Survey of Pakistan, Quetta, pp.5-24.
- Pudsey, C. J., 1986. The northern suture, Pakistan: Margin of a Cretaceous island arc. *Geological Magazine*, v.123, pp.405-423.
- Pudsey, C. J. & Maguire, P. K. H., 1986. Magnetic profiles across the northern suture, Kohistan, NW Pakistan. *Geological Bulletin University of Peshawar*, v.19, pp.47-60.
- Pudsey, C. J., Coward, M. P., Luff, I. W., Shackleton, R. M., Windley, B.F. & Jau M.Q., 1985. Collision zone between the Kohistan arc and the Asian plate in NW Pakistan. *Transactions of Royal Society, Edinburgh (Earth Sciences)*, v.77, pp.463-479.
- Roedder, E., 1977. Fluid Inclusions as Tools in Minerals Exploration. *Econ. Geol.* 72,

- Roedder, E., 1984. Fluid Inclusions, Mineralogical Society of America. Reviews in Mineral., v.12, 644p.
- Rollinson H. R., 1993. Using geochemical data, evaluation, Presentation, interpretation. John Wiley & Sons. Inc., New York, 344p.
- Routhier, P., 1969. Ser trois principes generous de la metallogenie et de la recherche minerals: Mineralium Deposita. v.42, pp.213-218.
- Routhier, P., 1980. Quelques Lois regissant la distribution disguisements de metaux au sein des plaques centimentals. C. R. Acad. Sci., Paris, 288, Ser. D., pp.859-862.
- Ruzhentsev, S. V. and Shvolman, V. A. 1981. Tectonics and structure of Pamir metamorphics. In: Saklani, P. S. (ed.), Metamorphic Tectonics of the Himalaya. Today and Tomorrow Publishers, New Delhi, pp. 27-41.
- Rye, R. O., & Sauciness, F. J., 1974. Fluid inclusion and stable isotope studies on the Casapalca Ag- Pb- Zn- Cu deposits, Central Andes, Peru: Geology, v.69, pp.181-205.
- Schneiderhohn, H., 1952. Genetische agerstattengliederung auf geotekonischer Grundlage: Stuttgart, E. Schweizervart sche Varlag, 42p.
- Searle, M. P., 1991. Geology and Tectonics of the Karakoram Mountains. J. Wiley & Sons, New York, 358p.
- Shah, M. T. & Hamidulllah, S., 1994. Field and Mineralogy constraints of the Dir Metavolcanic Sequence, Kohistan arc Terrane Northern Pakistan. Geological Bulletin University of Peshawar, v.27, pp.43-55.
- Shah, M. T. & Jan, M. Q., 1993. Mineralogical constraints of Shergarh Sar amphibolites of Allai Kohistan, Northern Pakistan. Geological Bulletin University of Peshawar, v.26, pp.59-73.
- Shah, M. T. & Majid, M., 1985. Major and trace element variations in the lavas of Shergarh Sar area and their significance with respect to the Kohistan tectonic anomaly. Geological Bulletin University of Peshawar, v.18, pp.163-188.
- Shah, M. T., Thorpe, R. I., & Siddique, S. A ., 1992. Lead isotope signature of the Proterozoic sediment-hosted base metal deposits at the margin of the Indian plate in Besham area, northern Pakistan. Geological Bulletin University of Peshawar, v.25, pp.59-65.

- Shah, M. T., Shervais, J. W. & Ikramuddin M., 1994. The Dir metavolcanic sequence: calc-alkaline magmatism within the Kohistan arc terrane, northern Pakistan. *Geological Bulletin University of Peshawar*, v.27, pp.9-27.
- Shams, F. A., 1972. Glaucophane-bearing rocks from near Topsis, Swat-First record from Pakistan. *Pakistan Journal of Earth Sciences*, v.24, pp.343-345.
- Shams, F. A., 1980. Origin of the Shangla blueschists, Swat Himalaya, Pakistan. *Geological Bulletin University of Peshawar (Spec. Issue)* v.13, pp.67-70.
- Sharp, Z. D., 1990. A laser-based microanalytical method for insitu determination of oxygen isotope ratios of silicates and oxides. v.54, pp.1354-1357.
- Shepherd, T. J., Rankin, A. H. & Alderton, D. H., 1985. A practical guide to fluid Inclusions studies. Blackie and Son, Glasgow, 239p.
- Sheppard, S. M. & Epstein, S., 1970. D/H and $^{18}\text{O}/^{16}\text{O}$ ratios of Minerals of possible mantle or lower crustal origin. *Earth and Planetary Science Letters*, v.9, pp.232-237.
- Shervais, J. W., 1982. Ti-V plots and petrogenesis of modern and ophiolitic lavas. *Earth Planetary Science Letters*, v.59, pp.101-118.
- Spooner E. T. C., Beckinsale R. D., Fyfe, W. S. & Snewing, J. D. 1974. ^{18}O enriched ophiolitic metabasic rocks from E. Liguria (Italy), Pindos (Greece), and Troodos (Cyprus). *Contributions to Mineralogy and Petrology*, v. 47, pp. 41-62.
- ✓ Stacey, J. S. & Kramers, J. D., 1975. Approximation of terrestrial lead isotope evolution by two-stage model. *Earth and Planetary Science Letters*, v.26, pp. 207-221.
- Sullivan, M. A., Windley, B. F., Saunders, A. D., Haynes, J. R. & Rex, D. C., 1993. A Paleogeographic reconstruction of the Dir group. Evidence for magmatic arc migration within Kohistan N. Pakistan. In: *Himalayan Tectonic* (Treloar, P. J. & Searle, M. P.: Editors). Geological Society of London, Special Publication, v.74, pp.139-160.
- Sun S. S. & McDonough W. F., 1989. Chemical and isotopic systematic of oceanic basalt's: Implications for mantle composition and processes. *Magnetism in Ocean basins*. Geological Society of London, Special Publication, v.42, pp.313-345.

- Tahirkheli, R. A. K., 1983. Geological evolution of Kohistan island arc on the southern flank of the Karakoram-Hindukush in Pakistan. *Bollitino Geofisica Teorica Applicata*, v.25, pp.351-364.
- Tahirkheli, R. A. K. & Jan, M. Q. 1979. A preliminary geological map of Kohistan and the adjoining areas, N. Pakistan. *Geological Bulletin University of Peshawar*, v.11 (in pocket).
- Tahirkheli, R. A. K., Mattaur, M., Proust, F. & Tapponier, P. 1979. The India-Eurasia suture zone in northern Pakistan: some new data for the interpretation at plate scale. In: Farah, A. & DeJong, K. A., (Eds.) *Geodynamics of Pakistan*. Geological Survey of Pakistan, Quetta, pp 125-130.
- Taylor, H. P., 1979. Oxygen and hydrogen isotope relationships in hydrothermal mineral deposits. In: *Geochemistry of hydrothermal ore deposits* (Barnes, H. L., ed.). Wiley interscience, New York, pp. 236-277.
- Taylor, H. P., Jr., & Epstein, S., 1962. Relationship between $^{18}\text{O}/^{16}\text{O}$ ratios in coexisting minerals of igneous and metamorphic rocks. Part 1: Geological Society of America. v.73, pp. 461-480.
- Taylor, H. P., Jr., 1971. Oxygen isotope evidence for large-scale interaction between meteoric ground water and tertiary granodiorite intrusions, Western Cascade Range, Oregon. *Journal of Geophysical Research*, v.76, pp.7855-7875.
- Taylor, H. P., Jr., 1974. The application of Oxygen and hydrogen isotope studies to the problems of hydrothermal alteration and ore deposition. *Economic Geology*, v.69, pp.843-883.
- Tera, F., 1981. Aspects of isochronism in lead isotope systematics: application to planetary evolution. *Geochimica et Cosmochimica Acta*, v.45, pp.1439-1448.
- Tipper, G. H., 1921. Orpiment mines in Chitral. *Records, Geological Survey India*, 54(1): pp.16-17.
- Tonarini, S., Villa, I.M., Oberli, F., Meier, M., Spencer, D.A., Pognante, U. & Ramsay, J. G., 1993. Eocene age of eclogite metamorphism in Pakistan Himalaya. *Terra Nova*, 5, 13-20.
- Treloar, P.J., Rex, D.C., Guise, P.G., Coward, M.P., Searle, M.P., Windley, B.F., Petterson, M.G., Jan, M.Q. & Luff, I.W., 1989. K-Ar and Ar-Ar geochronology of the Himalayan collision in NW Pakistan: constraints on the timing of suturing, deformation, metamorphism and uplift. *Tectonics*, 4, 881-909.

- Wadia, D. N., 1932. Notes on the geology of Nanga Parbat, Mt. Diamir, and adjoining parts of Chilas, Gilgit district, Kashmir. Records, Geological Survey India, v.66, pp.212-234.
- Wedepohl, K. H., Delvaux, M. H. & Doe, B. R., 1978. The potential source of lead in the Permian Kupferschiefe bed of Europe and some selected Paleozoic mineral deposits in the federal Republic of Germany. Contributions to Mineralogy and Petrology, v.65, pp.273-281.
- Wilson, M., 1989. Igneous Petrogenesis, A Global Tectonic Approach. Unwin Hyman, London.
- Zartman, R. E. & Doe, B. R., 1981. Plumbotectonics- the model. Tectonophysics, v.75, pp.135-162.
- Zeitler, P. K., 1985. Cooling history of the NW Himalaya, Pakistan. Tectonics, v.4, pp.127-151.
- Zeitler, P. K. & Chamberlain, C. P., 1991. Petrologic and tectonic significance of young leucogranites from the northwestern Himalaya, Pakistan. Tectonics, v.10, pp.729-1.
- Zeitler, P. K., Johnson, N. M., Naeser, G. W. & Tahirkheli, R. A. K., 1982. Fission-Trace evidence for quaternary uplift of the Nanga Parbat region, Pakistan. Nature v.298, pp.255-257.

- Woolley, A.R., 1969. Some aspects of fenitization with particular reference to Chilwa Island and Kangankunde, Malawi. British Mus. (Nat. History) Bull. Mineral. 2, 191-219.
- Woolley, A.R., Symes, R.F. and Elliott, C.J., 1972. Metasodmatized (fenitized) quartzite from the Borralan Complex, Scotlandland. Min. Mag. 38, 819-836.
- Woolley, A.R., 1982. A discussion of carbonatite evolution and nomenclature, and generation of sodic and potassic fenites. Min. Mag. 46, 13-17.
- Wright, T.L., 1967. The microcline-orthoclase transformation in the contact aureole of the Eldora Stock. Amer. Mineral. 52, 117-136.
- Wright, T.L., 1968. X-ray and optical study of alkali feldspar II. An x-ray method of determining the composition and structural state from measurement of 2 θ values for three reflections. Amer. Mineral. 54, 88-104.
- Wright, T.L. and Stewart, D.B., 1968. X-ray and optical study of alkali feldspar: 1. Determination of composition and structural state from refined unit-cell parameters and 2 θ . Amer. mineral. 53, 38-87.
- Varet, J., 1969. Les pyroxenes des phonolites du Cantal (Auvergne, France). Neues. Jb. Miner. Mh., 4, 174-184.
- Yagi, K., 1953. Petrochemical studies of the alkalic rocks of Morotu district, Sakhalin. Bull. Geol. Soc. Am. 64, 769-810.